

# Dynamic Processes in Supramolecular Gels

Jorge Ruiz Olles

PhD

University of York

Chemistry

October 2017

## **Abstract**

Supramolecular gels are self-assembled solid-like materials with a large solvent component making up a liquid-like phase. The 3D scaffold, which is self-assembled from low-molecular-weight building blocks, and is present in form of nanostructured fibres, holds the mobile liquid phase, preventing bulk flow. As a consequence, these gels have interesting dynamic properties, which were the subject of study in this thesis. Chapter One provides an introduction to dynamic processes in gels. Chapter Two focusses on the thermodynamics and kinetics of a two-component gelator system based on a peptide dendron acid combined with an amine. We used rheology, CD spectroscopy and NMR to characterise the gelation process at different length scales (macroscopic, nanoscale and molecular scale respectively). We conclude that thermodynamic stability of the gel network does not correlate with the rate of network formation. Chapter Three reports diffusion across a gel-gel interface, comparing the diffusion of self-assembling small molecules with those which do not form gel fibres. Chapter Four reports the gelation capabilities of certain choline chloride based deep eutectic solvents (DESs) using 1,3;2,4-dibenzylidenesorbitol (DBS) as gelator. We monitor the ionic conductivity and demonstrate that conductivities for the deep eutectic gels are similar to those of the DESs themselves, indicating that the ionic components do not suffer from immobilisation through interaction with the self-assembled gel nanofibres. These results are encouraging as they are the first example of supramolecular gels made for these specific kinds of DESs, and suggest potential applications, for example as gel electrolytes in battery applications. Chapter five reports all Experimental details, materials and methods. In summary, this thesis provides insights into a range of different dynamic processes in gels – (i) the formation of gels, (ii) the mobility of the solid-like fibres themselves, and (iii) the mobility/conductivity of ionic species in innovative DES gels.

## **Acknowledgements**

I would like to thank to my supervisor David Smith for giving me the opportunity of developing this exciting and innovative project. Also, I thank him because letting me to integrate risky ideas and experiments that in the end were successful. He has been a constant source of support and inspiration. I would like to thank to the European Union through the Marie Curie program which supported economically all the research involved in this project which was run by several universities across the continent. Collaborative programs like this one makes Europe a more integrated place and strength its capabilities of research and innovate. I have also been fortunate to meet and work with amazing people not only professionally but also extraordinary persons with excellent human background. I could mention some of my colleagues such as Philip Chivers, Tunde Okesola, Stephen Bromfield, Daniel Cornwell, Vania Vieira, Buthaina Albanyan, Ching Wan Chan (Rex), Nicole Whitelaw, Ana Campo, Marta Tena, Ian George, Andrew Steer, Elizabeth Wheeldon, Joshua Smith, Stefan Rohner and many others that I have met along this extraordinary journey that has been this European PhD program in York. I would also like to extend my gratitude towards all of the technical staff at University of York who have helped me with various experiments; Dr Karl Heaton (MS), Heather Fish for NMR, Meg Stark (TEM and SEM) and John Hawes for his extraordinary IT support.

Lastly, but most importantly, I would not be able to reach this stage without the support of my family which includes my parents Carlos and Margarita. I would specially mention to supportive persons such as Angélica, Pili, Jorge and Joaquín. Finally, this thesis is dedicated specially to my beloved grandmother Maria Larrull.

## **Declaration**

I declare that the work presented within this thesis is entirely my own, except where otherwise acknowledged. Aspects of this work have been published in the following journal article: *RSC Adv.* 2015, **5**, 27190-27196. This work has not been submitted in part or fully for examination towards any other degrees or qualifications.

Jorge Ruiz Olles

15/09/17

# Table of Contents

<b>Abstract .....</b>	<b>2</b>
<b>Acknowledgements .....</b>	<b>3</b>
<b>Declaration .....</b>	<b>4</b>
<b>Table of Contents.....</b>	<b>5</b>
<b>List of Figures .....</b>	<b>13</b>
<b>List of Tables.....</b>	<b>22</b>
<b>Abbreviations.....</b>	<b>24</b>
<b>Chapter 1 Introduction .....</b>	<b>29</b>
1.1. Brief History of Materials.....	29
1.2. General definition of gels. ....	29
1.3. Molecular interactions. ....	31
1.4. Supramolecular chemistry .....	34
1.5. Supramolecular Gels.....	37
1.6. DBS as gelation system. ....	39
1.7. Supramolecular bicomponent organogels based on lysine dendrons. ....	40
1.8. Crystallization and gelation. ....	43
1.9. Thermodynamics of gel formation. ....	45
1.10. Dynamic aspects of supramolecular gels. ....	46
1.10.1. Reversibility.....	46
1.10.2. Evolving nature.....	46
1.10.3. Internal mobility. ....	47
1.10.4. Tunability.....	47

1.11.	Kinetics of gel formation.....	47
1.11.1.	<sup>1</sup> H-NMR.....	48
1.11.2.	Circular dichroism spectroscopy.....	49
1.11.3.	Rheology.....	49
1.12.	Diffusion processes in gels.....	50
1.12.1.	Controlled release. ....	52
1.12.2.	Gel-gel diffusion. ....	53
1.12.3.	Fick's Law treatment of diffusion in gels. ....	56
1.13.	Electrolytes as conductive materials. ....	59
1.13.1	Ionic liquids.....	59
1.13.2.	Deep eutectic solvents (DESs).....	60
1.13.3	Types of DES .....	62
1.13.4.	Ionic conductivity of ILs and DESs. ....	64
1.13.5.	Deep eutectic gels and ionogels .....	66
1.14.	Project aims. ....	68
<b>Chapter 2 Thermodynamics and kinetics of supramolecular gelation.....</b>		<b>70</b>
2.1.	Thermodynamics of supramolecular gels formation .....	70
2.1.1.	Introduction .....	70
2.1.2.	Two-component dendrons and amines.....	71
2.2.1.	Synthesis of the second generation dendrons of various configurations G2 (Boc-Phe) <sub>2</sub> -Lys-OH, G2 (Boc-Val) <sub>2</sub> -Lys-OH and G2 (Boc-Ala) <sub>2</sub> -Lys-OH.....	73
2.2.2.	T <sub>gel</sub> measurements via tube inversion .....	76

2.2.3. VT <sup>1</sup> H-NMR and Van't Hoff treatment .....	77
2.2.4. Conclusions on Thermodynamics.....	84
2.3. Kinetics of gels formation.....	85
2.3.1. Introduction .....	85
2.3.2. Visual kinetics of gel formation. ....	86
2.3.3. Quantitative study kinetics of gel formation. ....	88
2.3.4. CD Spectroscopy:.....	89
2.3.4.1. CD as a Technique for Following the Kinetics of Gelation on the Nanoscale.....	90
2.3.4.2. Protocol of kinetics of gel formation by CD. ....	90
2.3.4. CD in hot conditions .....	91
2.3.5. CD in cold conditions.....	95
2.3.6. Conclusions of CD kinetic experiments.....	97
2.3.5. Rheology as the technique for studying kinetics of gel formation on the macroscopic length scale.....	98
2.3.5.1. Introduction .....	98
2.3.5.2. Experiment design and strategy of Rheology in cold conditions. ....	99
2.3.5.3. Treatment of kinetic rheological data.....	102
2.3.5.5. Conclusions on the kinetics rheology experiment.....	108
2.3.6. NMR as a molecular-scale technique for the study of gel formation.....	112
2.3.6.1. VT- <sup>1</sup> HNMR for studying kinetics of gel formation .....	112
2.4. Chapter Conclusions. ....	116
<b>Chapter 3 Diffusion processes at gel-gel interfaces .....</b>	<b>119</b>
3.1. Introduction.....	119
3.2. Supramolecular Organogel .....	120

3.3. Formation of a two-component gel.....	121
3.4. Diffusion and mobility in gels. ....	123
3.4. The design of a diffusion cell. ....	124
3.4.1. Selection of the material for the diffusion cell.....	125
3.5. Chemical Nature of the Gel .....	126
3.6. Gel characterization: .....	127
3.6.1. Images of kinetically produced samples. ....	127
3.6.2. Images of thermodynamically formed gels.....	129
3.6.3. Images of gels by SEM. ....	130
3.6.4. Images of gels in TEM.....	132
3.7. Stages of building the diffusion cell. ....	133
3.7.1. Diffusion System: A description.....	136
3.7.2. Diffusion experiment.....	140
3.7.3. First experiment at room temperature. ....	141
3.7.4. Diffusion of small molecules .....	143
3.7.5. Diffusion of amines at various temperatures.....	146
3.7.5.1. Diffusion across gel-gel interfaces at 25°C .....	146
3.7.5.2. Diffusions at 5°C .....	151
3.7.5.3. Diffusions at 45°C .....	153
3.7.6. Diffusion coefficients of gel-gel transfers.....	155
3.7.7. Diffusions of dendrons gels at 25°C by CD measurements. ....	159
3.7.7.1. Calibration curves.....	162
3.7.7.2. Explanation of CD experiment.....	165
3.8. Ultrasound influence in gel solid-like state.....	171

3.8.1. AFM as an imaging technique.....	175
3.9. Conclusions and future ideas.....	178
<b>Chapter 4 Ionogels Conductivity .....</b>	<b>181</b>
4.1. Introduction.....	181
4.1.1. Natural Deep Eutectic Solvents (DESs).....	182
4.1.2. Organic Ionic gels .....	183
4.1.3. Objectives of the Research .....	186
4.2. Preparation of natural deep eutectic solvents.....	188
4.3. Preparation of ionic deep eutectic gels .....	190
4.4. Comparing ionic conductivity of ionic liquids and their respective ionogels ...	192
4.5. Increasing ionic force in Ionogels .....	196
4.6. Gelation of DESs based on components other than glycols .....	200
4.7. Gelating second generation DESs based on ChCl and hydrogen bond donors .	203
4.8. Rheological properties of DESs.....	204
4.9. Rheological properties of ionogels .....	206
4.10. Sample preparation .....	206
4.11. Electron Microscopy of Ionogels.....	215
4.12. SEM images of ionogels .....	215
4.13. TEM images of ionogels .....	218
4.14. Sonication and ionic conductivity.....	220
4.15. Conclusions.....	223
4.15.1. Suggested Future Work.....	223

<b>Chapter 5 Conclusions and future work .....</b>	<b>225</b>
5.1. Thermodynamics and Kinetics of gelation. ....	225
5.2. Diffusion processes at gel-gel interfaces .....	226
5.3. Ionic conductivity of Deep Eutectic gels. ....	227
5.4. Summary .....	227
<b>Chapter 6 Experimental.....</b>	<b>228</b>
6.1. General Experimental Methods. ....	228
6.2. Chapter 2 and 3 syntheses.....	229
6.2.1. Synthesis of L or D lysine methyl ester dihydrochloride <sup>207</sup> .....	229
6.2.2. BOC protection of L or D Lysine.....	230
6.2.3. Coupling of L-(Boc) <sub>2</sub> -Lys-OH and L(Lys)-OMe. ....	231
6.2.4. Coupling of Boc-Phe-OH and Lys-OMe. ....	233
6.2.5. Coupling of Boc-Ala-OH and Lys-OMe.....	234
6.2.6. Coupling of Boc-Val-OH and Lys-OMe.....	236
6.2.7. Hydrolysis of L and D G2 ((Boc) <sub>2</sub> Lys) <sub>2</sub> -Lys-OMe.....	237
6.2.8. Hydrolysis of G2 ((Boc)Phe) <sub>2</sub> -Lys-OMe. ....	239
6.2.9. Hydrolysis of G2 (Boc-Ala) <sub>2</sub> -Lys-OMe.....	240
6.2.10. Hydrolysis of G2 (Boc-Val) <sub>2</sub> -Lys-OMe.....	241
6.3. Assay, analysis, materials and methods.....	243
6.3.1. Procedure for determining T <sub>gel</sub> values - Chapter 2.....	243
6.3.2. Electron Microscopy (TEM) – Chapter 3. ....	243
6.3.2.1. Toluene based gels sample preparation for TEM.....	243

6.3.2.2. DES based gels sample preparation for TEM .....	243
6.3.3. SEM sample preparation – Chapter 3. ....	244
6.3.3.1. Freeze-drying method.....	244
6.3.3.2. Ambient drying method.....	244
6.3.4. AFM technique - Chapter 3.....	245
6.3.4.1. Preparation of samples. ....	245
6.3.5. Kinetics of gelation by circular dichroism spectroscopy - Chapter 2. ....	245
6.3.5.1. Hot sol-gel transition gel formation.....	246
6.3.5.2. Cold (25°C) sol-gel transition formation. ....	246
6.3.6. Kinetics of gelation by VT <sup>1</sup> H-NMR spectroscopy – Chapter 2.....	246
6.3.6.1. Procedure Kinetic data VT- <sup>1</sup> HNMR - Chapter 2.....	247
6.3.8. Ionic conductivity method. Chapter 4 .....	249
6.3.9. Sonication ionic conductivity measurements .....	250
6.3.10. Rheology and viscosity measurements .....	251
6.3.10.1. Gel Disc preparation.....	251
6.3.10.2. Viscosity test in rheology. ....	252
6.3.11. Kinetics of gel formation in rheology – Chapter 2.....	252
6.3.11.1. Cold (25°C) sol-gel transition formation. Chapter 2. ....	253
6.3.12. The Diffusion cell testing – Chapter 3 .....	254
6.3.12.1. Placing gels in the cell. ....	254
6.3.12.2. Sampling of the various regions of the cell. ....	255
6.3.12.3. Diffusion procedure for dendron analysis with CD.....	256
6.3.12.4. Diffusion coefficients D calculation.....	257
<b>References.....</b>	<b>264</b>
<b>Appendix. ....</b>	<b>277</b>
L-LysOMe. Characterization spectra. <sup>207</sup> .....	277
D-LysOMe. Characterization Spectra.....	278

7.2. G1 (Boc) <sub>2</sub> -Lys-OH Characterization spectra.....	280
G2 ((Boc) <sub>2</sub> -Lys) <sub>2</sub> -Lys-OMe Characterization data.....	283
G2 (Boc-Phe) <sub>2</sub> -Lys-OMe Characterization data.....	285
G2 (Boc-Ala) <sub>2</sub> -Lys-OMe Characterization data.....	287
G2 (Boc-Val) <sub>2</sub> -Lys-OMe Characterization data.....	288
G2 ((Boc) <sub>2</sub> -Lys) <sub>2</sub> -Lys-OH Characterization data.....	290
G2 (Boc-Phe) <sub>2</sub> -Lys-OH Characterization data.....	292
G2 (Boc-Ala) <sub>2</sub> -Lys-OH Characterization data.....	293
G2 (Boc-Val) <sub>2</sub> -Lys-OH Characterization data.....	295
Diffusion coefficients calculations .....	297
Diphenylmethane Diffusion Coefficient.....	297
Naph diffusion coefficient at 25°C.....	298
Hex diffusion coefficient at 25°C.....	299
Naph diffusion coefficient at 5°C.....	300
Hex diffusion coefficient at 5°C.....	301
Naph diffusion coefficient at 45°C.....	302
Hex diffusion coefficient at 45°C.....	303

## List of Figures

<b>Figure 1-1</b> Molecular assembly of tris hydrazone hydrogelator leads to fibre formation of a gel. Figure reproduced from reference <sup>12</sup> .....	30
<b>Figure 1-2</b> Representation of the three main types of multi-component gels of LMWGs. Figure reproduced from reference <sup>13</sup> . .....	31
<b>Figure 1-3</b> Phase transition of water depending on the surrounding conditions. The properties of the various forms of water depend on the existence of molecular interactions between molecules.....	33
<b>Figure 1-4</b> Typical representation of the hydrogen bonds present in the DNA polymer chain <sup>20</sup> .....	34
<b>Figure 1-5</b> Typical self-assembly process of LMWG to form the 3D network <sup>26</sup> .....	36
<b>Figure 1-6</b> Example of a molecular machine that has two positions depending .....	36
<b>Figure 1-7</b> host guest chemistry of the encapsulation of a potassium cation. ....	37
<b>Figure 1-8</b> The modification of the molecular skeleton of DBS gives differential gelation ranges depending on the surrounding conditions <sup>59</sup> .....	38
<b>Figure 1-9</b> Chemical structure of the DBS <sup>62</sup> .....	39
<b>Figure 1-10</b> Chemical structure of the DBS and possible derivatives. <sup>58 62</sup> .....	40
<b>Figure 1-11</b> G2 ((Boc) <sub>2</sub> -Lys) <sub>2</sub> -Lys-OH dendron interacting with an amine by hydrogen bonding. <sup>65</sup> .....	40
<b>Figure 1-12</b> Low Molecular Weight Hydrogelator (Fmoc-Dipeptides) and Protein Structures which are self-assembled in a cooperative manner. <sup>77</sup> .....	41
<b>Figure 1-13</b> Two-component gelation system formed by acid–amine interactions at the focal point of the dendritic lysine .....	42
<b>Figure 1-14</b> The various resulting structures of self-assembly of gelators being (a) self-sorting; (b) random mixing; (c) specific co-assembly <sup>79</sup> .....	43
<b>Figure 1-15</b> Supersaturated solution of chemical species can result in crystallization, amorphous precipitation by agglomeration and gelation . ....	44
<b>Figure 1-16</b> Typical solubility plot where ln(sol) of components is represented.....	46
<b>Figure 1-17</b> Warfarin being release from a composite depending on the pH of the media. <sup>137</sup> .....	53
<b>Figure 1-18</b> The image represents a summary of the controlled, directional release experiment. <sup>140</sup> .....	53
<b>Figure 1-19</b> The dependence of the diffusion coefficient of probe molecules on the concentration of acrylamide in gel. <sup>123</sup> .....	54
<b>Figure 1-20</b> A scheme of the basic structure of a lithium ion cell. Where lithium ions have to move through the electrolyte at certain diffusion rates. <sup>150</sup> .....	56
<b>Figure 1-21</b> Diffusion set up with camera recorder to track the diffusion of dyes <sup>151</sup> ....	57
<b>Figure 1-22</b> Diffusion profile as seen in the set of images recorded .....	57
<b>Figure 1-23</b> Comparation and fitting between the model and the .....	58

<b>Figure 1-24</b> Schematic representation of selected structures of IL cations and anions <sup>165</sup> .....	60
<b>Figure 1-25</b> Structures of DESs based on choline chloride and glycerol. <sup>170</sup> .....	61
<b>Figure 1-26</b> Standard eutectic mixture where final melting temperature of the mixture is lower than ones of the isolated compounds. <sup>167</sup> .....	62
<b>Figure 1-27</b> Some examples of the hydrogen bond donators and the hydrogen bond acceptors that can be mixed in certain DESs.....	64
<b>Figure 1-28</b> Dynamic viscosity ( $\eta$ ) of polyol based DESs as a function of temperature <sup>186</sup> .....	65
<b>Figure 2-1</b> Dendrons which have been synthesized. Note that these dendrons are second generation and the inner core is based on the lysine. ....	71
<b>Figure 2-2:</b> Lys based dendron interacting by means of .....	72
<b>Figure 2-3:</b> Series of reactions to produce the second generation dendron of Lys <sup>17</sup> .....	72
<b>Figure 2-4:</b> Hexylamine (Hex), 1-Naphthylmethylamine (Naph) and Phenethylamine (Phen) were the amines tested in the gel formation experiments. ....	74
<b>Figure 2-5</b> Various $T_{gel}$ temperatures for the resulting gels obtained from the combination of dendrons and amines proposed. ....	76
<b>Figure 2-6</b> VT-NMR experiment with a temperature range of 25-90°C with 5°C intervals for the Phen-Val. ....	78
<b>Figure 2-7</b> The integration of the various peaks corresponding the molecules involved in the gel appear when gels are analysed by NMR at several temperatures give precise concentrations VS temperature data. The reference concentration is given by the Diphenylmethane.....	79
<b>Figure 2-8</b> Concentration profile of the VT <sup>1</sup> H-NMR of the Phen-Val Gel. ....	80
<b>Figure 2-9</b> Plot representing Ln of the concentration of components in the gel versus the 1/T. for the case of Val-Phen Gel. ....	82
<b>Figure 2-10:</b> $T_{gel}$ values for a range of dendron and amine combinations .....	88
<b>Figure 2-11:</b> Elliptical Absorbance Vs time of Hex-Lys gel under hot conditions.....	92
<b>Figure 2-12:</b> Variation of the CD signal for the Hex-Ala gel for a 206.5 nm. ....	93
<b>Figure 2-13:</b> Variation of the CD signal for the Hex-Val gel for a 216.5 nm. ....	93
<b>Figure 2-14:</b> Variation of the CD signal for the Hex-Phe gel for a 236.5 nm. ....	94
<b>Figure 2-15</b> Representation of the various CD absorbance experiments for each tested component. ....	95
<b>Figure 2-16</b> Comparison of CD signal progressions when the two components are mixed in ambient conditions. ....	96
<b>Figure 2-17</b> General scheme of the process of collecting a progression of viscosity from solution state of components to the sol-gel transition triggered by the addition of the second component. ....	99
<b>Figure 2-18:</b> Rheogram which shows the progression of gelation in Hex gels at 25°C. ....	101

<b>Figure 2-19</b> Rheogram which shows the progression of gelation in Naph gels at 25°C. .....	101
<b>Figure 2-20</b> Rheogram which shows the progression of gelation in Phen gels at 25°C. .....	102
<b>Figure 2-21</b> Typical rheogram of elastic modulus versus time. ....	103
<b>Figure 2-22:</b> Fitting of the two different regions for the gel formation process of Hex Lys Gel. ....	104
<b>Figure 2-23</b> Fitting of the two different regions for the gel formation process of Naph-Lys Gel. ....	105
<b>Figure 2-24</b> Fitting of the two different regions for the gel formation process of Naph-Phe Gel. ....	106
<b>Figure 2-25</b> Fitting of the two different regions for the gel formation process of Phen-Ala Gel.....	106
<b>Figure 2-26</b> CD absorption spectra of the Hex-Phe gel system Vs time.....	109
<b>Figure 2-27</b> Rheogram of the formation of various amine-dendron systems.....	110
<b>Figure 2-28</b> Rheological test of Phen based gels.....	111
<b>Figure 2-29:</b> Several spectra of the gel being cooled down from 90°C to 25°C and retained to that temperature while analysing that.....	113
<b>Figure 2-30:</b> Concentration of G2 ((Boc) <sub>2</sub> Lys) <sub>2</sub> -Lys-OH dendron mM Vs cooling time min. Starting from the temperature of 90°C to 25°C during several minutes.....	114
<b>Figure 2-31:</b> Concentration drop of the various combinations of dendrons and amines in the cooling experiment. ....	115
<b>Figure 3-1</b> A process of diffusion in liquid media. <sup>222</sup> .....	119
<b>Figure 3-2</b> Diffusion of a dye in agarose as a classic example of diffusion processes inside gels. Potassium Permanganate (MW=158) on the left and Methylene Blue (MW=320) on the right. <sup>225</sup> .....	120
<b>Figure 3-3</b> Self-assembly of a TTF-grafted C3 core <sup>228</sup> .....	121
<b>Figure 3-4</b> Representation of Acid-Amine two-component complex.....	122
<b>Figure 3-5.</b> Two-component complex formed between the acid on.....	122
<b>Figure 3-6</b> Controlled release of molecules loaded inside a gel being released to a... 124	124
<b>Figure 3-7</b> An example of first design of diffusion system. ....	126
<b>Figure 3-8</b> Gels kinetically formed which composition is NaphGel (left) and HexGel (right) as the xerogels evaporated at normal conditions.....	128
<b>Figure 3-9</b> Gels thermodynamically formed which composition is ..... 129	129
<b>Figure 3-10</b> HexGels 10mM concentration. Xerogels by freeze drying method. Left 20.000 magnification, right 33.439 magnification. ....	131
<b>Figure 3-11</b> Naph Gels 10 mM concentration Xerogels by freeze drying method Left 10.000 magnification, right 32.151 magnification. ....	131
<b>Figure 3-12</b> TEM NaphGel (right) and HexGel (left) both 16.500 magnification. ....	132

<b>Figure 3-13</b>	Vial filled with fluorescent and non-fluorescent gels being irradiated....	133
<b>Figure 3-14</b>	First diffusion experiment that was made in a vial. The two gels .....	134
<b>Figure 3-15</b>	Placement of the gels in the cuvette and removal of the.....	136
<b>Figure 3-16</b>	The diffusion chamber (desiccator) inside an incubator to maintain a stable temperature. Notice that the closed system (chamber) maintains rich the vapour pressure of toluene so gels don't dry out. ....	137
<b>Figure 3-17</b>	Assembly of glass cells for use in the diffusion experiments.....	138
<b>Figure 3-18</b>	The process of filling the central hole with white silicone in order to seal one side from the other with an aluminium barrier. Once silicone is in contact with toluene it swells and there was therefore a need to removing the excess of swollen white silicone with a very sharp blade to obtain a completely flat surface in the diffusion cell. ....	139
<b>Figure 3-19</b>	Visualizing the two gels loaded into the cell by pouring the hot liquid gels into each side of the cell while maintaining them separate with an aluminium barrier (left). Once the gels have solidified the barrier is removed and gels come into contact (right), representing time point zero of the diffusion experiment.....	140
<b>Figure 3-20</b>	Diffusion process of the 3D network of different gels. On the left, the cuvette at time 0, and on the right the cuvette as the experiment takes place, indicating diffusion of the fluorescent amine. ....	141
<b>Figure 3-21</b>	The cuvette is divided in 6 regions in order to .....	141
<b>Figure 3-22</b>	Concentration of Naph sampled from each of the six locations on either side of the gel-gel interface, at different timepoints of the experiment. ....	142
<b>Figure 3-23</b>	In the upper part of the cuvette HexGel is mixed with the .....	144
<b>Figure 3-24</b>	Concentration of diphenylmethane versus cell region in the.....	145
<b>Figure 3-25.</b>	<sup>1</sup> H-NMR signals to be integrated in the diffusion experiment. Notice the first two amines are part of the 3D network for each kind of gel. Naph Gel and Hex Lys Gel respectively. We highlight one of the protons that comes from the dendron (green) which was effectively used as an internal standard.....	147
<b>Figure 3-26</b>	<sup>1</sup> H-NMR of the region 1 of the diffusion cell of certain diffusion time. Notice that signals are integrated relative to the dendron proton highlighted. ....	148
<b>Figure 3-27</b>	Concentration profile for amines in a diffusion experiment between Naph Lys Gel and Hex Lys Gel for a given time and temperature.....	149
<b>Figure 3-28</b>	Concentration profile for Hexylamine in a diffusion cell for a range of various diffusion times at 25°C .....	149
<b>Figure 3-29</b>	Concentrations profile for 1-Naphthylmethylamine in a diffusion cell...	150
<b>Figure 3-30</b>	Concentrations profile for Hexylamine in a diffusion cell for a range of various diffusion times at 5°C. ....	152
<b>Figure 3-31</b>	Concentrations profile for 1-Naphthylmethylamine in a diffusion cell...	152
<b>Figure 3-32</b>	Diffusion concentration Hexylamine profiles for various times and at 45°C .....	153
<b>Figure 3-33</b>	Diffusion Naph concentration profiles for various times and at 45°C.....	155

<b>Figure 3-34</b> Comparison Between the model with $D=10^{-6}$ and the real diffusion profile corresponding to Naph at 96h at 25°C .....	156
<b>Figure 3-35</b> All the Naph concentration profiles which are fitted with the equation of the diffusion model proposed above and with a Diffusion coefficient determined by least squares. 25°C .....	157
<b>Figure 3-36</b> Comparative values of diffusion Coefficients according to the substance and the temperature. ....	158
<b>Figure 3-37</b> CD spectra for samples which are stereoisomers DDD and LLL of G2 ((Boc) <sub>2</sub> Lys) <sub>2</sub> -Lys-OH dendrons 5 mM concentrations. Methylcyclohexane: dioxane (95:5) .....	160
<b>Figure 3-38.</b> CD spectra that shows that equal amounts of a mixture of Hex L and D Lys Gels results in the cancelation of the resulting dichroic signal at 5mM concentration. Methylcyclohexane: dioxane (95:5) .....	161
<b>Figure 3-39</b> Calibration Curve for samples which are stereoisomers DDD and LLL of G2 ((Boc) <sub>2</sub> Lys) <sub>2</sub> -Lys-OH dendrons. Various concentration has been analysed to get the relation between concentration and CD Signal at 25°C and 220 nm. Solvent mixture of Methylcyclohexane: dioxane (95:5) .....	162
<b>Figure 3-40.</b> Calibration Curve fitting for the D Lys Hex Gel. ....	163
<b>Figure 3-41</b> Calibration Curve fitting for the Hex <sub>L</sub> -Lys Gel. 25°C, Methylcyclohexane: dioxane (95:5).....	163
<b>Figure 3-42</b> Calibration curve for the CD signal and the various proportions of mixtures LLL and DDD. ....	164
<b>Figure 3-43</b> Fitting of the data points presented in the table above for a given wavelength of 220nm.....	164
<b>Figure 3-44</b> CD spectra of the 6 different regions for a diffusion of 18h at 25°C.....	165
<b>Figure 3-45</b> CD spectra for a gel diffusion of 96h.....	166
<b>Figure 3-46</b> CD spectra for a gel diffusion of 144h.....	167
<b>Figure 3-47</b> CD spectra for a gel diffusion of 240h.....	167
<b>Figure 3-48</b> Percentage content of the L dendron concentration while diffusing in the cell at several times as deduced by CD measurements. ....	169
<b>Figure 3-49</b> Percentage content of the D G2 ((Boc) <sub>2</sub> Lys) <sub>2</sub> -Lys-OH dendron concentration while diffusing in the cell at several times as deduced by CD measurements. ....	170
<b>Figure 3-50</b> Gels diffusing under sonication conditions. Notice total.....	172
<b>Figure 3-51</b> Picture showing the difference between a .....	172
<b>Figure 3-52.</b> NMR Spectra of sonicated and non-sonicated Hex Gels. Both spectra are completely identical.....	174
<b>Figure 3-53</b> Gels thermodynamically formed and sonicated.....	177
<b>Figure 3-54</b> Gels thermodynamically formed which composition is Naph- <sub>L</sub> -Lys Gel and Hex- <sub>L</sub> -Lys Gel. ....	178
<b>Figure 4-1</b> Schematic representation of a eutectic point of two-component phase diagram. <sup>167</sup> .....	183

<b>Figure 4-2:</b> Picture represents such a mass transfer which .....	185
<b>Figure 4-3:</b> Typical Butterfly structure of DBS. <sup>242</sup> .....	186
<b>Figure 4-4:</b> The basic procedure to form the Ionic liquid based on the two main components. Proportions are two molecules of glycol every one of choline chloride. 188	
<b>Figure 4-5</b> Tgel determined for the first set of prepared DESs. ....	191
<b>Figure 4-6</b> Picture of ionogels as an example of the kind of gels that .....	192
<b>Figure 4-7</b> Set up which is used in order to measure ionic conductivities versus temperature. In the image above can be identified the various parts of the set up: Conductometer, probe and the programable thermostatic Bath. ....	193
<b>Figure 4-8:</b> presents the influence of temperature of the ionic conductivity of the DESs and the corresponding DEGs.....	194
<b>Figure 4-9:</b> Ionic conductivity Vs Temperature for MEG DES with 1M salts dissolved .....	198
<b>Figure 4-10</b> Conductivities Vs temperature of DESs and DESs Gels with some salts. ....	199
<b>Figure 4-11</b> Molecular structures of different potential molecules to be combined with Choline Chloride to form various DES's. ....	201
<b>Figure 4-12:</b> Logarithmic graph of the IC of the natural IL prepared from various combinations. "Ave" meaning average measurement of temperatures between the bath temperature and the probe temperature. ....	202
<b>Figure 4-13:</b> Logarithmic representation of IC measurements comparing and highlighting the small difference in IC between the IL and their respective Ionogels. 203	
<b>Figure 4-14:</b> Viscosity versus temperature of the various prepared DESs.....	205
<b>Figure 4-15:</b> Procedure of preparations of disc of gels. The obtained disk can be handled in one piece until it is placed in the rheometer for testing.....	207
<b>Figure 4-16:</b> Amplitude Sweep Rheogram for MEG based ionogel. ....	209
<b>Figure 4-17:</b> Amplitude Sweep Rheogram for MPG based ionogel.....	209
<b>Figure 4-18:</b> Amplitude Sweep Rheogram for PDO based ionogel. ....	209
<b>Figure 4-19</b> Comparison of the viscoelastic components of the ionogels that have been tested (MEG, MPG and PDO).....	210
<b>Figure 4-20</b> Values of $G'$ and $G''$ for the various ionogels with different kind of salts dissolved. ....	211
<b>Figure 4-21:</b> Amplitude Sweep Rheogram for Glycerol based IG. ....	212
<b>Figure 4-22:</b> Amplitude Sweep Rheogram for Sorbitol based IG.....	213
<b>Figure 4-23:</b> Amplitude Sweep Rheogram for Xylitol based IG.....	213
<b>Figure 4-24:</b> Amplitude Sweep Rheogram for Urea based IG. ....	213
<b>Figure 4-25</b> Various values of viscoelastic $G'$ and $G''$ for the prepared ionogels. ....	214
<b>Figure 4-26</b> SEM images of various gels at 30 thousand magnifications each.....	216
<b>Figure 4-27</b> SEM Images of various gels at 30 thousand magnifications each.....	217

<b>Figure 4-28</b> TEM Images of various gels of MEG, MPG and PDO .....	218
<b>Figure 4-29</b> TEM Images of various gels of MEG mixed with various salts at 1M ...	219
<b>Figure 4-30</b> TEM images of 1 micron for the glycerol and Sorbitol ionogels. ....	219
<b>Figure 4-31</b> TEM images of 1 micron for the Urea and Xylitol ionogels. ....	220
<b>Figure 4-32:</b> Effect on the ionic conductivity of the DES liquids .....	221
<b>Figure 6-1</b> Molecular structure of Lysine methyl ester dihydrochloride.....	229
<b>Figure 6-2</b> Molecular Structure of (Boc) <sub>2</sub> -Lys-OH .....	230
<b>Figure 6-3</b> Molecular structure of G2 ((Boc) <sub>2</sub> -Lys) <sub>2</sub> -Lys-OMe .....	231
<b>Figure 6-4</b> Molecular structure G2 (Boc-Phe) <sub>2</sub> -Lys-OMe.....	233
<b>Figure 6-5</b> Molecular structure G2 (Boc-Ala) <sub>2</sub> -Lys-OMe.....	234
<b>Figure 6-6</b> Molecular structure G2 (Boc-Val) <sub>2</sub> -Lys-OMe.....	236
<b>Figure 6-7</b> Molecular structure G2 ((Boc) <sub>2</sub> Lys) <sub>2</sub> -Lys-OH .....	237
<b>Figure 6-8</b> Molecular structure G2 (Boc-Phe) <sub>2</sub> -Lys-OH.....	239
<b>Figure 6-9</b> Molecular structure G2 (Boc-Ala) <sub>2</sub> -Lys-OH .....	240
<b>Figure 6-10</b> Molecular structure G2 (Boc-Val) <sub>2</sub> -Lys-OH .....	241
<b>Figure 6-11</b> Concentration profile of the process of cooling a NMR tube from 90 to 25 with HEX LYS gel. ....	248
<b>Figure 6-12</b> Concentration profile of the process of gelation from hot.....	249
<b>Figure 6-13</b> Thermoregulated ionic conductivity set up and conductivity probe with the ionic liquid or gel inside. ....	250
<b>Figure 6-14</b> Process of placing a formed gel inside a Jar and the careful extraction of it to the rheometer testing platform.....	252
<b>Figure 6-15</b> example of the set up where gels are introduced in liquid state and there is a transition to gel produce either the addition of a second component or the lowering of the temperature. ....	253
<b>Figure 6-16</b> the rheological response of the elastic modulus when adding the second component to the aluminium weight boat while the rheometer performs the analysis. ....	254
<b>Figure 6-17</b> Diffusion Cell (left)with the two sides easily observed and an incubator with the diffusion chamber filled with several diffusion cells performing the experiment at controlled temperature. ....	255
<b>Figure 6-18</b> Diffusion cell divided in each region (left) and the collection .....	255
<b>Figure 6-19</b> Dendron diffusion profile of two gels in a transfer cell for a given time of 240h .....	257
<b>Figure 6-20</b> Fitting of the Fickian model with a real diffusion profile of 96h at 25°C. The obtained value of Diffusion Coefficient is $1 \cdot 10^{-6}$ .....	258
<b>Figure 6-21</b> Data of diffusion for Naph at 24h and 25°C .....	259
<b>Figure 6-22</b> Model representation of Naph concentration Vs Position for a given value of 86400 seconds (24h) and diffusion parameter of $10^{-7} \text{ cm}^2\text{s}^{-1}$ .....	260

<b>Figure 6-23</b> Representation of both (Real and model) graphs for diffusion of Naph 24h and 25°C .....	261
<b>Figure 6-24</b> Example of such calculation by using solver analysis tool where cell set objective is the SUMMSQ function and the variable cell is the corresponding to the diffusion rate cell. ....	262
<b>Figure 6-25</b> Representation of modelled and real behaviour.....	262
<b>Figure 6-26</b> <sup>1</sup> H-NMR L-Lysine methyl ester dihydrochloride. ....	277
<b>Figure 6-27</b> <sup>13</sup> C NMR L-Lysine methyl ester dihydrochloride. ....	277
<b>Figure 6-28</b> Mass spectrum of L-Lysine methyl ester dihydrochloride .....	278
<b>Figure 6-29</b> <sup>1</sup> H-NMR of D-Lysine methyl ester dihydrochloride. ....	278
<b>Figure 6-30</b> <sup>13</sup> C NMR of D-Lysine methyl ester dihydrochloride. ....	279
<b>Figure 6-31</b> Mass spectrum of D-Lysine methyl ester dihydrochloride.....	279
<b>Figure 6-32</b> <sup>1</sup> H-NMR of G1 L-(Boc) <sub>2</sub> -Lys-OH.....	280
<b>Figure 6-33</b> <sup>13</sup> C NMR of G1 L-(Boc) <sub>2</sub> -Lys-OH .....	280
<b>Figure 6-34</b> <sup>1</sup> H-NMR of G1 D-(Boc) <sub>2</sub> -Lys-OH. ....	281
<b>Figure 6-35</b> <sup>13</sup> C NMR of G1 D-(Boc) <sub>2</sub> -Lys-OH.....	281
<b>Figure 6-36</b> FTIR spectra of G1 (Boc) <sub>2</sub> -Lys-OH .....	282
<b>Figure 6-37</b> Mass spectra of G1 L-(Boc) <sub>2</sub> -Lys-OH.....	282
<b>Figure 6-38</b> Mass spectra of G1 D-(Boc) <sub>2</sub> -Lys-OH.....	283
<b>Figure 6-39</b> <sup>1</sup> H-NMR of G2 L-((Boc) <sub>2</sub> -Lys) <sub>2</sub> -Lys-OMe. ....	283
<b>Figure 6-40</b> <sup>13</sup> C NMR of G2 L-((Boc) <sub>2</sub> -Lys) <sub>2</sub> -Lys-OMe. ....	284
<b>Figure 6-41</b> Mass Spectra of G2 L-((Boc) <sub>2</sub> -Lys) <sub>2</sub> -Lys-OMe. ....	284
<b>Figure 6-42</b> Mass Spectra of G2 D-((Boc) <sub>2</sub> -Lys) <sub>2</sub> -Lys-OMe.....	285
<b>Figure 6-43</b> <sup>1</sup> H-NMR of G2 L-(Boc-Phe) <sub>2</sub> -Lys-OMe. ....	285
<b>Figure 6-44</b> <sup>13</sup> C NMR of G2 L-(Boc-Phe) <sub>2</sub> -Lys-OMe. ....	286
<b>Figure 6-45</b> Mass Spectra of G2 L-(Boc-Phe) <sub>2</sub> -Lys-OMe. ....	286
<b>Figure 6-46</b> <sup>1</sup> H-NMR of G2 L-(Boc-Ala) <sub>2</sub> -Lys-OMe. ....	287
<b>Figure 6-47</b> <sup>13</sup> C NMR of G2 L-(Boc-Ala) <sub>2</sub> -Lys-OMe. ....	287
<b>Figure 6-48</b> Mass Spectra of G2 L-(Boc-Ala) <sub>2</sub> -Lys-OMe. ....	288
<b>Figure 6-49</b> <sup>1</sup> H-NMR of G2 L-(Boc-Val) <sub>2</sub> -Lys-OMe. ....	288
<b>Figure 6-50</b> <sup>13</sup> C NMR of G2 L-(Boc-Val) <sub>2</sub> -Lys-OMe. ....	289
<b>Figure 6-51</b> Mass Spectra of G2 L-(Boc-Val) <sub>2</sub> -Lys-OMe. ....	289
<b>Figure 6-52</b> <sup>1</sup> H-NMR of G2 ((Boc) <sub>2</sub> -Lys) <sub>2</sub> -Lys-OH. ....	290
<b>Figure 6-53</b> <sup>13</sup> C NMR of G2 ((Boc) <sub>2</sub> -Lys) <sub>2</sub> -Lys-OH.....	290
<b>Figure 6-54</b> Mass Spectra of G2 L((Boc) <sub>2</sub> -Lys) <sub>2</sub> -Lys-OH.....	291
<b>Figure 6-55</b> Mass Spectra of G2 ((Boc) <sub>2</sub> -Lys) <sub>2</sub> -Lys-OH.....	291

<b>Figure 6-56</b> $^1\text{H}$ -NMR of G2 (Boc-Phe) <sub>2</sub> -Lys-OH. ....	292
<b>Figure 6-57</b> $^{13}\text{C}$ NMR of G2 (Boc-Phe) <sub>2</sub> -Lys-OH.....	292
<b>Figure 6-58</b> Mass Spectra of G2 (Boc-Phe) <sub>2</sub> -Lys-OH.....	293
<b>Figure 6-59</b> $^1\text{H}$ -NMR of G2 (Boc-Ala) <sub>2</sub> -Lys-OH .....	293
<b>Figure 6-60</b> $^{13}\text{C}$ NMR of G2 (Boc-Ala) <sub>2</sub> -Lys-OH.....	294
<b>Figure 6-61</b> Mass Spectra of G2 (Boc-Ala) <sub>2</sub> -Lys-OH.....	294
<b>Figure 6-62</b> $^1\text{H}$ -NMR of G2 (Boc-Val) <sub>2</sub> -Lys-OH.....	295
<b>Figure 6-63</b> $^{13}\text{C}$ NMR of G2 (Boc-Val) <sub>2</sub> -Lys-OH.....	295
<b>Figure 6-64</b> Mass Spectra of G2 (Boc-Val) <sub>2</sub> -Lys-OH.....	296
<b>Figure 6-65</b> Diphenylmethane Diffusion Coefficient.....	297
<b>Figure 6-66</b> Naph Diffusion Coefficient at 25°C.....	298
<b>Figure 6-67</b> Hex Diffusion Coefficient at 25°C.....	299
<b>Figure 6-68</b> Naph diffusion coefficient at 5°C.....	300
<b>Figure 6-69</b> Hex diffusion coefficient at 5°C.....	301
<b>Figure 6-70</b> Naph Diffusion Coefficient at 45°C.....	302
<b>Figure 6-71</b> Hex diffusion coefficient at 45°C.....	303

## List of Tables

<b>Table 1-1</b> Typical covalent bond energies expressed in kJ/mol <sup>16</sup> .....	32
<b>Table 1-2</b> Typical supramolecular formation energies expressed in kJ/mol <sup>17</sup> .....	32
<b>Table 2-1</b> Various combinations of L enantiomers of dendrons and amines that are going to be tested. ....	75
<b>Table 2-2</b> Concentration of each component at each temperature. ....	80
<b>Table 2-3</b> Thermodynamic parameters for the gelation of different dendrons with Phen amine. ....	84
<b>Table 2-4</b> Monitoring gelation at three different time points for each two-component system. Soft = viscous liquid; Partial = Partial gel.....	86
<b>Table 2-5</b> Progression of CD signal Vs time at 221.5 nm .....	91
<b>Table 2-6</b> The $\lambda_{\max}$ values for each of the different dendron-amine .....	93
<b>Table 2-7</b> Table with the parameters of the calculated curve that .....	104
<b>Table 2-8</b> The term m linear and k exponential of the fitting .....	105
<b>Table 2-9</b> Set of values of m (linear part) and k (Exponential part) of the various gels analysed. ....	107
<b>Table 2-10</b> Visual transformation of Hex-Phe cold mixture. ....	109
<b>Table 2-11</b> Time of the process of cooling and gel formation versus concentration of free available Dendron in the deuterated solvent in the NMR tube.....	114
<b>Table 3-1</b> Values of the obtained diffusion coefficients in $\text{cm}^2 \text{s}^{-1}$ .....	158
<b>Table 3-2</b> Table of the calculated composition for a Dendron diffusion of 240h.....	168
<b>Table 3-3</b> representation of % of L dendron in different regions of the diffusion cell at various diffusion times. ....	169
<b>Table 3-4</b> Dendron Diffusion coefficients for 25°C.....	171
<b>Table 3-5</b> Values of Diffusion Coefficients D for the studied.....	179
<b>Table 3-6</b> Real concentrations of components when diffusing.....	179
<b>Table 4-1</b> Ionic conductivities values for the pure glycols and their.....	189
<b>Table 4-2</b> Various combinations of DBS with the prepared DES based on glycols and ChCl.....	190
<b>Table 4-3</b> Values of ionic conductivities expressed in mS/cm.....	194
<b>Table 4-4</b> Solubility test for determining the saturation concentration of these chlorides in MEG based ionic liquid. Where <b>sol</b> means soluble, <b>no</b> means no soluble in such concentration conditions.....	197
<b>Table 6-1</b> Correspondence with time in min temperature in °C .....	248
<b>Table 6-2</b> Experimental data of diffusion Naph for 24h at 25°C .....	258
<b>Table 6-3</b> Calculated parameters of the model proposed for 24h diffusion time and 10-7 of Diffusion constant. ....	259

**Table 6-4** Concentration in mM multiplied by 5 and the position in cm..... 260

**Table 6-5** Differences between real and modelled [Naph]. Notice calculation of Square sum ..... 261

## Abbreviations

- Ala: Alanine
- (Boc)<sub>2</sub>Lys-OH: Boc protected L-Lysine
- Boc: tert-Butyl Carbonate Group
- (Boc)<sub>2</sub>O: Di-tert-butyl-dicarbonate
- $\delta$ : Chemical shift
- CD: Circular dichroism
- <sup>13</sup>C NMR: Carbon Nuclear Magnetic Resonance
- ChCl: Choline Chloride
- d: Doublet (NMR)
- D: Diffusion Coefficient
- DCM: Dichloromethane
- D-Lys: D Lysine
- DBS: 1,3:2,4-Dibenzylidene-d-sorbitol
- DNA: Deoxyribonucleic acid
- DES: Deep Eutectic Solvent
- DEG: Deep Eutectic Gel
- DSSC: Dye sensitised solar cells
- EtOAc: Ethyl acetate
- Fmoc: Fluorenylmethyloxycarbonyl group.
- FTIR: Fourier Transform Infrared Spectroscopy.
- G': Storage modulus
- G'': Loss modulus
- $\Delta G$ : Gibb's free energy change

- G2: Second Generation
- G2 ((Boc)<sub>2</sub>-Lys)<sub>2</sub>-LysOMe: Methyl ester of the second generation dendron of G2 L-((Boc)<sub>2</sub>-Lys)<sub>2</sub>Lys-OH
- G2 L-((Boc)<sub>2</sub>-Lys)<sub>2</sub>Lys-OH: Second generation Dendron acid based of Lysine
- G2 L-(Boc-Phe)<sub>2</sub>-Lys-OH: Second generation dendron acid based on Phenylalanine and Lysine
- G2 L-(Boc-Val)<sub>2</sub>-Lys-OH: Second generation dendron acid based on Valine and Lysine
- G2 L-(Boc-Ala)<sub>2</sub>Lys-OH: Second generation dendron acid based on Alanine and Lysine
- ΔH: Change in enthalpy
- HBA: Hydrogen Bond Acceptor
- HBD: Hydrogen Bond Donor
- Hex: Hexylamine
- Hex-Ala gel: Hexylamine + G2 ((Boc-Val)<sub>2</sub>-Lys-OH based supramolecular gel.
- HexGel = Hex-Lys gel: Hexylamine + G2 ((Boc)<sub>2</sub>Lys)<sub>2</sub>-Lys-OH based supramolecular gel.
- Hex-Phe gel Hexylamine + G2 ((Boc-Phe)<sub>2</sub>-Lys-OH based supramolecular gel.
- Hex-Val gel: Hexylamine + G2 ((Boc-Val)<sub>2</sub>-Lys-OH based supramolecular gel.
- <sup>1</sup>H-NMR: Proton Nuclear Magnetic Resonance.
- Hz: Hertz

- HRMS: High resolution mass spectrometry
- IL: Ionic liquid
- IC: Ionic conductivity.
- J: Coupling constant
- IR: Infra-red
- L-Lys: L Lysine.
- LysOMe: Methyl ester L-Lysine.
- LMWGs: Low molecular weight gelators
- MEG: Mono ethylene glycol
- MeOH: Methanol
- MPG: Mono propylene glycol
- m: multiplet (NMR)
- mL: Millilitre
- mM: Millimolar
- m.p: Melting point
- MHz: Megahertz
- MS: Mass spectrometry
- MW: Molecular Weight
- Naph: 1-Naphthylmethylamine
- Naph-Ala gel: Hexylamine + G2 ((Boc-Val)<sub>2</sub>-Lys-OH based supramolecular gel.
- NaphGel: Naph-Lys gel: Hexylamine + G2 ((Boc)<sub>2</sub>Lys)<sub>2</sub>-Lys-OH based supramolecular gel.
- Naph-Phe gel Hexylamine + G2 ((Boc-Phe)<sub>2</sub>-Lys-OH based supramolecular gel.

- Naph-Val gel: Hexylamine + G2 ((Boc-Val)<sub>2</sub>-Lys-OH based supramolecular gel.
- NEt<sub>3</sub>: Triethylamine
- Pa: Pascal
- PAAm: Polyacrylamide
- PDO: 1,3-propanediol
- PFG-NMR: Pulsed Field Gradient Nuclear Magnetic Resonance
- Phe: Phenylalanine
- Phen: Phenethylamine
- Phen-Ala gel: Hexylamine + G2 ((Boc-Val)<sub>2</sub>-Lys-OH based supramolecular gel.
- Phen-Lys gel: Hexylamine + G2 ((Boc)<sub>2</sub>Lys)<sub>2</sub>-Lys-OH based supramolecular gel.
- Phen-Phe gel Hexylamine + G2 ((Boc-Phe)<sub>2</sub>-Lys-OH based supramolecular gel.
- Phen-Val gel: Hexylamine + G2 ((Boc-Val)<sub>2</sub>-Lys-OH based supramolecular gel.
- Phen-Lys Gel: Phenethylamine + ((Boc)<sub>2</sub>Lys)<sub>2</sub>-Lys-OH Based Supramolecular Gel.
- q: Quartet (NMR)
- (QSPR): quantitative structure-property relationship model
- ppm: Parts per million (NMR)
- R<sup>2</sup>: Correlation coefficient
- R<sub>f</sub>: Retention factor
- ΔS: Change in entropy

- SEM: Scanning Electron Microscopy.
- Sol: Solubility.
- TEM: Transmission Electron Microscopy.
- TBTU: O-(Benzotriazol-1-yl)-*N,N,N',N'*-tetramethyluronium tetrafluoroborate
- <sup>t</sup>BuOH: tert-Butyl alcohol.
- $T_{\text{gel}}$ : Glass Transition Temperatures.
- VT-CD: Variable temperature circular dichroism
- VT <sup>1</sup>H-NMR: Variable temperature proton nuclear magnetic resonance
- TLC: Thin-layer chromatography
- UV-Vis: Ultraviolet-visible
- Val: Valine

# Chapter 1 Introduction

## 1.1. Brief History of Materials.

Materials science is one of the broadest disciplines of<sup>1</sup> chemistry<sup>1</sup>. From the very beginning of humanity, indeed even some species of animals, the use of tools has been a critical step for gaining survival skills and hence an evolutionary advantage<sup>2</sup>. The basic concept of evolution combined with the use of increasingly complex tools led to the continuous development of ideas for using those tools. The specific composition of tools led to the specialization of professions. Biomaterials and naturally occurring materials were the first type of materials that led to the construction of archaic technologies. Specific advances have named certain periods of archaeological time due to the enormous impact that those materials had in the evolution of society<sup>3</sup> (i.e., stone, bronze, iron, silicon). It is interesting to reflect, however, that these ages were named in retrospect by archaeologists, as a result of the materials that were left behind – which are generally hard and robust. Since pre-history, soft materials have also been used by human society – including reeds, resins, waxes etc. As a result of their lack of persistence on the archaeological timescale, these intriguing soft materials are often overlooked.<sup>4</sup> Nowadays, technology is the driving force that pushes societies to better positions of sustainability and economic progress. This thesis explores fundamental dynamic aspects/properties of soft materials – specifically gels – and in later chapters, hopes to indicate how such materials may impact on further developments in technological progress.<sup>5</sup>

## 1.2. General definition of gels.

Gels are colloidal materials<sup>6,7</sup>, which comprise a sample-spanning solid-like network embedded within a liquid. They have solid-like properties on the analytical characterisation timescale, but also have some properties resulting from the extensive

liquid-like phase. It is these liquid-like properties of gels, specifically the diffusion characteristics, which are of key interest in this thesis.<sup>8</sup> Gels prevent the bulk flow of the internal liquid due to capillary forces and surface tension, although there is mobility of the fluid phase on the molecular scale.<sup>9</sup>

Gels can be classified according to the nature of the bonds that sustain the ‘solid-like’ 3D network. Polymer gels are those which the ‘solid-like’ network is based on polymers, which can be connected into an entangled nanoscale network either by covalent chemical bonds (so-called chemical polymer gels) or via non-covalent interactions (so-called physical polymer gels).<sup>10</sup> On the other hand, there also exist supramolecular gels based on LMWGs (Low Molecular Weight Gelators)<sup>11</sup>, which under certain conditions of temperature and in specific solvents, spontaneously form a solid-like nanoscale network by means of molecular self-assembly as shown in Figure 1-1.

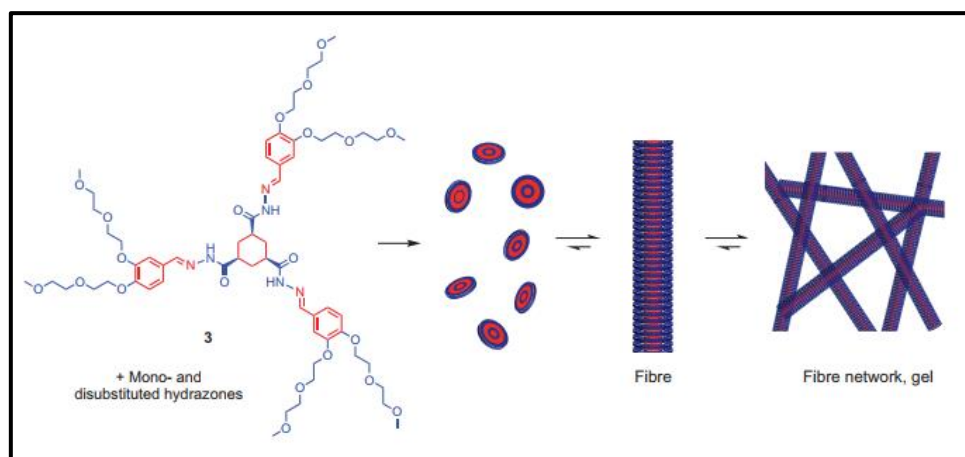


**Figure 1-1** Molecular assembly of tris hydrazone hydrogelator leads to fibre formation of a gel. Figure reproduced from reference<sup>12</sup>

In the example above, the extended discotic molecule self-assembles via a hierarchical process into a 3D fibrillar network, with molecules assembling into fibres that then entangle and interact to form a sample-spanning network. Most gelators self-assemble based on a single molecular building block. However, in some cases formation of the 3D network is the result of combining several substances that interact to form a complex,

which then self-assembles into nanofibres, and hence a network – such systems are referred to as two-component gels

Multicomponent gels can be classified into three basic groups according to the key review by Buerkle and Rowan **Figure 1-2**:<sup>13</sup>

1. Two component gel-phase materials where each component alone does not form a gel, and the combination of the two molecules is necessary for self-assembly.
2. Two gelator, two-component gels in which both compounds are gelators in their own right. Such systems have two possibilities for gelation either by cooperation (co-assembly) or the two gelators forming fibres separately (self-sorting).
3. Two component gels in which a gelator is combined with a non-gelating additive, which can interact with the gelator and hence affect the performance of the generated 3D network.

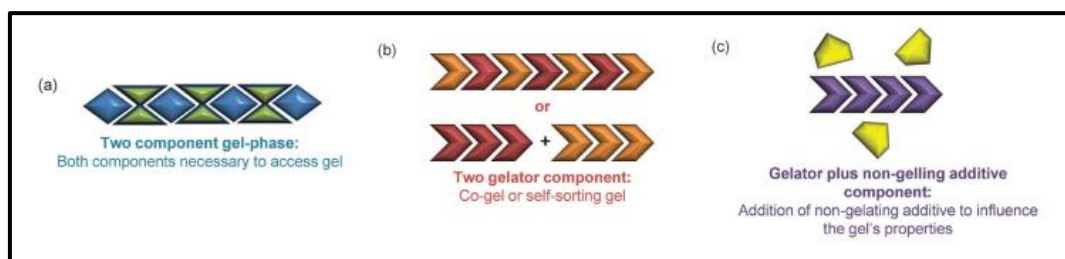


**Figure 1-2** Representation of the three main types of multi-component gels of LMWGs. Figure reproduced from reference<sup>13</sup>.

### 1.3. Molecular interactions.

Given the importance of self-assembly in forming supramolecular gels, it is important to consider the types of non-covalent interactions that can underpin supramolecular systems. Supramolecular chemistry is a discipline that studies the non-covalent interactions between molecules.<sup>14</sup> The main difference between covalent and supramolecular bonding is the strength of the bonds formed, which means that supramolecular interactions, which

are weaker than covalent bonds, tend to be reversible (**Table 1-1 and 1-2**). This gives rise to key properties of supramolecular materials such as their adaptiveness and responsiveness. Some of the most important supramolecular interactions<sup>15</sup> take the form of ionic interactions (100-350 kJ mol<sup>-1</sup>), hydrogen bonding (4-60 kJ mol<sup>-1</sup>), van der Waals forces (<5 kJ mol<sup>-1</sup>) and  $\pi$ - $\pi$  interactions (5-20 kJ mol<sup>-1</sup>). Solvophobic effects can also be of considerable energetic significance, although of course this depends strongly on the solvent environment in which assembly is taking place. In general, multiple non-covalent interactions act in combination within many supramolecular systems.

Type of Bond	Energies (kJ/mol)	distance Å
C-O	340	1.43
C-C	360	1.53
C-H	430	1.11
C=C	600	1.33
C=O	690	1.21

**Table 1-1** Typical covalent bond energies expressed in kJ/mol <sup>16</sup>

type of interactions	Energy in kJ/mol
Hydrophobic	<40
Electrostatic	≈20
Hydrogen bond	12 - 30
Van der Waals	0.4 - 4
Cation- $\pi$	5 - 80
$\pi$ - $\pi$ stacking	0 -50

**Table 1-2** Typical supramolecular formation energies expressed in kJ/mol <sup>17</sup>

The strength of non-covalent intermolecular interactions is responsible for phase transitions.<sup>18</sup> As an example of such a transition, water is represented in Figure 1-3. Intermolecular interactions play a key role in allowing the molecules to self-interact and reorganize according to the lowest energy content and the time available to do so – the strength of hydrogen bonding in water means it maintains its liquid state to significantly higher temperatures than might otherwise be expected for such a small molecule. These hydrogen bond interactions also play a key role in controlling the crystal structure of the solid ice form of water. The vital importance of the surrounding conditions for a phase transition to occur are clear with pressure and temperature being the main parameters that govern these transitions.

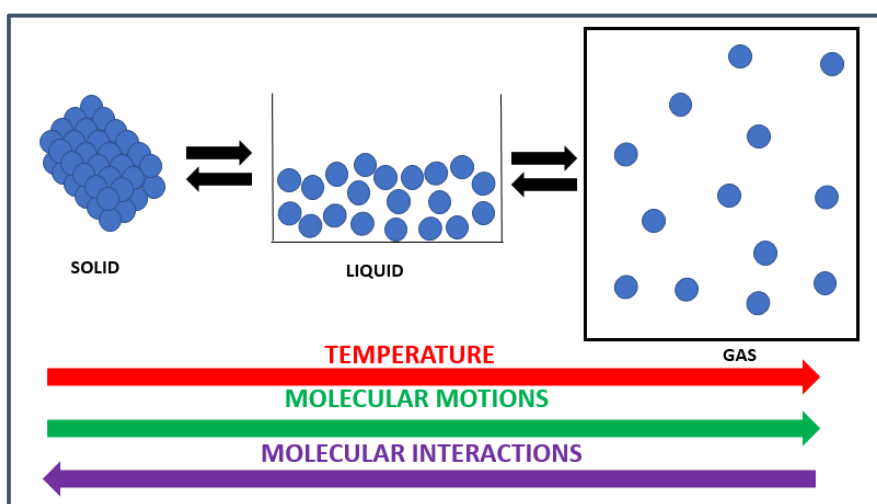


**Figure 1-3** Phase transition of water depending on the surrounding conditions. The properties of the various forms of water depend on the existence of molecular interactions between molecules.

In terms of more complex molecular structures which depend on non-covalent interactions, DNA<sup>19</sup> (Deoxyribonucleic acid) is a biochemical example of a molecule which relies on complementary non-covalent interactions to control its phase transition, self-assembly and the replication of its encoded information (Figure 1-4).

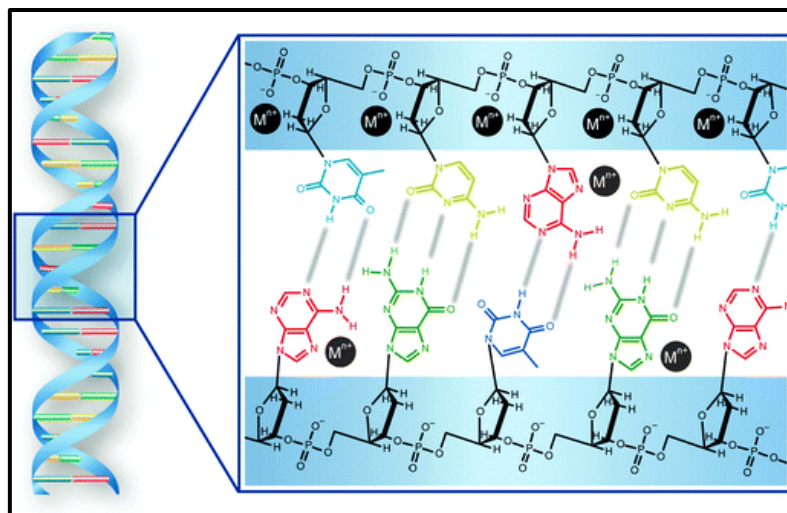


**Figure 1-4** Typical representation of the hydrogen bonds present in the DNA polymer chain<sup>20</sup>

Other biomolecules such as proteins<sup>21</sup> are also fundamentally dependent on supramolecular interactions that are critical to enable protein folding<sup>22 23</sup> that allows the system to take on the more stable structural characteristics. Non-covalent interactions then enable them to interact with their binding partners and express their biological function. As such, non-covalent interactions are of fundamental importance across a wide-range of physical and biological sciences and represent the ‘language’ through which molecules can interact with one another.<sup>24</sup>

#### **1.4. Supramolecular chemistry**

Supramolecular chemistry is the study of non-covalent interactions between molecules and is often described as ‘chemistry beyond the molecule’.<sup>15</sup> One of the main characteristics of supramolecular chemistry is that although individual interactions are weak, the accumulation of many of them can provide a strong overall interaction, which results in the formation of bulk macroscopic materials.

Due to the existence of labile supramolecular links, variation in the strength of interactions can change the macroscopic properties<sup>25</sup> of the bulk material. For example, in terms of gels, when temperature is increased, the increasing importance of the entropy term gives rise to disassembly of the gel. The key equation (1-1) describes the relation between entropy, enthalpy and Gibbs free energy:

$$\Delta G = \Delta H - T \cdot \Delta S \quad \text{Equation 1-1}$$

In the equation 1-1  $\Delta G$  defines how thermodynamically spontaneous the process is according to the value of Gibbs variation (the more negative the better). The variation in enthalpy ( $\Delta H$ ) and entropy ( $\Delta S$ ) are the parameters that underpin this process. These two terms are in balance, and the surrounding temperature which drives the process spontaneously in one direction controls their relative balance and hence determines the supramolecular equilibrium.

The existence of intermolecular forces is the key for reversible gel fibre formation. This provides gels with the ability to assemble and disassemble using a variety of triggers (external stimuli) and is one of the reasons why this subgroup of materials is sometimes referred to as “smart materials”. One such trigger is temperature as a result of the enthalpy/entropy balance. In general, gelation is enthalpically favoured and entropically disfavoured, and for this reason as the temperature increases, many gels break down into a sol. The self-assembly of gels passes by a series of ordered interactions that hierarchically assembles the various structures (through fibrils, and fibres) and building in the end the 3D network that immobilises the surrounding bulk solvent as can be seen in Figure 1-5.

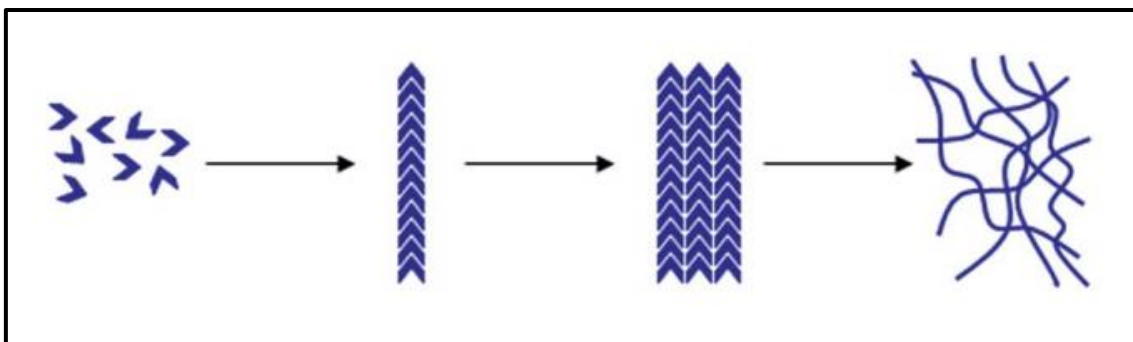


**Figure 1-5** Typical self-assembly process of LMWG to form the 3D network<sup>26</sup>

It is worth noting that to form a supramolecular gel, an energy barrier has to be overcome that is normally related to temperature and also reflects the molecular orientation that is required for self-assembly. This can give rise to an often-observed kinetic barrier to gelation, which will be discussed in more detail below.

An important field of application of self-assembly is the construction of molecular devices<sup>27</sup> or nanodevices from the ‘bottom-up’.<sup>28</sup> There are many examples of this kind of supramolecular systems, such as molecular switches<sup>29</sup> or molecular machinery<sup>30</sup> (Figure 1-6) that in 2016 was the topic for winning the Nobel prize. Some are activated by visible light<sup>31</sup> and some others by changing the oxidation state.

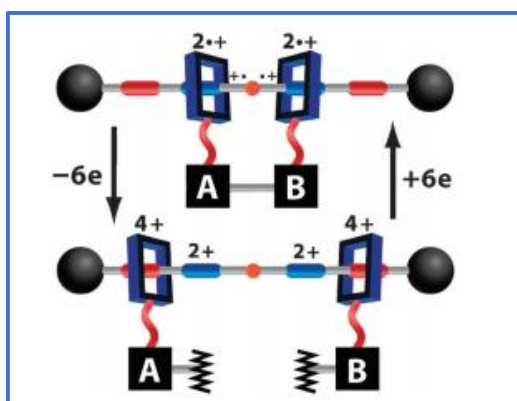


**Figure 1-6** Example of a molecular machine that has two positions depending on the molecular oxidation state.<sup>30</sup>

There are other supramolecular systems that are also important ranging from biomolecules such as DNA<sup>32</sup> and proteins to the synthetic or predesigned molecules that are able to host ions such as crown ethers<sup>33</sup> and other cyclic polyethers<sup>34</sup> (Figure 1-7).

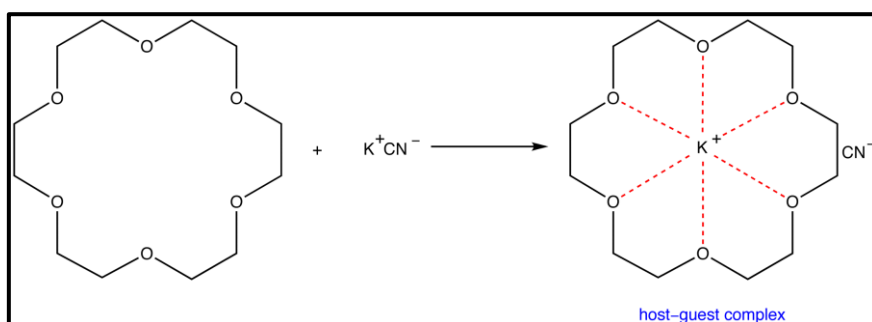


**Figure 1-7** host guest chemistry of the encapsulation of a potassium cation.

Because the forces involved in the self-assembly are physical, thus reversible, the formation of these supramolecular structures is also reversible. Reversibility ensures that the whole process of formation and disintegration favours the most thermodynamically stable product. This leads to the concept of ‘bottom up’ synthesis which is the basis of the nanotechnology<sup>28 35-37</sup> in which designed molecules have been consciously programmed to self-assemble under certain conditions into desired functional architectures.

### 1.5. Supramolecular Gels.

Even though they have been recognized and studied since the nineteenth century, supramolecular gels have been difficult to define properly<sup>38 6</sup>. They have been described as ‘jelly like’ materials which have soft solid appearances that don’t flow and they are basically formed by two main components – solvent and gelator.<sup>39</sup> They have also been described as materials which are easier to recognise than define.<sup>9</sup> Gelators can be found in a number of everyday applications and uses<sup>39</sup> ranging from cosmetics, hygiene and food, to more high-tech applications such as the creation of nanostructures for solar cells,<sup>40-42</sup> or battery electrolytes.<sup>43-45</sup> They also have potential medicinal applications such

as controlled release of functional molecules,<sup>46</sup> tissue engineering<sup>47</sup> and 3D printing.<sup>48-50</sup> It is worth mentioning that cell culture and the creation of synthetic organs<sup>51-56</sup> and tissues are of intense current interest, and exploit the biocompatible properties of this kind of supramolecular material. For this kind of application the search for gels with rapid kinetics of formation is of key importance. Supramolecular gels usually require only a very small amount of gelator<sup>57</sup> to start gelation, which is often a highly cooperative process – indeed many supramolecular gels require <1% wt/vol of gelator in order to give rise to solvent immobilisation. If we compare polymer gels with LMWGs there is a better chance of chemical tunability and increased diversity in the molecular structures of LMWGs as a result of the ability of organic synthesis to easily programme small molecules with highly variable structural modifications (Figure 1-8) Such changes in molecular structure can lead to variations of the conditions in which the gel is gelating (pH, gelation speed...) and the properties of the gel. It may also endow the materials with new forms of behaviour and potential applications as a result of the new functionality introduced. 1,3;2,4-Dibenzylidenesorbitol (DBS) has this behaviour as a functionality is introduced in the aromatic part.<sup>58</sup>

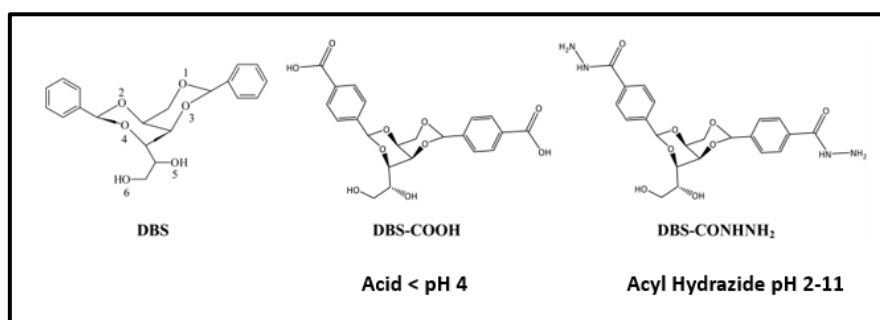


**Figure 1-8** The modification of the molecular skeleton of DBS gives differential gelation ranges depending on the surrounding conditions<sup>59</sup>

## 1.6. DBS as gelation system.

DBS (Figure 1-9) is a chiral low molecular weight gelator with a butterfly shape conformation. The synthetic simplicity and the benign non-toxic nature of the molecule and its derivatives make DBS a great formulation agent in cosmetics, personal care, adhesive sticks and indeed in numerous industrial applications,<sup>60</sup> such as electrically conductive gel composites.<sup>61</sup> The benzylidene groups constitute the ‘wings’ of this molecule and the sorbitol backbone the ‘body’ with the nature of solvent playing a key role in controlling the precise assembly mode. In non-polar solvents it is considered that hydrogen bonding between the sorbitol units dominates, whereas when the solvent becomes more polar, solvophobic and  $\pi$ - $\pi$  stacking interactions between the benzylidene groups make a greater contribution to the intermolecular interactions. The way in which DBS self assembles is therefore facilitated by the aromatic part and mediated by the most external 6-hydroxy group, Figure 1-9, which forms intermolecular hydrogen bridges with the acetal oxygens of DBS “neighbours”, and is hence crucial for the self-assembly event.

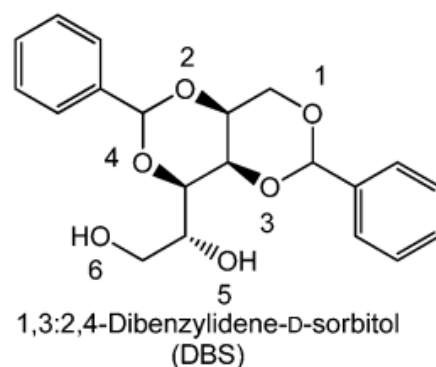


**Figure 1-9** Chemical structure of the DBS<sup>62</sup>

There are various possible derivatives resulting from the chemical modification of the aromatic part, and this modifies the solubility and packing conformations that could be obtained on self-assembly depending on the solvent medium.<sup>63</sup> Figure 1-10 shows some possible chemical modifications of DBS.

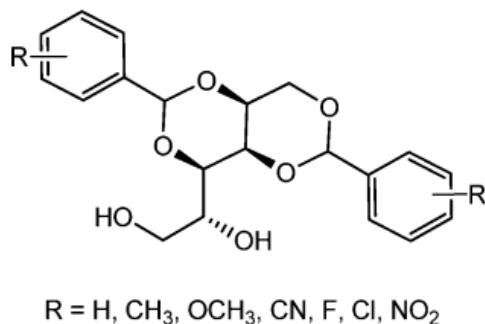


**Figure 1-10** Chemical structure of the DBS and possible derivatives. <sup>58 62</sup>

Daniel Cornwel and co-worker's were able to modify DBS<sup>58</sup> molecules so its gelation properties were pH dependent. Acyl hydrazide, acid and glycine derivatives had different ranges of gelation depending on the pH of the medium.

### 1.7. Supramolecular bicomponent organogels based on lysine dendrons.

As described above, two-component gels are based on the formation of a complex between two molecules, which then underpins gelation. One example of this is provided by the specific combination of a G2 dendron constructed from L-lysine (G2 ((Boc)<sub>2</sub>-Lys)<sub>2</sub>-Lys-OH) and an amine (Figure 1-11).<sup>64</sup>

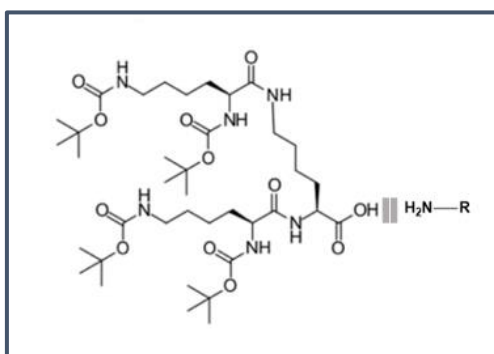


**Figure 1-11** G2 ((Boc)<sub>2</sub>-Lys)<sub>2</sub>-Lys-OH dendron interacting with an amine by hydrogen bonding. <sup>65</sup>

The acid residue of the dendron interacts with the amine through the formation of an acid-base interaction and that triggers the formation of the fibres, which grow by self-assembly

as a result of intermolecular hydrogen bond interactions between the peptide groups in the lysine dendron. This system has been extensively studied by Smith and co-workers.<sup>65–69</sup> and we were able to publish a recent paper which relates thermodynamics and kinetics of these kind of bicomponent systems<sup>69</sup>.

Lysine is a versatile molecular building block for the preparation of various gelators in a range of solvents. It has several advantages such as biocompatibility and easy orthogonal functionalization. It has therefore been explored in a range of peptidic gelators.<sup>70</sup> For example, Suzuki, Hanabusa and co-workers have used lysine as a key building block to develop functional soft materials in organic solvents.<sup>71</sup> More widely, peptide gelators have been of considerable interest, particularly Fmoc-modified dipeptides<sup>72,73</sup>. Ulijn<sup>74</sup> et al reported one of these peptide gelators which self assembles cooperatively with proteins to form a multi-component system (Figure. 1-12) It was suggested this system might give an insight into assembly mechanisms of relevance to the origin of life and the development of synthetic mimics of living systems. There are some other examples where Fmoc-peptides (Fluorenylmethyloxycarbonyl-peptides) are used as anti-infective materials.<sup>75 76</sup>

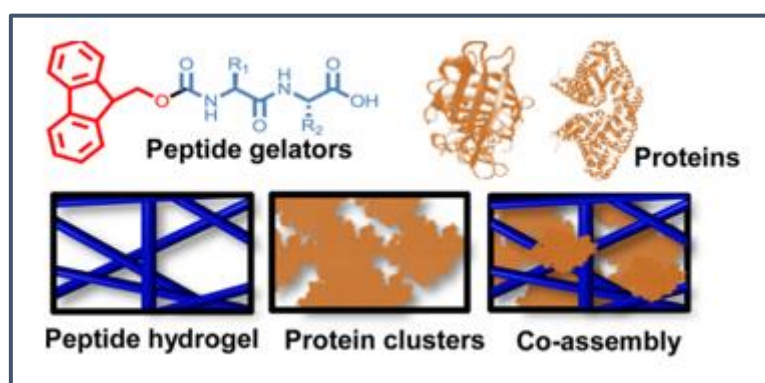


**Figure 1-12** Low Molecular Weight Hydrogelator (Fmoc-Dipeptides) and Protein Structures which are self-assembled in a cooperative manner.<sup>77</sup>

There have also been examples in which three molecules are part of the primary assembly. For example, as a result of the acid-amine interactions at the focal point of the dendritic lysine with a diamine linking unit (Figure 1-13).<sup>66</sup>

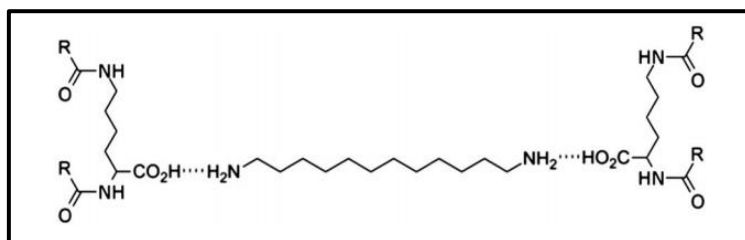


**Figure 1-13** Two-component gelation system formed by acid-amine interactions at the focal point of the dendritic lysine

The self-assembly of these three-component systems is known to be based on establishing assembly with an intermolecular hydrogen bond primarily between the amide groups, with carbamate groups playing a secondary role.<sup>78</sup> Cooperative assembly plays an important role in the assembly pathway.

In terms of multi-component self-assembly, Adams and co-workers<sup>79</sup> proposed a clear picture of the way in which LMWGs can have different pathways of assembly resulting in diverse structures. As shown in Figure 1-14, various combinations of gelators can result in different distribution of components while forming a network depending on whether they co-assemble randomly (a), co-assemble in an alternating manner (b) or self-sort into individual nanofibres (c). Adams and co-workers noted that such processes depended on the molecular structure and also on the pathways used for gel formation. Importantly, this illustrates that the structure and performance of gel nanostructures depends not only on thermodynamic factors, but also on kinetic factors associated with the overall energy profile of the gelation landscape.

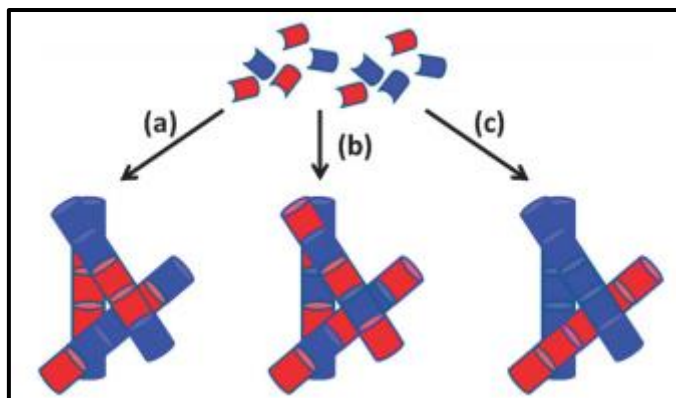


**Figure 1-14** The various resulting structures of self-assembly of gelators being (a) self-sorting; (b) random mixing; (c) specific co-assembly<sup>79</sup>

### 1.8. Crystallization and gelation.

In the case of the two-component lysine-based gels described above, the solvent of choice is typically toluene, which is an apolar aprotic organic solvent, able to dissolve the two components. It is also able to maintain an adequate balance between solubility,<sup>80</sup> the ability to support the required interaction between dendron acid and amine, as well as providing enough insolubility to encourage the formation of intermolecular hydrogen bonds between the peptide dendrons. This balance between solubility and insolubility is a key factor in all LMWGs, as gels can be considered intermediate between solution-phase species and a crystalline phase. In contrast, the Fmoc-based peptide gels described above and reported by Ulijn, Adams and others, typically form in water, but only on protonation of the carboxylic acid group, which tips the balance of solubility of the system such that it wants to start aggregating.<sup>77</sup>

The simplest and most common method to prepare gels is by dissolving the gelators in a hot solution of an appropriate solvent. A supersaturated solution of gelator molecules is thus created and then cooled in order to let the fibres nucleate and then assemble further.<sup>81</sup> The creation of nanofibres depends on the ability of the gelator to self-assemble into fibres instead of ordered 3D crystals.<sup>82</sup> Both processes rely on the delicate equilibrium between

solvation and self-interaction. Bhadha and co-workers described the intimate balance between crystallization and gelation between in specific metallogels.<sup>83</sup>

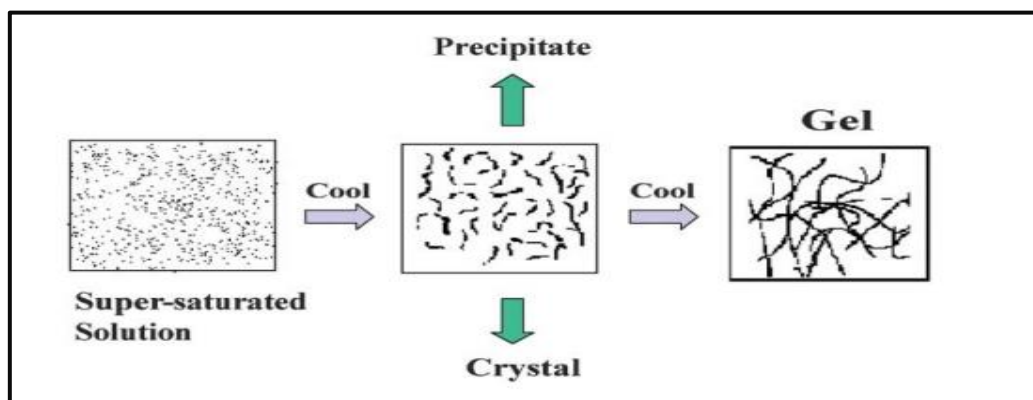


**Figure 1-15** Supersaturated solution of chemical species can result in crystallization, amorphous precipitation by agglomeration and gelation .

Figure 1-15 illustrates the balance that is relevant in gelation – in general, gels can be considered to be balanced somewhere between systems which are fully soluble, and those which are completely insoluble and hence just precipitate. Rogers and co-workers<sup>80</sup> showed that there is a predictive correlation between some solvent parameters (e.g. partition coefficients, Henry’s law constants, solvatochromic parameters, Hansen solubility parameters) and the gelation ability of numerous classes of molecular gelators. In particular, they have found that gelating systems tend to cluster together in Hansen solvent space, which would indicate there is a specific ‘ideal zone’ of solubility for gelation to be favoured. Gelation can therefore be considered as a kind of linear crystallization where molecules of solvent become trapped inside the gel nanostructured scaffold.

## 1.9. Thermodynamics of gel formation.

Gels are in most cases not the most stable state thermodynamically, i.e., they are a metastable state, so they are not in equilibrium and they can slowly develop into various systems that can contain larger crystals and fibrous networks. Thus, because most supramolecular gels are in a metastable state their formation is often governed by a subtle interplay between kinetics and the thermodynamics. For example, the rate of cooling when forming a gel from a supersaturated solution can be of critical importance in the final stability of the formed fibres.<sup>84</sup>

Meijer and co-workers revealed that the gelation process requires a nucleation step before the assembly of nanofibres can take place.<sup>85</sup> This can therefore be considered as a cooperative process, which has many similarities with crystallization – indeed gelation is sometimes referred to as a frustrated crystallization event. Clearly the kinetics of assembly should depend on the kinetics of nucleation as well as the kinetics of fibre growth and entanglement. Obviously, each of these steps may take place with different kinetics.

One of the most effective ways of studying the thermodynamic stability of supramolecular gels is to use variable temperature <sup>1</sup>H-NMR (VT <sup>1</sup>H-NMR). Mirabet and co-workers<sup>78</sup> used VT <sup>1</sup>H-NMR to determine the solubility of a gelator at a range of temperatures, and by treating the conversion from gel to sol as being analogous to a dissolving crystal, they could derive thermodynamic parameters for the gel-sol transition. Linear fitting using the van't Hoff approach gives thermodynamic parameters as expressed by the equation 1-2.

$$\ln (Sol) = -\frac{\Delta H_{diss}}{RT_{eq}} + \frac{\Delta S_{diss}}{R} \quad \text{Equation 1-2}$$

Where  $-\frac{\Delta H_{diss}}{R}$  is the slope of the function (m) and  $\frac{\Delta S_{diss}}{R}$  is the c term of the same linear function. Also R has the value of  $8.314 \cdot 10^{-3} \text{ kJ} \cdot \text{K}^{-1} \text{ mol}^{-1}$  and the  $T_{eq}$  is the temperature in kelvin corresponding that concentration of liberated gelator. Once  $\Delta H_{diss}$  and  $\Delta S_{diss}$  are obtained (Figure. 1-16), the  $\Delta G_{diss}$  value can be calculated. They reported this approach using lysine based gelators with various different protecting groups on their peripheries (Boc carbamate and benzyl carbamate groups) and reported the impact of gelator structural modification on the thermodynamics of assembly.

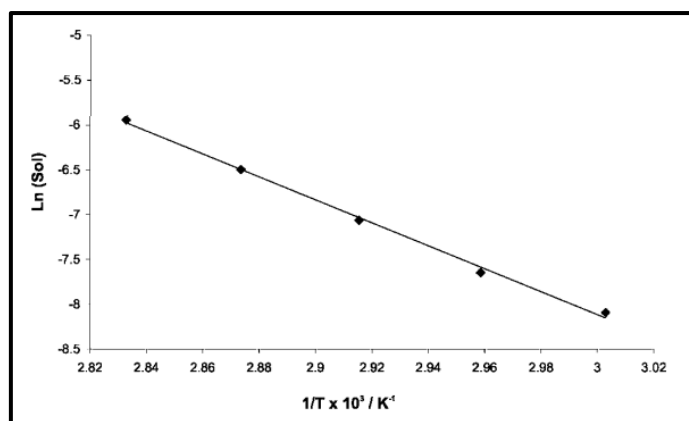


**Figure 1-16** Typical solubility plot where  $\ln(\text{sol})$  of components is represented versus the temperature inverse

## 1.10. Dynamic aspects of supramolecular gels.

Supramolecular gels are dynamic materials because of several intrinsic properties. These are detailed in the following list.

1.10.1. **Reversibility.** The reversible nature of supramolecular interactions is due the lability of those interactions and forces that are created between molecules and the structures that are the result of the various intermolecular forces.<sup>86 87</sup>

1.10.2. **Evolving nature.** Gels are formed at a certain pace depending on many aspects that includes the stability of the formed compounds and the appropriate orientation of the molecules to achieve efficient self-interaction.

The more effective the orientation of those potential functional groups, the faster the self-assembly should be. On the other hand, if there are functional groups that could hinder the process of self-assembly this may slow down the process of gel formation.<sup>88,89</sup>

1.10.3. **Internal mobility.** Gels are solid materials full of solvent. These solvent molecules are in the liquid form which means that they are free to move everywhere within the margins of the solid piece of material. The only potential exception is those solvent molecules directly interacting with the gel nanofibres. Solvent molecules can even leave the gel as a result of solvent evaporation. This internal mobility and dynamic behaviour leads to intriguing potential diffusion capabilities of substances inside the material. The rate of diffusion will be dependent on many factors such as the affinity of the diffusing compounds with the 3D network (steric and electronic), the density of the 3D network and physical parameters such as temperature, pressure and the presence of substances or stimulus that could affect the 3D network stability. Some techniques based on the relaxation NMR phenomena have been applied to obtain the diffusion constants of molecules inside the gels.<sup>90</sup>

1.10.4. **Tunability.** Two-component systems permit a tremendous number of possible combinations that could work as gelation systems. This remarkably high structural variability has considerable potential for developing gels which have appropriate properties for a wide range of different applications.

### 1.11. Kinetics of gel formation.

In general terms, there have been relatively few studies of self-assembly systems focusing on the rate of gelation speed.<sup>91</sup> It is known that rarely, in some supramolecular systems, instant gelation can occur.<sup>92</sup> In most other cases a trigger is necessary for gelation – most

usually this might be a change in the temperature or pH of the solution.<sup>93</sup> Moreover, gelation can be a difficult process to predict and control.<sup>80</sup>

There have been several methods or models proposed to describe quantitatively the gelation rate. Avrami type kinetic study gives an idea of the degree of crystallinity of the gelation, i.e., the dimensionality of the self-assembly process.<sup>94,95</sup> Even sometimes from a Hansen solubility parameter perspective<sup>92</sup> gelation can be kinetically predicted.

Gelation kinetics can be of critical importance in terms of the application of gels. For example, the use of gelation as a mechanism to immobilise crude oil on the surface of the ocean requires rapid gelation kinetics to be practically useful.<sup>96,97</sup> Every gel forms at a certain rate from the solubilized gelator and this will be expected to depend on the energy barrier to the self-assembly event combined with the need to nucleate a gel nanofibre, which in turn will depend on aspects such as the saturation of the solution, the temperature etc. Self-assembly can be almost instant or it can take longer times, even hours/days. In general, however, there is very little predictive understanding of the factors which control gelation kinetics, with much more attention in the literature having been focussed on gel stability.

To study the rate of gelation, several techniques can be employed to track the formation of fibres.

1.11.1. **<sup>1</sup>H-NMR.** Molecules that are immobilised in the 3D network and therefore have no freedom of movement within the solvent on the NMR timescale cannot be observed in the NMR spectrum. In contrast, molecules which are mobile and dissolved within the liquid-like gel phase give sharp signals in the <sup>1</sup>H-NMR spectrum and thus can be quantified as the amount of mobile gelator decreases during gel formation. Saal Wachter and co-workers used this

method<sup>98</sup> based on <sup>1</sup>H-NMR to track the evolution of gelation in a system. Other experiments have been performed by Romero-Zeron using the same kind of procedure.<sup>99</sup> After these experiments, concentration profiles are obtained which can be treated with the Avrami model to get the n and K parameters.<sup>100-102</sup>

1.11.2. **Circular dichroism spectroscopy** is a type of spectroscopy that is able to differentiate between the absorption of right and left polarized light, which is then represented as an elliptical signal. Only chiral molecules are active in this kind of spectroscopy, and equal and opposite signals are obtained for enantiomers. In the case of gel formation, if there are chiral molecules or nanostructures involved, a genuine spectrum will be generated of certain intensity and sign. In general, nanosystems have larger signals than isolated molecules, as chiral nanostructures are formed, and as such, CD spectroscopy is a highly effective technique to monitor self-assembly events on the nanoscale. In order to measure the kinetics of gel formation, there have been various authors like Veerman and co-workers<sup>103</sup> who used the intensity at the maximum absorbance region ( $\lambda_{\text{max}}$ ) to track the formation of the gel and hence obtain kinetic parameters by comparing with a calibration curve that related concentration and signal. In recent work from Cornwell and Okesola<sup>104</sup> the use of CD (and quantitative NMR) has been used to calculate the gelation rates. Meijer and co-workers used Variable Temperature Circular Dichroism (VT-CD) methods to comprehend the kinetics of the nanofibre formation in a system where the solvent was playing an important role.<sup>105</sup>

1.11.3. **Rheology.** This is the systematic study of the flow and deformation of materials.<sup>26,106</sup> Materials can flow and can be deformed in an elastic and

viscous way (viscoelastic materials).<sup>107,108</sup> Rheology is a powerful technique to gain insight into these materials properties on the macroscopic length scale. In the case of gel formation, the transition between a solution of components and a solid like viscoelastic material can thus be determined. Furthermore, the way this varies with temperature can also be studied. There are many models that can be applied to process kinetic data for gel formation. For instance, Goudoulas<sup>109</sup> adapted a kinetic gelation model designed by Djabourov, Maquet and co-workers which fitted the kinetic rheological data well. Fernandez Farrés<sup>110</sup> and Norton<sup>111</sup> applied rheological methods to track gel formation by the application of an exponential equation and were able to extract effective rate constant (k) parameters using this approach (Equation 1-3).

$$G'(t) = G'_{\infty} - (G'_{\infty} - G'_0) \text{Exp}(-k_i t) \quad \text{Equation 1-3}$$

Other methods to study gel kinetics have also been used. For example, Hamley and Banerjee employed the time-dependent fluorescent response on the gel formation<sup>112</sup> to calculate kinetics.

### **1.12. Diffusion processes in gels.**

Diffusion is one of the most basic processes that takes place in nature on a regular basis allowing molecules to travel according to the volatility and their affinity with the mobile phase (liquid or gas).<sup>113-115</sup> For example, when pouring a drop of dye solution into clean water, diffusion takes place as a result of the turbulence<sup>116</sup> of the addition, compatibility of both the dye and the liquid (solubility), convection currents, and also by the Brownian

motion<sup>117</sup> that is acting as a result of molecular collisions between the solvent molecules and the solubilized dye in the liquid phase. When talking about diffusion processes in gels, the movement of internal molecules can be produced by spontaneous Brownian motion or also, in the presence of an electric field, by electrophoretic effects<sup>118–120</sup> that can drive the internal movement of (e.g.) charged biomolecules. Within gels, convection currents and turbulence are largely eliminated – which is an advantage of using them, for example, to enable the crystallisation of various substances – from pharmaceutical drugs to proteins.<sup>121</sup>

Mobility in supramolecular gels is allowed and gives rise to diffusion processes within these materials. Transport of substances through gels is a topic that is gaining increasing attention lately due to the advantages that involves controlled release in diverse fields.<sup>122</sup> Diffusion depends on the effective pore size of the gel and the steric demands of the diffusing substance. Furthermore, if the substance of interest interacts with the solid-like gel network, then its diffusion will be slower. In a recent paper,<sup>123</sup> Tokita has clearly presented the main diffusion parameters that can be recovered from gels when testing them as media for diffusing substances and flow of solvents. When an interface is created between gel and air, the potential diffusion of substances is blocked due to the absence of transporting liquid-like molecules. The liquid reaches the boundaries between the solid wet piece of material and the air phase, then an interface is created and the only mass transport that can occur is in the form of evaporation into the gas phase. Solvent is thus retained due to the surrounding vapour pressure, capillarity effects and surface tension of the solvent.<sup>124 125</sup> Also crosslinking affects the rate of diffusion as is reported, for example, in the studies of Diaz and co-workers.<sup>126</sup>

### 1.12.1. Controlled release.

Diffusion processes have often been studied from a controlled release point of view, which has great significance in the field of drug formulation and delivery.<sup>47,127</sup> In this regard, nanoparticles can be diffused through gels and liberated,<sup>128</sup> a strategy that could be applied medical systems such as where stable levels of functional substances are needed in the blood stream e.g. antibiotics<sup>129,130</sup> or antiinflammatories.<sup>131,132</sup>

There are many stimuli that can be used to trigger more rapid diffusion. In particular, the ability to break down supramolecular gels allows them to be considered as self-assembled ‘boxes’ that keep the substances unaltered and blocked until a physical signal interacts with the gel, converting it into a sol, and hence liberating in a controlled manner the encapsulated substances. These stimuli can be of diverse nature as explained in the influential Steed review.<sup>133</sup> One of the simplest and most ubiquitous stimuli in supramolecular materials is temperature,<sup>134</sup> however other stimuli can also be applied. In this regard there is an example of controlled release of an implantable gel in the form of a capsule which is “activated” by the effect of a focused ultrasonic stimulus.<sup>135</sup> This interacts at distance with the implanted capsule and starts to liberate in a controlled manner the substances, which are kept inside this small supramolecular container. In this way we can potentially impact the properties of supramolecular materials with the use of focused ultrasound, which is a recent technique, being used in surgeries to eliminate tumours and other related diseases<sup>136</sup> without the need for open surgery. Controlled liberation of substances depending on a variation of pH as widely studied by several research groups (Figure 1-17).<sup>63,137,138</sup> Typically, changing the pH modifies the protonation state of either the gel network or the drug, and therefore changes the interactions between them, hence modifying the release rate of the encapsulated drug into the surrounding medium.

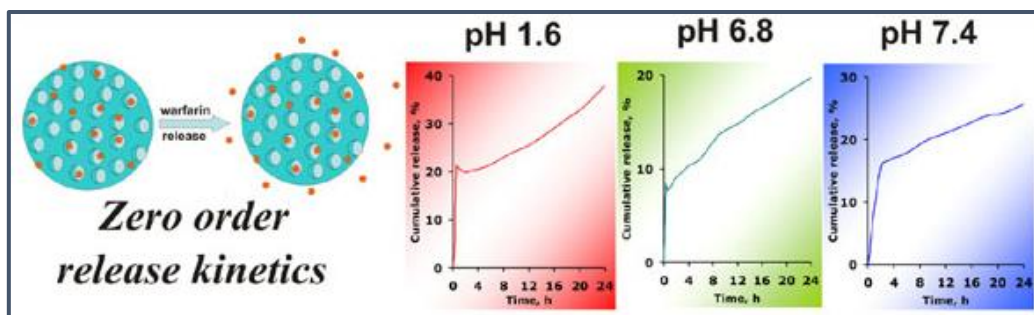


**Figure 1-17** Warfarin being release from a composite depending on the pH of the media. <sup>137</sup>

In a recent example from our research group, a functional molecule (anti-inflammatory drug, naproxen) has been released in a controlled manner by means of changing the environmental pH.<sup>139</sup> By creating hybrid gels combining a polymer gel (for robustness) and a supramolecular gel (for pH-controlled release), it has been possible to pattern gels which can release the drug in a directional sense depending on the pH value of the solvents which it is brought into contact with (Figure 1-18).<sup>140</sup> Drug release is enabled in this system only when naproxen becomes deprotonated, and stops interacting with the self-assembled LMWG network.

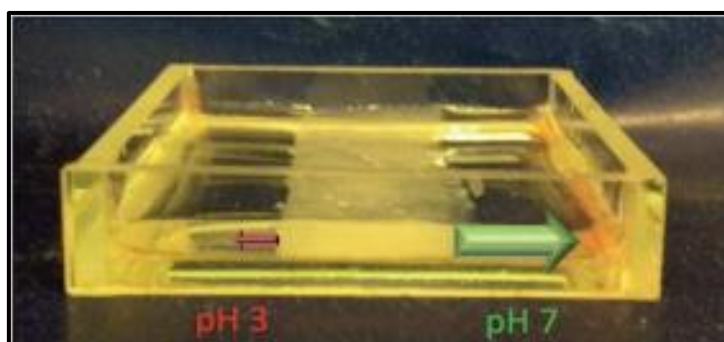


**Figure 1-18** The image represents a summary of the controlled, directional release experiment. <sup>140</sup>

### 1.12.2. Gel-gel diffusion.

Diffusion processes are of critical importance in nature. Oxygen needs to diffuse inside our lungs, penetrate the alveolar area and be molecularly interchanged by the

haemoglobin, expelling the CO<sub>2</sub> simultaneously and continuing the cycle indefinitely. This process is a natural one, which is carried out in gaseous phase where diffusion is very rapid, but diffusion processes in the solid state<sup>141,142</sup> depend on other parameters and have very different rates. In this regard, diffusion within gels has been studied and the mass transport that has been generated of various substances determined.

One of the main techniques which have been used to study the diffusion of molecules inside a gel is the pulsed field gradient nuclear magnetic resonance method (PFG-NMR). Tokita<sup>123</sup> applied this method to obtain diffusion coefficients within a polymer gel network (polyacrylamide, PAAm) for a series of encapsulated molecules, including water, ethanol, glycerin, poly(ethylene glycol) and sucrose. This method is quite straightforward and enables determination of the diffusion parameters and properties of molecules in an individual gel at various densities and with varying degrees of crosslinking (Figure 1-19).

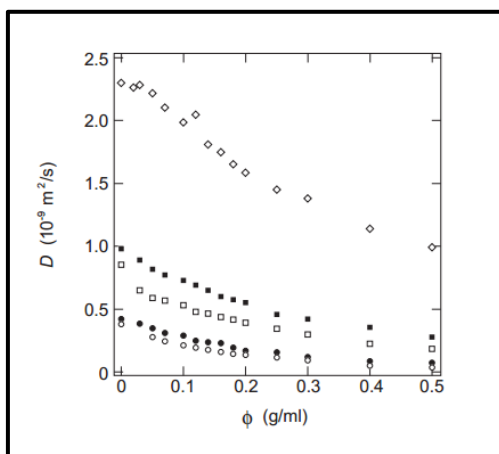


**Figure 1-19** The dependence of the diffusion coefficient of probe molecules on the concentration of acrylamide in gel.<sup>123</sup>

There remains, however, a need to understand molecular dynamics on gels.<sup>143</sup> For example Canet et al<sup>144</sup> were interested in determining the diffusion coefficients of toluene (solvent) depending on the degree of density and temperatures of the organogelators.

Once again, they employed an NMR relaxation technique to analyse those parameters. Bielejewski et al <sup>145</sup> also studied the relationship between solvent molecules and 3D network by means of NMR relaxometry. They found a clear difference between the molecules which are next to the scaffold and those others which are more freely dispersed within the matrix. The interaction of solvent molecules with the gel matrix introduced an additional relaxation mechanism, not found in the bulk solvents. In general, the solvent interacting directly with the gel nanofibres only constitutes a very small percentage of the overall solvent (<5%). Tritt-Goc et al<sup>145</sup> also found this particular behaviour between solvent and gelator and expressed it in terms of different diffusivity.<sup>146</sup> They clearly demonstrated that NMR relaxometry can be successfully applied to study the solvent-gelator interaction between the 3D network by observing the dynamics in the vicinity of the liquid solid interfaces.

Berk et al<sup>147</sup> produced examples of determination of diffusion coefficients for various biological molecules such as proteins, dextrans, polymer beads and DNA, which were measured by fluorescence recovery after photobleaching in 2% agarose.

Diffusion coefficients can be also determined in electrolytes representing the propagation rate at which ions can move through the gel electrolyte (see Section 1.12 below for further details).<sup>148</sup> NMR is a powerful technique in this particular study. Hayamizu<sup>149</sup> and co-workers showed how to determine self-diffusion coefficients in polymer gel electrolytes of lithium ion batteries. Diffusion processes and electrochemistry are highly related in battery technology (Figure 1-20), and investigation of diffusion processes in gels is a vital study in this applied field of gel technology.

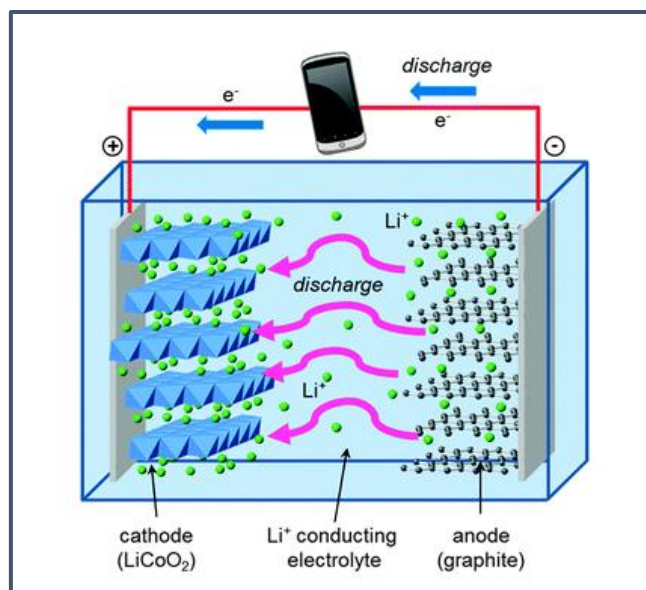


**Figure 1-20** A scheme of the basic structure of a lithium ion cell. Where lithium ions have to move through the electrolyte at certain diffusion rates. <sup>150</sup>

### 1.12.3. Fick's Law treatment of diffusion in gels.

In another study of diffusion of dyes in agar gels made by Samprovalaki,<sup>151</sup> diffusion coefficients were determined at various temperatures (30, 50, 70°C). The diffusion process was studied using image analysis techniques and the diffusion coefficients (D) were then estimated using Fick's second law. The objective of this work was to study diffusion in gels, the effect of temperature and the impact of the size of the diffusing molecule. Figure 1-21 illustrates the experimental set-up.

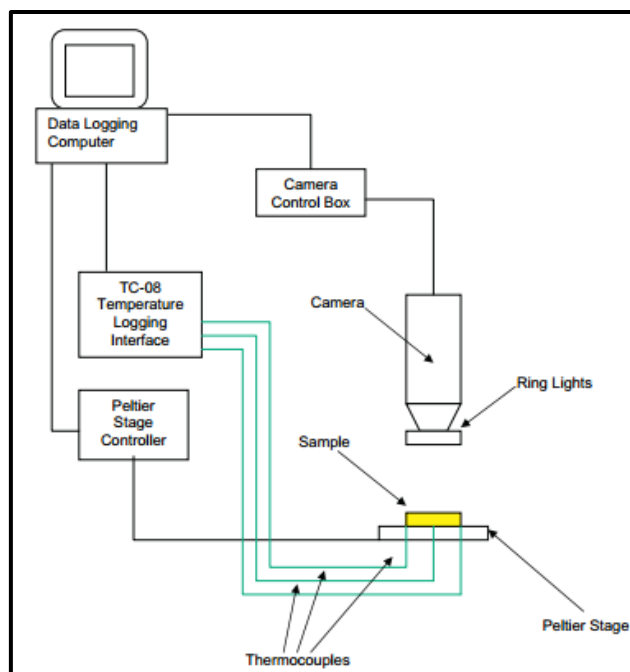


**Figure 1-21** Diffusion set up with camera recorder to track the diffusion of dyes<sup>151</sup>.

The experiment utilized a camera to record the change in gel colour that was produced by the dye permeation inside the gel. The dye reservoir and gel block were brought into contact so the diffusion could start and the process was recorded (Figure 1-22). Colours were converted to a concentration and thus a concentration profile was able to be produced (Figure 1-23).

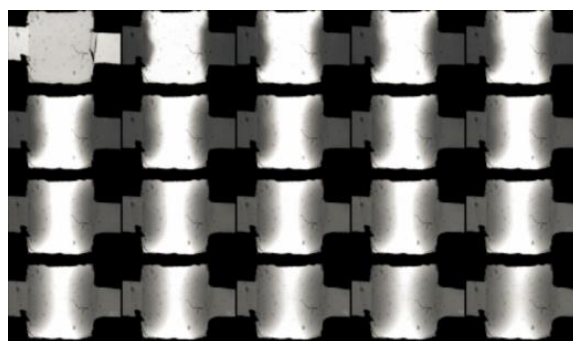


**Figure 1-22** Diffusion profile as seen in the set of images recorded by the video camera at certain times.<sup>151</sup>

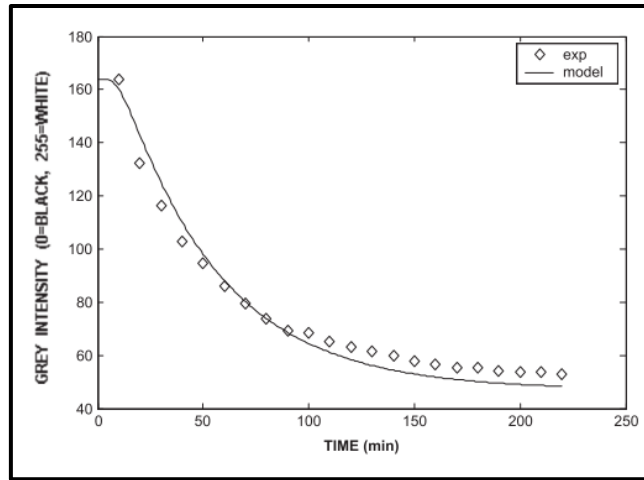


**Figure 1-23** Comparison and fitting between the model and the experimental data where diffusion coefficients are obtained. <sup>151</sup>

These data were then analysed using Fick's laws of diffusion. In more detail, the first law of diffusion was established by Fick in 1855. Crank<sup>152</sup> proposed a clear explanation of diffusion processes according to the geometry and the nature of the material diffused. In order to calculate and determine diffusion coefficients within gels, Fick's Law can be used, where the concentration of the diffusing substance can be determined in different ways (in the examples outlined above, NMR and visual coloured gradient using camera recording and image analysis). Then Fick's equations can be transformed as García-Aparicio and co-workers did (Eqn. 1-4).<sup>153</sup>

$$J_x = -D \frac{dN}{dx} \quad (\text{Eq. 1-4})$$

where  $J_x$  is the diffusion flux,  $D$  is the diffusion coefficient,  $dN/dX$  is the gradient of matter over distance.

$$\frac{dC(x,t)}{dt} = D \frac{d^2C(x,t)}{dx^2} \quad (\text{Eq. 1-5})$$

Equation 1-5 presents Fick's second Law of diffusion. It is a one-dimensional Laplacian and represents how sharply concentration changes with position.

In his work, García Aparicio used proton localized NMR spectroscopy to study three small molecules in chitosan gels of different concentrations. Concentration profiles were compared with theoretical curves based on solutions of Fick's diffusion equations to achieve the best fitting and hence determine diffusion parameters.<sup>153</sup>

### **1.13. Electrolytes as conductive materials.**

Electrolytes are generally liquid materials that allow propagation of ions for various purposes. Clearly, the diffusion of active species is of key importance in these materials. There is however no need for the electrolyte itself to flow on the bulk scale because the conductivity mechanism does not require such a flow. As a result of this, there are various solid porous polymer materials<sup>154</sup> that have the function of propagating the charges between plates of a battery. Indeed, the replacement of liquid electrolytes with solids, and more recently gels, are topics of intense current interest in energy technology.<sup>155–158</sup> The following sections explore liquids in which ionic diffusion becomes possible and which are compatible with gel formation.

#### **1.13.1 Ionic liquids.**

An ionic liquid (IL) is a salt in a liquid state usually at room temperature (less than 100°C) which clearly differentiates such liquids from molten salts.<sup>159</sup> They differ from normal solvents because the solvent molecules are not neutral but are instead ions or short-lived ion pairs. These kinds of compounds can also be called ionic melts,<sup>160</sup> ionic fluids or fused salts. If comparing 'normal' salts (e.g. NaCl) and those that are found to be liquid at room temperature, the major difference comes from the strength of the electrostatic ion-ion interaction created between the pair of counterions.<sup>161</sup> In general, ionic liquids have larger

ions, that interact with one another less strongly, and are unable to pack so effectively into crystalline solid-like forms (for examples see, Figure 1-24). Ionic liquids can have symmetric or asymmetric counterions<sup>162 163 164</sup> (cations and anions) – this affects the strength of the supramolecular interactions created between ions and then the resulting melting point is hence lowering due to the inefficient interactions.

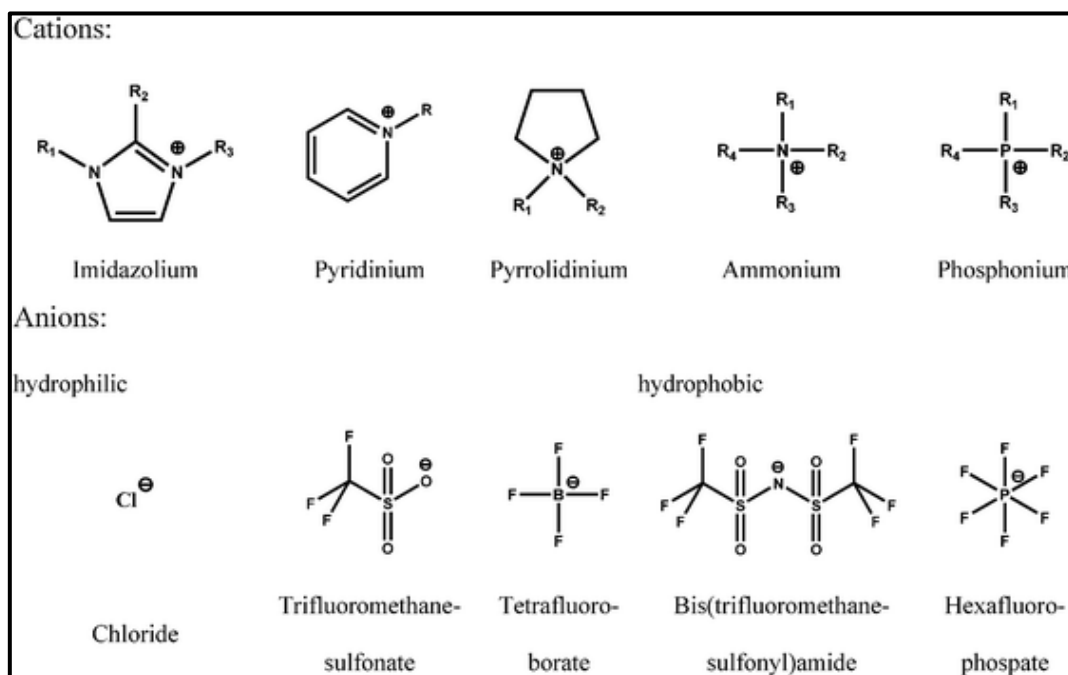


**Figure 1-24** Schematic representation of selected structures of IL cations and anions<sup>165</sup>

However, ILs suffer from some drawbacks – for example they are relatively toxic<sup>166</sup> and can also have relatively high cost. For this reason, there has been increasing interest in green ionic liquids, and one class of ‘ionic liquid’ which has recently emerged are so-called deep eutectic solvents (DESs).<sup>167</sup>

### 1.13.2. Deep eutectic solvents (DESs)

DESs are a relatively new class of ionic liquids which share many characteristics and properties with ILs.<sup>168</sup> DESs are formed from a eutectic mixture of Lewis or Bronsted acids and bases, which can contain a variety of anionic and cationic species (complexes)

– examples are presented in Figure 1-21. In contrast, ILs are primarily formed by a discrete anion and cation combination. Even though they (ILs and DESs) share many physical properties, the different chemical nature between them suggests different application areas.<sup>169</sup> DESs typically form from mixtures of a quaternary ammonium salt (1, Figure 1-24), a metal salt and a hydrogen bond donor (HBD) such as glycerol (2, Figure 1-25) or urea.

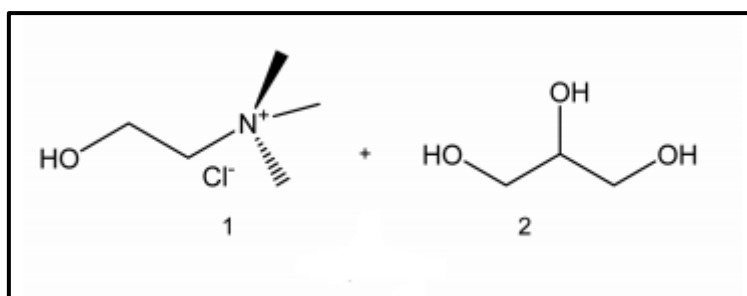


**Figure 1-25** Structures of DESs based on choline chloride and glycerol.<sup>170</sup>

The unique advantages of DESs are that they are low cost, non toxic,<sup>171</sup> easy to prepare, have high biocompatibility & biodegradability,<sup>172,173</sup> and low volatility.<sup>174</sup> In terms of electrochemical uses of DESs, they have a very large electrochemical window<sup>175</sup> which gives them the potential to be a reliable electrochemical platform for a wide range of electrochemical and energy applications without the DESs starting to alter or decompose.

Generally, DESs are formed by mixing a hydrogen bond donor (HBD) and a hydrogen bond acceptor (HBA), associated with each other by means of hydrogen bond interactions, upon which a eutectic mixture with a melting temperature much lower than its constituents is formed. (Figure 1-26).

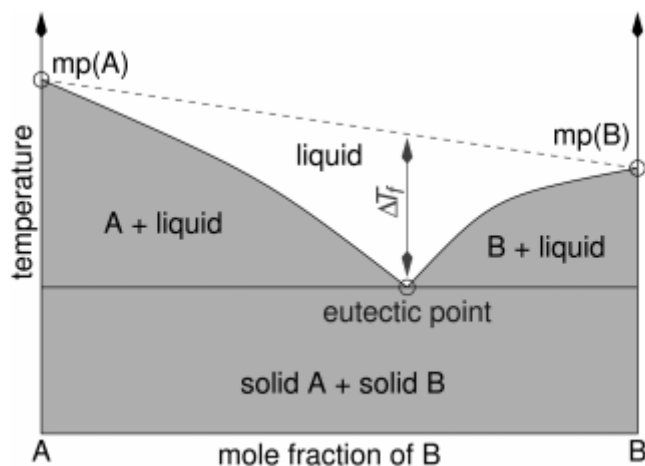


**Figure 1-26** Standard eutectic mixture where final melting temperature of the mixture is lower than ones of the isolated compounds.<sup>167</sup>

In some cases, the effect of lowering the initial melting points of the starting materials that are combined to form the DES is remarkably large. As one example, combining choline chloride (m.p. 302 °C) and urea<sup>176</sup> (m. p. 133 °C) by means of heating, leads to the formation of a viscous liquid (m.p. 12 °C) without any intervention of solvent. Obviously, the resulting liquid DES has charged electrolyte-like properties as a result of the presence of the ionic choline chloride. This is therefore an effective way of formulating ionic compounds into liquid-like form, suitable for energy (and other) applications.

### 1.13.3 Types of DES

There are four kinds of DESs according to the precise composition of the mixture.

**Type 1: Quaternary ammonium salt + metal chloride.** The association between a metal halide and a halide anion from the quaternary ammonium salt can produce halometallate species. Hurley and co-workers<sup>177</sup> used this eutectic combination to electrodeposit aluminium chlorides with pyridinium bromides.

**Type 2: Metal halide hydrates and quaternary ammonium salts.** The existence of water makes the resulting melting point lower than for Type 1 DESs. However, the presence of a molecule of water makes it harder to combine these systems with species that are water sensitive. Some of the hydrated molecules used are  $\text{CrCl}_3 \cdot 6\text{H}_2\text{O}$ ,  $\text{CaCl}_2 \cdot 6\text{H}_2\text{O}$ ,  $\text{MgCl}_2 \cdot 6\text{H}_2\text{O}$ ,  $\text{CoCl}_2 \cdot 6\text{H}_2\text{O}$ ,  $\text{LaCl}_3 \cdot 6\text{H}_2\text{O}$ , and  $\text{CuCl}_2 \cdot 2\text{H}_2\text{O}$ .<sup>178</sup>

**Type 3: Quaternary ammonium salt + hydrogen bond donor.** This constitutes one of the most common DES, and one of the most important. A quaternary ammonium salt is combined with a range of hydrogen bond donors to obtain ionic liquids which are ionically conductive. Some combinations of choline chloride have been studied<sup>170</sup> when incorporating 2,2,2-trifluoroethanol and hexamethylphosphoramide to the resulting mixture.

**Type 4: Metal chloride hydrate and a hydrogen bond donor.** Again, there is water present in form of a hydrate and thus the restriction on the selection of metal compatible chlorides is quite high. The range of electrochemical applications is also quite limited due to the existence of water and thus limitations of electro decomposition. Cruz's team has reported the use of this kind of DES in combinations with lithium chloride.<sup>179</sup>

Of most interest here are type 3 DESs based on choline chloride with various different hydrogen proton donor (glycols, polyols and urea). Typical examples of Type 3 DESs are shown in Figure 1-27. It is evident that there is a very high level of structural versatility in this class of DES and this makes them of significant interest in a range of potential applications.

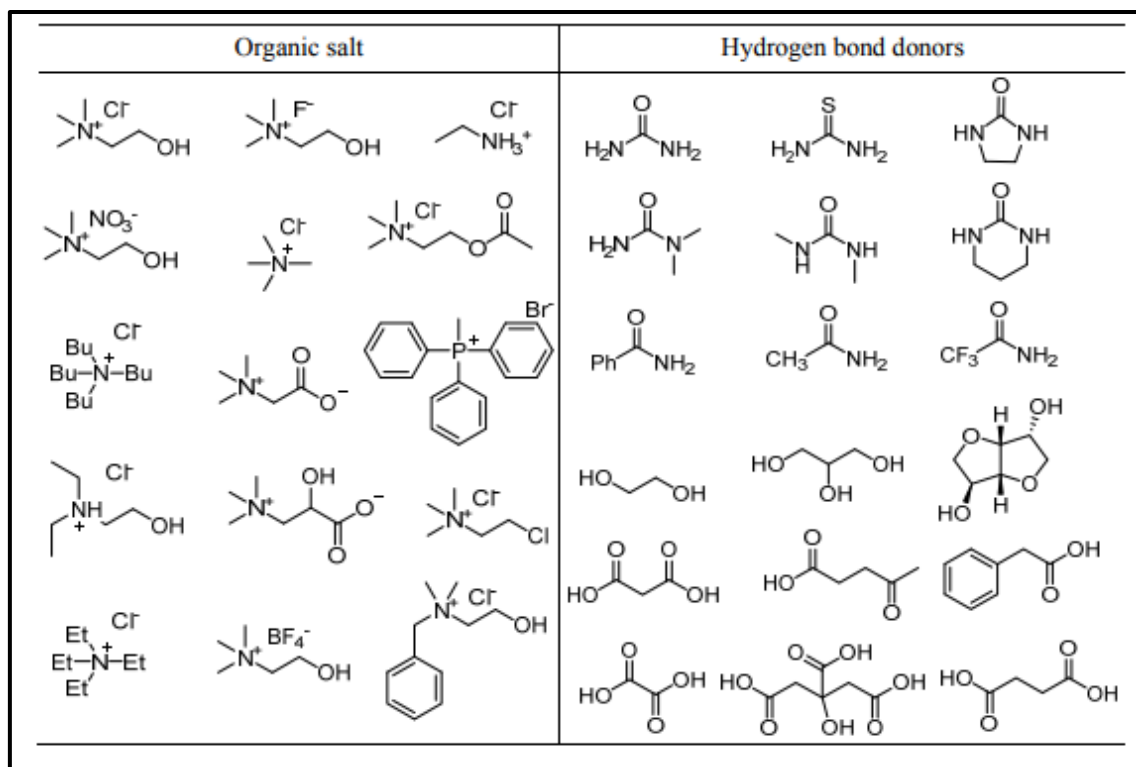


**Figure 1-27** Some examples of the hydrogen bond donors and the hydrogen bond acceptors that can be mixed in certain DESs.

#### 1.13.4. Ionic conductivity of ILs and DESs.

ILs have inherent ionic conductivity (IC) because of the ionic nature and liquid properties. There is a direct link between viscosity and ionic conductivity in a IL,<sup>174</sup> indeed, many studies have tried to relate viscosity,<sup>180</sup> ionic conductivity and self-diffusion coefficients.<sup>181,182</sup> Brennecke and co-workers had an important role in elucidating the transport properties of aprotic heterocyclic anion based ILs<sup>183,184</sup> The more readily the ions can move, the better the conductivity. This can be related to the diffusion coefficient<sup>185</sup> of every ion depending on the liquid nature of the IL (ionic strength and presence of other molecules). Hashim et al<sup>186</sup> investigated a series of DESs based on different glycols, choline chloride and *N,N*-diethylenethanol ammonium chloride obtaining various DESs that had diverse viscosities depending always on the temperature (Figure 1-28).

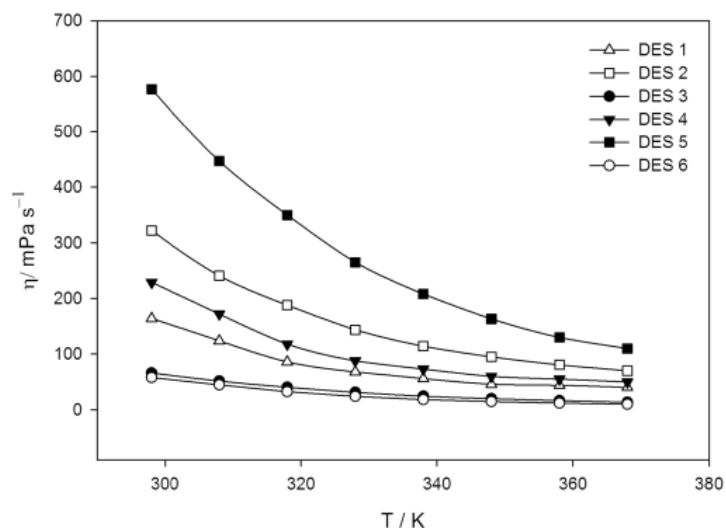


**Figure 1-28** Dynamic viscosity ( $\eta$ ) of polyol based DESs as a function of temperature<sup>186</sup>

In DESs, there is also a relationship between viscosity and conductivity. If there is continuous addition of choline chloride to the glycerol,<sup>187</sup> this lowers the viscosity and increases the conductivity due to the presence of more available charge carriers in an increasingly less viscous solvent.<sup>186</sup> Another way of increasing conductivity is to select cations and anions that are going to be involved in the transport of charge. This will affect the self-diffusion parameter<sup>188</sup> of the introduced species and influence the conductivity.<sup>184</sup> Also, temperature is one of the main parameters that will affect the viscosity of these DESs as is clear in some studies that have been done by Popescu.<sup>189</sup> It has also been noted that the addition of smaller solvent molecules such as methanol could lead to the formation of a less viscous media, thus becoming more conductive, but having the possibility of predicting the expected levels of viscosity according to ionic radius predictions.<sup>190</sup> However, this can also introduce some of the problems of working with such solvents that DESs are avoiding in the first place. The quantitative structure-property relationship model (QSPR) for ionic conductivity and viscosity of ionic liquids in the Yamamoto study<sup>191</sup> gave a reasonable correlation accuracy of IC and viscosity.

### 1.13.5. Deep eutectic gels and ionogels

The use of ILs as gelation fluids led to the development of ionogels (IGs) – indeed IGs have become a major field of research.<sup>192</sup> In 2001, Kimizuka and Nakashima were the first to realise the potential of this approach, reporting glycolipids that self-assembled into bilayer membrane structures capable of immobilising ILs.<sup>193</sup> Hanabusa and co-workers went on in 2005 to report a family of gelators based on dipeptides functionalised with a branched alkyl chain, which they described as specialist gelators for ILs.<sup>194</sup> Importantly, they noted that the IC of these gels were similar to those of the ILs. Later work with other gelators in ILs also indicated that the electrochemical properties of the gels were very similar to those of the native ILs.<sup>195</sup> Intriguingly, in recent work, Šantić and co-workers demonstrated that their oxalamide gelator actually even enhanced the conductivity of ionogels at low gelator concentrations.<sup>196</sup> Specifically, they postulated, on the basis of molecular dynamics calculations, that this phenomenon resulted from the higher affinity of the gelator towards  $\text{BF}_4^-$ , which reduced its electrostatic attraction to the countercation  $[\text{BMIm}]^+$  and thus increased the ionic mobility. As the gelator concentration increased further, the IC decreased because the denser gel network hindered ion transport – although even at very high gelator concentrations, the decrease in conductivity was less than an order of magnitude. The gelator network can therefore impact in subtle ways on the overall performance of ionogels. Maruyama and co-workers have blended self-assembled LMWGs with crosslinked polymer gel networks to yield tunable IGs,<sup>197</sup> with the presence of the poly(methyl methacrylate) (PMMA) network enhancing overall materials performance.

As early as 2003, Yanagida and co-workers demonstrated that dye sensitised solar cells (DSSCs) could be formulated including ionogels using a lipopeptide as LMWG.<sup>40</sup> Energy conversions of ca. 5% were obtained in this early device. Grätzel and co-workers also incorporated supramolecular IGs into DSSCs and achieved 6.3% efficiency,<sup>198</sup> noting that the thermoreversibility of the IG was advantageous for filling the device, using a liquid at elevated temperatures and then allowed to set into a gel *in situ*. In later work, these researchers developed an ionogel-based DSSC using a urea/amide gelator that achieved 7.8% power conversion efficiency.<sup>199</sup> These cells were tested outdoors in Jeddah, Saudi Arabia where, impressively, the power conversion efficiency PCE of the cells was close to 9% around midday when the temperature reached nearly 37°C. This indicates excellent performance under hot conditions.

Clearly there is significant potential to apply gel electrolytes in real-world settings, and LMWGs offer an effective and simple way of modifying devices to yield desirable electrolyte rheological properties. Excitingly, it is evident that the gelator structure, both on the molecular scale and in terms of the nanoscale network and macroscopic properties tunes the performance of these devices. Overall, it seems likely that LMWGs will be employed with conductive fluids in new technologies in the near future.

Gels based on DESs have been much less studied than the ionogels described above. Recently, polymeric gels were prepared by means of chemical polymerization of 2-hydroxyethyl methacrylate (HEMA) within a choline chloride-based DES with Vinyl acetate (VA).<sup>200</sup> There has also been recent interest in polymer gels as the basis for the creation of internal matrix in DESs. As an example, it can be mentioned the work of Panzer and co-workers the use of UV copolymerization of 2-hydroxyethyl methacrylate (HEMA) inside the mixture of the gel.<sup>201</sup> However, DES's are hugely under-exploited in

terms of their potential for supramolecular gel formation, and clearly there are many interesting questions to answer about the potential for diffusion and conductivity in this family of materials.

#### **1.14. Project aims.**

The key goals of this PhD thesis were to study dynamic processes in self-assembled gels, and to gain new insights into these phenomena. In particular, we wanted to interrogate a variety of different dynamic processes considering: (i) the formation of the supramolecular gel, (ii) the mobility of the solid-like network in a supramolecular gel and (iii) the mobility of the liquid-like phase within supramolecular gels. The main objectives that were targeted in this research are described here:

- 1) Chapter 2: Thermodynamic and kinetics of gelation: Study the thermodynamics and the stability of a family of two-component organogels in toluene and importantly, to gain insight into their rates of gelation. Rates of gelation are rarely studied, and the systems investigated here have the benefit of forming gels on simple mixing of the two components under ambient conditions. As such, the energy barrier to gelation is relatively low. We thus hoped to gain an understanding of the different factors which control both the thermodynamics and kinetics of gel formation.
- 2) Chapter 3: Study of diffusion of supramolecular gels across a gel-gel interface. There are many examples on controlled release of substances from within the liquid-like phase of a gel. However, very rarely has anyone ever studied the migration of components of the solid-like network itself across a gel interface. Such processes should give important insights into how gels can adapt and

self-heal and the extent to which solid-like networks can actually be considered dynamic in their own right. This study strikes at the heart of understanding the unique dynamic characteristics of self-assembled gels.

- 3) Chapter 4: To develop innovative supramolecular gels based on deep eutectic solvents and understand the diffusion of conductive components of the liquid-like electrolyte solvent through the gel network. In particular, we aimed to study, DESs based on choline chloride and a range of various proton donors. We hoped to demonstrate the impact of gelation on conductivity, and hence understand how the dynamic properties within these gels might have potential energy applications.

## **Chapter 2 Thermodynamics and kinetics of supramolecular gelation**

This chapter investigates the thermodynamics and focusses on the kinetics of assembly of supramolecular gel systems. Although there are number of studies of gelation thermodynamics<sup>202</sup>, and gelation kinetics<sup>203,204</sup>, it is relatively rare that both are investigated for the same system. We wanted to determine which factors affects thermodynamics and kinetics, and whether these are connected in the overall gelation process. Gel thermodynamics will reflect the overall stability of the self-assembled material, as such they can be considered to reflect the non-covalent interactions that underpin the self-assembled gel. On the other hand, gelation kinetics depend on the energy barrier to gel formation and assembly – this is much less well understood, and might be considered to depend on the dispersion and mixing of the gelator, as well as the energy barrier associated with reorganisation of the gelator molecules into self-assembled nanostructures. We reasoned that studying kinetic aspects of gelation would shed unique insight into gel dynamics – the key underpinning topic of this thesis, as well as providing new insights into gel assembly. Some of the results presented in this Chapter have been published in *RSC Adv.* 2015, **5**, 27190-27196.

### **2.1. Thermodynamics of supramolecular gels formation**

#### **2.1.1. Introduction**

There are different ways of determining the thermodynamic character and stability of soft gel-phase materials. One approach is simply to measure the thermal stability of gels. This can be done in terms of a simple  $T_{\text{gel}}$  measurement – determining the temperature at which the gel is converted into a sol. This temperature reflects the point at which the enthalpy of gel assembly is balanced with the entropy of gel dissolution, and provides some general

insight into the overall thermodynamic stability of a gel. However, in order to accurately determine thermodynamic parameters, it is also necessary to apply a more detailed study of response to temperature. In order to achieve this, we selected a technique based on variable temperature NMR (VT-NMR). In combination with Van't Hoff treatment<sup>69,78,205</sup> of the data, this allows us to determine  $\Delta S$ ,  $\Delta H$  and  $\Delta G$  values for the dissociation process, thus providing detailed insight into the self-assembly process of the 3D gel nanofibre network.

### 2.1.2. Two-component dendrons and amines

The gels selected for investigation in this case were supramolecular, two-component organogels based on combining certain amines and dendron acids, as illustrated in Figure 2-1. The Smith group has previously extensively studied dendrons based exclusively on lysine amino acids, such as G2 ((Boc)<sub>2</sub>Lys)<sub>2</sub>-LysOH (see introduction),<sup>17,66,206</sup> but has not previously studied the other dendrons in which different amino acids are coupled to the lysine core unit.

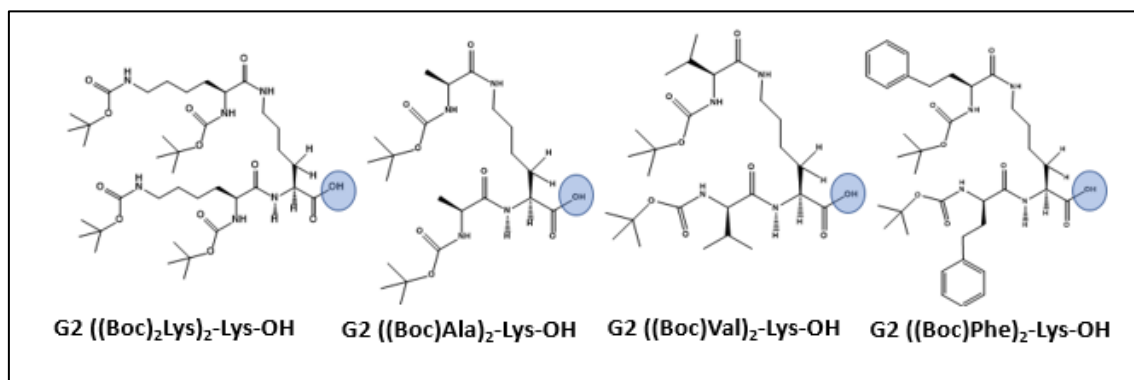


**Figure 2-1** Dendrons which have been synthesized. Note that these dendrons are second generation and the inner core is based on the lysine.

The organogels that are targeted consist of two simple components.<sup>64</sup> The first is a lysine based second generation dendron (Figure. 2-2) which is obtained using a series of peptide coupling reactions (Figure 2-3).

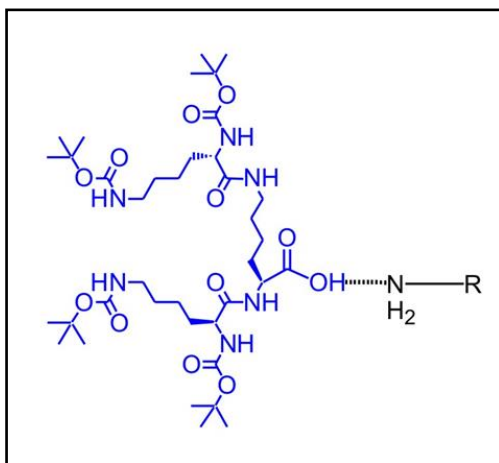


**Figure 2-2:** Lys based dendron interacting by means of hydrogen bonds with a standard amine.

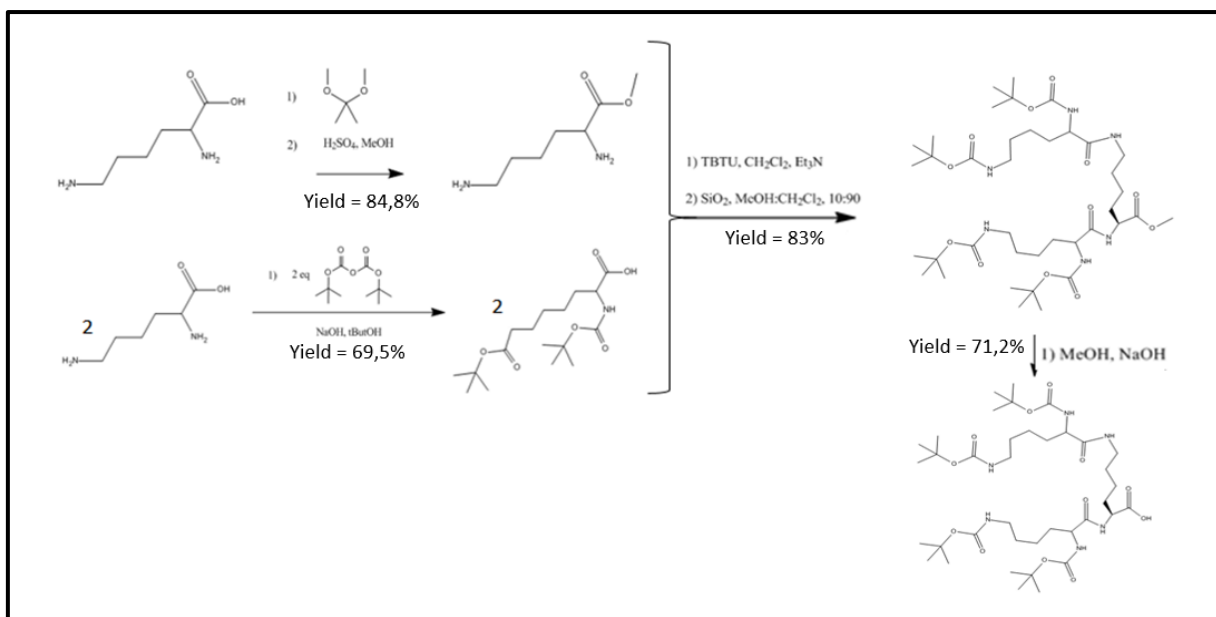


**Figure 2-3:** Series of reactions to produce the second generation dendron of Lys<sup>17</sup>

Starting from Lys, the first reaction was the esterification to obtain the methyl ester derivative (Lys-OMe).<sup>207</sup> The activation of the carboxylic acid group takes place because of the presence of the catalytic amount of acid that is added to the reaction mixture. The

second reaction was the Boc protection of the amino groups of the Lys.<sup>208</sup> The amine attacks one of the electrophilic carbonyl groups of (Boc)<sub>2</sub>O. The key step was the coupling reaction of the two orthogonally protected substances produced in the previous two reactions to make the second generation dendron.<sup>209</sup> In order to synthesise the second generation dendron of the Boc-protected Lysine, a coupling reagent (TBTU)<sup>210 211</sup> was employed to connect the carboxylic group in (Boc)<sub>2</sub>Lys-OH to the amino groups in the Lys-OMe via amide bond formation. Finally, deprotection of the ester provided the target carboxylic acid. The dendron obtained in the previous step was hydrolysed via a very simple procedure using base in methanol. In addition to synthesising the dendron based on *L*-Lys, we synthesised the enantiomer, starting from *D*-Lys, using identical methods. Full characterisation of all systems was in agreement with previously published data for lysine dendrons, and can be found in the Experimental Section 6.

### **2.2.1. Synthesis of the second generation dendrons of various configurations G2 (Boc-Phe)<sub>2</sub>-Lys-OH, G2 (Boc-Val)<sub>2</sub>-Lys-OH and G2 (Boc-Ala)<sub>2</sub>-Lys-OH**

The organogels that are targeted consist of dendron acids based on a variety of different amino acids at the peripheral sites – phenylalanine (Phe), valine (Val) and alanine (Ala) were selected as they are simple modifications which introduce increasing amounts of apolar character to the system. These dendrons were synthesised using the same approach as that used for the all-lysine based system.

The only difference between dendrons was the purification step in terms of flash chromatography. The nature of the dendrons was essentially sticky and very viscous. This viscosity disappeared when the substances were able to be completely dry but due to this particular behaviour when using flash column, the crude reaction partially purified was in some cases not easy to separate with a mixture of solvents proposed (DCM:MeOH:Et<sub>3</sub>N in the 95:5:0.1 proportion. The only solution to this problem was the

use of a high diameter (7cm) diameter chromatography column and a big volume of silica ( $3.5^2 \cdot \pi \cdot 13 = 500 \text{cm}^3$ ) for a relatively small amount of crude (1g). Each of the dendrons had distinctive NMR spectra associated with the side chains on the peripheral amino acids and had mass spectra molecular ions consistent with the molecular formula. Full characterisation can be found in the experimental section 6.

Commercially available amines that form a two-component acid-amine complex with the dendrons and hence give rise to gelation, were supplied by Aldrich. Their structures are illustrated in Figure 2-4. Amines were selected to represent both aliphatic and aromatic types of amine, and also different sizes of aromatic unit. Furthermore, naphthylmethylamine has a distinctive chromophore which can be useful for further characterisation study, while phenethylamine is the pharmacophore of a key class of neurotransmitter type drugs (e.g. dopamine, amphetamine etc.) and there is potential interest in terms of detection or delivery of this type of unit.

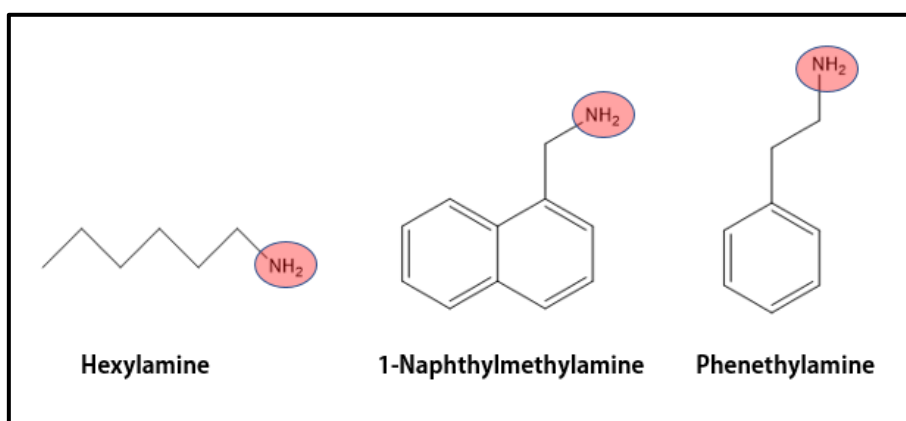


**Figure 2-4:** Hexylamine (Hex), 1-Naphthylmethylamine (Naph) and Phenethylamine (Phen) were the amines tested in the gel formation experiments.

The various combinations of amines and dendrons resulted in a range of gels. Table 2-1 represents the range of 12 gels that can be assembled in this way, and presents their nomenclature as used in this chapter.

	G2 ((Boc) <sub>2</sub> Lys) <sub>2</sub> -Lys-OH	G2 (Boc-Phe) <sub>2</sub> -Lys-OH	G2 (Boc-Ala) <sub>2</sub> -Lys-OH	G2 (Boc-Val) <sub>2</sub> -Lys-OH
Hex	Hex-Lys	Hex-Phe	Hex-Ala	Hex-Val
Naph	Naph-Lys	Naph-Phe	Naph-Ala	Naph-Val
Phen	Phen-Lys	Phen-Phe	Phen-Ala	Phen-Val

**Table 2-1** Various combinations of L enantiomers of dendrons and amines that are going to be tested.

In Table 2-1 is important to realize that all combinations resulted in stable gels in toluene. Interestingly, we noted through visual observation that each of these gels had significantly different kinetics of gelation (see below for further discussion of kinetics). This system is relatively unique,<sup>64,65</sup> in that it forms gels on simple mixing of the components – no heating or ultrasound are required for gelation. The vast majority of gels have a significant energy barrier to gelation – this is clearly not the case in this family of gels. As such, it makes an ideal testbed for understanding the processes of gelator assembly, which can often be confused by the need to apply an ill-defined ‘activation’ step. These observations therefore led us to realise that understanding both the thermodynamics and kinetics of these subtly variable gelation systems would be highly valuable. It should be noted that the phenylalanine-based dendron itself was capable of some gelation even in the absence of the amine if ultrasound stimulation was used. This may be a result of  $\pi$ - $\pi$  interactions allowed by the potential  $\pi$  stacking of the aromatic part of phenylalanine.

It is important to realise that the thermodynamic gel stability may depend on the maturation time of the gel in each case, as it is well known that ageing can affect gel morphology and stability.<sup>112</sup> Therefore, in order to have an accurate determination of thermodynamics we always aged gels for 24h.<sup>212</sup>

### 2.2.2. $T_{\text{gel}}$ measurements via tube inversion

The first approach to monitoring the thermodynamics and stability of the prepared gels was a  $T_{\text{gel}}$  determination. In order to obtain the corresponding values for each combination, we performed a vial inversion experiment<sup>26 213</sup> while heating samples in a thermoregulated oil bath using a programmed ramp of temperatures (5°C/min). When each gel was starting to melt and slide down the internal walls of the vial, the  $T_{\text{gel}}$  temperature was recorded (Figure 2-5). This standard, simple, reproducible table top rheology method gave rise to  $T_{\text{gel}}$  values with errors of  $\pm 2^\circ\text{C}$ .

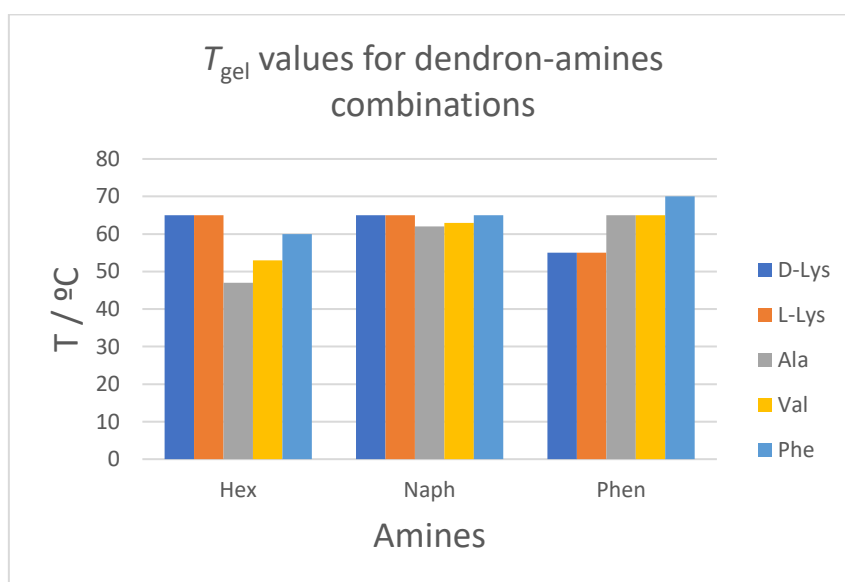


**Figure 2-5** Various  $T_{\text{gel}}$  temperatures for the resulting gels obtained from the combination of dendrons and amines proposed.

In general terms, the gels based on Phenylalanine (Phe) dendrons are more stable than those based on Valine (Val) or Alanine (Ala) dendrons. This might suggest some contribution from  $\pi$ -stacking to gel stability. This would be in agreement with the observation that even in the absence of amine, some gelation was possible for this dendron. The Lysine (Lys) dendrons are more stable with the aliphatic amine hexylamine

(Hex), but less stable with a Phenethylamine (Phen) aromatic amine, whereas the Phe dendrons are more stable with the aromatic amines than they are with aliphatic Hex. As would be expected, the <sub>L</sub>-Lys and <sub>D</sub>-Lys gels have identical  $T_{\text{gel}}$  values in each case, reflecting their enantiomeric relationship – mirror image gels should be identical in terms of thermal stability.

### 2.2.3. VT <sup>1</sup>H-NMR and Van't Hoff treatment

The thermodynamics of some of the compounds based on the Phen amine gels were studied alongside visiting undergraduate student Stefan Rohner. These results have already been published.<sup>69</sup> We performed thermodynamic studies of these gels using <sup>1</sup>H-NMR methods and also visually monitored the kinetics of gelation.

We applied a VT- <sup>1</sup>H-NMR technique to determine the thermodynamic parameters. Importantly, on heating the gel, it transitions from a gel to sol and this can be monitored by NMR. Solid-like self-assembled gel nanofibres cannot be observed in the NMR spectrum because they are immobile on the NMR timescale, affecting their relaxation. However, in the sol state, gelator molecules can be observed, because they are mobile on the NMR timescale. Heating an NMR sample, in the presence of a mobile internal standard, therefore provides us with the ability to quantify how much gelator is mobilised at each temperature and hence follow in molecular-scale detail the transition of the gel into its sol state. Treating the process as being analogous to the dissolution of a crystal then allows us to apply a Van't Hoff treatment in order to determine the thermodynamic parameters associated with the phase transition. For example, an NMR tube with the Phen-Val gel was prepared using deuterated toluene as solvent at a final concentration of 20 mM. An internal standard for later integration of peaks and calculation of

concentrations was present. The reference of choice is diphenylmethane which is selected as the recommended non interacting substance to use for quantitative purposes in various works.<sup>64,65,67</sup> The gel was generated and kept for 24 hours for gelation to be complete. VT <sup>1</sup>H-NMR experiments were then programmed and executed. The range of temperatures used in this experiment was 25°C-90°C at intervals of 5°C for each <sup>1</sup>H-NMR analysis. The result is a set of spectra (Figure 2-6) showing the effect of increasing temperature. This reflects the liberation of the two-components as the 3D network disassembles in response to the temperature increase. The equilibration time for each temperature in the ramp was 3 min each.

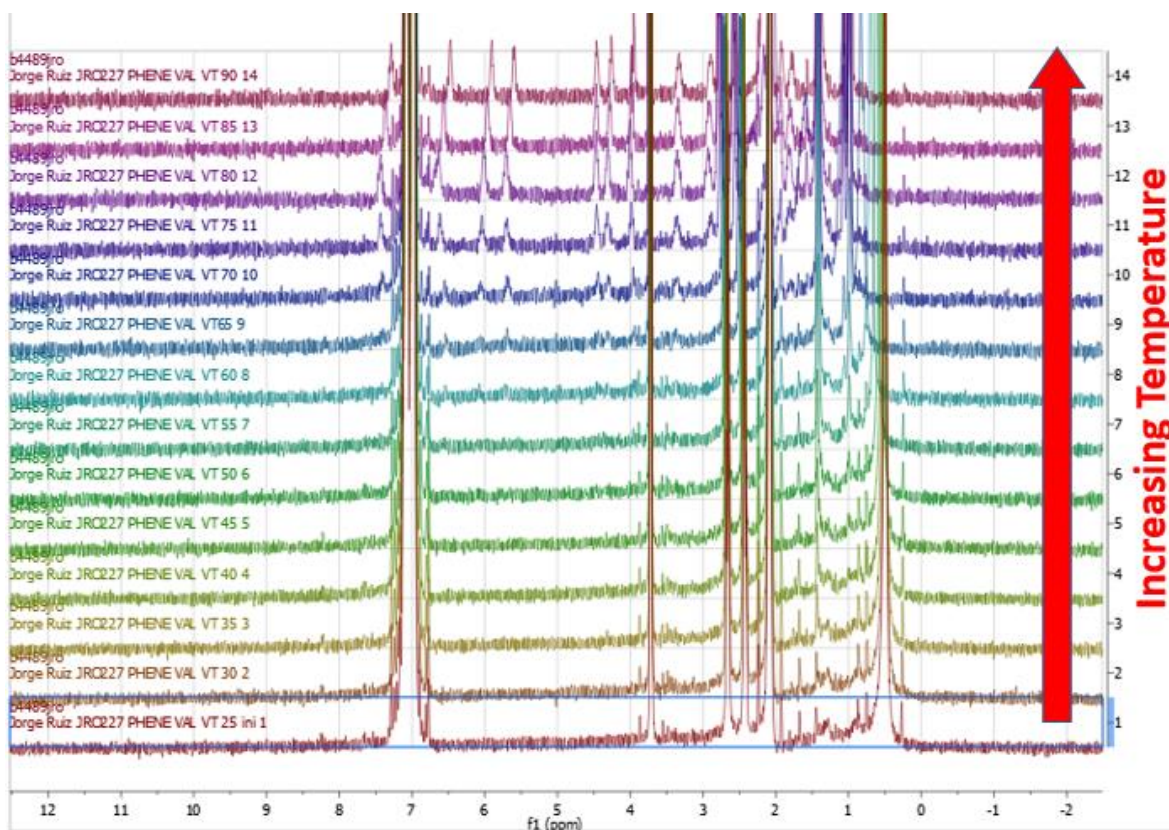


**Figure 2-6** VT-NMR experiment with a temperature range of 25-90°C with 5°C intervals for the Phen-Val.

Furthermore, as the peaks for the gelator increase in size as they are liberated from the gel, they also generally shift upfield (to the right). This reflects the loss of hydrogen bond

interactions as the gel network disassembles and the molecules aggregate to a lesser extent, ultimately becoming individual non-interacting molecules.

The various peaks that are visible in the spectra are identified and integrated according to the reference material (diphenylmethane). In the following picture (Figure 2-7) such peaks and the corresponding parts of the molecules that are involved in the formation of the Phen-Val gel are represented.

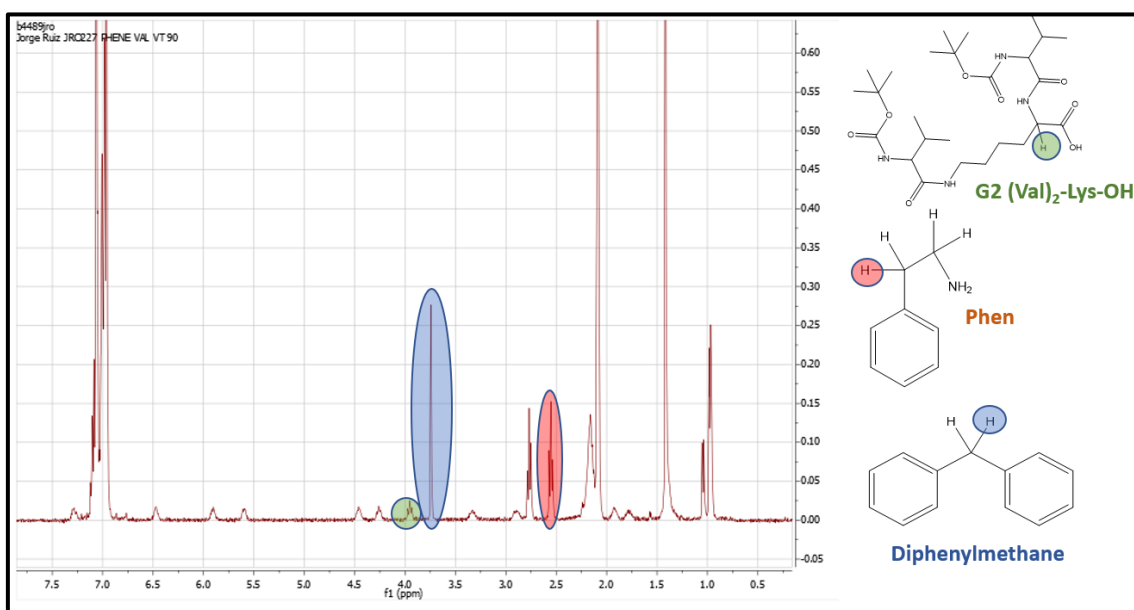


**Figure 2-7** The integration of the various peaks corresponding the molecules involved in the gel appear when gels are analysed by NMR at several temperatures give precise concentrations VS temperature data. The reference concentration is given by the Diphenylmethane

The NMR spectra are integrated and converted in a concentration profile versus temperature, yielding both concentration of amine and dendron. In particular we integrated the peaks associated with one proton of the dendron against the two aliphatic peaks of diphenylmethane, as these peaks were distinct within the spectra and hence easily and accurately integrated. This approach allowed us to quantify the free dendron at each concentration.

mM Phen	mM Val	Temperature °C
2.98	2.79	25
3.8	2.98	30
4.63	3.86	35
5.37	4.29	40
5.29	5.51	45
5.79	6.57	50
8.1	9.43	55
12.07	12.75	60
16.53	17.35	65
19.75	19.78	70
19.83	19.98	75
20	20	80
19.5	19.69	85

**Table 2-2** Concentration of each component at each temperature.

If such set of data (Table 2-2) is plotted then a graph such as Figure 2-8 is obtained.

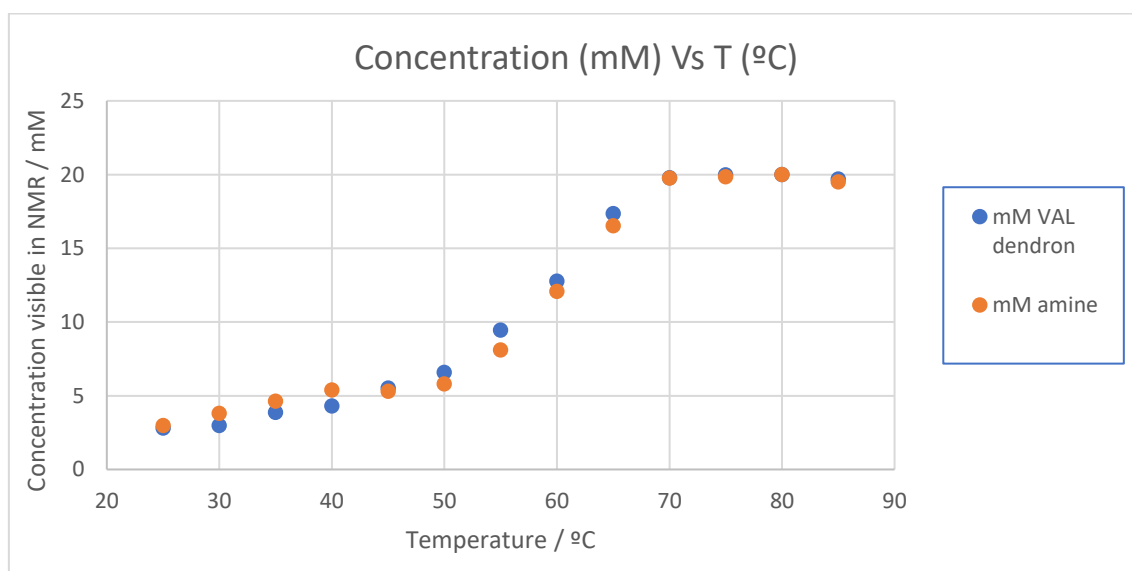


**Figure 2-8** Concentration profile of the VT <sup>1</sup>H-NMR of the Phen-Val Gel.

Figure 2-8 clearly demonstrates that as the temperature is increased, the amount of dendron (and amine) liberated from the self-assembled gel nanofibres also increases. As

such, more dendron is detected by NMR because it moves freely through the gel network. Eventually, the concentration reaches a maximum, which means that the gel has been dissolved completely so the concentration equals to the initial concentration of components. From the example in Figure 2-6 it can be seen that the gel-sol transition in the NMR tube is occurring at ca. 50-70°C – this is in good agreement with the visually observed  $T_{gel}$  value of 65°C. It should, however, also be pointed out that gel-sol transition measured in this way may not always agree with those measured visually by tube inversion for two reasons:

- The shape of the vial can influence the  $T_{gel}$  value, as side walls and diameter have an impact on the ability of a gel to support its own weight.
- The NMR method probes molecular mobility, and it is not fully clear, especially in cases where the transition between gel and sol is less ‘sharp’ (see Figure 2-6) exactly at what point the visual transition between gel and sol will occur – i.e., exactly how much gelator is required in the ‘solid-like’ network’ in order to form a stable sample-spanning gel.

To calculate the thermodynamic values that corresponds to the gel formation we then apply Van’t Hoff treatment (equation (2-1)) treating the gel breakdown like the dissolution of a crystal:

$$\ln(sol) = \left(-\frac{\Delta H_{diss}}{RT_{eq}}\right) + \left(\frac{\Delta S_{diss}}{R}\right) \quad \text{Equation 2-1}$$

where:

- **Sol** is the solubility (it is assumed that in this case Sol is approximately the concentration of dendron or amine observed),
- $\Delta H_{diss}$  is the dissociation enthalpy associated with the destruction of fibres by means of heating.

- $\Delta S_{diss}$  is the dissociation entropy associated for the gel-sol transition where supramolecular fibres are melted down.
- $T$  is the temperature in Kelvin.
- $R$  is the gases constant with a value of  $8.314 \text{ J}/(\text{mol} \cdot \text{K})$

We process the data taking the values in which the concentration changes from Figure 2-6, that is, for the example shown, the range between  $50^\circ\text{C}$  and  $70^\circ\text{C}$  and plot  $\ln [\text{sol}]$  vs  $1/T$  (Figure 2-9) and apply a straight-line fit to the data.

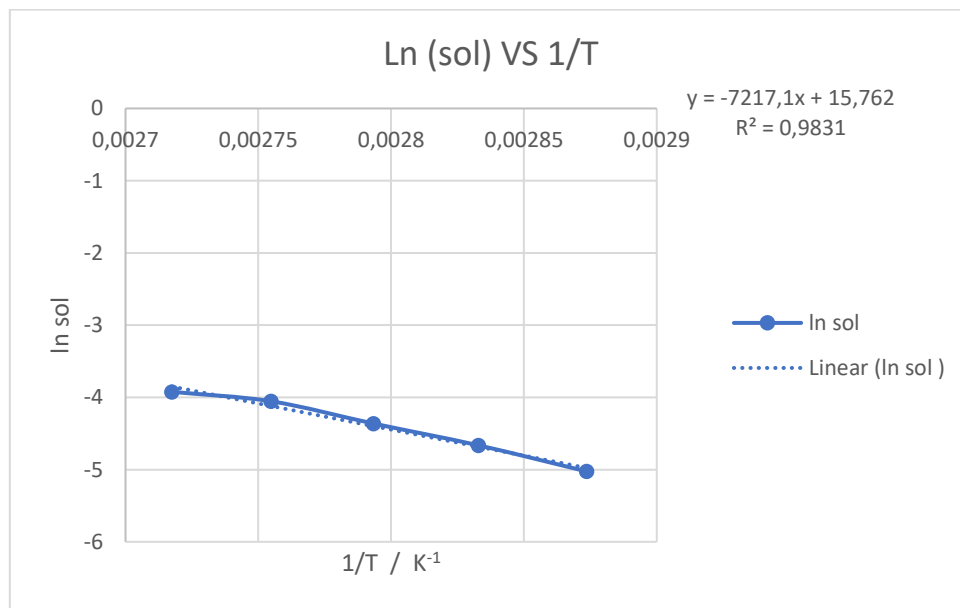


**Figure 2-9** Plot representing  $\ln$  of the concentration of components in the gel versus the  $1/T$ . for the case of Val-Phen Gel.

As a result of Van't Hoff equation (2-1), we can then derive thermodynamic parameters from this treatment corresponding to the entropy and the enthalpy.

In the case presented,

$$\Delta H_{diss} = 48.1 \text{ KJ/mol}$$

$$\Delta S_{diss} = 108 \frac{\text{J}}{(\text{mol} \cdot \text{K})}$$

These values indicate that the gel-sol transition is enthalpically disfavoured (+ve). This is to be expected as non-covalent interactions are being broken as the gel is converted into a sol. Conversely, the gel-sol transition is entropically favoured (+ve). Once again, this is expected on the grounds that as the gel disassembles from its ordered solid-like state, free molecules are released into a more disordered liquid-like phase.

These values can then be combined to determine the Gibbs free energy for the dissolution process (equation (2-2)).

$$\Delta G_{diss} = \Delta H_{diss} - T\Delta S_{diss} \quad \text{Equation 2-2}$$

For a given temperature of 25°C (298 K) we can thus determine if the process is spontaneous.

$$\Delta G_{diss} = 48.1 \text{ KJ}/(\text{mol} \cdot \text{K}) - 298 \text{ K} \cdot 108 \cdot 0.001 \text{ KJ}/(\text{mol} \cdot \text{K}) = 15.9 \text{ KJ}/\text{mol}$$

In order to have a spontaneous process the Gibbs Free energy variation has to be negative. In this case the variation of Gibbs energy is positive for the gel-sol transition. This means that at 25°C, the assembly of the system into a gel will be favoured in terms of free energy in agreement with the observation that a gel at room temperature is indeed observed for this system. This is a very useful approach to obtain thermodynamic parameters that are closely linked with the stabilization interactions that underpin a particular supramolecular gel system.

This value is positive, and we can therefore conclude that the sol to gel transition is thermodynamically favoured at room temperature and has the potential to be spontaneous. Obviously, the precise kinetics of the process will depend on the energy barrier to gelation, which we explore in the following section.

Using the same approach, we also obtained the thermodynamics of the assembly of the other dendrons with the Phen amine. The results can be found in Table 5. It is evident

from this data that of these three gels, the dendrons incorporating alanine formed the least thermodynamically stable gels, and as the amino acid side chain became larger and more apolar, the gel stability at room temperature increased, with Phen-Phe being the most stable two-component gelation system based on this amine. This is fully in agreement with the observations from the simple  $T_{\text{gel}}$  measurements, which indicated that the order of thermal stability of these three gel systems was Phen-Ala < Phen-Val < Phen-Phe.

Gel	$\Delta H_{\text{diss}} / \text{kJ mol}^{-1}$	$\Delta S_{\text{diss}} / \text{J mol}^{-1} \text{K}^{-1}$	$\Delta G_{\text{diss}}$ at 298 K /
Phen-Ala	56.6	121	14.3
Phen-Val	48.1	108	15.9
Phen-Phe	27.7	45	20.5

**Table 2-3** Thermodynamic parameters for the gelation of different dendrons with Phen amine.

#### 2.2.4. Conclusions on Thermodynamics.

Thermodynamics of gel formation allows the user to know how thermally stable a supramolecular gel is. In order to assess this stability, we can use a simple tube inversion method or a more detailed calculation of the thermodynamic parameters. According to the results obtained in the  $T_{\text{gel}}$  inversion method, and the VT  $^1\text{H-NMR}$  approach, the less stable Phen gels are the ones based on Ala dendron and the most stable ones the ones are based on the Phe dendron. Surprisingly, however, the Phe dendrons, although forming the most stable gels, had significantly slower kinetics of gelation than the other systems (see below for details). This particular contradiction made us focus in detail on measuring properly the kinetics of gel formation. In our published work,<sup>69</sup> we only did this visually, but moving on from that study, we wanted to achieve more detailed insight into gelation kinetics using a range of different techniques. Surprisingly, gelation kinetics are relatively rarely studied, and we reasoned that using a variety of different approaches would allow us to consider the kinetics of gelation from three different perspectives:

- Macroscopically: Using rheometry<sup>110</sup> to track the formation of gels.
- Nanoscopically: Using CD spectrometry to track the assembly of chiral nanostructures.
- Molecularly: Using <sup>1</sup>H-NMR to detect and quantify the rate at which molecules are assembled into solid-like form and hence disappear from the NMR spectrum.

## 2.3. Kinetics of gels formation.

### 2.3.1. Introduction

It is worth mentioning that thermodynamically ‘spontaneous’ (i.e., favoured) processes are not necessarily the fastest in kinetic terms. This is because all species have to overcome an energy barrier and an adequate geometric orientation to interact, and this may, or may not, correlate with the thermodynamic stability of the system. This energy barrier will depend on a variety of factors such as structural hindrance, mobility etc. This process is defined by the Arrhenius formula.

$$k(T) = A \cdot e^{-\frac{E_a}{RT}} \quad \text{Equation 2-3}$$

Where k is the rate constant, T refers to the temperature in Kelvin, A is a pre-exponential factor and has a relationship with the number of collisions necessary for the molecule to react, E<sub>a</sub> is the energy barrier and R is the gas constant.

There has been considerable study of thermodynamics in gel formation processes but much less discussion of the rate at which these gels are formed. Indeed, in many cases, gelation requires activation such as heating and cooling or sonication in order for self-assembly to take place. Such systems are not amenable to detailed kinetic study. However, the ability of this two-component gel to form spontaneously on mixing two solutions together made it ideal for kinetic study. In some cases, gelation is fast and instant, such that it is quite difficult to measure the kinetics of gel formation. There have

been a number of approaches to try to measure the speed at which gels are formed<sup>214</sup> but when talking about instant gel formation the measurements become more complex and sometimes impossible. We present here a series of techniques developed to measure evolution in gel formation for various systems (fast and slow) and a protocol is developed for each particular case. The first approach to measure kinetics of gels formation was simply a visual check of gel formation in vials when mixing components – this part of this study was performed in collaboration with Stefan Rohner and has been previously published.<sup>69</sup>

### 2.3.2. Visual kinetics of gel formation.

We qualitatively assessed the formation of gels when combining our range of dendrons and amines as described earlier in the chapter. These combinations are represented in the Table 6 which presents the visual observations of the system at different times after mixing.

t = 1 h	D-Lys	L-Lys	Phe	Ala	Val
Hex	Hard	Hard	Liquid	Soft	Liquid
Naph	Hard	Hard	Partial	Partial	Partial
Phen	Liquid	Liquid	Liquid	Hard	Liquid
t = 2 h	D-Lys	L-Lys	Phe	Ala	Val
Hex	Hard	Hard	Liquid	Soft	Soft
Naph	Hard	Hard	Partial	Partial	Partial
Phen	Soft	Soft	Soft	Hard	Partial
t = 3 h	D-Lys	L-Lys	Phe	Ala	Val
Hex	Hard	Hard	Hard	Hard	Hard
Naph	Hard	Hard	Hard	Hard	Hard
Phen	Hard	Hard	Hard	Hard	Hard

**Table 2-4** Monitoring gelation at three different time points for each two-component system. Soft = viscous liquid; Partial = Partial gel

By the end of the experiment (3 hours), all combinations of amines and dendrons (10mM concentration) had formed stable hard gels. The only clear difference is the speed at which

those gels are formed. In the table, we can observe that the fastest gels to form were combinations of G2 ((Boc)<sub>2</sub>Lys)<sub>2</sub>-Lys-OH based dendrons and Hex and Naph. On the other hand, Phen and combinations of dendrons were quite slow in terms of gel formation except the combination with the alanine based dendron, which was actually relatively rather fast (minutes).

In order to measure the maturation of the gel in more detail, it is necessary to select a physical property that changes as gelation progresses. Such properties can be visual properties such as a transition between liquid to solid appearance (sol-gel transition) as described above, or more specific transition properties such as viscosity, viscoelasticity<sup>110</sup> and spectroscopic properties,<sup>215</sup> even changes in turbidity for a sol-gel transition.

To get a better picture of these evolution of these gels over time, we performed the  $T_{gel}$  experiment after just three hours of maturation time in order to see whether the gels were different to those described above which had been aged overnight. This process of aging is quite important because all gel related properties (rheological, thermodynamics and spectroscopically) will be dependent on the stage of gel formation. However, Figure 2-9 makes it clear that after 3 hours, the gels are actually very similar to those formed after 24 hours, so gelation can be considered to be largely complete in this initial 3 hour period. As such, we need to focus our attention on the first 3 hours of gelation in order to understand the kinetics of assembly.  $T_{gel}$  values in figure 2-10.

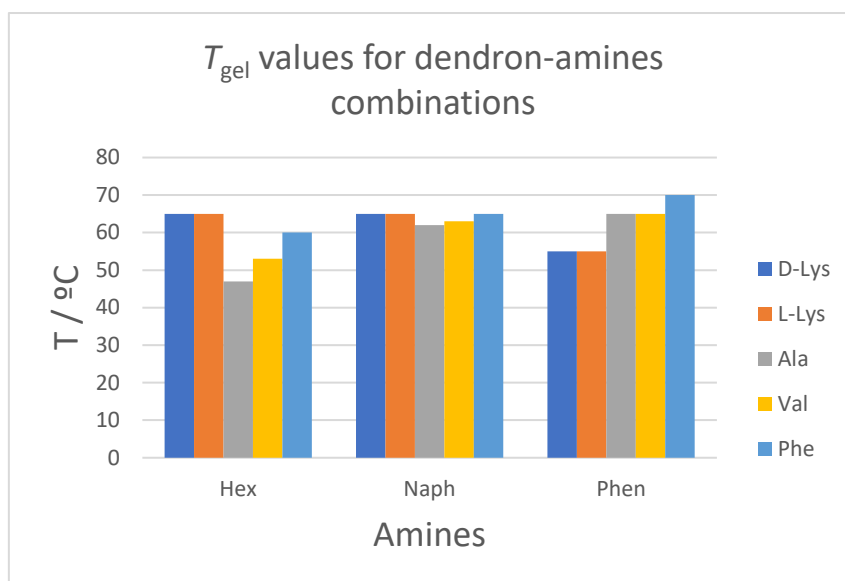


**Figure 2-10:**  $T_{gel}$  values for a range of dendron and amine combinations measured three hours after mixing the components together.

### 2.3.3. Quantitative study kinetics of gel formation.

In order to study gelation rate properly and go beyond our published simple visual study of gelation kinetics, there is a need to use instrumental approaches that are able to detect certain properties of those generated gels in a systematic and quantitative way. This became a key target of my ongoing PhD work after Stefan Rohner had finished his placement in York. Some of the most interesting properties to track in gel formation are the following:

- **Spectroscopic properties** such as polarized light absorption in a circular dichroism spectrometer (CD) – chiral self-assembled nanostructures undergo a significant increase in ellipticity during the assembly process as a result of the formation of chiral nanoscale superstructures.
- **Rheological properties** – as gelation progresses, the  $G'$  value will increase, and the  $G'$  will become an order of magnitude greater than  $G''$ , reflective of gel-type materials behaviour.

- **H-NMR** signals for variable time experiments – on rapid cooling, the length of time required for gel formation, and loss of signal intensity as a ‘solid-like’ network forms, provides an insight into the rate of gelation. This is due to an effect that appears by the rapid tumbling of molecules averages these anisotropic, which are direction dependent, constituent to zero. Because of this, liquid or solution NMR spectroscopy provides very narrow and well-defined peaks in contrast to peaks produced by the substances which are not well dissolved or have solubility problems.

It should be noted that different techniques provide insight into the self-assembly process on different time scales. NMR provides information on what individual molecules are doing, CD reports on the nanoscale assemblies, and rheology reports on the overall macroscopic material. We therefore decided to use each of these tools to track the changing properties over time as the sol-gel transition occurs.

#### **2.3.4. CD Spectroscopy:**

Circular dichroism (CD) Spectroscopy can be considered as a ‘chiral’ form of optical spectroscopy.<sup>216</sup> Basically, it is a technique that employs UV-Vis using circular polarized light, with a detector able to quantify the difference in absorption between right handed and left handed circularly polarized light, which is reported as an ‘ellipticity’ of polarisation. Molecules with no chirality have no absorption band in the CD spectrum. When molecules assemble into chiral nanostructures, a large CD signal appears at wavelengths in which UV-Vis light would be adsorbed. Typically the CD signal associated with assemblies is much larger than that observed for isolated chiral molecules, thus CD is a very powerful technique to demonstrate the presence of chiral nanostructures in the 3D scaffold of gels.<sup>213,217</sup>

#### **2.3.4.1. CD as a Technique for Following the Kinetics of Gelation on the Nanoscale**

A key requirement of the CD technique is that the substances involved in the gel have to be non-absorbent in the wavelength range 200-300 nm. These wavelengths are of interest because peptides absorb at ca. 220 nm, while the aromatic components of some of our gels would absorb at ca. 250 nm. For this reason, the gelation solvent, toluene, was substituted by a mixture of methylcyclohexane and dioxane (95/5) which is optically transparent in this region and has been shown in previous studies to support self-assembly of this type of system.<sup>64</sup> In the following section, we present an example of how to use CD as the technique to track the kinetics of gel formation using the hexylamine based two-component systems. We selected these systems because they show a range of different gelation kinetics under the visual inspection methodology.

#### **2.3.4.2. Protocol of kinetics of gel formation by CD.**

We used CD spectrometry to study the kinetics of assembly of hexylamine-based gels. There were two different of approaches to studying gel formation kinetics:

1. In **hot conditions**. The two components (amine and dendron) are introduced into the CD cell and heated with a heat gun until the gel forms a hot sol. The sample is then introduced into the CD instrument and allowed to cool under ambient conditions until gel assembly occurs.
2. In **cold conditions**. The solutions of components are mixed in the CD cell once it has been introduced in the instrument and data are then collected of gelation kinetics. This approach has fewer thermal errors (e.g. initial temperature, cooling rate etc.) and should give better data.

We chose to use both different methods, as the kinetics of gel formation can depend heavily on the available surrounding thermal energy and we reasoned it would be useful

to gain insight into the possible variations that can appear on the kinetic process to nanoscale assembly and also determine which method is more effective.

#### 2.3.4. CD in hot conditions

In order to monitor the assembly of the gel, we probed the CD signal at 221.5 nm over time on mixing and heating solutions of the dendron and amine (final gel concentrations of 10 mM). The wavelength was selected because it coincides with the maximum absorbance in the CD when the gels is formed in such concentration and solvent conditions. This signal is associated with the intermolecular self-assembly of the peptide groups in the dendron, which have a chromophore at this wavelength. This gives rise to the data in Table 2-5,

Hex-Lys HOT	
CD signal	time (s)
-23.51	11
-32.2	33
-154.38	55
-165.35	78
-167.65	97
-167.73	115
-168.17	146
-167.44	165
-167.88	188

**Table 2-5** Progression of CD signal Vs time at 221.5 nm for the Hex-Lys gel formation.

which can also be plotted in the form of a graph, as shown in Figure 2-11.

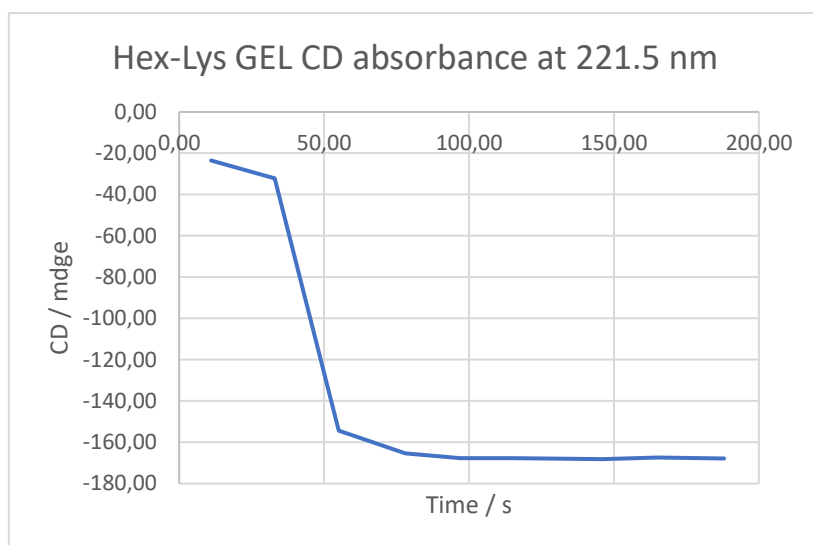


**Figure 2-11:** Elliptical Absorbance Vs time of Hex-Lys gel under hot conditions

If we describe the process reflected in the graph it can be said that the experiment starts with a very small CD signal indicative of dissolved molecular scale components with no self-assembly being observed. At some time, point (around 30 s) the CD signal starts to increase significantly until it reaches its maximum intensity at a time of 55 seconds. This increase in CD signal is consistent with the self-assembly of the molecular building blocks into nanoscale fibres, which have an amplified CD signal as a result of nanoscale chirality. Clearly, this process is fast, being essentially complete in 30 seconds under these conditions – after 1 minute, a plateau value is reached, indicative of complete assembly into chiral nanoscale objects.

We then went on to perform the same experiment for the other gels based on hexylamine with each of the different peptide dendrons. In each case, we had to monitor a slightly different wavelength, as the different amino acids present in the dendron changed the  $\lambda_{\max}$  value as a result of perturbing the chromophore. The wavelengths used are presented in Table 2-6.

Compound	Wavelength / nm
Hex-Lys	221.5
Hex-Ala	206.5
Hex-Val	216.5
Hex-Phe	236.5

**Table 2-6** The  $\lambda_{\max}$  values for each of the different dendron-amine

The same data analysis was then performed on each of these other hexylamine based gelation systems giving rise to Figures 2-12, 2-13 and 2-14.

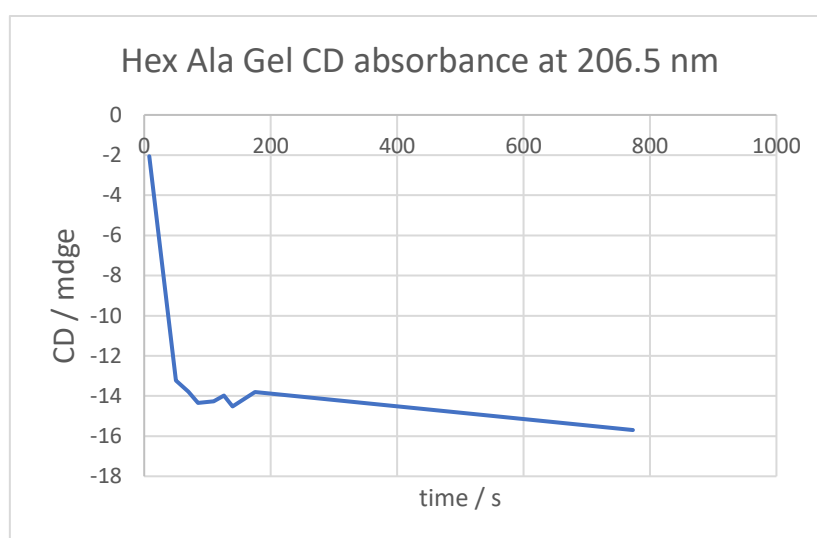


**Figure 2-12:** Variation of the CD signal for the Hex-Ala gel for a 206.5 nm.

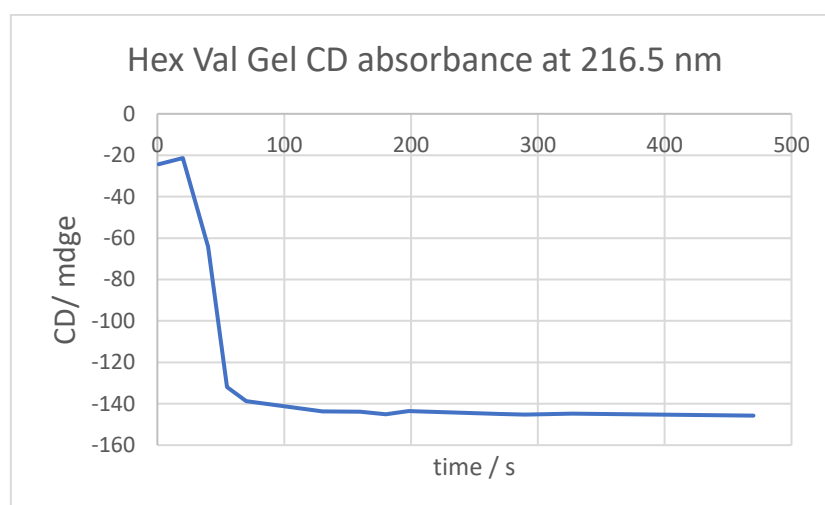


**Figure 2-13:** Variation of the CD signal for the Hex-Val gel for a 216.5 nm.

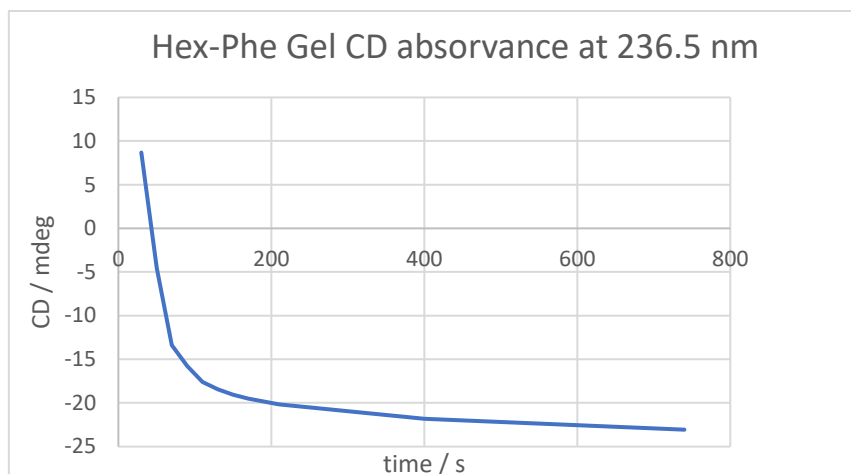


**Figure 2-14:** Variation of the CD signal for the Hex-Phe gel for a 236.5 nm.

In each case, the gelation process is relatively fast, and is complete in less than 100 seconds. Of all the gelation systems, that based on the phenylalanine dendron appears to show the slowest increase in CD signal. This agrees with the observation from visual experiments in which the Phe-Hex gel was formed significantly more slowly at room temperature (several hours) than any of the others: Hex-Lys gel (<1 hour), and Hex-Ala gel and Hex-Val gel (< 2 hours). It is evident, however, that at elevated temperatures of this experiment, the kinetics are very significantly faster, as a result of the thermal energy available to the system, which will help it overcome the energy barrier associated with self-assembly. It is important to note that all of the final gelled systems show very different CD spectra, as would be expected given that they are composed of different amino acids. In Figure 2-15, It is noticeable that Hex-Lys gel and Hex-Val gel have the largest CD signals, while those for Hex-Ala gel and Hex-Phe gel are significantly smaller. This may suggest different packing into chiral nanostructures dependent on the precise nature of the amino acid side chains.

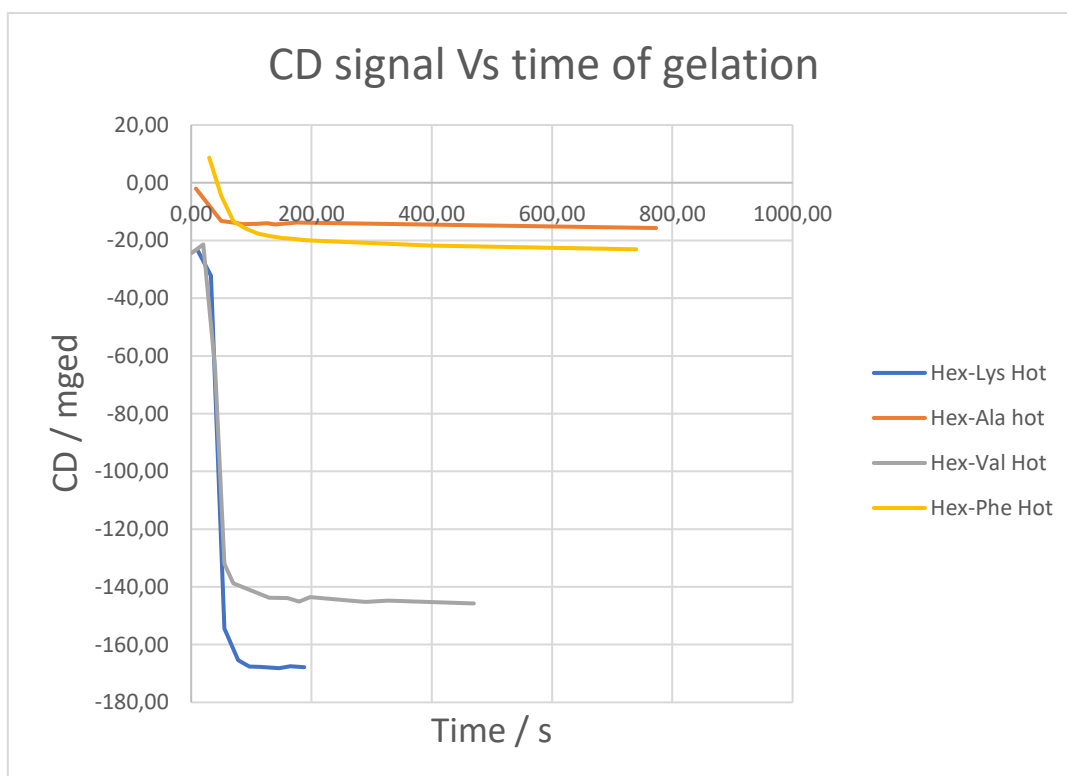


**Figure 2-15** Representation of the various CD absorbance experiments for each tested component.

### 2.3.5. CD in cold conditions.

We then performed CD studies of the room temperature gelation of the same family of systems based on hexylamine on mixing room temperature solutions of the dendron and amine (Final gel concentrations of 10 mM ). Unfortunately, we were unable to study the phenylalanine dendron, as its solubility was too low in the replacement solvent of methylcyclohexane-dioxane 95/5. The results are represented in Figure 2-16.

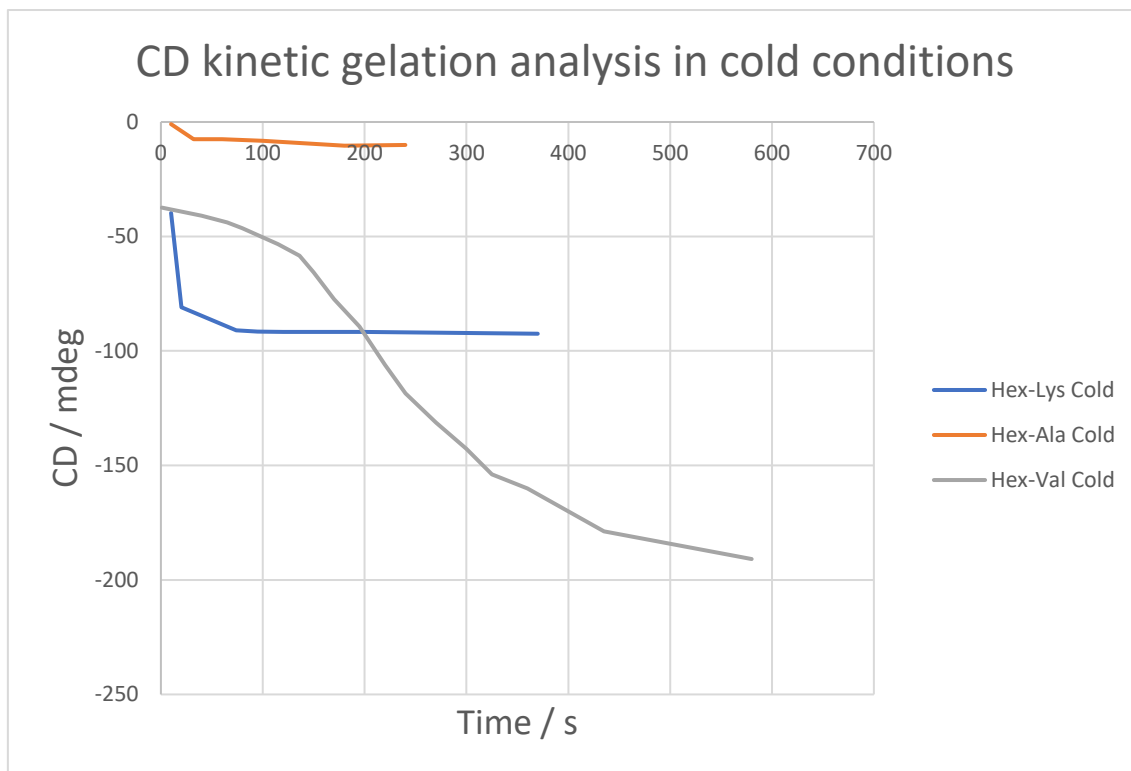


**Figure 2-16** Comparison of CD signal progressions when the two components are mixed in ambient conditions.

We observed that in this experiment, Hex-Lys gel and Hex-Ala gel rapidly progressed into their assembled state and reached a plateau region. For Hex-Val gel, however, the progress of assembly was significantly slower. This is in agreement with the visual observations of gelation, which had shown that this system also took longer to form gels in toluene.

In terms of CD intensity, it is interesting to note that once again Hex-Ala gel  $\ll$  Hex-Lys gel or Hex-Val gel. However, under these ambient conditions, there are some differences in the absolute final intensity values compared to the systems formed at elevated temperatures. Although the Hex-Ala gel forms an assembled system with a similar intensity, Hex-Lys forms a gel with an ellipticity of ca. -100 mdeg, rather than ca. -165 mdeg in the hot experiment. This suggests there are some differences in the self-assembled state that is formed dependent on whether the experiment is hot or cold.

Similarly, Hex-Val gel forms final states with different ellipticities, ca. -140 mdeg in the hot experiment and ca. -200 mdeg in the cold experiment. Overall, this suggests that the evolution of the gel state is somewhat different depending on the thermal energy available to the system. It is well understood that gel-phase nano-assemblies are metastable kinetically trapped states and that the conditions of their formation can affect their structures – these experiments support this view, and emphasise the importance of carefully considering the effect of experimental conditions when performing kinetic experiments on gels, as they can have very significant impacts, potentially changing assembly pathways as well as just kinetics.

### **2.3.6. Conclusions of CD kinetic experiments.**

CD spectroscopy allowed us to monitor the kinetics of nanofibre assembly, and also provide insight into the final state of the chiral nanostructures formed. We selected the structures including hexylamine for study via this technique because, under the visual inspection approach, they had shown a range of different gelation kinetics. Overall, under hot conditions, the phenylalanine dendron showed the slowest assembly by CD, and at room temperature conditions, the solubility was insufficiently good for it to be studied. This would suggest a significant energy barrier to gel formation. The next slowest assembly was that of the valine-based dendron, which in particular showed slower assembly at room temperature than in the hot experiment, as would be expected based on the thermal energy available. The other two dendrons both exhibited rapid nanofibre assembly under all conditions. The final CD spectra of the self-assembled systems were quite different, in part as a result of the different amino acids used in the construction of the four dendrons. Hex-Val gel and Hex-Lys gel had larger CD signals than Hex-Ala gel and Hex-Phe gel. Interestingly, the final CD signals were different depending on the

conditions under which the nanofibres were assembled - hot or room temperature, demonstrating that dependent on the thermal energy available in the system, different self-assembled states can be accessed. The concept of energy landscapes is increasingly well-known in assembly processes.<sup>26</sup>

### **2.3.5. Rheology as the technique for studying kinetics of gel formation on the macroscopic length scale.**

#### **2.3.5.1. Introduction**

Rheology is the optimal technique<sup>106,108</sup> to use to study the macroscopic viscoelastic properties of gel-phase materials. There is an intimate relationship between the macroscopic properties of materials and their micro and nanoscopic structure. Viscoelasticity is a macroscopic property that results from the supramolecular interactions between the various molecules present in a material although rheological studies are a standard way of characterising gel-phase materials, they are very rarely used to probe gelation kinetics. We reasoned that our system, based on simple mixing of two solution phase components, offered a unique opportunity for this kind of investigation.

The sol–gel transition is the process in which gel components are in solution and progressively start to interact by means of supramolecular interactions and self-assemble into nanostructures which eventually form a sample-spanning network that supports the gel. By performing this experiment on the rheometer stage, we reasoned that we could macroscopically detect the assembly of the gel-phase network in situ – a unique way of probing the kinetics, and rheological ageing of a two-component gel.

### 2.3.5.2. Experiment design and strategy of Rheology in cold conditions.

To study this transition and investigate the macroscopic kinetics of gel formation, an experiment was designed to monitor the variation of viscosity properties of the sol-gel transition over time. Such a variation was initially being measured at room temperature by mixing the two components under ambient conditions on the rheometer stage. The rheometer was programmed to record viscoelastic values (viscosity program). A toluene 1 mL solution of dendron (10 mM) was introduced into an aluminium weighing boat in which the viscosity analysis was going to be performed. The aluminium vessel was placed in the rheometer and the probe was placed touching the solution of dendron. The rheometer was then activated and starts to record typical values of viscosity for a solution. At time = 0, we then rapidly added the 1 mL solution of another component (amine, concentration = 10 mM, which means final gel concentration of 5mM) into the aluminium vessel. From that moment, the two components will in principle start to interact and the viscosity will increase as the sol-gel transition progresses. The increase in viscosity over time can be analysed both to determine the kinetics of the process, and the final viscosity of the resulting self-assembled gel.



**Figure 2-17** General scheme of the process of collecting a progression of viscosity from solution state of components to the sol-gel transition triggered by the addition of the second component.

Figure 2-17 presents typical data for this experiment as performed using the combination of G2 ((Boc)<sub>2</sub>Lys)<sub>2</sub>-Lys-OH based dendrons and Hex amine. This Figure illustrates the disposable aluminium vessels used to perform the viscosity experiments. It is worth mentioning that toluene could evaporate, so these experiments were as fast as possible to limit problems with solvent evaporation and that is why it was maintained covered to minimize solvent evaporation. It can be observed that in the experiment, the elastic modulus (in Pa) increased rapidly, suggestive of a fast self-assembly step, and then continued to increase more slowly over time, suggesting that the gel-phase network continues to evolve diffusing the components or aging slowly over time. This is in agreement with a hierarchical assembly model<sup>218</sup> in which a network may rapidly assemble, but then the nanoscale fibres underpinning the network slowly reorganise in order to optimise the strength of the overall macroscopic material. As such, this technique provides insight not possible using the molecular scale (NMR) or nanoscale (CD) experimental methods, which only report on either molecular immobilisation, or nanofibre formation respectively. Interestingly, when using CD spectroscopy as described above, we observed that for this Hex based gel system, the maximum signal at one wavelength was achieved after 30 seconds. Clearly in rheology, however, we see that macroscopically, the assembly was not truly complete at this point. CD indicates that chiral nanostructure formation was complete at this point, but clearly rheology shows us that these nanofibres could assemble and rearrange in order to form the optimal three dimensional sample spanning network on the macroscopic length scale. That process is what we can uniquely observe on the rheometer stage. Indeed, in rheology, we observe the maturation of the network,<sup>219</sup> which is also impossible to observe visibly, because once the gel is formed, we normally consider the experiment to be complete. As such, in

principle our new rheological method can provide insights into the gel forming process that cannot be achieved using other approaches.

We tested all 12 combinations of dendron and amine using this approach. Consequently, rheograms were measured for each of these combinations, and Figures 2-18, 2-19 and 2-20 present the elastic modulus vs time in each case.

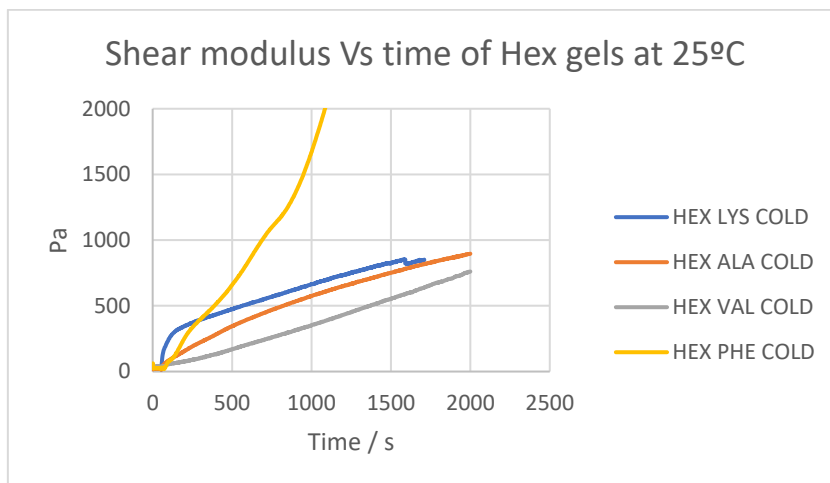


**Figure 2-18:** Rheogram which shows the progression of gelation in Hex gels at 25°C.

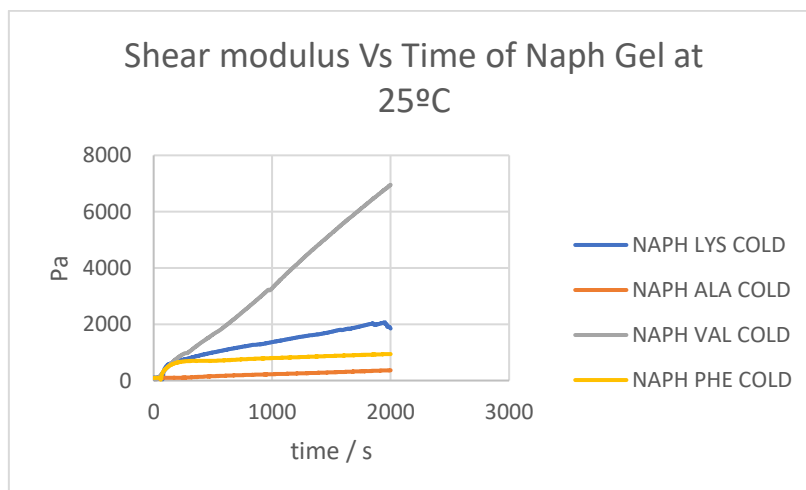


**Figure 2-19** Rheogram which shows the progression of gelation in Naph gels at 25°C.

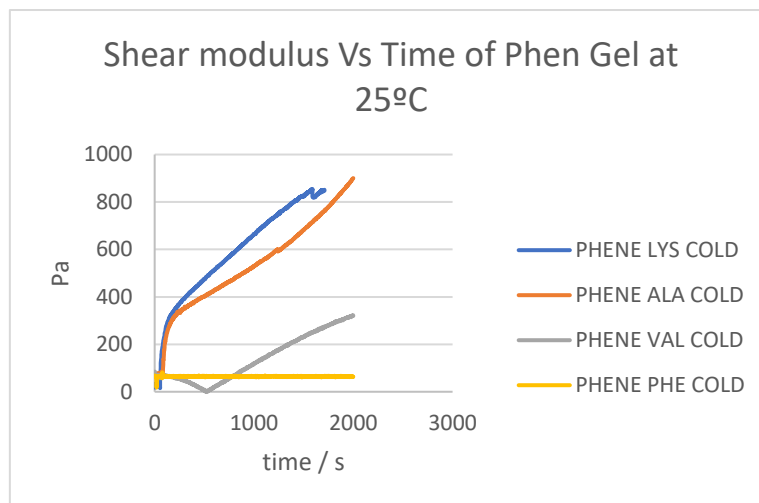


**Figure 2-20** Rheogram which shows the progression of gelation in Phene gels at 25°C.

Different gels exhibit quite different types of rheological responses over time. In some cases, the kind of two-step response described earlier is observed. In other cases, a more linear increase in modulus over the timescale of the experiment is observed, which could indicate that gel network formation proceeds more slowly over the timescale of the experiment. In some other cases, very little increase in modulus is seen, which would perhaps suggest inefficient gel network building under the conditions of imposed shear on the rheometer plate. In particular, we decided to focus in on the gels which form in a two-step process because the kinetics were clearer to process mathematically.

### **2.3.5.3. Treatment of kinetic rheological data.**

We made some attempts to treat the data to obtain kinetic insight – in particular, we focussed on the initial linear gel building region, and aimed to determine the relative rate at which this network formation was taking place. For example, Figure 2-21 shows how we divided the plot into two regions – an initial gel building stage, followed by a second gel maturation or selfdiffusion step.

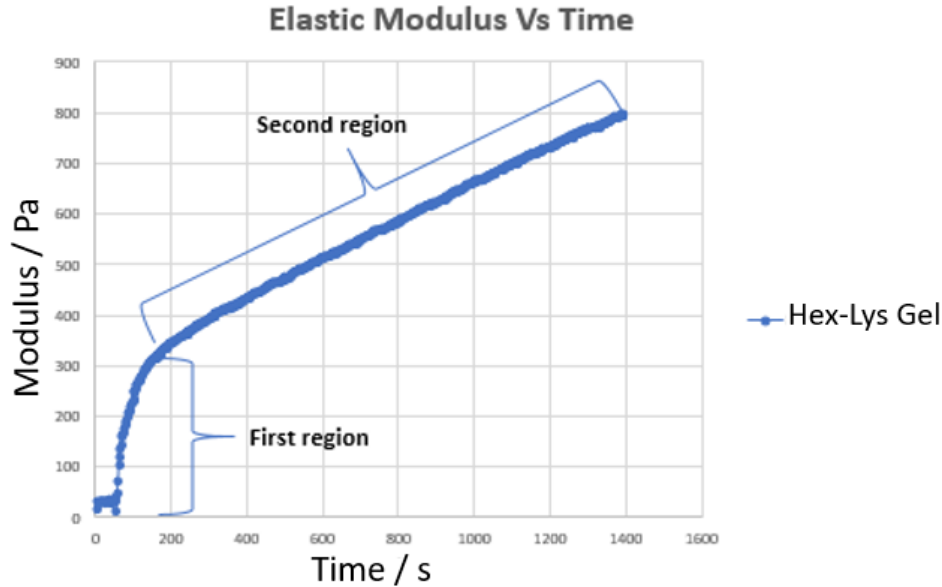


**Figure 2-21** Typical rheogram of elastic modulus versus time. Notice the two regions that there are in there are in graph.

The selected method was to fit the initial increase of elastic modulus on mixing the two components to an exponential function in order to determine an apparent rate of assembly for this rapid gel building step (first stage of gelation). We note that linear fitting gave a reasonable approximation to the second observed region of maturation., Therefore a fitting was prepared which has two different components, an exponential initial step followed by a linear region. It is not clear in these cases what kinetic model should be applied to the process of macroscopic network building, but we reasoned this empirical approach would allow us to obtain useful comparative data.

The equation that was fitted to the observed kinetic behaviour was equation 2-4.

$$y = n + mx + A \cdot e^{kx} \quad \text{Equation 2-4}$$

Where n and m represents the components of the linear behaviour and the A the factor that multiplies the exponential part of the fitting.

The equation incorporates the linear and exponential behaviour that is observed in the kinetic experiments. This equation was then fitted as an approximation of least squares

deviation to optimise the parameters of the equation (m, n, K). The fitting of the experimental data for HexGel is illustrated in Figure 2-22. The key parameters extracted from this fit are presented in Table 2-8.

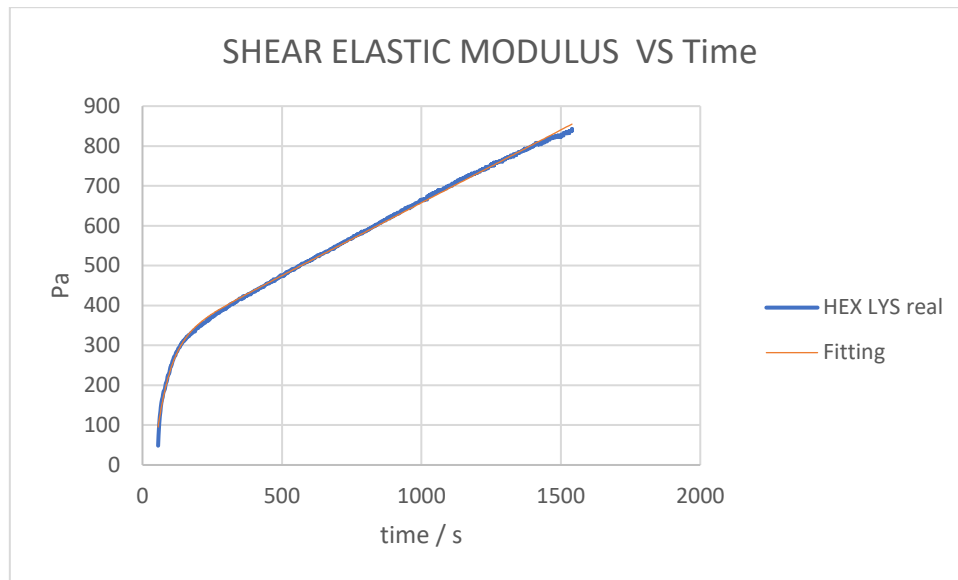


**Figure 2-22:** Fitting of the two different regions for the gel formation process of Hex Lys Gel.

The resulting equation which is fitted is therefore:

$$y = 292.28 + 0.37x + 217.70 \cdot e^{1.986E-2 \cdot x}$$

n	m	A	k
292,28	0,37	217,70	1,986E-02

**Table 2-7** Table with the parameters of the calculated curve that is adjusted to the gelation of Hex Lys.

The exponential part of this equation corresponds to the region in which gelation occurs really fast and the elastic component grows really quickly, so it is considered that the k value corresponds to the kinetic constant of this initial rapid gel assembly step. Apart from that, in the linear region, the value of the rate at which diffusion processes or aging occurs also has a rate, which is given by the m value of the equation which is the slope of the linear behaviour. Both terms are expressed in the table 2-9.

m	K
0,37	1,986E-02

**Table 2-8** The term m linear and k exponential of the fitting for kinetics for Hex Lys gel.

In this case, linear fitting of the macroscopic network growth region gives a slope of 0.37 Pa/s which can be considered an approximation of the rate of macroscopic change when mixing the two components in the rheometer. A set of gels were then studied using the same approach so that the relative data could be compared. Figure 2-23, 2-24 and 2-25 present the fitting of rheological kinetic studies of these gels and Table 2-10 collects together the extracted data.

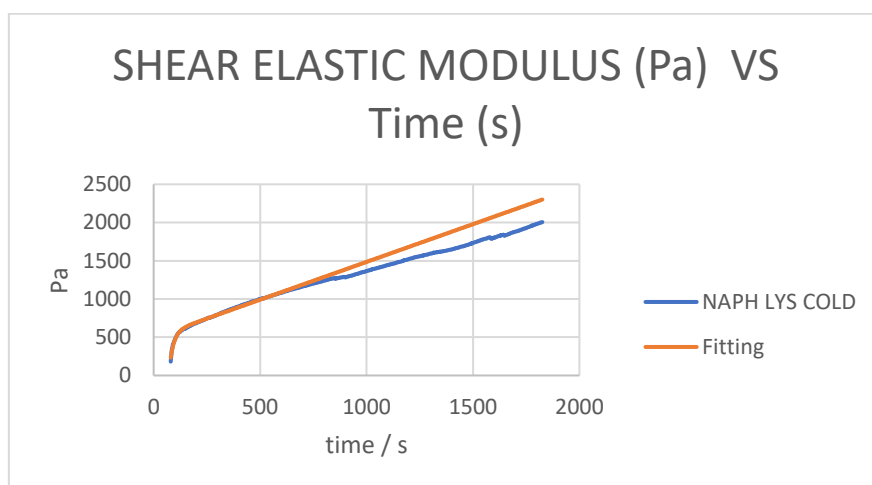


**Figure 2-23** Fitting of the two different regions for the gel formation process of Naph-Lys Gel.

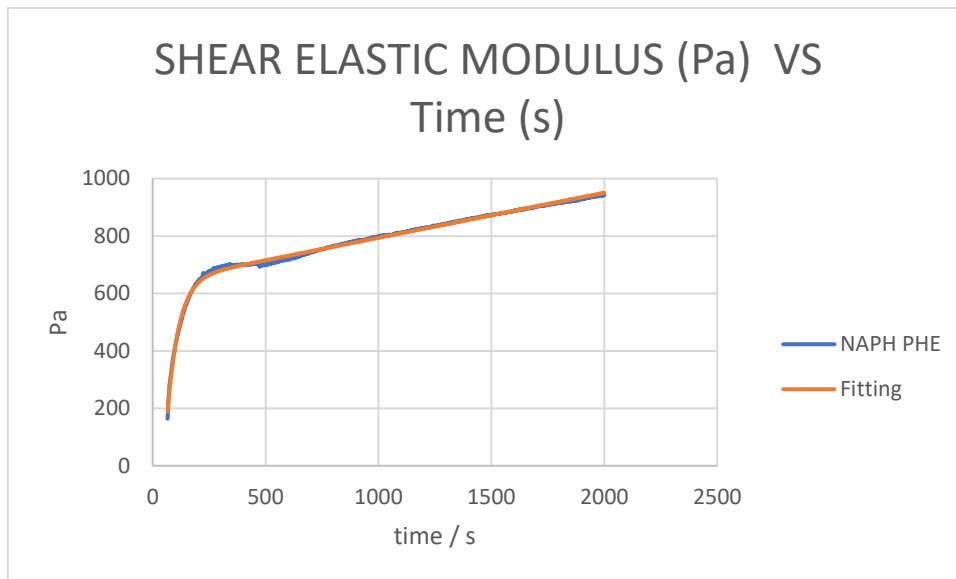


**Figure 2-24** Fitting of the two different regions for the gel formation process of Naph-Phe Gel.

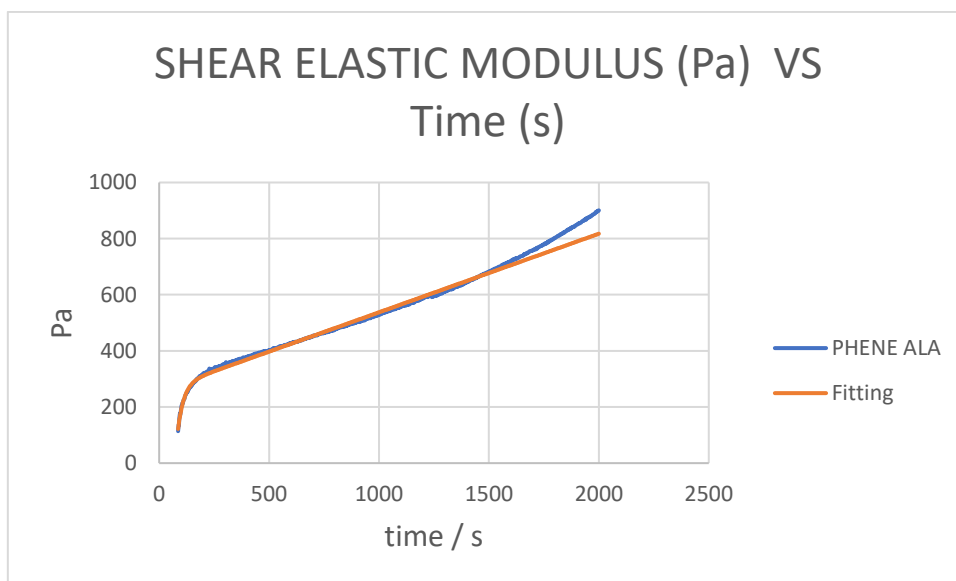


**Figure 2-25** Fitting of the two different regions for the gel formation process of Phen-Ala Gel.

	m	m <sub>rel</sub>	k
Naph-Lys	0.73	3.65 x 10 <sup>-4</sup>	4.86 x 10 <sup>-2</sup>
	m	m <sub>rel</sub>	k
Phen-Ala	0.28	3.11 x 10 <sup>-4</sup>	3.63 x 10 <sup>-2</sup>
	m	m <sub>rel</sub>	k
Hex-Lys	0.37	4.30 x 10 <sup>-4</sup>	1.99 x 10 <sup>-2</sup>
	m	m <sub>rel</sub>	k
Naph-Phe	0.16	1.74 x 10 <sup>-4</sup>	1.96 x 10 <sup>-2</sup>
	m	m <sub>rel</sub>	k
Phen-Lys	0.34	3.58 x 10 <sup>-4</sup>	1.26 x 10 <sup>-2</sup>

**Table 2-9** Set of values of m (linear part) and k (Exponential part) of the various gels analysed.

In the table 2-9 m<sub>rel</sub> is the relation between the maximum value of m and the maximum level of signal that is reached in the experiment. The order of compound in the table is according to the value of the kinetics of the exponential part. Having a maximum value of kinetics for the Naph-Lys GEL system and the lowest value for the Phen-Lys GEL:

$$k_{\text{Naph-Lys}} > k_{\text{Phen-Ala}} > k_{\text{Hex-Lys}} > k_{\text{Naph-Phe}} > k_{\text{Phen-Lys}}$$

This is in agreement with the visual observations of gel formation, in which it was noted that Naph-Lys and Hex-Lys formed gels more rapidly than Phen-Lys. Furthermore, simple visual observation also demonstrated that Naph-Lys assembled into a gel more rapidly than Naph-Phe. Furthermore, Phen-Ala had already been identified (see above) as one of the more rapidly assembling systems. As such, the rheology experiment allows us to quantitatively compare these initial gel formation rates, suggesting that for Naph Lys (the fastest of these systems) is ca. 4 times larger than that for Phe-Lys (the slowest of these systems).

We also calculated relative m values, with the m (gradient of linear increase) being divided by the maximum level of signal that is reached in the experiment so they can be

compared. According to the data of the linear part there is a trend in gelation.  $m_{rel}$  relative values have no units.

$$m_{rel} \text{ Hex-Lys} > m_{rel} \text{ Naph-Lys} > m_{rel} \text{ Phen-Lys} > m_{rel} \text{ Phen-Ala} > m_{rel} \text{ Naph-Phe}$$

This would suggest that after taking place most of the gelation there is still a remaining amount of free available gelators that could diffuse under the rheology probe due to the small gap between the bottom of the aluminium plate and the rheology probe.

### **2.3.5.5. Conclusions on the kinetics rheology experiment**

As conclusions we can propose that the exponential component is more related to the gelation process as visualised by the naked eye when the two components are mixed together. We then consider the linear part to correspond to a process that could be related with slower aging of the material which cannot normally be visualised or the slow diffusion of gelator that is constantly diffusing after most of the gelation takes place. This may suggest that size of the gap left in between aluminium plate and rheology probe and the specific geometry of the rheology experiment can affect to this potential diffusion process that could affect the rheogram as seen in the presented results.

Other kinetic experiments (Hex-Ala, Hex-Val, Hex-Phe, Naph-Ala, Phen-Val, Phen-Phe) did not show the exponential behaviour when mixing the cold components. Instead, the behaviour was remarkably linear so the kinetics of gelation was given basically for the linear fitting and the relative slope of the curve.

Talking about the discrepancies, if we compare the various approaches that have been used to study the various gel combinations, it turns out that there are some miscorrespondences. For example, Hex-Phe gels are visually slow forming systems that took at least 2 hours' time to get the gel formed. (Table 2-10)

Hex-Phe	
time	Appearance
First hour	liquid
Second hour	liquid
Third hour	Hard

**Table 2-10** Visual transformation of Hex-Phe cold mixture.

However, the CD technique showed that for this system there was a rapid formation of gel till a stable CD signal level of -25 that was reached at 750 seconds (12 min) approx. (Figure 2-26), that is to say, from a nanoscopic point of view there was formation since the beginning of the mixing of components (Hex-Phe). We have to bear in mind that the CD measurements are performed using a similar solvent that could modify the gelation properties and thus a kinetic experiment should be considered qualitatively.

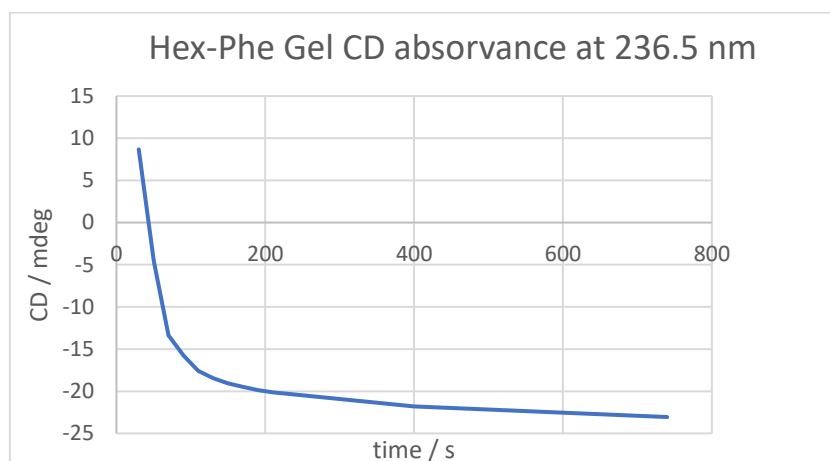


**Figure 2-26** CD absorption spectra of the Hex-Phe gel system Vs time.

Finally, if we look to the rheological results of simple cold mixing for the same gel system we find that there is a constant increase of elastic modulus to very elevated levels compared to the other tested systems (Figure 2-27).

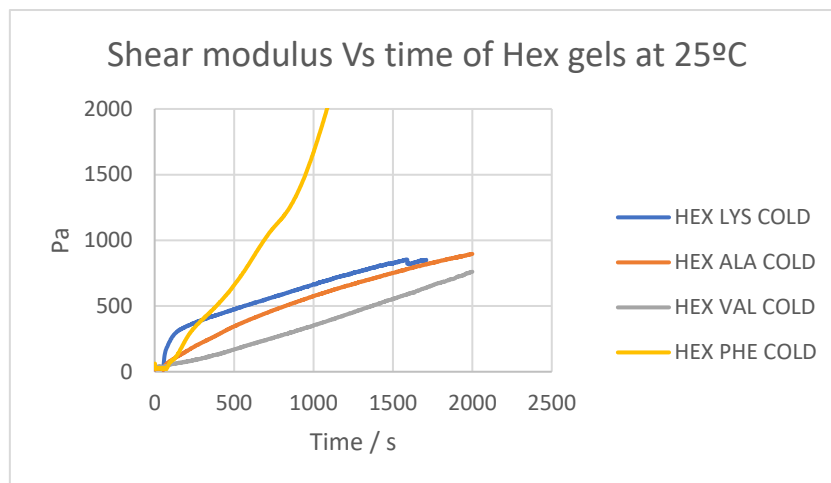


**Figure 2-27** Rheogram of the formation of various amine-dendron systems.

The conclusion to this discrepancy could be caused because the various techniques have naturally different possible ambient conditions. That's why one of the main conclusions and future possible plans must be the cautious repetition of every experiment, paying attention to the particular misbehaviours and discrepancies to substances that appear to behave differently depending on the chosen technique. In the case of future studies using the presented approach the separation between plate and torsional probe has to be sufficiently separated one from another to ensure total and easy diffusion of components while testing the elastic modulus increase when mixing components. Possibly the potential problems that have to be overcome are related to the practical aspect of sample preparation rather than the nature of the components themselves.

Another discrepancy can be the one corresponding to the system Phen-Lys gel which forms slowly (from a visual perspective) and very fast when it is tested under rheology. (Figure 2-28)

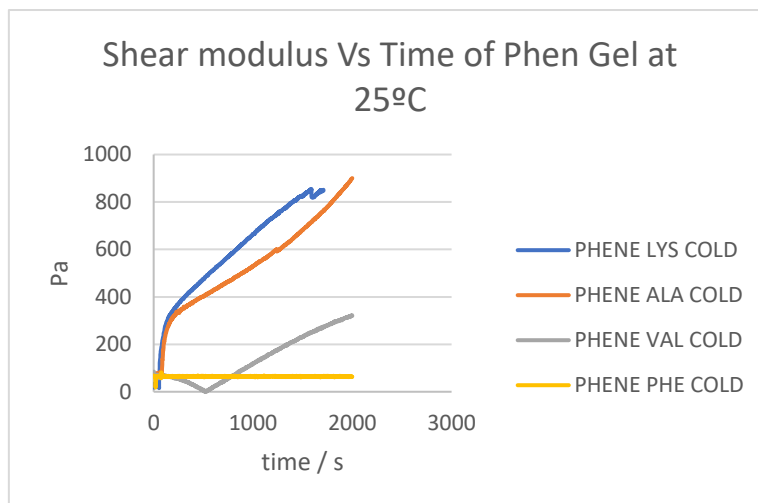


**Figure 2-28** Rheological test of Phen based gels.

Only the fast formation of Phen-Ala gel is comparable with the rate at which the Phen-Lys gel is forming. In this case we see an exponential behaviour at the beginning and a linear increase (or maturing) of the elastic modulus after such initial period. This discrepancy can be due to several reasons that could affect to the experiment. The movement of the plate in rheology can affect to the formation of nucleation points for the later gelation process if this was true such perturbation could affect in the same manner to the other tested systems.

In principle now, considering the data as a whole, we can see that the fastest gelation rates are generally achieved by the gels based on the lysine amino acid component as dendron. Amongst the amines, naphthylamine (and to a lesser extent hexylamine) generally give rise to the fastest macroscopic gel formation processes, while phenylethylamine was significantly slower. Pleasingly, this is in good general agreement with the visual observations of gel formation kinetics made above, and also agrees with the CD studies of hexylamine based systems, in which Lys-Hex was demonstrated to be one of the fastest systems in terms of gelation kinetics

It is worth considering if the results obtained using these techniques were satisfactory. This method is, overall, better applied for systems which are very fast like the gels Hex and Naph but less ideal for systems which are extremely slow in terms of kinetics such as some of the Phen Gels –. Nonetheless, we were able to use this method to detect significant differences in gelation kinetics, such as the more rapid gelation of Lys dendron based systems, and the slower overall gelation of phenylethylamine based systems, however limitations of the methodology mean precise numbers should be treated with some caution.

### **2.3.6. NMR as a molecular-scale technique for the study of gel formation.**

Solution phase NMR is a technique that allows the user to track molecules which are mobile in the deuterated NMR solvent, but, as outlined earlier in the chapter, molecules which are part of the ‘solid-like’ gel network will present very broad signals and essentially be invisible in the spectrum. As such, NMR provides a technique to visualise on the molecular scale whether individual molecules are being incorporated into the solid-like network, and hence is complementary to CD methods (nanoscale) and rheological studies (macroscale). We therefore designed an NMR experiment to gain insight into the gel assembly process.

#### **2.3.6.1. VT-<sup>1</sup>H-NMR for studying kinetics of gel formation**

As an approach to kinetics of gel formation from a molecular point of view we wanted to develop a technique based on quantitative <sup>1</sup>H-NMR that could allow us to track the gel formation. The methodology we developed was based on starting with a 5 mM gel in the NMR tube. The sample was then heated from 25°C to 90°C in steps of 5°C in order to convert the gel into a sol. This part of the experiment is as described previously in the thermodynamic study, and indeed thermodynamic data could be derived from this approach. Once the sample had equilibrated at 90°C, the NMR spectrometer was set to

cool rapidly to 25°C and maintained there for several minutes while performing  $^1\text{H-NMR}$  analysis at fixed time points in order to determine the concentration of components as gel formation progresses on cooling. Figure 2-28 illustrates the  $^1\text{H-NMR}$  spectra obtained over several minutes with the system being cooled to 25°C after being at 90°C at the end of the VT- $^1\text{H-NMR}$  cycle. As such, we performed all of our NMR experiments in a single cycle. A fast heating process to 90°C and a rapid cooling, followed by NMR at fixed timepoints to gain insight into assembly kinetics on the molecular scale as in Figure 2-31.

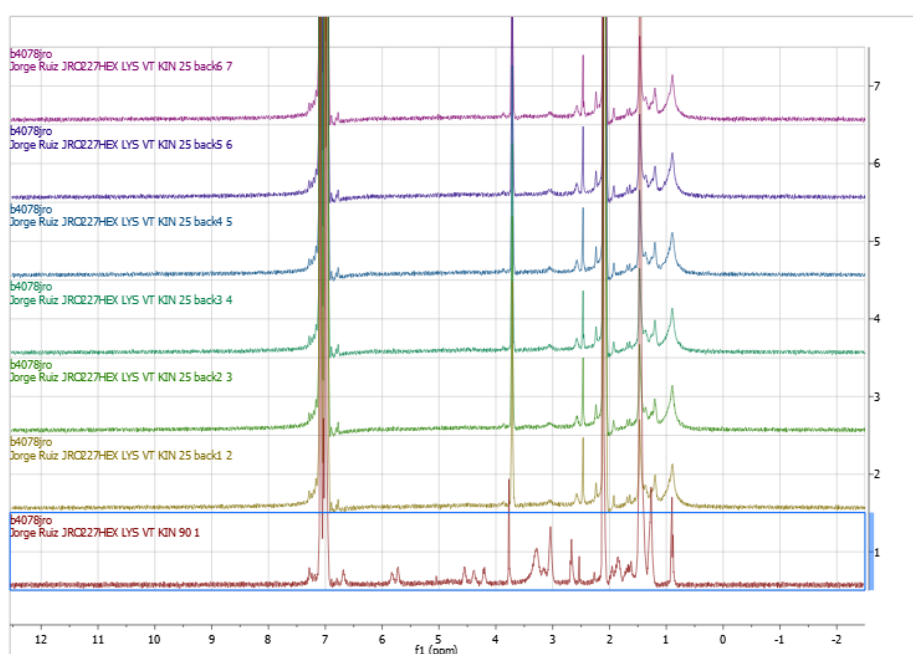


**Figure 2-29:** Several spectra of the gel being cooled down from 90°C to 25°C and retained to that temperature while analysing that.

After picking one by one the peaks corresponding to each dendron in every sample, data was determined from one of these experiments are presented in Table 2-11.

Time min	Probe temperature °C	[G2 ((Boc) <sub>2</sub> Lys) <sub>2</sub> -Lys- OH] mM
0	90	4.2
14	25	0.5
26	25	0.65
38	25	0.45
49	25	0.75
61	25	0.75
72	25	0.7

**Table 2-11** Time of the process of cooling and gel formation versus concentration of free available Dendron in the deuterated solvent in the NMR tube.

The data in Table 2-13. is the accumulated time in minutes versus dendron concentration for the experiment of cooling down the tube in the NMR machine after the maximum temperature of 90°C has been reached. If we represent this table in a graph of concentration vs time, for the Hex-Lys Gel we obtain Figure 2-29.

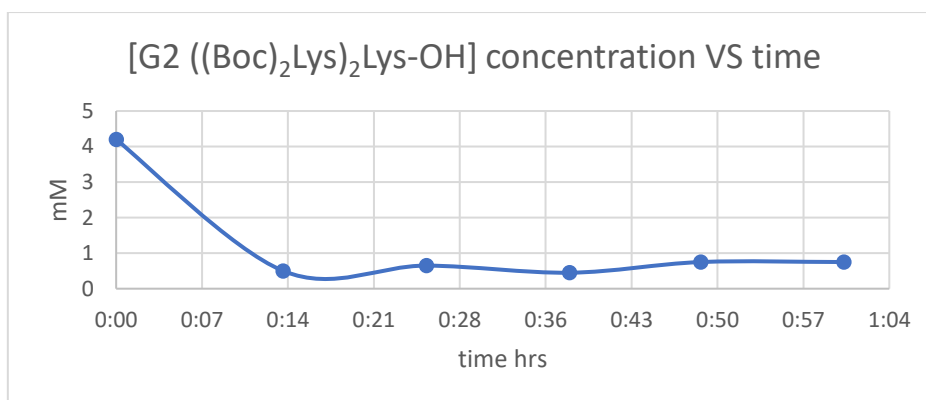


**Figure 2-30:** Concentration of G2 ((Boc)<sub>2</sub>Lys)<sub>2</sub>-Lys-OH dendron mM Vs cooling time min. Starting from the temperature of 90°C to 25°C during several minutes.

The progress of this gelation is very fast and under these experimental conditions we cannot actually monitor the decrease of dendron concentration. Indeed, by the first measurement point at 14 minutes, gelation was essentially complete. If the gelation process had been slower, we would have observed a gradual decrease in dendron concentration. In contrast, we see that when gel is cooled down and the first acquisition

made, the dendron concentration is already very low, and it would appear that on the molecular scale, gelation is essentially complete. However, we already knew that the Hex-Lys gelation system was particularly rapid, and we therefore believed that this approach may shed more light onto the gels which were formed more slowly. We tested each of the combinations of amines and dendrons and the data are presented in Figure 2-30.

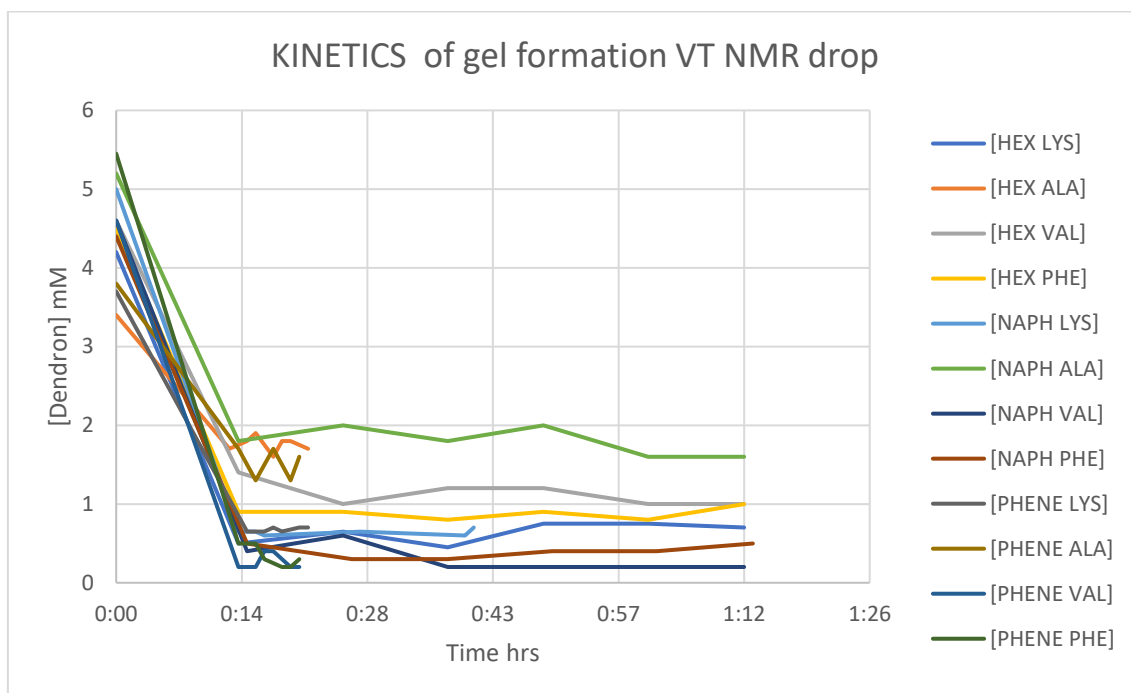


**Figure 2-31:** Concentration drop of the various combinations of dendrons and amines in the cooling experiment.

The result of this experiment, however, is that none of the tested combinations gave us a clear gelation kinetic trend because in each case, gelation was essentially complete after 14 minutes under cooling conditions. This was somewhat surprising as under ambient conditions, many of these gels took >1 hour to form which was consistent with the CD data. There could be possible reasons for the rapid gelation under these conditions:

- i) Gelation starting from 90°C under ambient cooling to 25°C is very fast as a result of the large amounts of thermal energy allowing the molecules to overcome the energy barrier for self-assembly.

- ii) The ability of NMR to report on molecular scale assembly, may indicate that the molecular scale self-assembly is somewhat faster than the formation of the overall macroscopic gel, which occurs more slowly.
- iii) The time needed for the gel to completely melt and convert into the solubilized form was not enough for the sample to stabilize at 90°C.
- iv) Gelation process occurs within the initial 14 min where the temperature is lowering rapidly and triggering the cascade self-assembly process for each tested system.

Although the method as applied here was not effective in measuring differences in gelation kinetics between each of the different systems, we believe the method is highly applicable to gel systems that have gelation times on the order of minutes-hours – or could be useful if applied with shorter timepoints between each NMR measurement. In particular, this is a potentially highly efficient way to determine both thermodynamic and kinetic insights from a single VT NMR cycle, which we believe could be of very high value in terms of gelation future studies

#### **2.4. Chapter Conclusions.**

We synthesised a family of dendron acids based on a lysine unit functionalised with peripheral amino acids – either lysine, alanine, valine or phenylamine. Interaction of these dendron acids with three different amines gave rise to gel-phase materials. Thermodynamic study of the gels based on phenylethylamine demonstrated that the most thermally stable two-component gel incorporated the Phe dendron, while Val and Ala

were less stable. However, intriguingly, the rates of formation of each of these gels were in the opposite order, with the Ala dendron rapidly forming gels with this amine, while Val and Phe were significantly slower. This led us to be interested in studying the kinetics of assembly process, and in particular to understand this process on multiple length scales. The two-component nature of this system, and the ability to form gels on simple mixing made it particularly amenable for study.

Three different methods have been utilized in order to screen the dynamic behaviour in the formation of gels. Rheology to gain macroscopic insight, CD spectroscopy to understand the assembly of nanofibres and NMR to visualise the molecular immobilisation. Furthermore, we have been interested in two approaches to the gelation process: cold conditions for gelation mean the available energy for the molecules to interact is limited, while hot conditions mean there is more thermal energy available for the molecules to self-assemble.

In terms of nanofibre assembly as probed using CD spectroscopy using the hexylamine based gels, it was evident that this process is fast (seconds) under both cold and hot conditions. The relative rates correlated with the observations made visually of gelation speed. Interestingly, the resulting gels had very different CD signatures, suggesting different chiral packing was achieved by the different dendrons. Furthermore, different CD intensities were obtained depending on whether the assembly was performed cold or hot, which suggests that nanostructure assembly is dependent on the energy available, and that the gels formed may be different depending on the exact conditions used.

On the macroscopic level, a significant number of gels underwent a ‘two step’ process, with an initial rapid increase in viscosity followed by a slower ongoing increase over time. We suggest that the rapid increase corresponds with the visual observation of gelation and the assembly of nanofibres as observed using CD, but the slow further

increase indicates a process which could be the diffusion of gelators under the probe of the Rheometer. The rapid onset of gelation was in the order:

Naph-Lys > Phen-Ala > Hex-Lys > Naph-Phe > Phen-Lys

We noted that this process was particularly clearly marked for lysine based dendrons. It should be noted that these rheological experiments were quite challenging and difficult to interpret due to the slow linear increase in viscosity rather than exhibiting a rapid gelation.

On the molecular scale, we used NMR methods in a cooling spectrometer to observe the molecules being immobilised into the ‘solid-like’ network. This process worked, with all systems showing immobilisation of the gelator. However, the process was much more rapid than expected based simply on visual observation of gelation (which can take hours). Indeed, all systems showed complete molecular immobilisation in 14 minutes. This most likely suggest that kinetics are much faster when cooled from hot conditions – future work should involve performing these experiments with much shorter times between acquisitions, or alternatively starting from lower temperatures.

In summary, this chapter reports a rare study of both thermodynamic and kinetic study of a family of gels, and in particular uses different experimental methods to gain insight into gelation kinetics across different length scales and with different amounts of thermal energy available. Such fundamental studies are of importance in understanding the dynamic behaviour of gel-phase assembly.

## Chapter 3 Diffusion processes at gel-gel interfaces

### 3.1. Introduction

Diffusion processes play vital roles in a huge number of processes as a consequence of the tendency of molecules to move. There are diffusion processes in gaseous, liquid and even in solid phases.<sup>152</sup> These processes occur as a result of Brownian motion<sup>119,220,221</sup> (statistical thermal movement) or other kinds of processes, such as electromagnetic interactions (electrophoresis) and supramolecular interactions (molecular affinity). Clearly the density of the medium will play a key role in controlling the relative ability to diffuse, and hence the diffusion rate.



**Figure 3-1** A process of diffusion in liquid media.<sup>222</sup>

Diffusion processes in liquids and gases have been extensively studied giving rise to famous laws (e.g. Fick's Law<sup>128,152,223,224</sup>) that describe such behaviour and allowing researchers to determine the main parameters that affect normal diffusion processes. Gels are fascinating materials in terms of their diffusion properties as in one regard they are 'solid-like' materials which have solid rheological properties, but they also have a very large amount of solvent inside (typically  $\gg 90\%$  by weight) leading to high internal diffusional mobility of the 'liquid-like' solvent molecules, or other small solvated species that can be incorporated inside the gel. In one regard, the process of diffusion in gels is

reasonably well understood, and has been studied for some years, however, in self-assembled gels, the self-assembled gel nanofibers are themselves molecular in composition, and this opened the question of interest for us in this chapter – to what extent could components of a gel nanostructure itself diffuse within, or even out of, a gel-phase material.

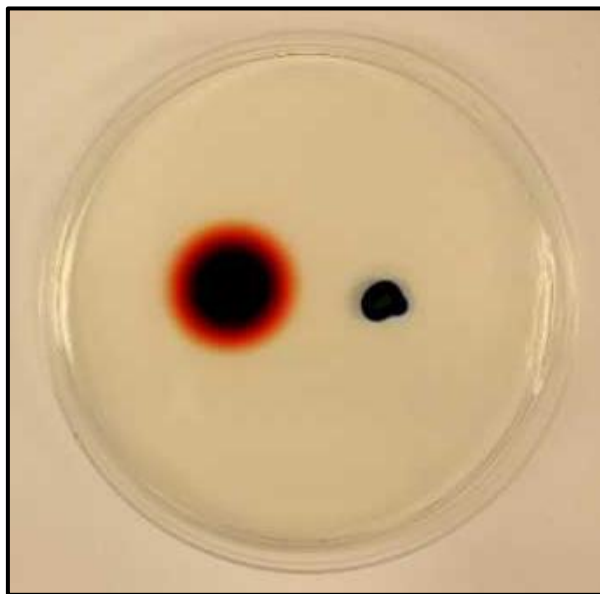


**Figure 3-2** Diffusion of a dye in agarose as a classic example of diffusion processes inside gels. Potassium Permanganate (MW=158) on the left and Methylene Blue (MW=320) on the right.<sup>225</sup>

### 3.2. Supramolecular Organogel

In the system studied here, we deal with a supramolecular multicomponent organogel which is a solid-like gel-phase material that contains a 3D network formed by means of supramolecular interactions when certain molecular scale components are mixed together in an organic solvent.<sup>226</sup> An essential property of organogels is that they are a solid-like material in which rheological properties<sup>227</sup> are similar to ordinary solids on the analytical timescale, but at the same time, they have liquid-like characteristics.

Multi-component gel-phase systems occur when two or more components have some kind of affinity and an appropriate geometry to interact with each other by means of

supramolecular interactions to form complexes that can further self-assemble and hence lead to extended hierarchical supramolecular structures. Such a hierarchical process gives rise a series of different types of multidimensional self-assembled structures (see for example Figure. 3-3)

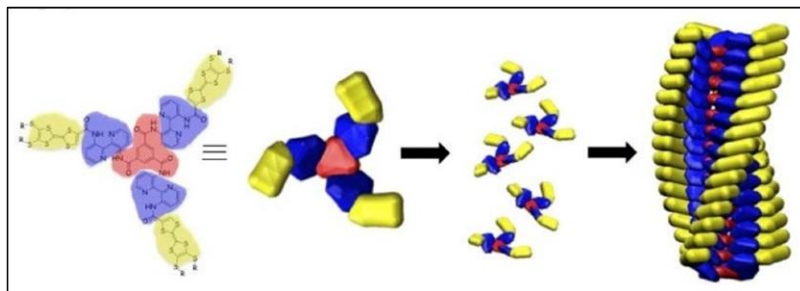


**Figure 3-3** Self-assembly of a TTF-grafted C3 core<sup>228</sup>

### 3.3. Formation of a two-component gel

The specific system investigated in this chapter forms an organogel in the presence of toluene as solvent, and has two components that only act as a gelator when present in combination with one another (Figure 3-4). These two components interact with one another as the consequence of an acid-amine interaction, with the acid at the focal point of the synthetic peptide-based dendron interacting with a selected amine. The acid-amine complex self-assembles into fibres because of intermolecular hydrogen bonds between the amide groups in the peptidic dendron component. These fibres entangle and ultimately give rise to the supramolecular gel.

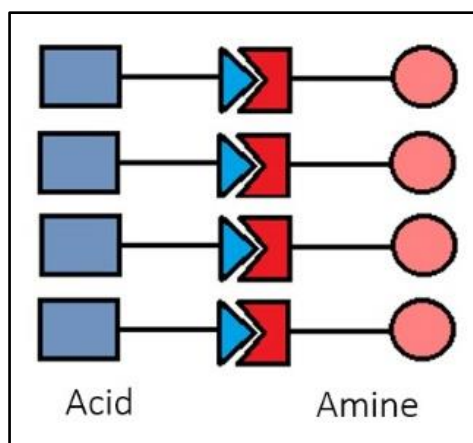


**Figure 3-4** Representation of Acid-Amine two-component complex which assembles into a fibrillar 3D network in our gel.

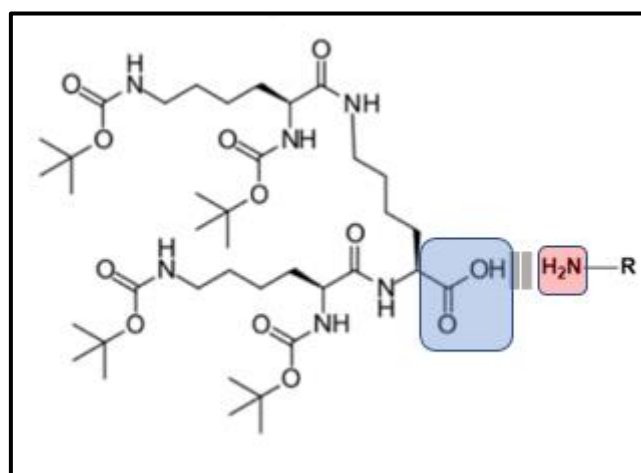


**Figure 3-5.** Two-component complex formed between the acid on the dendritic peptide and the amine group.

As described in Chapter 2, the potential interactions that can occur between molecules in a given solvent can generate an equilibrium that could lead to the assembly of gels with different rates of formation and thermal stabilities. The geometry and the nature of the molecular moieties of each molecule (dendron-acid and amine, Figure 3-5) will define the kind and effectiveness of interactions that will lead to a faster or slower process of assembly.<sup>69</sup> It is therefore interesting to reflect on the dynamic properties of these gels. In particular, in this study, we were interested in the mobility of the self-assembled gel network itself. It might be considered that a gel is a fixed solid-like material but we hoped to demonstrate that these multicomponent systems are much more dynamic than

previously thought. In particular, we hoped to demonstrate their self-healing and adaptive characteristics. Diffusion of the gel network itself opens the possibility of self-healing, because it suggests that network components can freely diffuse, and hence should be able to repair damage. There are examples of self-healing gels that can self-repair by simply re-joining the two gels that have been sliced by the interchange of material and components that are part of the 3D network.<sup>229</sup> A number of researchers have previously demonstrated that gel cubes can be ‘stuck together’ and have hypothesised this can occur as a result of self-healing supramolecular interactions across the gel-gel interface. For example, in a landmark *Nature* paper from 2011, Aida and co-workers made a bridge out of gel cubes, and demonstrated that the cubes became adhered together, and were hence able to form a self-supporting structure.<sup>230</sup> However, perhaps surprisingly, there have been no effective physical chemistry studies of diffusion across a gel-gel interface, and for this reason, we targeted a system that could deliver some understanding of this type of process. Synthesis and Characterization of the G2 ((Boc)<sub>2</sub>Lys)<sub>2</sub>-Lys-OH can be found in the 6<sup>th</sup> chapter relating with the experimental part.

### **3.4. Diffusion and mobility in gels.**

In general, the most commonly performed diffusion experiments with gel-phase materials concern the phenomenon of release of substances within the gel into a surrounding solvent medium. This can be achieved in a controlled manner by means of exerting different stimuli on the gel. The stimulus is the trigger to liberate substances, potentially by disrupting interactions between the substance being released and the gel network itself. Alternatively, the substance may simply be released by a Fickian diffusion mechanism.<sup>231</sup> In such a case, we are dealing with mass transfer of molecules kept inside the gel, which are being transferred from a solid-like phase within a nanoscale network present to a

liquid phase where the mobility of the molecules and pure diffusion is not impeded in any way by a 3D network.

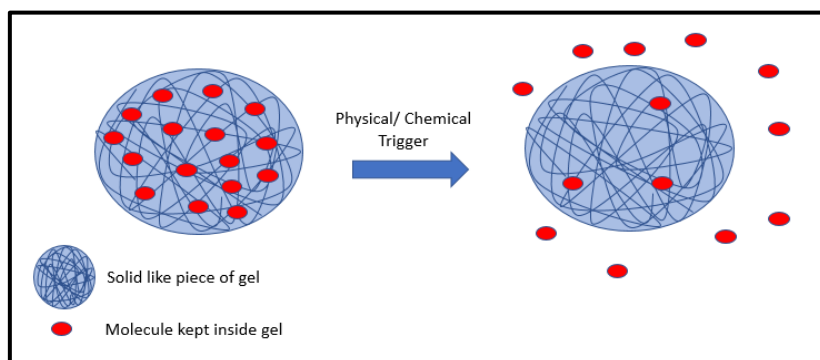


**Figure 3-6** Controlled release of molecules loaded inside a gel being released to a liquid phase in a controlled manner.

It is important to note that the solid-like fibres inside a gel are not necessarily fixed. Firstly, they might move on a length scale of tens of nanometres as a result of nanofiber flexibility, but more significantly for supramolecular gels, they can also move because their structures are only held by means of supramolecular interactions. If an external stimulus can affect the stability of those intermolecular interactions the stability of the whole material may be compromised (Figure 3-6). We therefore reasoned that by directing our attention to diffusion processes inside gels, we might find them interesting and new phenomena.

### **3.4. The design of a diffusion cell.**

The specific case that we want to study involves the potential of transferring matter from one gel to another gel, which is similar in molecular and nanoscale structure and macroscopic properties but has small differences in composition. The experiment will therefore consist of joining together two different gels with a common interface and after a period of time analysing them in terms of their composition and physical properties. This is an innovative approach that has not been applied before in the field of

supramolecular gels, and thus throws up a number of specific challenges. This aspect of research therefore required significant experimental design, and trial and error optimisation, which will be described in the sections below. The key requirements of the experiment were a design that enabled two gels to be brought into close intimate contact with one another, with an interface between them, in a defined geometry, which could be sampled at certain points in time in order to assess the progress of diffusion. Ideally, the experimental design should be robust, easy to use, give reproducible results, and not suffer from problems such as solvent evaporation, leakage or induce any gel damage. This was a challenging set of criteria for experimental design. Furthermore, given that each individual gel-based diffusion experiment may be relatively slow (e.g. days), and as such, this optimisation process took considerable time and effort to achieve.

#### **3.4.1. Selection of the material for the diffusion cell.**

The material selected for the diffusion cell depends heavily on the nature of the gel. There is a big difference in chemical stability and resistance of a cell depending on the solvent that forms the gel. In our case, we were working with toluene, and this provided a significant challenge. The toluene in our organogels is a relatively harsh solvent compared with the water found in hydrogels. There are many more materials that are resistant to an aqueous environment than there are which are resistant to toluene. So the selection of material with which the cell has to interact is a critical step in the design of the cell itself. Toluene is known to dissolve plastics and even if not, toluene can leach into the plastic leading to swelling and deformation, damaging the structure of the whole cell. Early cell designs in our lab suffered significantly from this problem. Thus, there were few materials available to resist the conditions of long-term diffusion (hours, days, weeks). The materials selected were glass and metal. It is important to note that experimental design

will depend on the system being studied, for example, if we were studying a hydrogel, metals would not be a desirable choice because of corrosion issues.

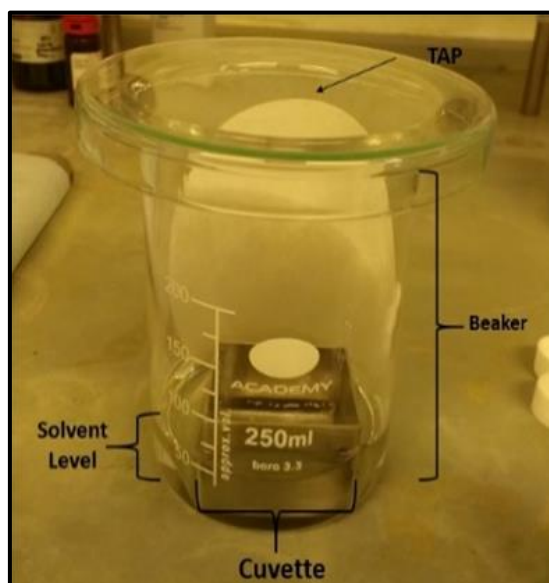


**Figure 3-7** An example of first design of diffusion system. The cell is metal, the chamber is a beaker with high vapour pressure of toluene.

Such a design (Figure 3-7) didn't work properly due to the of reliability in the placement of materials in each side of the cell before starting the experiment. So it was necessary redesigning both the cell and the diffusion chamber.

### 3.5. Chemical Nature of the Gel

As explained above, we were investigating a two-component organogel based on an L-lysine acid and an amine<sup>65</sup>. In order to explore diffusion of gel components between two different gels across an interface, we realised that we had two options for our two-component system:

- Monitor the diffusion of the amine by making gels with two different amines
- Monitor the diffusion of the dendron acid by making gels with two different acids

During the course of our studies we investigated each of these. Initially, we focussed on modification of the amine, and as a starting point, rationalised that using a fluorescent amine would provide us with easy visualisation of whether diffusion processes were taking place or not. As such, we decided to make gels based on: (i) hexylamine (non-fluorescent) and (ii) 1-naphthylmethylamine (fluorescent). We reasoned that if such gels were brought into contact with one another, and diffusion of the amine takes place across the interface, then we should be able to visualise this very simply as a fluorescent output. We refer to these two gels as Hexylamine based gels (HexGel) and 1-naphthylmethylamine based gel (NaphGel) respectively.

### **3.6. Gel characterization:**

It was important to characterize<sup>213</sup> the gels we proposed to use for diffusion experiments. For HexGel, some of this detailed characterization was reported in Chapter 2, and we do not go through it all again in detail here. However, it is important to note that we also studied NaphGel using the similar methods and we present a comparison of some of the key points – particularly in terms of nanoscale characterization.<sup>232</sup> Firstly, at a concentration of 10 mM, both samples formed gels, and both had very similar thermal stabilities of 65°C as monitored using simple reproducible tube inversion methodology. This suggests that replacing one amine with the other does not significantly impact on the gelation ability or macroscopic performance – important in our proposed diffusion experiment.

#### **3.6.1. Images of kinetically produced samples.**

The AFM images of the kinetically-formed, formed at room temperature conditions by just mixing the two components and ambient drying are shown in Figure 3-8.

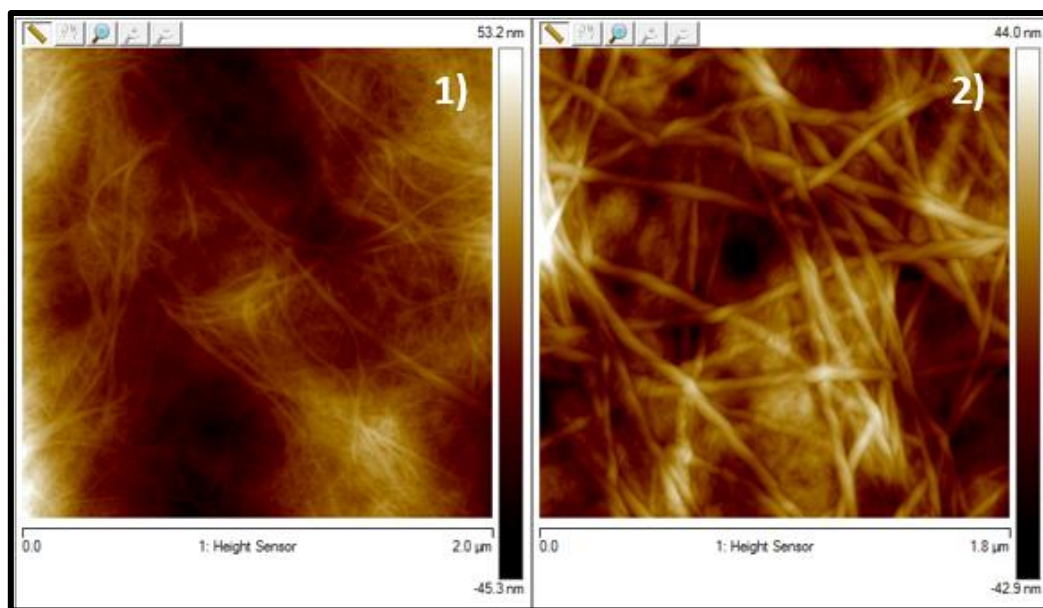


**Figure 3-8** Gels kinetically formed which composition is NaphGel (left) and HexGel (right) as the xerogels evaporated at normal conditions.

There is a significant difference between NaphGel and HexGel in terms of observed nanoscale morphology. It appears that the HexGel fibres are thicker in terms of diameter than those from NaphGel, which are almost molecular sized. This may be the result of supramolecular interactions between HexGel fibres making possible interaction and hence bundling between one another, giving rise to bigger secondary and tertiary structures. This is an interesting effect that may change the mechanical properties of the overall gel network. It has to be taken into account that the solvent retention properties of gels are related to the nano and micro structure. Bundling might suggest that the relative solvent compatibility of the HexGel nanofibers is less, which encourages greater aggregation. There is some logic to this argument as the NaphGel might be expected to have  $\pi$ - $\pi$  stacking interactions with the solvent (toluene), which would enhance their compatibility and maintain them with molecular-scale diameters. Such  $\pi$ - $\pi$  stacking interactions are not available to HexGel, which may as a result bundle instead in order to minimise unfavourable contacts with the aromatic solvent.

### 3.6.2. Images of thermodynamically formed gels.

Figure 3-9 illustrates the AFM images of the gels formed after a heating and cooling cycle. As will be explained below, this is more typical of the conditions used to form gels in our diffusion experiments.

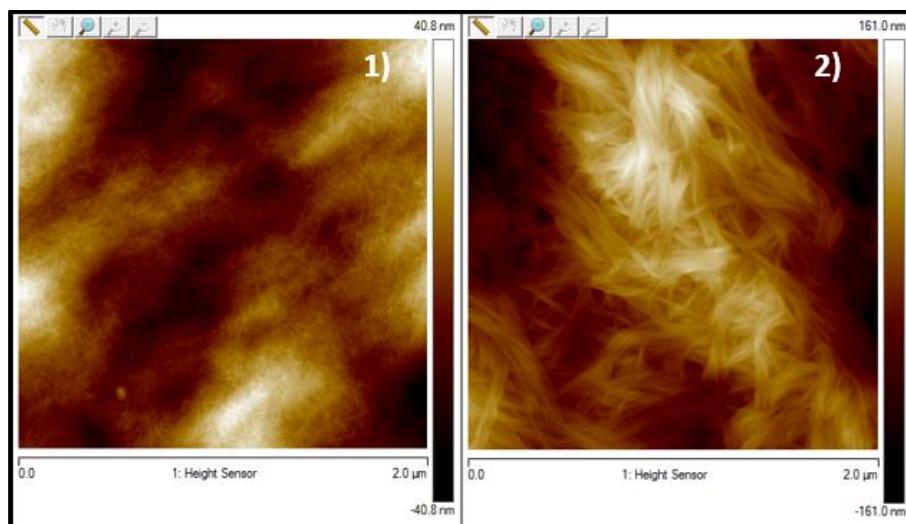


**Figure 3-9** Gels thermodynamically formed which composition is L-NaphGel and L-HexGel.

Once again, HexGel appears to have slightly larger diameter fibres than those formed by NaphGel. However, they are significantly smaller, and more flexible in appearance than those that were formed under the kinetic conditions of simple mixing of hexylamine and the acid dendron. As such, we suggest that the heating and cooling process has enabled reorganisation of the HexGel nanofibers into a more thermodynamically favoured form. The NaphGel sample again appears to show narrower fibres, although they are harder to visualise than in the previous sample.

### **3.6.3. Images of gels by SEM.**

In order to try and confirm the results of AFM imaging of these two systems, we also imaged the gels by scanning electron microscopy (SEM). Using this technique, it was challenging to prepare xerogels without damaging the nanostructure. Xerogels were obtained by evaporating gels while freezing with liquid nitrogen. This works well with hydrogels; however, it is more challenging for organogels. We also have to take into account that the SEM internal chamber is under high vacuum and this requires pre-removal of any chemicals that could be volatilized in such a chamber. This doesn't happen for samples analysed in AFM because the working platform is at normal conditions of pressure and temperature. In the case of (SEM) we needed to fully remove volatiles without damaging the nanostructure that we needed to image. Freeze-drying is important to try and limit any thermally induced reorganisation during the drying process. The process used employed a high vacuum pump, introducing the gel in a round bottomed flask inside a Dewar thermo bottle. At that point, the gel was solid-like and protected from surrounding ambient moisture (to avoid humidity condensation). After freezing, the high vacuum is opened to the sample flask gently till the flask is completely under vacuum conditions. After several hours of freeze-drying, the sample was dry and ready to be analysed. Before developing this enhanced protocol, there were many failures related to recrystallization of gel components because of the condensation of ambient water in the prepared xerogels before the sample. Figures 3-10 and 3-11 illustrate SEM images for samples produced from HexGel and NaphGel respectively. Both of these images suggest the formation of nanofibrillar networks for each of these gels. As observed by AFM, the nanofibers formed by HexGel appear to be somewhat larger than those formed by NaphGel – plausible reasons for this associated with nanofiber solvent compatibility and bundling were explained in the section above.

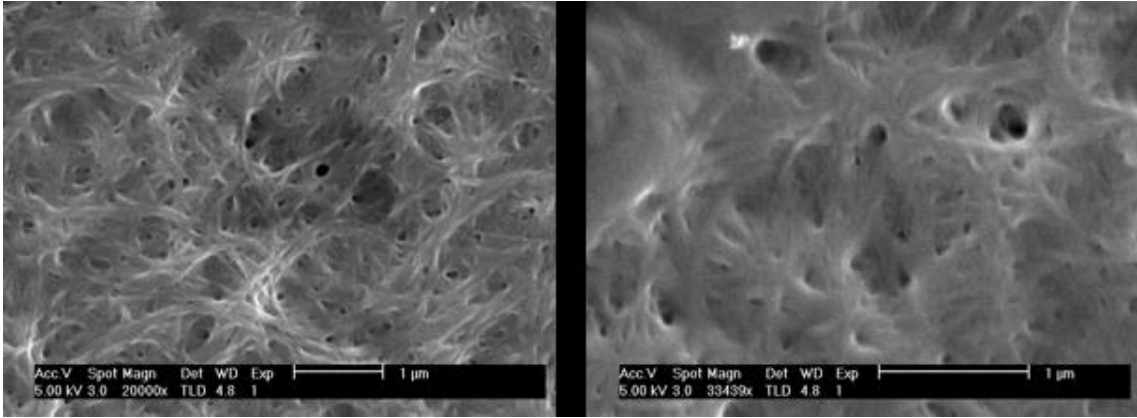


**Figure 3-10** HexGels 10mM concentration. Xerogels by freeze drying method. Left 20.000 magnification, right 33.439 magnification.

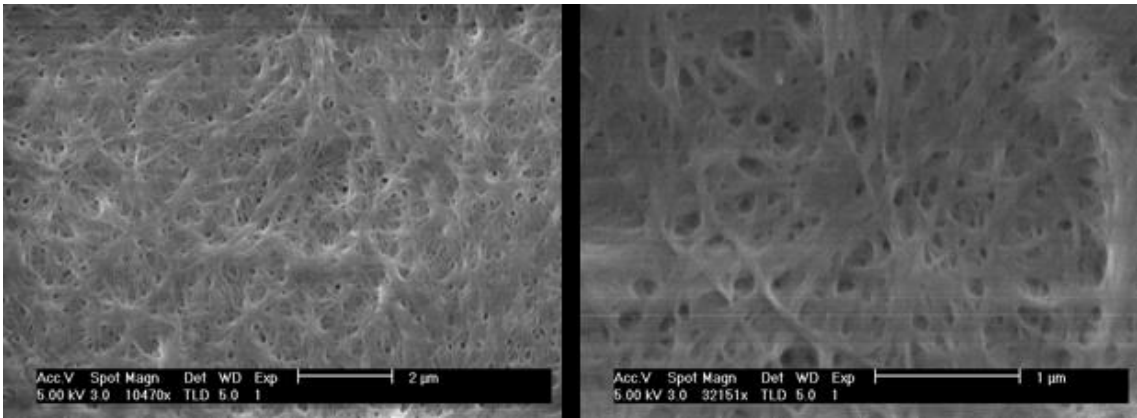


**Figure 3-11** Naph Gels 10 mM concentration Xerogels by freeze drying method Left 10.000 magnification, right 32.151 magnification.

### 3.6.4. Images of gels in TEM.

An alternative technique to image 3D gel networks was provided by transmission electron microscopy (TEM). Again, because of the vacuum conditions of the technique, we needed xerogels. A thin layer of gel sample was placed on the metallic TEM sample grid and allowed to dry at room temperature and pressure. This is a slightly different approach for sample preparation from the one used in SEM and more similar to AFM.

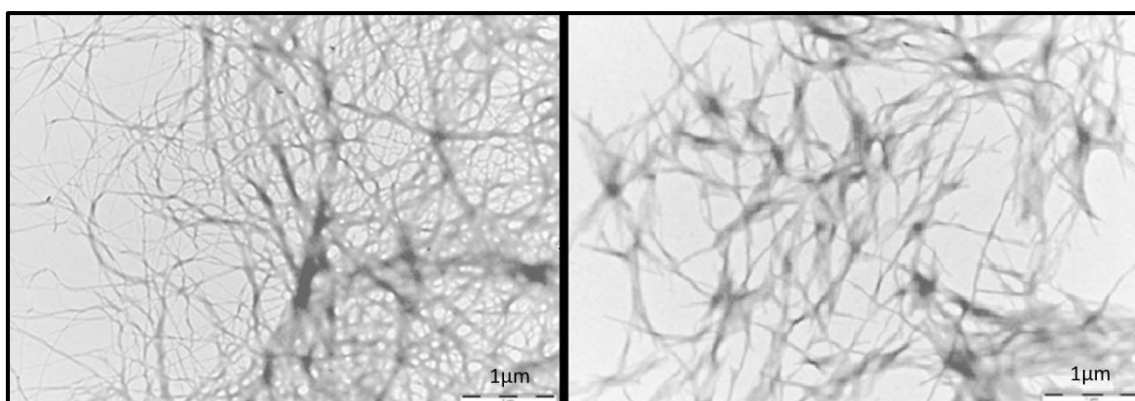


**Figure 3-12** TEM NaphGel (right) and HexGel (left) both 16.500 magnification.

In the pictures above Figure 3-12, we can see the nanofibrillar networks of the gels, which could clearly be visualised even in the absence of a contrast agent. Once again, this provides evidence that the HexGel fibres are somewhat larger than those formed by NaphGel – in support of both AFM and SEM imaging methods.

In summary, both systems formed gels with similar thermal stabilities ( $T_{gel}$ ) underpinned by fibrillar solid-like self-assembled morphologies on the nanoscale. There were some differences in diameter of the self-assembled nanostructures dependent on the amine being used, however, overall, these gels have good similarity and were considered suitable for study in our diffusion cell.

### 3.7. Stages of building the diffusion cell.

In order to get a simple visual insight into what was happening, we decided to initially use simple vials, and form two different gels, with an interface between them, and observe what happens. Taking advantage of the different properties of the gel in terms of fluorescence, we designed a diffusion process that could be tracked by the naked eye when UV radiation was applied to the vial with the two gels as shown in Figure 3-13.

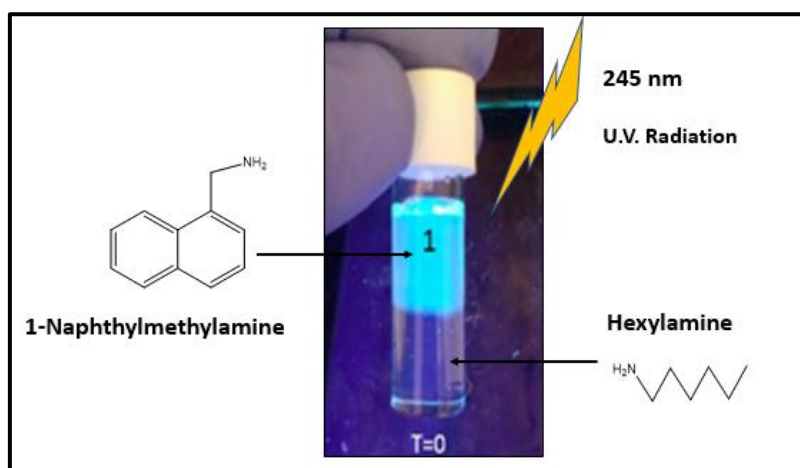


**Figure 3-13** Vial filled with fluorescent and non-fluorescent gels being irradiated.

Figure 3.13 shows a lower gel based on hexylamine combined with (G2 ((Boc)<sub>2</sub>Lys)<sub>2</sub>-Lys-OH), ie, Hex-Lys Gel, with a second gel layered on top, formed using 1-naphthylmethylamine and the same dendron (Naph-Lys Gel). The concentrations of each of these gels were 10mM. In Figure 3.13 the vial is being irradiated with UV light. The contents of the vial are two solid gels separated by a gel-gel interface. The 'blue' gel in the upper part is formed from the bicomponent system with the fluorescent amine (1-naphthylmethylamine) and the gel in the lower part is the non-fluorescent hexylamine based gel. When the two gels are joined together there may be some kind of interchange of matter as described earlier. This mass transfer may only be molecules of solvent (toluene), or may include molecules which are part of the 3D network of the gel matrix,

or alternatively could be molecules which are neither solvent nor 3D scaffold but are simply formulated within the gel. This experiment was left to stand for 48 hours, and the results observed (Figure 3-14). In this experiment, the positions of the fluorescent gel and the non-fluorescent gel at the start of this experiment were opposite to those shown in the previous Figure, with the fluorescent gel forming the lower layer. Under UV irradiation, it becomes clear that the fluorescent amine is diffusing from one side of the gel-gel interface to the other. This diffusion has started even after 5 hours, and after 48 hours, appears (visually) to be reasonably complete. Thus, mobility of one of the components of the self-assembled nanoscale network inside of this solid like material therefore appears to be allowed. This was a remarkable result – such networks are usually labelled as ‘solid-like’ and as such, it was surprising to us that diffusion appeared to be taking place. It suggests that the ‘solid-like’ nanoscale network (or at the very least, the amine component of it) may be effectively in equilibrium with the liquid-like phase. We anticipated that the non-fluorescent amine is also diffusing in the opposite direction, although obviously, this cannot be detected using this simple qualitative fluorescence technique illustrated here.

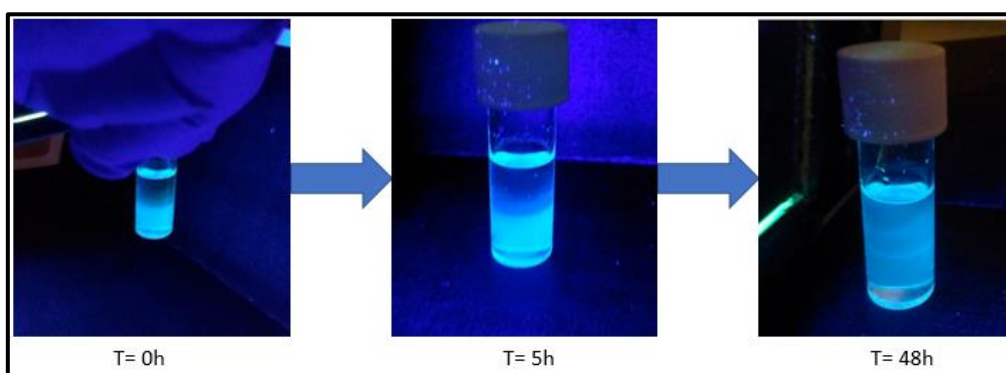


**Figure 3-14** First diffusion experiment that was made in a vial. The two gels were made one on top of the other.

The experiment described above was only qualitative in nature, and we therefore hoped to gain more detailed insight into this diffusion process. It is important to realise that various parameters may impact on the diffusion rate:

- **Temperature.** Temperature will affect not only the speed of Brownian motion (thus evolution of diffusion) but also the equilibrium of supramolecular interactions and affinities. Self-assembly processes depend on supramolecular interactions; thus, temperature can lead to lability of physical bonding, which may affect the diffusion rate of self-assembled systems.
- **Gradient concentration of components.** The concentration of components which are added (amine and dendron acid) will affect not only the concentration of components available to diffuse but also the density of the 3D scaffold of the gel matrix, both of which may impact on diffusion rate.
- **Area of contact.** The area of contact at the gel-gel interface is one of the most important parameters to control, because it will affect dramatically the flux of matter (directly proportional according to the Fick's Law)

All these parameters can be expressed in a formula – Fick's law which can be described in the following equation according to Crank<sup>152</sup>, 1975.

$$F = -D\nabla C \quad \text{Equation 3-1}$$

Which can be written for a 1D slab geometry as:

$$F = -D \frac{\partial C}{\partial x} \quad \text{Equation 3-2}$$

Where D is the diffusion coefficient ( $\text{m}^2 \text{s}^{-1}$ ) and  $\nabla C$  is the gradient concentration and F the rate of transfer per unit area of section ( $\text{kg m}^{-2} \text{s}^{-1}$ )

### 3.7.1. Diffusion System: A description.

The designed cells in which we analysed diffusion within these gel systems have defined length (4 cm), width (3.5 cm) and height (2.5 cm), and were made of soda glass. The volume of gel introduced in the cell was 5.44 mL which makes an interfacial area of 1.6 cm<sup>2</sup> between the two gels. Separation between the two sides of the cell was achieved by means of a aluminium made 'separator' (see below). The placement of the gels (Figure 3-15) in the cell was achieved by pouring each of the solutions into either side of the cell and to obtain a homogeneous gel it was necessary to heat the system until the gel was completely melted and then lower the temperature to gelate the system and thus obtain homogenous and separated gels. The homogeneity of the gels has to be as high as possible in order to ultimately achieve the most effective gel-gel interface and enable effective even diffusion through the system. Simple pouring and mixing could not achieve this, as the rapid rate of gel formation competed with the diffusion mixing rate. For this reason, the thermal cycle approach was employed.

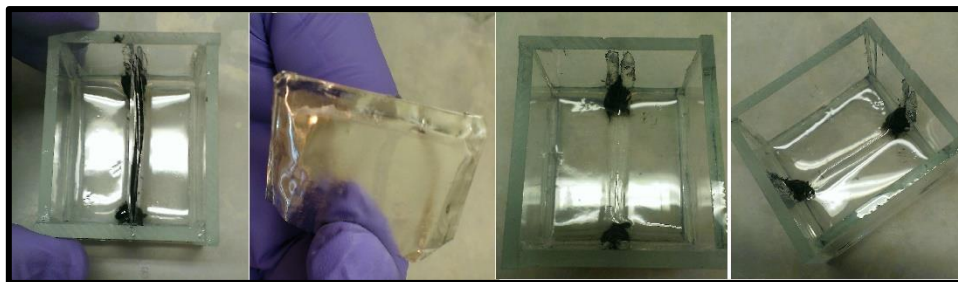


**Figure 3-15** Placement of the gels in the cuvette and removal of the separator to start the diffusion experiment.

The separator (Figure 3-15) keeps these two gels apart prior to the start of the experiment, at which point it is removed in order to bring the two gels into contact at the interface and allow diffusion to begin. The separator is an aluminium handmade piece that is thin enough to allow gel-gel contact when removed. The separation of the different gels until the diffusion experiment takes place is a key parameter, because when heating the

different gels for homogenization they turn into a liquid state. At this point the importance of separating both gels is a critical issue that can affect the whole experiment dramatically as mixing could easily occur if separation was ineffective. This aspect of experiment design was particularly problematic, and took considerable effort to solve even though there are other possible designs that could meet also the experimental requirements such as the shown in the work of Lefaucheu<sup>233</sup> where they used a curved column as diffusion cell.

Another important factor that has to be taken into account is that toluene is a highly volatile solvent, and the system is therefore vapour rich. Indeed, if the gel itself is open to the room it rapidly loses solvent by means of evaporation. To avoid these losses, it is therefore necessary to create a rich vapour atmosphere of toluene and keep the gel solvated. To obtain these conditions the experiment required the diffusion cell to be placed in a chamber full of solvent. In the final set up, a desiccator vessel containing toluene was used in order to maintain a solvent vapour pressure and ensure the gel remained at the right level of solvation. This desiccator was then placed in an incubator, to ensure the entire system was also kept at constant temperature. (Figure 3-16)



**Figure 3-16** The diffusion chamber (desiccator) inside an incubator to maintain a stable temperature. Notice that the closed system (chamber) maintains rich the vapour pressure of toluene so gels don't dry out.

Once diffusion has begun, sampling must take place. Although one of our component amines is fluorescent, and potentially could be followed by fluorescence, the other amine is not. The use of fluorescence was very useful in a qualitative sense to check that diffusion was taking place, but was not ideal for more quantitative insight. Given we wanted to follow the diffusion of both amines within the gel, we therefore opted to use a different analytical technique in order to track diffusion quantitatively – we selected NMR analysis. In order to do this efficiently each region of the cuvette has to be sampled properly and not mixed with others. To get quantitative results about the concentration profiles there is a need to sample the material from the cell (at certain diffusion times). This limited the range of designs for the cell. In the end, a cell as illustrated in Figures 3-17 and was the optimal design.

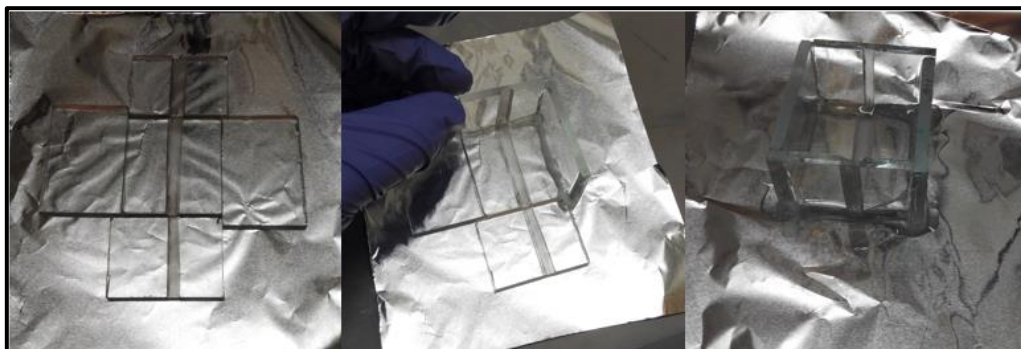


**Figure 3-17** Assembly of glass cells for use in the diffusion experiments.

The cell is constructed from glass pieces that are glued by a strong and chemically-resistant epoxy resin. This glue is particularly resistant to the toluene-enriched environment. Apart from the assembly of the cell itself, it is necessary to isolate one side of the cell from the other before the experiment starts. To do so, as outlined above, a temporary barrier has to seal one side from the other. This was achieved by using a silicone seal between the glass sides of the cell. Once silicone is in contact with toluene it swells and there was therefore a need to removing the excess of swollen white silicone with a very sharp blade to obtain a completely flat surface in the diffusion cell. The

aluminium separator described above could then contact this silicone seal and prevent solution leakage. Figure 3-18 provides a representation of the process of adding the silicone necessary for the isolation of the two sides of the cell.



**Figure 3-18** The process of filling the central hole with white silicone in order to seal one side from the other with an aluminium barrier. Once silicone is in contact with toluene it swells and there was therefore a need to removing the excess of swollen white silicone with a very sharp blade to obtain a completely flat surface in the diffusion cell.

After the construction of the cell, we began the diffusion experiments using a collection of diffusion cells. The reason for this, is that sampling from the cell damages the gel, and means that further diffusion timepoints cannot be studied – therefore a number of experiments were run in parallel, such that each could be sampled at a certain time after the experiment had started. The melted gels were poured into the cells on each side of the cell. In order to maintain one gel isolated from the other while in a hot sol state, the aluminium barrier was installed between those areas and inserted in the silicone. After solidification of the gels in the cell, the barrier was removed and the gels came into contact for the first time with a contact area of  $1.6 \text{ cm}^2$ . Figure 3-19 represents a cell that has been loaded with NaphGel on the left-hand side and HexGel on the right-hand side. As can be seen, the fluorescence of the 1-naphthylmethylamine provides an excellent way of qualitatively surveying the gels in this experiment.

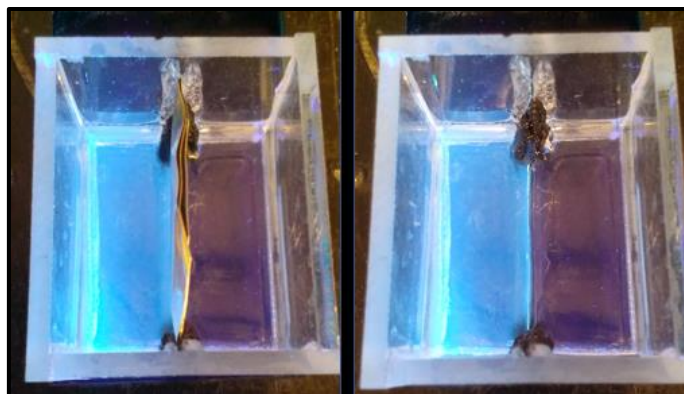


**Figure 3-19** Visualizing the two gels loaded into the cell by pouring the hot liquid gels into each side of the cell while maintaining them separate with an aluminium barrier (left). Once the gels have solidified the barrier is removed and gels come into contact (right), representing time point zero of the diffusion experiment.

### 3.7.2. Diffusion experiment.

The first gel-gel transfer experiments measured the rate at which the 3D networks of both gels were able to diffuse into one another. The experiment consisted of placing different gels, NaphGel and HexGel (Figure 3-20) in each side of the experiment, both gels were formed in the cuvette separately and homogenised as explained in the standard procedure. Once both gels were prepared, the separator was removed carefully and the gel-gel interface was checked to make sure there were no bubbles that could interfere with the transfer process. The experiment started at that point and was followed qualitatively using UV irradiation to visualize the progress of the diffusion of 1-naphthylmethylaniline.

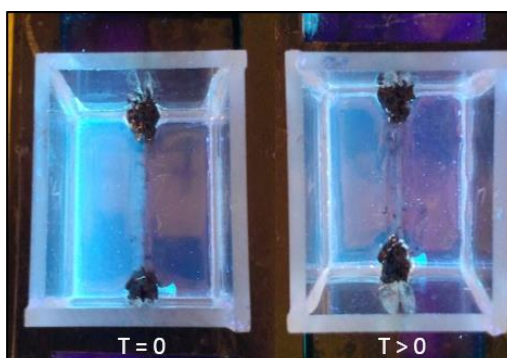


**Figure 3-20** Diffusion process of the 3D network of different gels. On the left, the cuvette at time 0, and on the right the cuvette as the experiment takes place, indicating diffusion of the fluorescent amine.

Samples were taken at specific times to check the progress of diffusion in more quantitative terms. To do that, the cuvette was divided into six regions equivalent in transferred amounts (Figure 3-21). The gel was transferred to numbered vials and put under vacuum conditions to remove solvent. The contents of the vial were then fully dissolved up in d8-toluene to determine the concentration of 1-naphthylmethylamine in each region. The vials were analysed by  $^1\text{H-NMR}$  using an internal standard to quantify concentration.



**Figure 3-21** The cuvette is divided in 6 regions in order to obtain the concentration of amine in each region.

### **3.7.3. First experiment at room temperature.**

We were uncertain how much diffusion we would observe, as the 1-naphthylmethylamine is, of course, part of the self-assembled gel nanostructure. However, our previous ‘in-cuvette’ experiment had led us to believe that some diffusion would take place. We therefore sampled from the cells on days one, three and seven – using visual fluorescence to monitor progress and help us decide the optimal timepoints for sampling. The results of diffusion progress are presented in Figure 3.22. This graph represents the six samples

removed from the gel, with their average distance (in cm) from the gel-gel interface. At the start of this experiment, the concentration of NaphGel on the right hand side of the experiment was 10 mM, and on the left hand side, it was 0 mM. As can be seen, as time progresses, the concentration of NAPH on the left hand side of the experiment increases, while that on the right hand side decreases. Furthermore, it can be seen that the increase in this amine on the left-hand side of the experiment appears to be more pronounced closer to the gel-gel interface. Although this experiment has some quite significant errors, associated with the sampling methodology – it is evident from the combination of fluorescence observations and NMR quantification, that diffusion of the 1-methylnaphylamine is taking place.

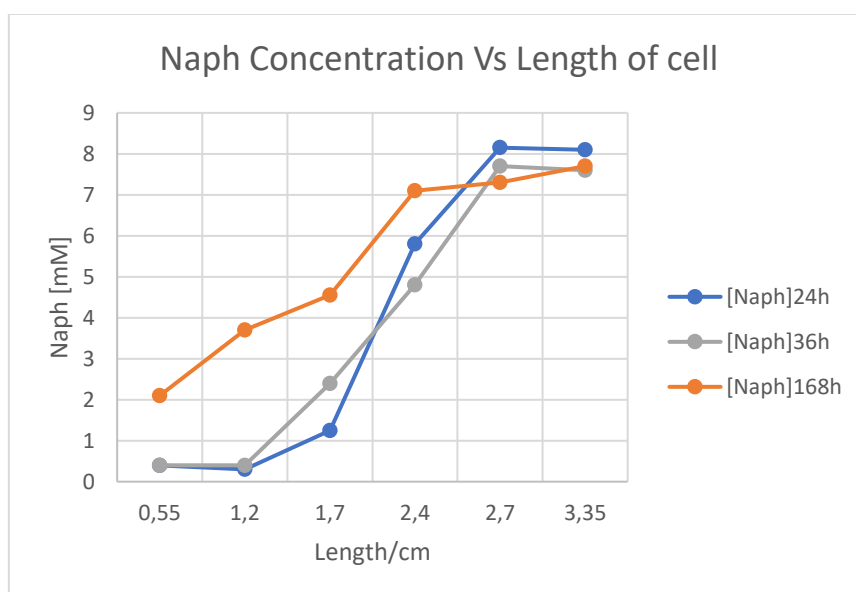


**Figure 3-22** Concentration of Naph sampled from each of the six locations on either side of the gel-gel interface, at different timepoints of the experiment.

In the test, it is therefore demonstrated that some diffusion takes place and gives rise to slow equilibration of the system components –at least for the 1-naphthylmethyamine. This intriguing result shows that in these multicomponent gels, the amine components can indeed exchange across the gel-gel interface and that the composition of the gels in either side of the experiment can slowly evolve and adapt. This indicates that these gels

can adapt and let their components to flow within the bulk material, and we suggest that this type of observation – the diffusion of gel network components – is of major significance with regard to self-healing and adaptivity properties. It is, however, also evident, that diffusion of the amine component of the 3D nanofiber network is a slow process, taking a period of days. We suggest this is because the amine network component must equilibrate on and off the fibres, in addition to diffusing through the gel before binding to a different acid. Indeed, we might propose a diffusion mechanism in which the amine building block diffuses through the gel by hopping from one acidic binding site to another. There should be therefore an energy barrier to produce this diffusion and rearrangement. Such an energy barrier has a relationship with the supramolecular bonds that sustain the overall gel scaffold.

In order to better understand the kinetics of this diffusion process, we therefore decided to test how a simple inert non-interactive small molecule would diffuse through the gel. This should help us quantify the inherent diffusion capacity of the gel interior in the absence of any specific non-covalent interactions.

#### **3.7.4. Diffusion of small molecules**

In this second diffusion experiment, the gel on each side of the experiment was HexGel. The only difference between them was that to one of them was added a small molecule, diphenylmethane at 5 mM, which is known to not interact with the 3D network (indeed, we have used it as an internal NMR standard in gel studies because it is mobile within the gel on the NMR timescale<sup>64 69</sup>). The system filled with the gels is shown in Figure.3-23.

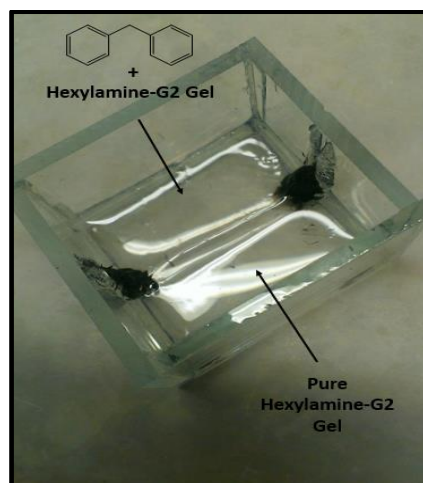


**Figure 3-23** In the upper part of the cuvette HexGel is mixed with the diphenylmethane at 5 mM in the bottom, the HexGel has no molecule formulated into it.

The conditions of the experiment were exactly as in the previous experiment. The cuvettes were analysed at certain times and sampled in their different regions by  $^1\text{H-NMR}$ . The concentrations in the different areas of the cuvette were measured against time (Figure.3-24). However, in this case, we sampled out of the gel at time points of hours rather than days. Once again, it was evident that the concentration of diphenylmethane on the right-hand side of the gel decreased, while that on the left-hand side of the gel increased. After 48 hours, it is evident that a concentration of ca. 5 mM is observed across almost the entire cell – suggesting that diffusion of the small molecule is complete, and diphenylmethane has equilibrated fully between both sides of the gel over this timescale.

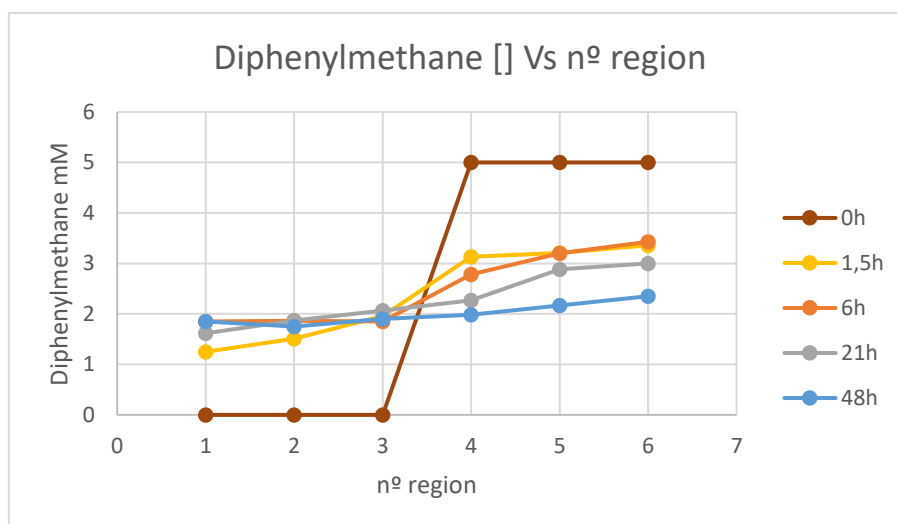


**Figure 3-24** Concentration of diphenylmethane versus cell region in the cell for a diffusion at 25°C.

This experiment therefore clearly showed that for diphenylmethane, rapid diffusion occurs. Comparing this molecular diffusion with the one in which an interactive amine component was transferred, it is evident that molecular diffusion of an inert non-interactive molecule through the gel is a much faster process than transferring a component which is intimately interacting with the 3D nanoscale network. This supports the view that an energy barrier has to be overcome when the components that are involved in the construction of the 3D network are themselves diffused. Nonetheless, although the timescale of network transfer for the amine is days, rather than the hours observed for diphenylmethane, it remains fascinating that it can indeed be observed at all. This ability to reorganise on a molecular level is a unique feature of supramolecular gels, in sharp contrast to their polymer gel analogues, and demonstrates a clear advantage of using reversible non-covalent interactions in the construction and assembly of soft materials. If diffusion coefficients are determined for this concentration profile a value of  $3.2 \cdot 10^{-4} \text{ cm}^2 \text{ s}^{-1}$  is obtained, which is extraordinarily high compared to the other obtained for diffusions of components in the 3D network. The process of obtaining this will be explained in detail in the section 3.7.6. and in the appendices.

### **3.7.5. Diffusion of amines at various temperatures.**

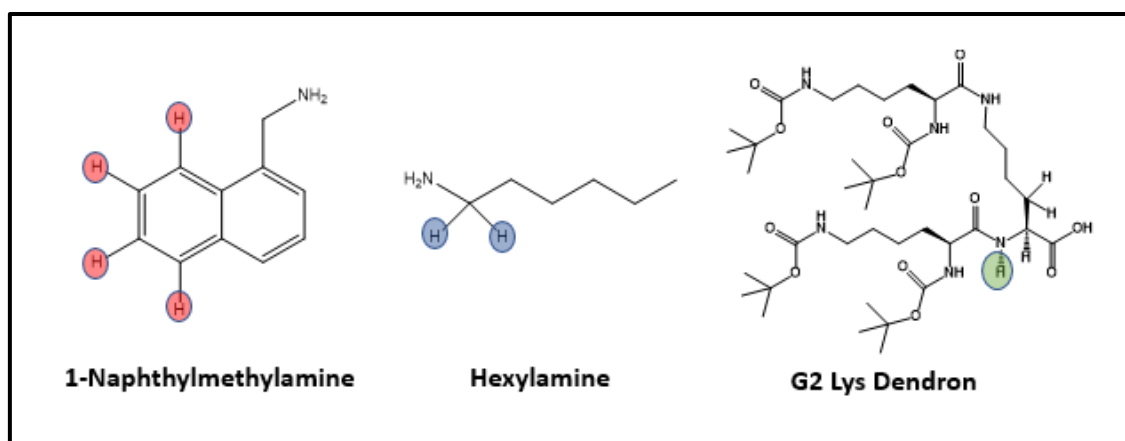
After the preliminary experiments described above, we moved forwards with an optimised procedure in order to obtain better quality data, and attempt to probe the impact of other variables on diffusion rates within the gels. Importantly, in addition to following the movement of Naph through the gel, we also wanted to probe the diffusion of the other component, Hex, as a part of our optimised methodology.

Temperature is one of the main parameters in Fick's diffusion law, so if we modify this parameter we may expect a change in diffusion rate. Experiments were performed at various temperatures using an incubator for the hot temperature (45°C) and room temperature (25°C), and a fridge for the cold temperature (5°C). As before, all diffusion experiments were performed in a saturated environment of toluene inside a desiccator. The results are described in the following sections.

#### **3.7.5.1. Diffusion across gel-gel interfaces at 25°C**

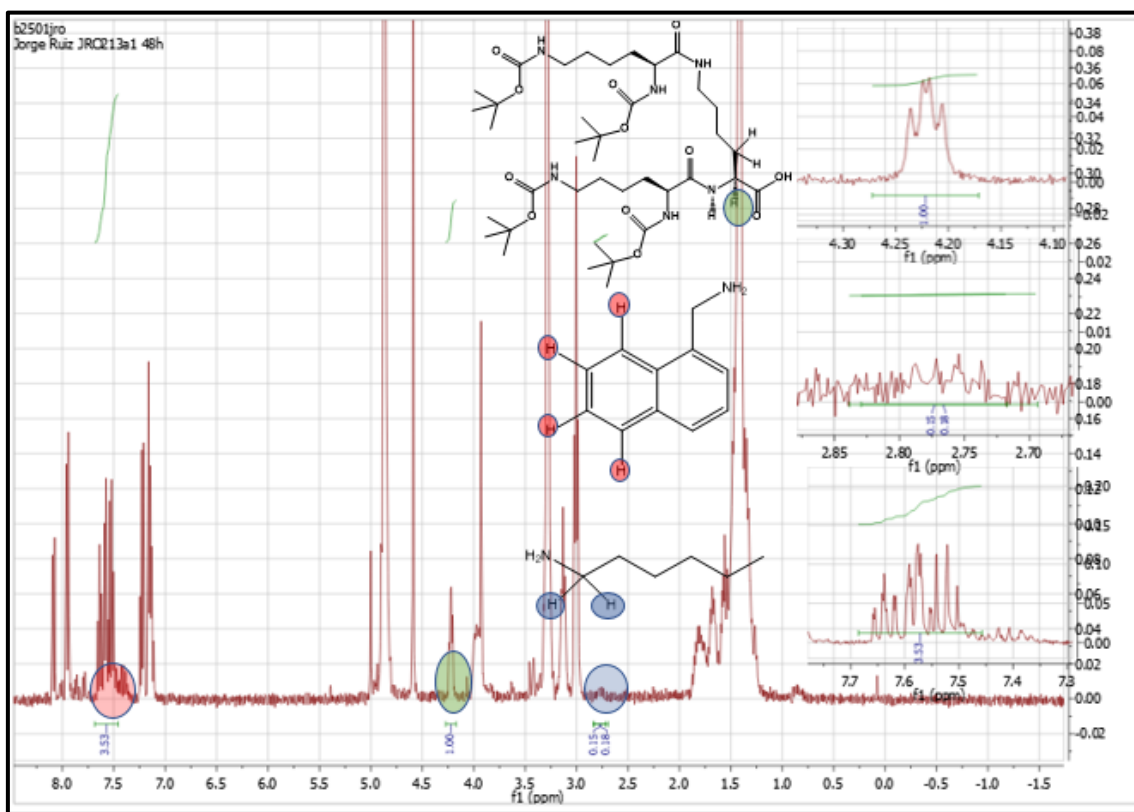
Diffusion cells were prepared and filled with respective gels of 5 mM of components (a lower concentration than that used in our previous experiments) and also a non-interactive additive (diphenyl methane) at 5 mM, which acts as an internal reference to integrate later in the <sup>1</sup>H-NMR peaks and more accurately determine the concentration of amines when gels have been diffused. This is a much better procedure than that described in the experiment above, in which the standard was added after sampling had taken place, hence introducing errors depending on the precise amount of gel sample being removed in each case. The experiment then proceeded essentially as described previously.

After sampling pieces of gel (which importantly already include the internal standard) from different regions of the cell, as before gels were evaporated to remove all the solvent, then fully dissolved in deuterated methanol for NMR analysis. Sadly, we found that diphenylmethane was a surprisingly poor reference in this experiment. The reasons for this are unclear, as the additive had performed normally in our previous diffusion experiment (see Figure 3-24), but it is possible that there is some degree of unhomogenization or loss of the compound (perhaps during the sample drying step) that resulted in very erratic concentrations. Therefore, in order to calculate and determine the amine concentrations, we elected instead to use the dendron acid as the internal reference, as it also has a constant concentration across the cell (5 mM). It was important to find a dendron  $^1\text{H}$ -NMR signal that could be used as an internal reference to integrate other  $^1\text{H}$  peaks against, and hence determine the amine concentrations for each region of the cell at each diffusion time. Fortunately, this could be achieved. Figure 3-25 illustrates the selected protons which were integrated and referenced against the dendron proton (green).



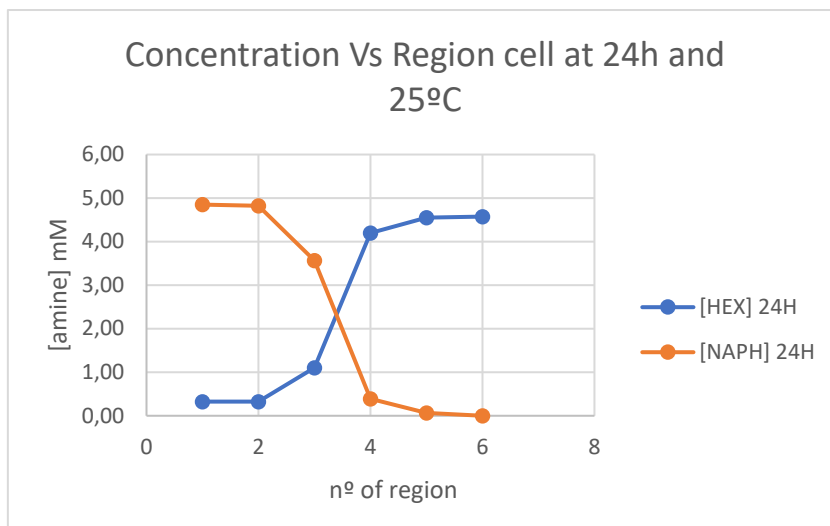
**Figure 3-25.**  $^1\text{H}$ -NMR signals to be integrated in the diffusion experiment. Notice the first two amines are part of the 3D network for each kind of gel. Naph Gel and Hex Lys Gel respectively. We highlight one of the protons that comes from the dendron (green) which was effectively used as an internal standard.

Figure 3-26 illustrates a typical NMR spectrum obtained after sampling and clearly indicates how we integrate the proton peaks in order to determine the concentrations.



**Figure 3-26** 1H-NMR of the region 1 of the diffusion cell of certain diffusion time. Notice that signals are integrated relative to the dendron proton highlighted.

If we integrate the peaks for each region of the cell at a given diffusion time (e.g. 24 h) we can determine the concentration profile for both of the amines (Hex and Naph). This is a useful profile which represents concentration and space for a given diffusion time and temperature. In addition to being referenced against the internal standard (the dendron acid), this data is now effectively self-referenced as both amines are being measured simultaneously. This therefore provides much more robust data than the preliminary experiments described previously,



**Figure 3-27** Concentration profile for amines in a diffusion experiment between Naph Lys Gel and Hex Lys Gel for a given time and temperature.

It is worth mentioning that this graph is the result of an experiment optimisation process which took ca. 1 year overall. With that being said, and repeating the same process four different times (0, 24, 48, 140, 300 hours) a graph of diffusions for a given temperature of 25°C could be made (Figure 3-28).

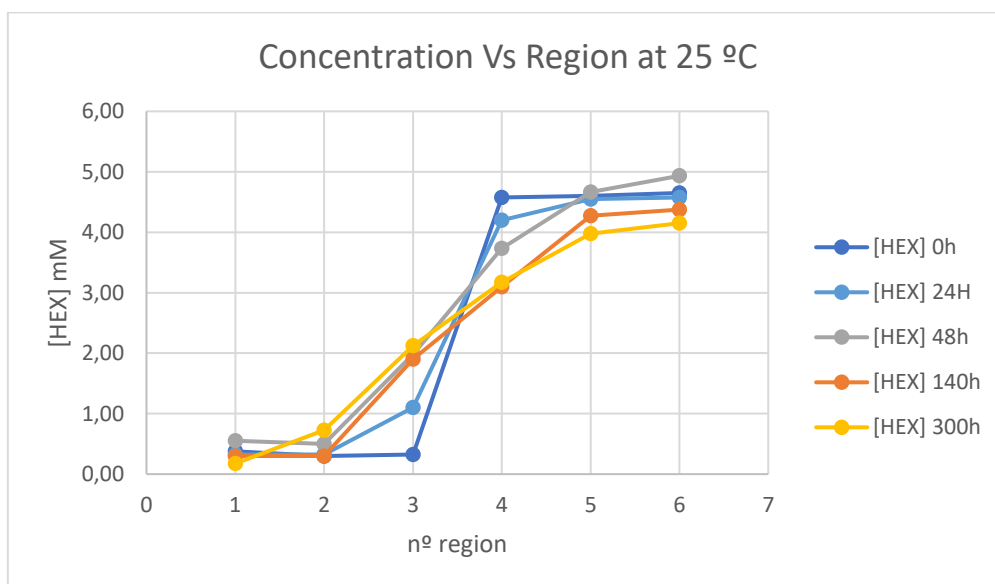


**Figure 3-28** Concentration profile for Hexylamine in a diffusion cell for a range of various diffusion times at 25°C

Very pleasingly, this graph is symmetrical and shows reliable and reproducible trends much better than those preliminary experiments performed in the previous section. Clearly as time progresses, the concentration in cell region 3 increases, while that in cell region 4 decreases, suggesting the diffusion of hexylamine from the right to the left. The same trends are seen, but with smaller concentration changes in sections 2 and 5, as would be expected given that they are further away from the gel-gel interface. This supports the view described earlier that amines can diffuse through these gels as the result of a mechanism in which they hop from one acid binding site to the next, with a relatively slow diffusion rate, as a result of the energy barrier to this process.

Figure 3-29 illustrates the 1-naphthylmethylamine concentration profiles of the same sample for several diffusion times (0, 24, 48, 140, 300 hours) and a temperature of 25°C

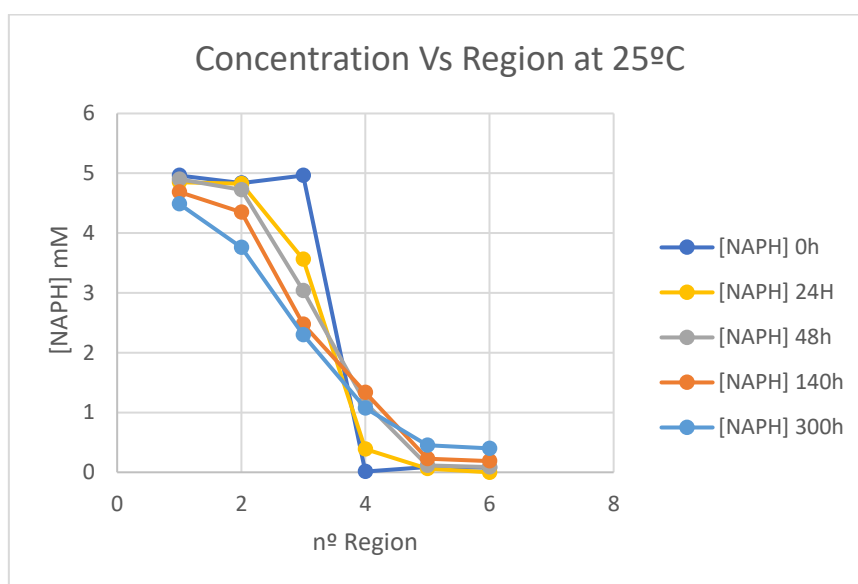


**Figure 3-29** Concentrations profile for 1-Naphthylmethylamine in a diffusion cell for a range of various diffusion times.

This time, the Naph is diffusing in the opposite direction – i.e. from left to right. Again, the same trends as seen for hexylamine are observed here. Interestingly, the increase in concentration of Naph in cell region 4 is less than that of Hex in cell region 2, which

might suggest that the aromatic amine is somewhat less able to diffuse through the gel – this may be a result of enhanced interactions, which lead to differences in the gel nanostructure (as described above in the microscopy imaging section). Nonetheless, it is clear that overall, across the gel-gel interface, the two amines are able to diffuse, and are exchanging with one another, even though they are an integral part of the nanoscale fibre network. Such progress could be compared in terms of diffusion speed for a given molecule. There are various parameters that can be compared having these kinetic constants such are the following list:

1. Region of the cell,
2. Temperature,
3. Diffusion time,
4. Initial concentration of two-component materials,
5. Density of the 3D network,
6. Nature of fibres (supramolecular affinity with the diffusing substances).

The list could be endless due to the enormous diversity of potential parameters that could affect the process of diffusion and because it will depend on the nature of the diffused molecules and the surrounding environment.

#### **3.7.5.2. Diffusions at 5°C**

We then performed the same experiment at lower temperature: 5°C, which gave rise to the results presented in Figures 3-30 and 3-31 for hexylamine and 1-naphthylmethanamine respectively.

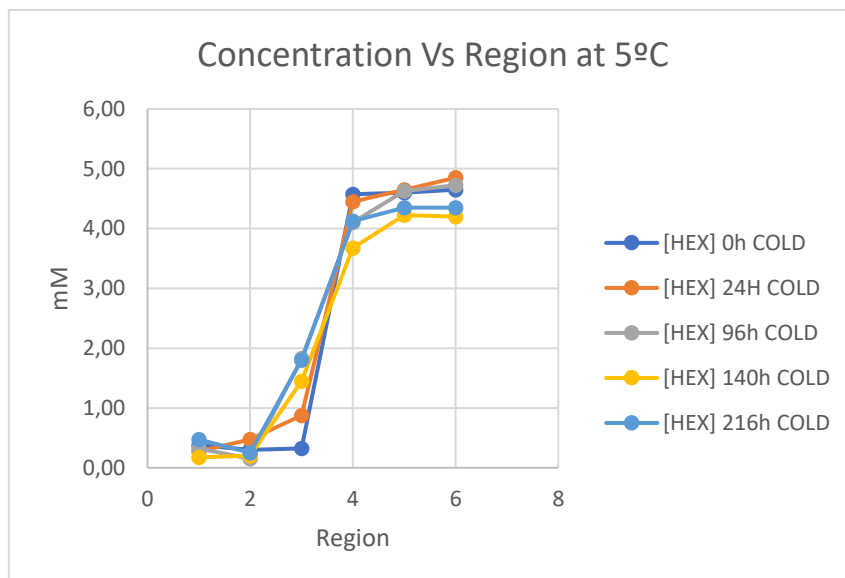


**Figure 3-30** Concentrations profile for Hexylamine in a diffusion cell for a range of various diffusion times at 5°C.

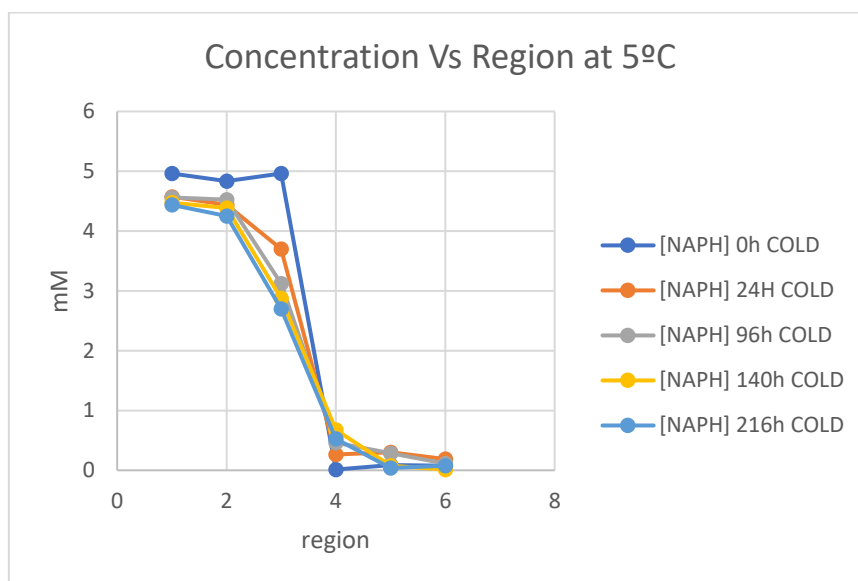


**Figure 3-31** Concentrations profile for 1-Naphthylmethylamine in a diffusion cell for a range of various diffusion times at 5°C.

As in the previous graphs we can observe the expected trend of diffusion from one side of the gel to the other, and with increasing time there is more diffusion (as is normal). However, the progress of diffusion is significantly lower at 5°C than was observed at

25°C. In particular, the diffusion has barely progressed at all into sections 2 and 5 of the cell (further from the gel-gel interface) unlike in the experiment performed at room temperature. For these diffusions, we can calculate a range of kinetic constants that will allow us to compare the various speeds for every region of the cell and the various temperatures.

### 3.7.5.3. Diffusions at 45°C

We then performed diffusion at elevated temperature: 45°C, which importantly remains below the  $T_{gel}$  value for these gels, and they are therefore not converted into sols. One of the main difficulties to get reliable results was that in some cases cells appeared to become dry after several days so that it was impossible to measure quantitatively with accuracy – this made it difficult to obtain diffusion profiles for longer than 96h. However, Figure 3-32 presents the data from this experiment.

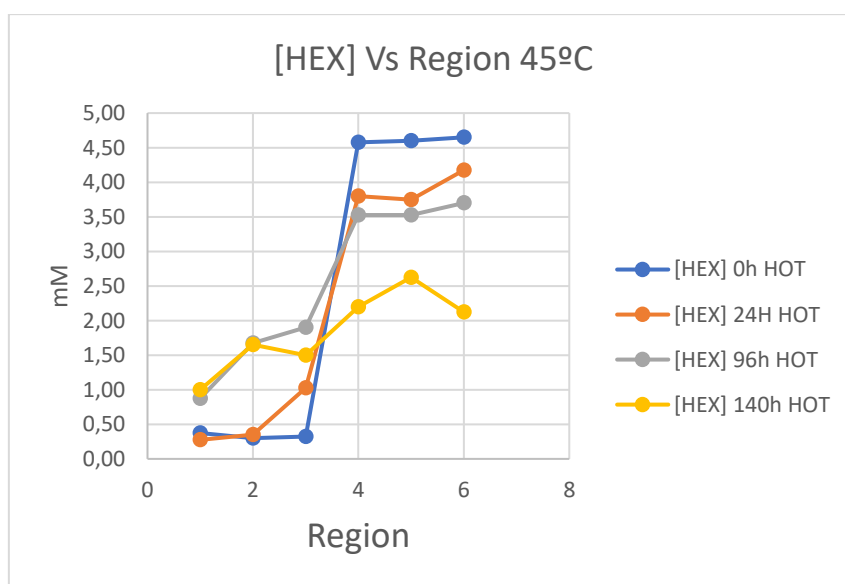


**Figure 3-32** Diffusion concentration Hexylamine profiles for various times and at 45°C

It is evident that the rate of change of concentration is now significantly greater, as indeed would be expected as a result of the elevated temperature. Indeed, after just 96 hours, the

concentration in cell region 3 has risen to ca. 2 mM and even that in cell region 1 has risen to 1 mM. Show a table of concentration versus time.

This could be due to two main factors.

- Increase of free available amines due to the displacement of the equilibrium between the two components in solution (amine + dendron). This is a reversible process. Supramolecular interactions are labile and affected by the surrounding physical and chemical conditions. Any variation in temperature will significantly affect the dissociation of complexes. Given we are proposing a hopping mechanism of diffusion, an increase in the amount of free amine (and the on-off rate) should have significant impact on the resulting diffusion rate.
- Increase of internal mobility of all liquid-like substances within the gel because of an increase of translational kinetic energy. Brownian motion will be faster and the molecular path will be longer in the same period of time.

Figure 3-33 reports the equivalent data for 1-naphthylmethylamine. The trend is almost the same which means that, as expected, higher temperature increases the diffusion rate across gel-gel interfaces.

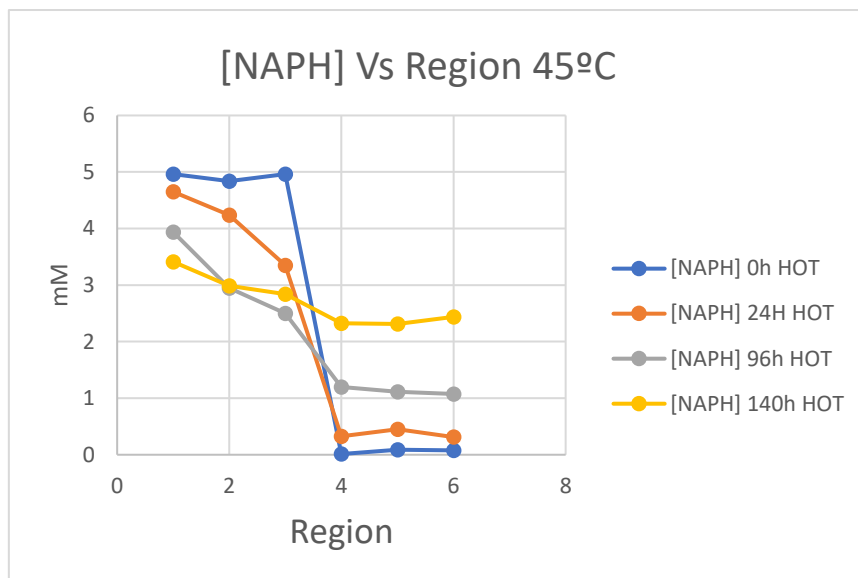


**Figure 3-33** Diffusion Naph concentration profiles for various times and at 45°C

As noted before one of the main reasons that could increase in the components diffusion is that increasing temperature can release more amine from the complex into the mobile liquid-like phase. This can, indeed, be seen by VT NMR experiments, where the concentration of available components can increase as temperature rises. Such experiments were reported in the previous chapter.

### 3.7.6. Diffusion coefficients of gel-gel transfers.

If we want to compare quantitatively the various diffusion conditions, it is necessary to calculate some kind of diffusion constant that will reflect the rate of mass transfer. The Fick's law give us an approximation to calculate diffusion coefficients which is shown in the following equation.

From the second law of diffusion.

$$\frac{\partial C(x,t)}{\partial t} = D \frac{\partial^2 C(x,t)}{\partial x^2} \quad \text{Equation 3-3}$$

The equation 3-3 says that the rate of change of the concentration of the chemical species at position  $x$  is the diffusion coefficient,  $D$  ( $\text{cm}^2\text{s}^{-1}$ ), that is multiplied times the rate of change of the gradient of the concentration at the position.

If we assume that we have cell in which the solute is present in half of the container. The concentration is taken initially as 1mM. The concentration profile at any time can be computed by:

$$C(x, t) = \frac{1}{2} \operatorname{erf} \left( \frac{x}{2\sqrt{DT}} \right) + \frac{1}{2} \quad \text{Equation 3-4}$$

Where  $\operatorname{erf}$  is the error function,  $C$  is the concentration,  $T$  is the diffusion time,  $D$  is the diffusion coefficient, with units of  $\text{cm}^2\text{s}^{-1}$ .

If we represent this model of diffusion and compare with the data obtained we can see some similarity that will depend on the value of  $D$  (figure 3-34)

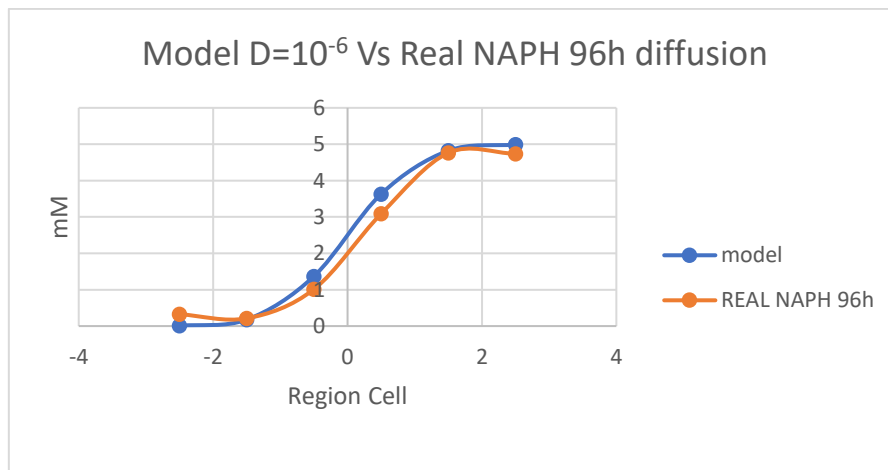


**Figure 3-34** Comparison Between the model with  $D=10^{-6}$  and the real diffusion profile corresponding to Naph at 96h at  $25^{\circ}\text{C}$

After realising that the model works and can be fitted in the set of concentration profiles that we obtained for each temperature we propose to calculate the values of  $D$  for each

cell, temperature and substance. This is done by summarizing all the concentration diffusion profiles and calculate for each substance and temperature the common diffusion coefficient. The selected procedure is collecting all the diffusion concentration profiles for each temperature and substance a diffusion coefficient is determined by the procedure of Least squares of each fitting for a specific time. (Figure 3-35)

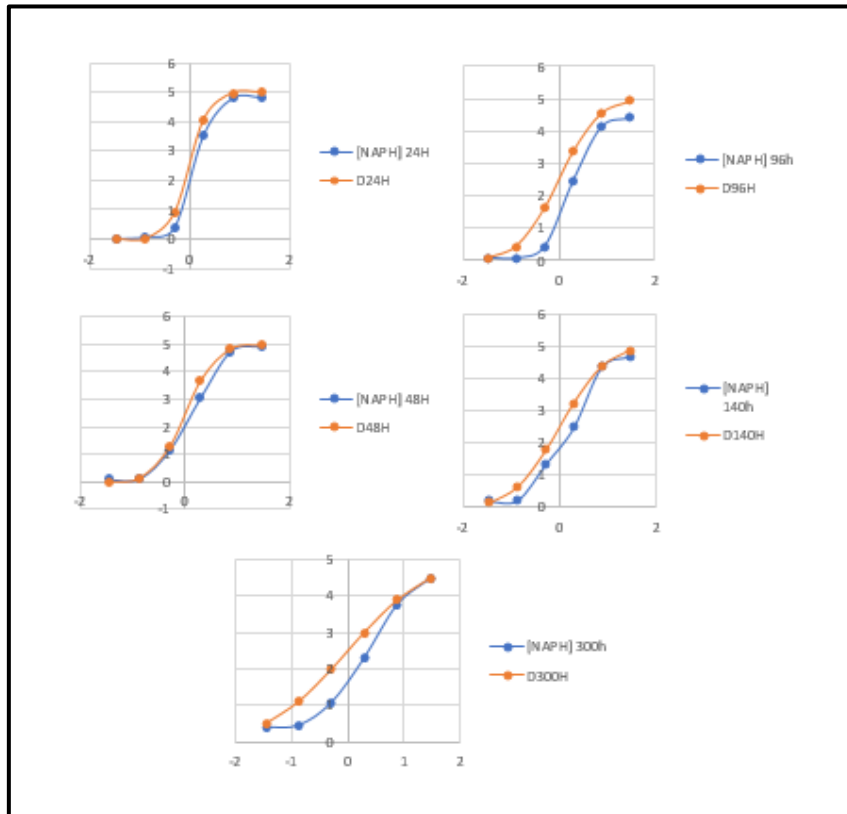


**Figure 3-35** All the Naph concentration profiles which are fitted with the equation of the diffusion model proposed above and with a Diffusion coefficient determined by least squares. 25°C

Then what we obtain by applying this least square method to the series of concentration profiles we collected is the determination of the diffusion coefficients associated at the experimental conditions that were developed. In the following table 3-1, diffusion values of amines at different temperatures of diffusion are shown.

Diffusion coefficients.			
Temperature °C	5	25	45
HEX	$1 \cdot 10^{-7}$	$7 \cdot 10^{-7}$	$5.69 \cdot 10^{-6}$
NAPH	$3 \cdot 10^{-7}$	$5 \cdot 10^{-7}$	$5.19 \cdot 10^{-6}$

**Table 3-1** Values of the obtained diffusion coefficients in  $\text{cm}^2\text{s}^{-1}$

From the data above we can figure out some trends. At room temperature both amines are moving at the same speed approximately  $7 \cdot 10^{-7} \text{ cm}^2\text{s}^{-1}$  for the Hex and  $5 \cdot 10^{-7} \text{ cm}^2\text{s}^{-1}$  for the Naph. When dropping the temperature to  $5^\circ\text{C}$  the difference between  $D$ s is growing having  $1 \cdot 10^{-7}$  for the Hex and  $6 \cdot 10^{-7}$  for the Naph. When increasing the experimental temperature to  $45^\circ\text{C}$  the both values of  $D$  increase one order of magnitude having  $5.69 \cdot 10^{-6}$  for the Hex and  $5.19 \cdot 10^{-6}$  for the Naph both in  $\text{cm}^2\text{s}^{-1}$  units. We can plot the values of  $D$  to have a better picture of the trend. (Figure 3-36)

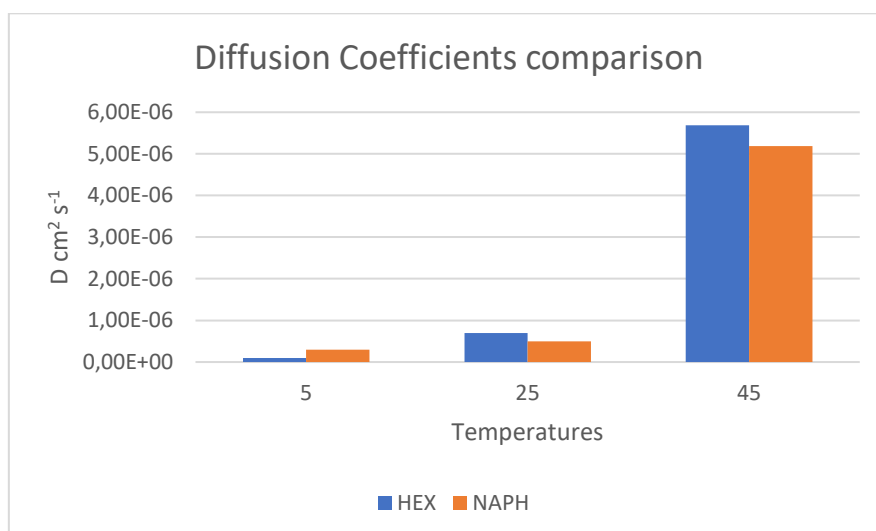


**Figure 3-36** Comparative values of diffusion Coefficients according to the substance and the temperature. This leads us to suggest that the effect of temperature on amine diffusion in this system is not only to increase the diffusion of the particles. We propose it does indeed also operate through a mechanism in which the supramolecular acid-amine interaction is plausible perturbed by temperature (as demonstrated by VT NMR), and hence the ability of the amine to diffuse through the gel via a hopping mechanism is significantly enhanced,

as a result of the reduction in the energy barrier to it hopping from one acidic site to the next as the temperature is raised.

In summary, we have therefore identified an unexpected diffusion process in which one of the components of a two-component gel can diffuse across a gel-gel interface, which allows its relatively slow, but consistent diffusion through these materials. Ultimately, this amine exchange mechanism gives rise to compositional change of these gels, which impacts on physical properties such as fluorescence.

### **3.7.7. Diffusions of dendrons gels at 25°C by CD measurements.**

So far, the diffusion systems described above have focussed primarily on the mobility of the amine through the gel network. However, this supramolecular gel is formed from a two-component system (amine + dendron acid). We have demonstrated above that the amine can diffuse through a gel-gel interface and that diffusion processes are therefore allowed, even for components which in principle are part of the 3D network. However, we were also interested to know whether the dendron acid also able to travel through the gel-gel interface. The generally understood model for gelation of these two-component peptide-based gels relies on intermolecular amide-amide hydrogen bond interactions between these peptidic dendron acids, and it might therefore be anticipated that this component is less able to diffuse through the gel network.

We were unable to easily use NMR methods to probe this, as changing the structure of the dendron acid can quite radically affect its ability to self-assemble. In order to address this question; an experiment was thus proposed taking advantage of a characteristic

possessed by this dendron acid - chirality. There are various stereoisomers for this dendron acid and we proposed to use  $D$ -G2  $((\text{Boc})_2\text{-Lys})_2\text{-Lys-OH}$  and  $L$ - $((\text{Boc})_2\text{-Lys})_2\text{-Lys-OH}$ . These dendrons have an enantiomeric relationship, and as such, gels formed from them will be identical in every way – except for properties associated with chirality. When combined with amines (hexylamine or 1-naphthylmethylamine) the gels form with equal and opposite circular dichroism spectroscopy signals. CD signals are well-known to be amplified for self-assembled systems, and this is known to be the case for these  $L$ -Lysine based dendron gels,<sup>67</sup> as intermolecular interactions between the amides pack the dendrons into a helical arrangement. Figure 3-37 illustrates the CD spectra of  $D$  and  $L$  enantiomers of the dendron acid. As is evident, they are mirror image spectra, reflecting the enantiomeric relationship of these molecules. The peak maximum at ca. 222 nm is associated with the UV absorption of the peptide chromophore. It should be noted that CD spectra must be measured in methylcyclohexane: dioxane (95:5) as this is optically transparent in the part of the spectrum where the peptide bond absorbed light – if toluene were used, it absorbs in the same region of the spectrum.

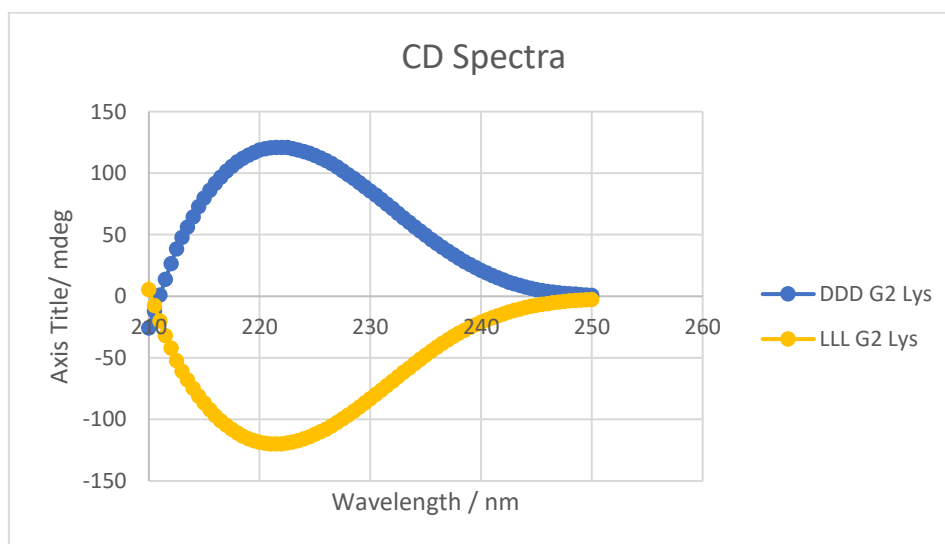


**Figure 3-37** CD spectra for samples which are stereoisomers DDD and LLL of G2  $((\text{Boc})_2\text{Lys})_2\text{-Lys-OH}$  dendrons 5 mM concentrations. Methylcyclohexane: dioxane (95:5)

To determine whether the dendron acids are, like the amines, able to move by means of diffusion through gel-gel interfaces, an experiment was set up in which we proposed to use CD spectroscopy to probe the movement of the dendrons. The gels on either side of the cell were assembled from G2 ((Boc)<sub>2</sub>-Lys)<sub>2</sub>-Lys-OH dendrons and hexylamine. The only difference between them was the stereochemistry of the dendron used, which was either L-G2 ((Boc)<sub>2</sub>-Lys)<sub>2</sub>-Lys-OH or D-((Boc)<sub>2</sub>-Lys)<sub>2</sub>-Lys-OH. As such, the gels were enantiomers of one another, with the same physical properties. This stereochemical difference is expressed, as mentioned before, in the opposite signal which is generated in a CD spectrometer; when mixing equal amounts of L-G2 ((Boc)<sub>2</sub>-Lys)<sub>2</sub>-Lys-OH and D-G2((Boc)<sub>2</sub>-Lys)<sub>2</sub>-Lys-OH gels, the CD signal self-cancel and becomes null as shown in Figure 3-38.

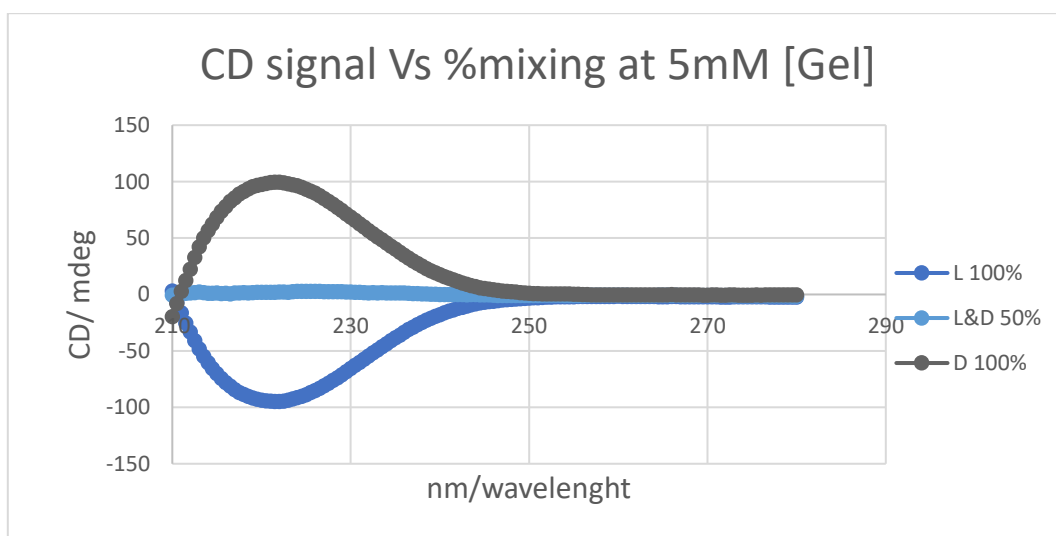


**Figure 3-38.** CD spectra that shows that equal amounts of a mixture of Hex L and D Lys Gels results in the cancellation of the resulting dichroic signal at 5mM concentration. Methylcyclohexane: dioxane (95:5)

CD spectroscopy can therefore be used to monitor diffusion because if the dendrons diffuse through the gel interface, signals that come from those regions closest to the interface will become weaker due to the mixing between L and D G2 ((Boc)<sub>2</sub>-Lys)<sub>2</sub>-Lys-OH dendrons and the cancelling of stereochemical information. Further, thanks to a

simple calibration curve it will be possible to gain quantitative insight using the intensity of CD signal to elucidate the % of mixing L and D Hex-Lys Gels.

### 3.7.7.1. Calibration curves

Firstly, we constructed a calibration curve to make sure that our concentrations and CD signals (D and L Hex-Lys Gels) have a clear correspondence at 25°C, and to test whether this was linear. Various samples were prepared adding increasing amounts of solvent (methylcyclohexane: dioxane 95:5) Consequently various concentrations were prepared for each stereoisomer (Figure 3-39).

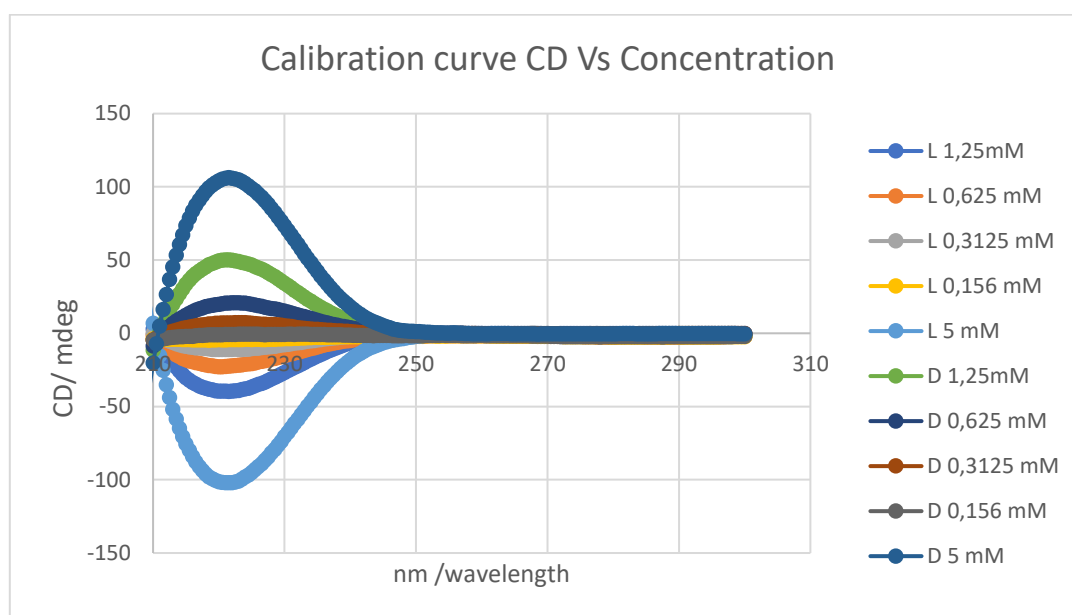


**Figure 3-39** Calibration Curve for samples which are stereoisomers DDD and LLL of G2 ((Boc)<sub>2</sub>Lys)<sub>2</sub>-Lys-OH dendrons. Various concentration has been analysed to get the relation between concentration and CD Signal at 25°C and 220 nm. Solvent mixture of Methylcyclohexane: dioxane (95:5)

To relate CD intensity with concentration we selected the maximum ellipticity wavelength and created a graph. Figure 3.40 shows such a fitting for DDD and LLL respectively. There is a reasonable linear correspondence between concentration and CD intensity. There may be some deviation which suggests that CD intensity increases

slightly more rapidly at lower concentrations, which could indicate some assembly-induced non-linear chirality effects, but overall, a linear fit is a reasonable approximation.

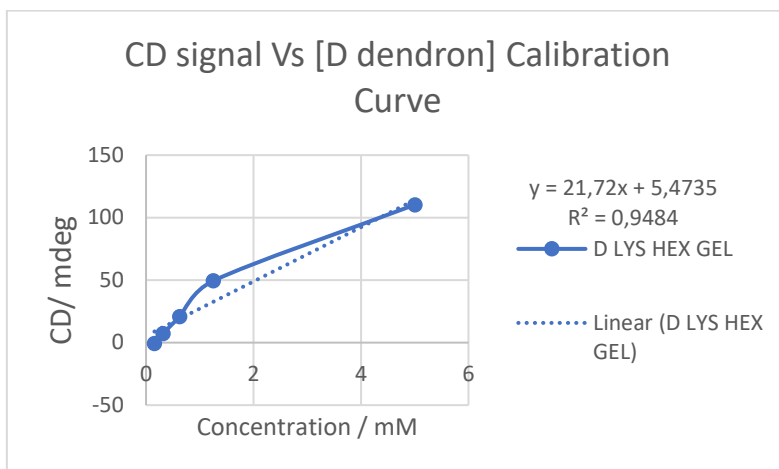


**Figure 3-40.** Calibration Curve fitting for the D Lys Hex Gel.

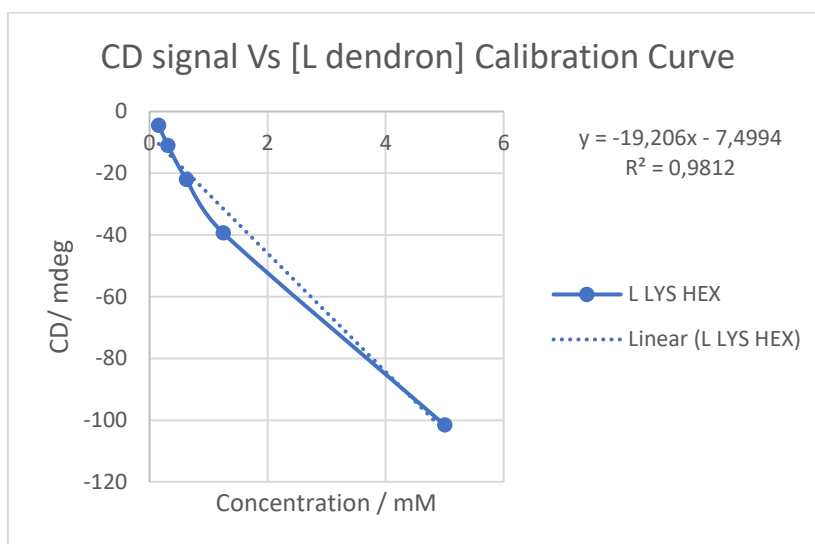


**Figure 3-41** Calibration Curve fitting for the Hex<sub>L</sub>-Lys Gel. 25°C, Methylcyclohexane: dioxane (95:5)

We then made mixtures of Hex Lys Gel based on both LLL and DDD dendron acids and constructed a calibration curve based on their CD signal intensity (Figure 3-41). This mixing experiment is more similar to what we would expect to happen across the gel-gel interface of our diffusion cell.

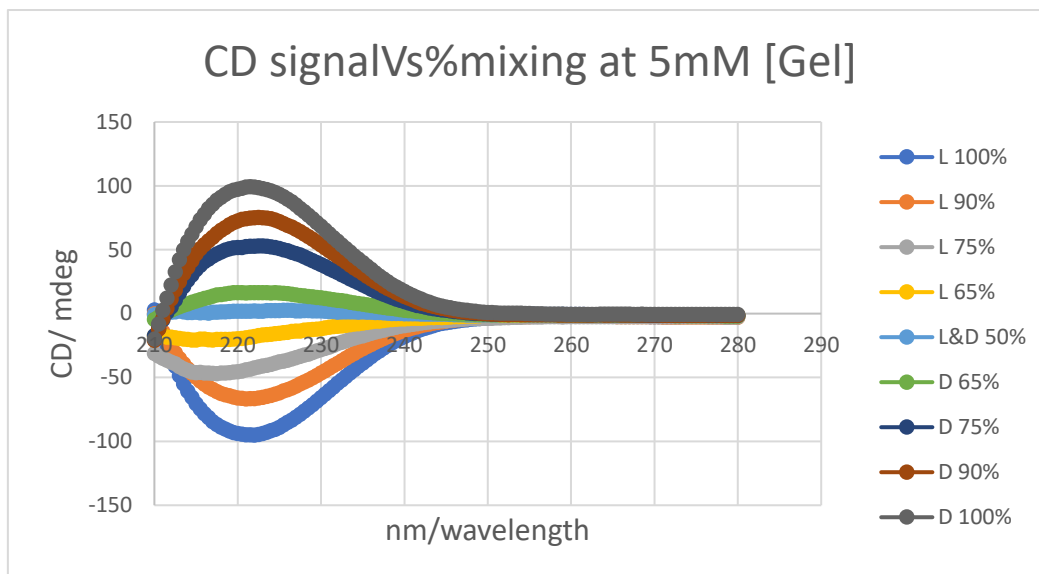


**Figure 3-42** Calibration curve for the CD signal and the various proportions of mixtures LLL and DDD.

We extracted the ellipticity at 220 nm, and constructed a calibration curve (Fig, 3-43) to calculate the % of dendron in any specific mixed system.

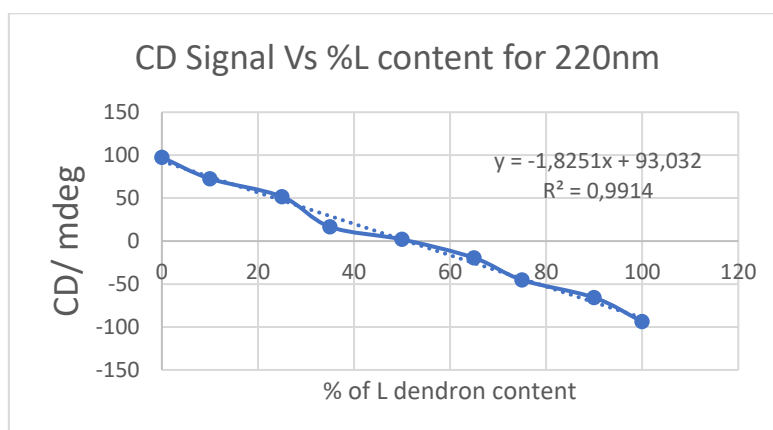


**Figure 3-43** Fitting of the data points presented in the table above for a given wavelength of 220nm

This mixing calibration curve showed a good linear fit. It has previously been proposed that such a fit suggests that the L and D systems are capable of self-sorting within a gel system,<sup>67</sup> as in the absence of self-sorting, significant non-linear effects would be

expected as the chirality of one enantiomer should be able to dominate the other through majority rules type principles.<sup>234</sup>

### 3.7.7.2. Explanation of CD experiment.

We then went on to perform the diffusion experiment. The experiment puts two different gels composed of DDD and LLL dendron acids respectively into contact, each with a concentration of 5 mM. The protocol for preparing the cells was identical to that used for amine diffusion. After specific diffusion times, the cells were sampled from their different regions into 6 different vials, evaporated and weighed. CD solvent (Methylcyclohexane-Dioxane 95/5) was added to the weighed samples in order to get certain equivalent concentrations (5mM) in all vials and then the samples were analysed by CD spectroscopy. All samples were left for 15 min in the CD quartz cell for a gel to form and maturing time. This is an important detail because depending on the maturation time, the intensity of the CD signal can change. Figure 3-44 presents the CD spectra that were obtained from the sampling of a diffusion experiment of 18 h (Figure.3-44).

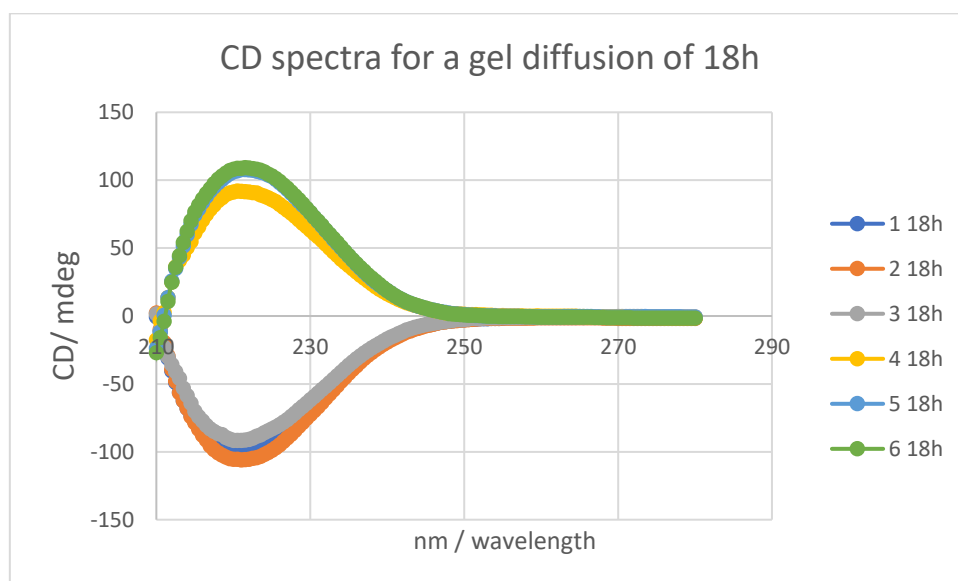


**Figure 3-44** CD spectra of the 6 different regions for a diffusion of 18h at 25°C

At this point, it is necessary to explain the meaning of the graph above. The most intense signals (negative and positive) correspond to the 1<sup>st</sup> and 6<sup>th</sup> regions of the cell. They have the highest absolute values because they have not experienced any mixing of chirality as they are most distant from the gel interface and hence from the diffusing enantiomeric form of the dendron. However, it is evident in Figure 3-45 that as we approach the limiting region of the gel-gel interface (3 and 4) there is a noticeable decrease of the CD signal expected for a concentration of 5 mM. This suggests that diffusion of dendrons may be beginning to start. Diffusion of dendrons, i.e., the ability to move the enantiomeric dendrons to move through the interface, would be reflected in the decrease of those signals as predicted from the calibration curve. If we go to longer diffusion times, Figures 3-46 and 3-47 present the results.

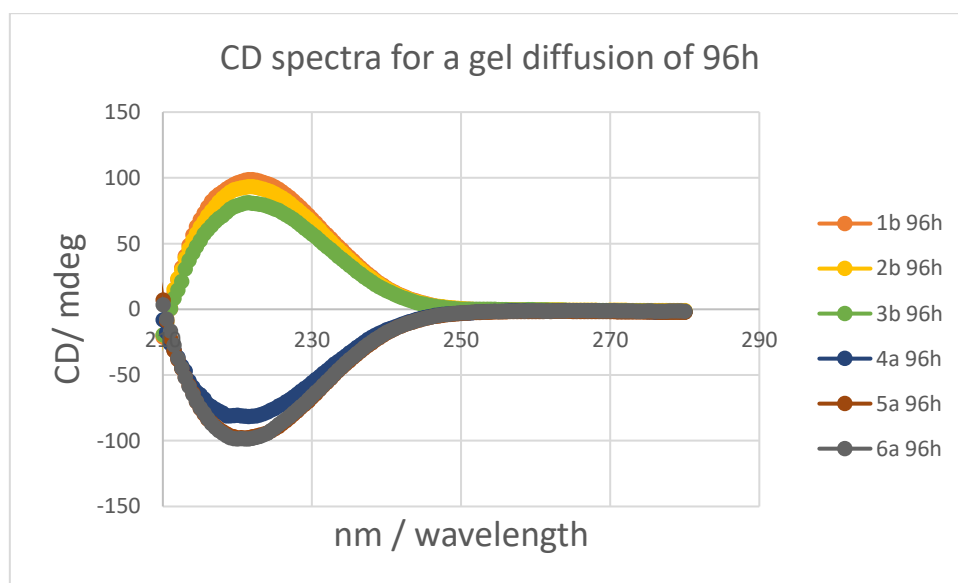


**Figure 3-45** CD spectra for a gel diffusion of 96h

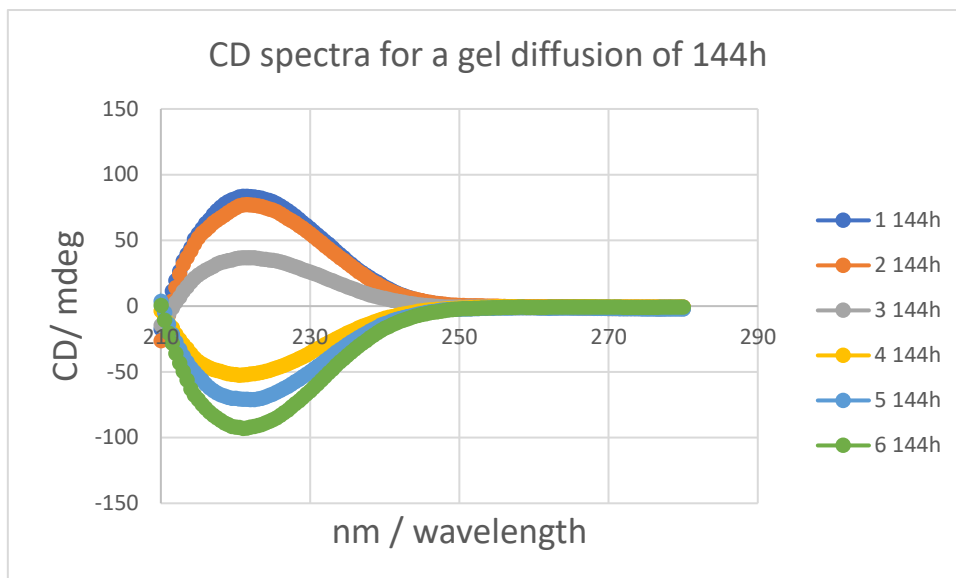


**Figure 3-46** CD spectra for a gel diffusion of 144h

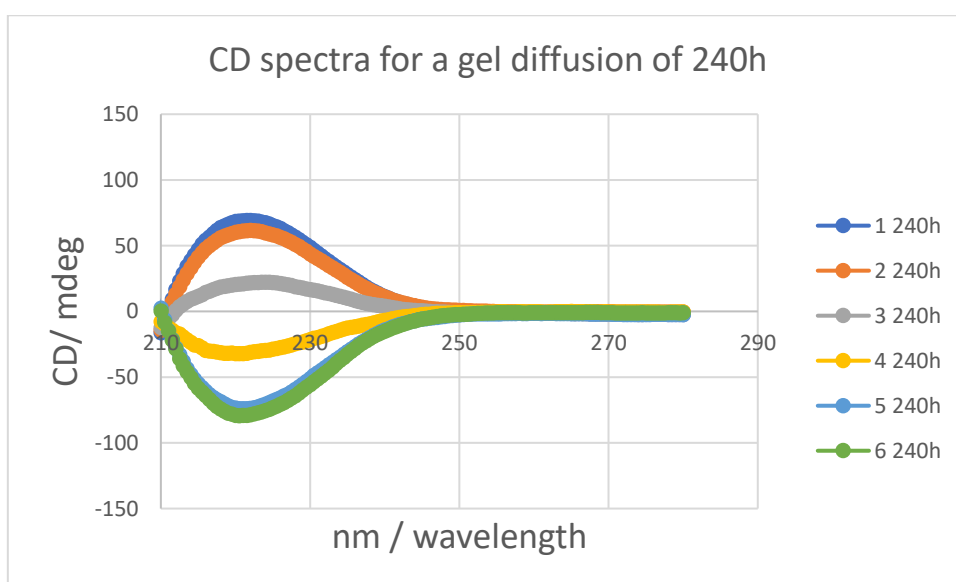


**Figure 3-47** CD spectra for a gel diffusion of 240h

The previous graphs Figures 3-45, 3-46 and 3-47 are a succession of diffusion experiments for various diffusion times in which can be seen the progressive decrease in signal particularly for the central region close to the gel-gel interface. These results confirm the concept that dendrons are also able to move through the gel. This was a very surprising result given that these dendron acids were expected to be even more intimately involved in the self-assembled gel-phase network than the amines, as result of the

intermolecular peptide-peptide hydrogen bonds which hold these materials together on the nanoscale. Qualitatively the results therefore confirm the proposed original idea of mobility for dendrons too.

Quantitatively, it is then necessary to use the calibration curve to understand the precise degree of mixing of DDD and LLL G2 ((Boc)<sub>2</sub>Lys)<sub>2</sub>-Lys-OH gels. As an example of the calculation will be presented based on the longest diffusion experiment of 240 h where L and D dendrons had reached the maximum progress of diffusion.

at 220 nm		
Region	Signal	% L Dendron content
1	68.43	13.48
2	60.31	17.93
3	20.63	39.67
4	-32.1	68.56
5	-73.42	91.2
6	-79.06	94.29

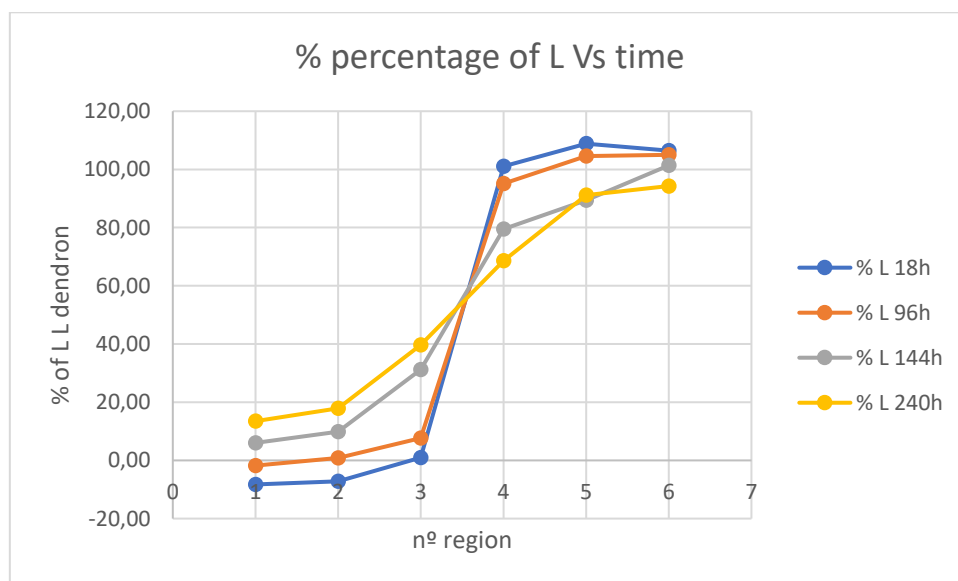
**Table 3-2** Table of the calculated composition for a Dendron diffusion of 240h.

Using our calibration curve (Figure 3-43), assuming the approximate nature of the CD signals of such calibration curve, we can determine the various percentages for the content of L Dendron in each region (Table 3-2). If we do the same for every diffusion time we can collect the various composition in percentage % of L Dendron in every region of the cells at certain times (Table 3-3) always taking into account the approximate nature of the calibration fitting that is used in order to calculate each dendron composition.

at 220 nm	region	18H		96H		144H		240H	
		Signal	% L dendron content	Signal	% L dendron content	Signal	% L dendron content	Signal	% L dendron content
	1	108,12	-8,27	96,28	-1,78	82,04	6,03	68,43	13,48
	2	106,14	-7,18	91,59	0,79	74,98	9,89	60,31	17,93
	3	91,25	0,98	78,95	7,72	36,09	31,20	20,63	39,67
	4	-91,48	101,10	-80,54	95,10	-52,03	79,48	-32,10	68,56
	5	-105,61	108,84	-97,83	104,58	-70,15	89,41	-73,42	91,20
	6	-101,19	106,42	-98,63	105,01	-91,98	101,37	-79,06	94,29

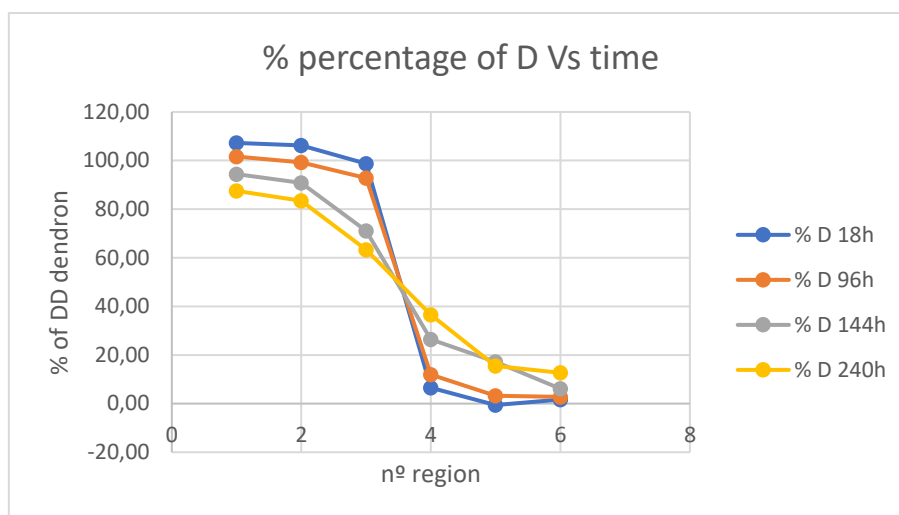
**Table 3-3** representation of % of L dendron in different regions of the diffusion cell at various diffusion times.

Table 3-3 represents the % of L dendron in different regions of the diffusion cell at various diffusion times. So if they are plotted like diffusion profiles according to regions then we obtain representations such as in Figure 3-48



**Figure 3-48** Percentage content of the L dendron concentration while diffusing in the cell at several times as deduced by CD measurements.

Note that due to the approximate nature of the calibration curve there is a lower content of L G2 ((Boc)<sub>2</sub>Lys)<sub>2</sub>-Lys-OH dendron than possible, particularly in the 1, 2 and 3 regions. For the D dendron we find a similar concentration profile which could be considered as a mirror image of the L dendron profile shown above. (Figure 3-49)



**Figure 3-49** Percentage content of the D G2 ((Boc)<sub>2</sub>Lys)<sub>2</sub>-Lys-OH dendron concentration while diffusing in the cell at several times as deduced by CD measurements.

Comparing these results against the diffusion of the amines (Based on NMR measurement) as outlined in earlier sections, it is clear (By CD) that at ca. 140 hours, the dendron has diffused ca. 30% diffusion into section 3, and 10% diffusion into section 2. At the same time, hexylamine had diffused by 40% into section 3 and by ca. 10% into section 2, while 1-naphthylmethylamine had diffused by ca. 30% into section 4 and <10% into section 5. As such, it would appear that the dendron acid and the amine each have relatively similar mobilities in these materials. This is a surprising result, and suggests that as the complex between the acid and amine breaks, both components are equally able to move within the gel, and that the dendron acid is not further immobilised as a result of non-covalent peptide-peptide hydrogen bonding interactions. Indeed, this suggests that when the acid-amine complex is broken, the two individual components disassemble from the gel nanofibres and start their diffusion process, where if they come into contact with their complementary binding partner, they would then reassemble into the gel network. This was a somewhat counter-intuitive finding, and demonstrates the power and interest of performing controlled diffusion experiments within self-assembled materials of this type.

In total, these observations suggest the ability of one gel to diffuse into another, and adaptive mixing to occur across gel-gel interfaces. This speaks in a remarkable way for to the dynamics of these materials, and helps envision a wide range of possible experiments in which the dynamic characteristics of gels can be used – not only in terms of their highly dynamic liquid-like phase, but also in terms of dynamics of their self-assembled solid-like networks. After this treatment we could try to obtain the diffusion coefficients corresponding the movement of the dendrons.

	D cm <sup>2</sup> s <sup>-1</sup>
Temperature °C	25
L Dendron	$3 \cdot 10^{-7}$
D Dendron	$3 \cdot 10^{-7}$

**Table 3-4** Dendron Diffusion coefficients for 25°C

If we compare diffusion coefficients between amines and dendrons we can say that diffusion of dendrons is slightly slower than the amines.

### **3.8. Ultrasound influence in gel solid-like state.**

Ultrasound stimulation can be a good way to promote and accelerate diffusion processes. We were therefore interested to understand the impact of ultrasound on these gelation systems.

Initially, a simple experiment was therefore set up and conducted with gels based on different amines layered up in a single vial, as originally performed and described earlier in this chapter in the absence of ultrasound stimulation. This was a qualitative and rapid experiment to track the diffusion of the fluorescent component by naked eye. The key point was to stimulate the two-gel system continuously with an ultrasound bath once the

gels have been brought into contact with one another. In Figure 3-50, we can clearly see that the diffusion process is apparently significantly accelerated by the effect of ultrasound. In fact, however, in this case, the acceleration is produced by the disintegration of the gel structure itself and eventually (45min) the destruction of the solid-like appearance the gel, which now has a liquid like appearance giving rise to effective mixing between layers. As such, the gel-gel interface has been destroyed by the effect of ultrasound.

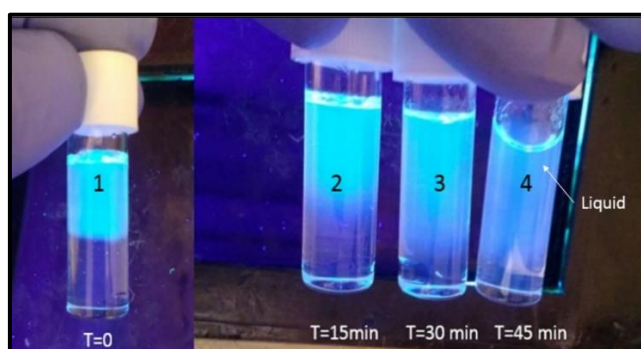


**Figure 3-50** Gels diffusing under sonication conditions. Notice total fracture of the gel material to become after 45 min of sonication in a liquid.

We were interested to understand the nature of the new liquid after continuous sonication for 45 min. Was it simply an isotropic liquid, or did it have any remaining structure. To answer this, we prepared samples of gel, and sonicated one of them. The final appearance of the two vials was as shown in Figure 3-51.

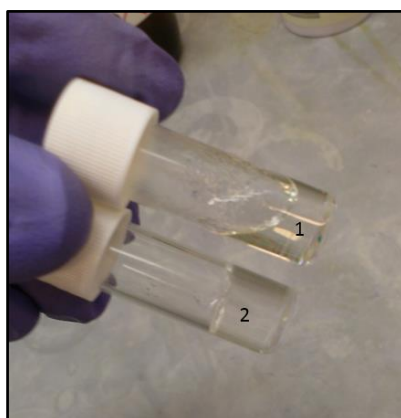


**Figure 3-51** Picture showing the difference between a sonicated HexGel (1) and non-sonicated HexGel (2).

Two different gels were sonicated in 2 mL vials: HexGel and NaphGel. HexGel was sonicated for 20 min controlling the temperature of the bath at 15-20 °C by adding ice. The temperature of the bath was checked with a laser thermometer. After 20 min of sonication the gel was transformed into a liquid state even though the temperature of the vial was only 17 °C – i.e. the system was significantly below the gel-sol transition temperature. This liquid state was then cooled to 5 °C in an ice cooled bath. The gel remained, perhaps surprisingly, in a liquid-like form. To check that the components of gel had not changed composition, the liquid state was then heated with a heat gun and cooled down in an iced bath. On this treatment, the gel regained its characteristic solid-like structure. This suggests that at room temperature the sonicated gel becomes a metastable liquid-like state, which is only able to re-enter into the gel-phase if it is treated thermally in order to overcome the kinetic barrier associated with self-assembly. There is considerable current interest in the academic literature in kinetically trapped, metastable, self-assembled states.<sup>235,236</sup>

To probe that sonicated gels are basically the same after sonication and that there are not variations in composition of the material but instead variations in the nanostructure of the material produced, an experiment was performed. Two identical Hex Gels of 10 mM were prepared, and one of them sonicated until complete formation of the viscous liquid from the original solid. The resulting liquid and solid gel were then analysed by <sup>1</sup>H-NMR after generating the xerogels by evaporation and redissolving in d<sub>4</sub>-methanol. The resulting spectra (Figure 3-52) were compared and no chemical differences in terms of shift and intensity of the peaks were found – indicating that there has not been any change in molecular-scale composition –rather the changes are only in terms of nanoscale structure. CD experiment check of the sonicated and non-sonicated gel remains as one of the key

analysis that in future experiments could give essential information about the nanoscopic reorganization under this sonication stimulus to gels.

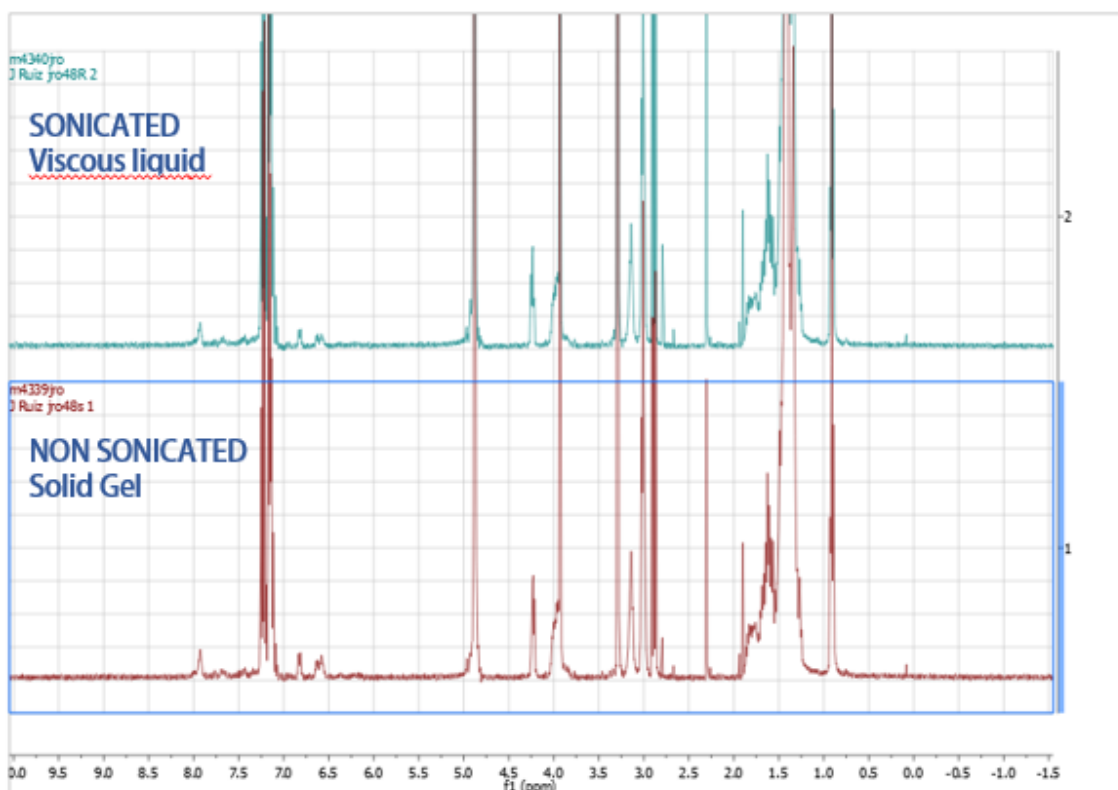


**Figure 3-52.** NMR Spectra of sonicated and non-sonicated Hex Gels. Both spectra are completely identical.

The NaphGel had the same behaviour as that described above. The gel was sonicated for at least 30 min. Interestingly, gel breakdown took longer than HexGel, which might indicate a more stable gel network (possibly in agreement with the characterisation above which indicated that Naph-Lys Gel forms smaller diameter nanofibres than Hex-Lys Gel, which may result from greater solvent compatibility and hence less bundling). A liquid like state was obtained at 17°C. The gel was then cooled to 5°C and remained in a liquid state. On heating with the heat gun and cooling in an ice bath, this gel also once again regained its solid-like gel form.

After both experiments, the organogels were dissolved and analysed by <sup>1</sup>H-NMR and both the liquid form and the solid-like gel showed similar signals and shifts. This allows

us to determine that there were no reactions at the molecular level. This is therefore an interesting behaviour in which sonication disrupts gelation and leads to a very unusual kinetically-trapped liquid state which can only rearrange into a gel on heating and cooling. Most importantly, it must be remembered that the formation of these gels does not normally require heating and cooling – simple mixing of the two components at room temperature is usually sufficient to give rise to self-assembly and gel formation. As such, the need for heating and cooling of the sonicated solution suggests that after breaking down the gel fibres in this way (as seen in the AFM images), we access a state which is not able to reassemble and reorganise sufficiently at room temperature. It seems plausible to suggest that the sonicated system may contain larger assemblies, rather than molecular-scale species, and that the reorganisation of these are therefore kinetically limited as a result of their size. Conversely, when mixing molecularly dissolved dendron acid and amine components at room temperature, the self-assembly process, which occurs through a cooperative nucleation and chain extension mechanism, can occur because the molecular-scale components have much higher diffusional mobility, and ability to reorganise and optimise their non-covalent interactions.

### **3.8.1. AFM as an imaging technique.**

In order to gain greater insight into differences between the sonicated liquid-like state and the solid non-sonicated gel, atomic force microscopy (AFM) was employed in Brussels as part of an internship coordinated by the SMARTNET program and the chemical company Solvay. Imaging was performed comparing the sonicated and non-sonicated states of Naph-Lys Gel and Hex-Lys Gel. Samples were imaged in xerogel form – we note that this can introduce morphological change as a result of sample drying, but is a fair comparative technique where all samples of chemically related systems have been prepared by drying in the same way. In order to visualize the nanostructure of the

xerogels, four different gels were prepared. Four combinations of two amines and two dendrons of different stereochemistry (L and D stereoisomers). The produced gels were labelled according to their composition. The final concentration of all gels was 10 mM.

One of the main objectives of this experiment was to assess differences in the nanostructures of materials depending on the conditions of their formation. So, there were three different ways in which the samples were treated prior to drying.

- 1) **Kinetic formation of gels:** The first way of forming the gels was the kinetic approach in which the two solutions components of gel (both amine and dendron acid) are simply mixed and instantaneous gelation takes place. This occurs in about one second for Naph-Lys Gel and around five seconds for Hex-Lys Gel.
- 2) **Thermodynamic formation of gels.** Once the gel was formed kinetically (explained above) the gel was melted by means of heating and reformed on slow cooling in order to rebuild the 3D network (heating-cooling process). This is a kind of annealing processes in polymer science and allows the gel to form while more energy is present and the system is under a greater degree of thermodynamic control.
- 3) **Sonication treatment:** Thermodynamically formed heat-cool gels were treated with sonication in a standard sonicator bath (Elmasonic P, 37kHz, 120W, 5 litres). Gels were treated simultaneously to exert the same sonication time (45 min) to all the samples. In each case, the gel was converted into a liquid-like form.

**Production of Xerogels from gels:** In order to image the produced gels there is the need to dry the gels. Even though AFM allows wet imaging, the images obtained in this way can have poor resolution, and comparative work can be very difficult. Further, it is very hard to achieve this in volatile organic solvents such as toluene being used here. As such, it was preferred to prepare dry samples from the formed gels. The procedure to prepare the dried gel was by placing a sample on a small piece of the silicon wafer (5mm\* 10 mm) and allowing the solvent to simply evaporate over one hour. This simple procedure was an effective approach to sample drying.

The AFM images of the kinetic and thermodynamically formed gels were presented earlier in this chapter (Figure 3-8 and 3-9). Here we present the AFM images of the sonicated materials

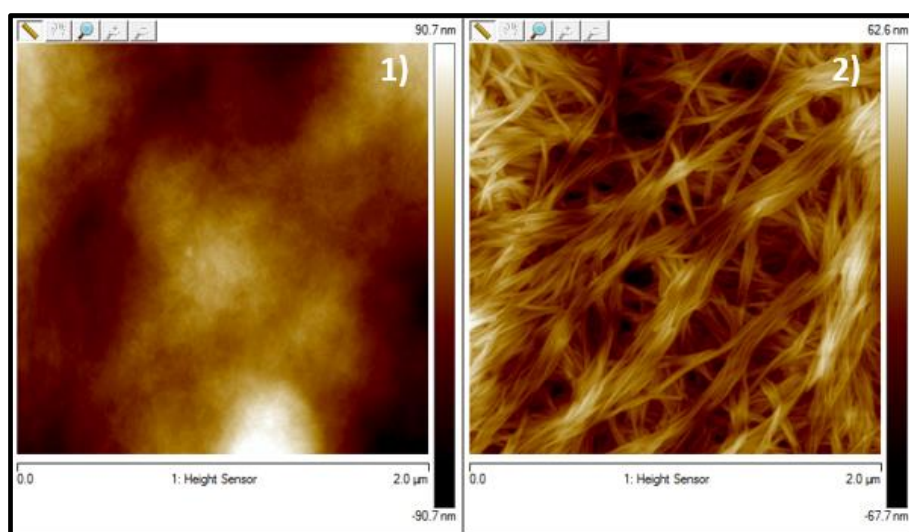


**Figure 3-53** Gels thermodynamically formed and sonicated which composition is Naph-L-Lys Gel and Hex-L-Lys Gel.

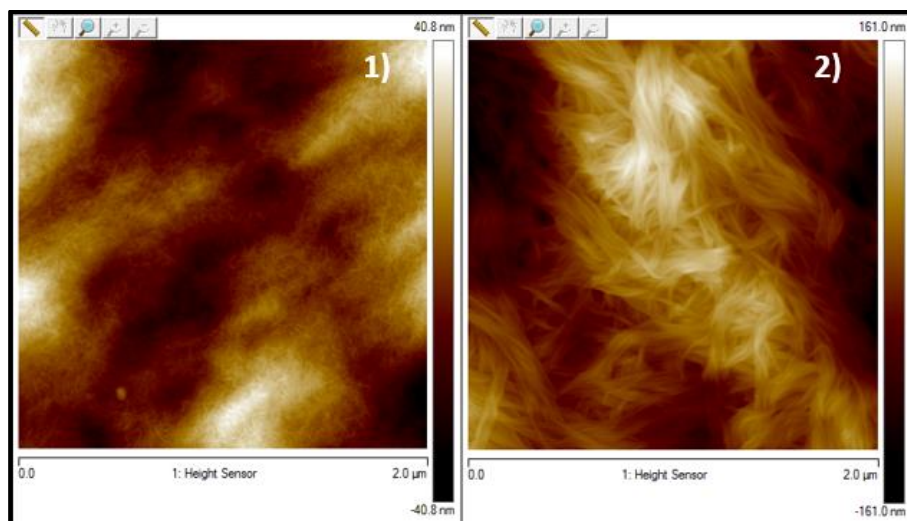


**Figure 3-54** Gels thermodynamically formed which composition is Naph-L-Lys Gel and Hex-L-Lys Gel. Comparing with these fibers with the ones that were not sonicated it can be seen that there is an expansion making the material more porous and thus, structurally more fragile.

### 3.9. Conclusions and future ideas.

Chapter three reports diffusion across a gel-gel interface, and in particular compares and contrasts the diffusion of small molecules which are mobile within the gel with the diffusion of the small molecules that actually self-assemble into the solid-like fibres. Such gel-gel diffusion processes are underinvestigated and are important in helping understand release processes that gels can have when they are loaded with functional chemicals. We find that although as expected, small molecules diffuse rapidly through the gel, even those small molecules which are part of the solid-like network can also diffuse and exchange across the gel-gel interface. This latter process is quantified in detail by means of determining the respective diffusion coefficient  $D$ . We find that diffusion of fully mobile diphenylamine small molecules is much higher ( $D = 10^{-4}$ ). We find that the amine is slightly more mobile than the acid dendron, which may reflect the latter being more integrated in the gel network through hydrogen bonding. The diffusion of self-assembled nanofibre components has important consequences for the potential ability of supramolecular gels to self-heal. The great milestone of this chapter is the development

of a method which allows to put into contact two different gels and measure the kinetics of the mass transfer between them of various substances. Thus we can study the dynamics of the transfers of virtually any substance that can move from one gel to the other by passing through that gel-gel interface created between the two regions of the diffusion cell. Finally, we can highlight the values of Diffusion Coefficient (by NMR and CD) to get a better idea of the rate of diffusion depending on the nature of the gel conditions (components, crosslinking, temperature) and the kind of substances which are being diffused.

Temperature °C	Diffusion coefficients.		
	5	25	45
Hex	$1.00 \cdot 10^{-7}$	$7.00 \cdot 10^{-7}$	$5.69 \cdot 10^{-6}$
Naph	$3.00 \cdot 10^{-7}$	$5.00 \cdot 10^{-7}$	$5.19 \cdot 10^{-6}$
Dendron		$3.00 \cdot 10^{-7}$	
Diphenylmethane		$3.29 \cdot 10^{-4}$	

**Table 3-5** Values of Diffusion Coefficients D for the studied diffused substances. Units are in  $\text{cm}^2\text{s}^{-1}$

It can be concluded that the diffusion values clearly depend on the temperature and on the concentration gradient of the diffused substance. If we compare the gradient of the Diphenylmethane introduced (5mM) with the concentration of components that are free available when gel is formed at the temperature of gelation and diffusion (0.5 mM for Naph, 1.2 mM for Hex and 0.5 mM for the dendron at 25°C).

Temperature °C	Concentration mM	
	25	45
Hex	1.2	2
Naph	0.75	1.3
Dendron	0.5	0.93
Diphenylmethane	5	5

**Table 3-6** Real concentrations of components when diffusing

In future investigations the system can be enhanced and adapted for any solvent conditions. Also it can be explored the use of this cells to study ionic movement in gels where ions are present such as aqueous electrolytes, ionogels (IGs) and deep eutectic gels (DEGs).

## Chapter 4 Ionogels Conductivity

### 4.1. Introduction

This Chapter describes the understanding and the design of a strategy to form supramolecular gels in ionic solvents. Gels are such dynamic materials that allow self-diffusion due to the large amount of solvent they contain ( $\gg 90\%$ ), even though they have solid-phase appearance and rheological properties over short timescales. There are a number of examples of gel systems which are aqueous and are used in various ionic conductive applications such as electrolytes<sup>237</sup> for batteries<sup>238</sup> and supercapacitors,<sup>239,240,241</sup> pollutant removal,<sup>242</sup> molecular reactors,<sup>243</sup> and electrophoretic media.<sup>244</sup> However, we were interested in the development of gels in inherent non-aqueous ionic media as described in the sections below.

There is an inherent interest in the development of gellified versions of ionic liquids – indeed ionogels are well explored in the literature.<sup>192,245,246</sup> In particular, as outlined in Chapter 1, there is developing interest in a variation of developing gels based on ionic deep eutectic solvents (DESs).<sup>247</sup> These ILs or DESs can function as electrolytes, and it is therefore quite understandable that for applications which encapsulate these electrolytes, such as batteries<sup>248</sup> or electrochemical solar devices<sup>249,250,251</sup> would benefit from the use of solid-like electrolytes which allows high ionic conductance, whilst also limiting problems associated with leakage, flammability<sup>252</sup> electrochemical stability<sup>175</sup> and volatility, which are present inherently in liquid electrolytes which may cause safety issues. Gels offer a potential solution to this problems while maintaining other characteristics of DESs and being easily processed at an industrial scale (high processability).<sup>252,253,254</sup>

#### 4.1.1. Natural Deep Eutectic Solvents (DESs)

Deep eutectic solvents (DESs)<sup>167</sup> have been of considerable recent interest. As outlined in Chapter 1, such systems are defined by a mixture of solid Brønsted or Lewis acids and hydrogen bond donors to generate liquid-like materials. The result of such a combination can be low temperature ionic melts with high ionic conductivity, chemical stability, low cost of materials and low toxicity. Deep eutectic solvents are classified in several groups:

- Type I: Quaternary ammonium salt + metal chloride.
- Type II: Quaternary ammonium salt + metal chloride hydrate.
- Type III: Quaternary ammonium salt + hydrogen bond donor.
- Type IV: Metal chloride hydrate + hydrogen bond donor.

In this study, we focussed on type III DESs. These consist of a quaternary ammonium salt combined with a hydrogen bond donor which allows great versatility when selecting each component to use. Choline chloride is a versatile salt that can be combined with a myriad of compounds, such as carboxylic acids, urea derivatives and alcohols. Depending on the substance the ideal molar ratio between the two is either 1:1 or 2:1. The substances can be solid or liquid, and the mixture of both always results in the creation of an ionic liquid of a certain viscosity and ionic conductivity. Importantly, these components have low toxicity and good environmental profiles making them of considerable relevance for industrial use.

These unusual properties give rise to a variety of potential applications of extraordinary impact, particularly in green chemistry<sup>255</sup> and electrochemistry.<sup>175</sup> These systems are able to completely change their physical properties as a result of the stabilising supramolecular

interaction between the two different components. As explained in Chapter 1, this can be represented in physical terms by means of comparing the melting point of the starting materials and the mixture as shown in Figure 4-1.

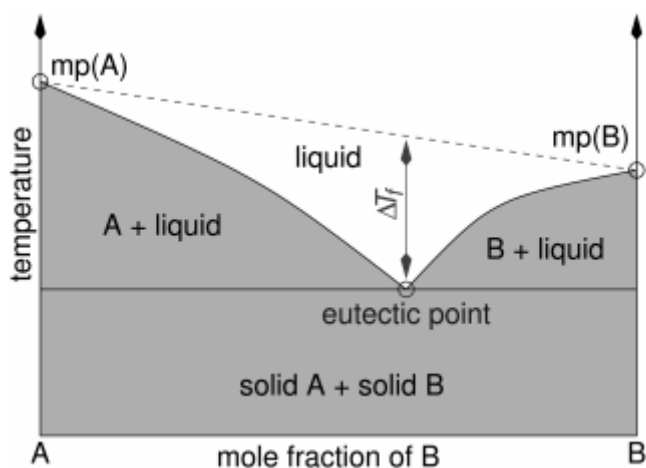


**Figure 4-1** Schematic representation of a eutectic point of two-component phase diagram.<sup>167</sup>

#### 4.1.2. Organic Ionic gels

The proven potential of deep eutectic solvents in electrochemical applications is relatively recent and has deep implications in technology.<sup>167</sup> Advances in this field can impact hugely on battery technology due to the very broad electrochemical window<sup>175</sup> in which the DES and its basic components are chemically stable during normal electrochemical processes, that is, when certain potentials and voltages are applied. This critical application of battery energy storage<sup>200</sup> has tremendous potential implications on environmental, economic and social issues, thus leading to the importance of these DESs.

There is a need to develop gel systems which integrate ionic liquids (ILs) due to these potential applications in battery technology<sup>183</sup> – there are not many examples of DESs which have been gellified.<sup>196,256</sup> Thus, trying to develop a gel based on DESs was a key objective in this third stage of research. We therefore proposed to develop an ionogel based on deep eutectic solvents and explore the mobility of the ionic deep eutectic solvent

phase within the overall soft material. Intriguingly, the Smith lab has developed significant experience in forming gels in glycol-type solvents for a range of industrial applications. These gels were based on 1,3:2,4-dibenzylidenesorbitol (DBS) that is able to gelate (thus self-assemble) in multiple solvent environments. This system, as well as some derivatives of DBS, have been shown to be excellent gelators of glycols and mixed aqueous glycol media.<sup>62</sup> Knowing that in the field of DESs there are various ionic liquids based on several types of glycols such as PDO (1,3-propanediol), MPG (propane-1,2-diol), MEG (mono ethylene glycol)<sup>189</sup> each combined with choline chloride there was therefore an ideal opportunity to test gelation on these particular deep eutectic systems. PDO is obtained naturally from corn, and is considered to be a 'green' glycol.<sup>257,258</sup> This is a significant advantage of DESs over ionogels formed from traditional ionic liquids. Of particular interest was determining (i) whether gelation could be achieved and (ii) the impact of gelation on the physical properties of the deep eutectic solvent, including diffusion of ions and hence conductivity.

The introduction of a gel network in a liquid media does not necessarily decrease the mobility of the liquid-like molecules, which in principle makes ionic conduction possible, regardless of the specific ionic mechanism of charge conduction. This is reasonably well established in ionic liquid ionogels<sup>259</sup> but has not been demonstrated for supramolecular gels formed in DESs. There was some concern that the presence of a self-assembling LMWG additive, which assembles as a result of non-covalent interaction might adversely affect the interactions between the two components in a DES, and limit their physical properties, or their ability to diffuse.

If a voltage is applied to a gel and there are charged molecules inside that gel there will occur induced diffusion motivated by an electrical interaction between the electric field and the charged molecules or complexes being this process the basis of electrophoretic<sup>260</sup>

processes. A similar process can happen in electrolytes which are part of batteries or supercapacitors<sup>261</sup>. There is a diffusion process in these devices, and then certain substances are converted into others when reacting at the plates.

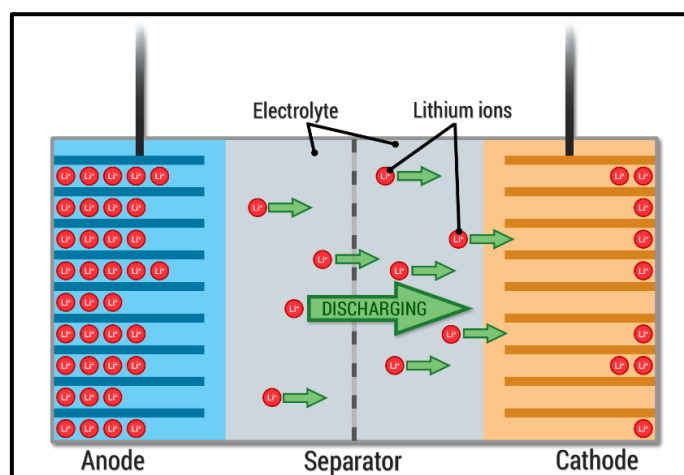


**Figure 4-2:** Picture represents such a mass transfer which is required when an electrochemical device such as a battery is running.

It is clear that in order to transfer ions from one side of the cell to the other ions have to move. That movement is driven by electrostatic forces between the plates and ions. The speed of such a transfer will be dependent on the propagation mechanism. An ideal electrolyte should be highly conductive in order to reduce the whole internal resistance of an electrochemical device. If high ionic conductivity is reached within the electrolyte that means that propagation of key ions is allowed very easily and thus mass transfer is produced almost instantly. This kind of system is ideal to apply in batteries, supercapacitors and even hybrid systems of those two. Such ionic conductivity decreases the internal resistance of the cell and thus the generated temperature in the process of discharging and charging is insignificant compared to other more traditional systems such as lead acid batteries or lithium based cells. This mentioned property should enable rapid charging processes.<sup>262</sup>

### 4.1.3. Objectives of the Research

As outlined in Chapter 1, DBS was first reported by Meunier in 1891. In the Smith research group there has been an intense study of DBS low molecular weight gelators (LMWG) as gelator for both organic (polyols) and aqueous solvents (Figure 4-3).<sup>242</sup> The minimum gelator concentration for DBS and its derivatives is quite low (1% by weight) and the chemical nature of gelator is sufficiently simple to have a very low cost for preparation, which can be achieved on an industrial scale. Indeed, this gelator is synthesised by simple one-step condensation of sorbitol with two equivalents of benzaldehyde – both of which have the potential to be naturally-derived compounds. The low-cost and simple nature of this gelator has tremendous advantages in terms of potential industrial applications, and means this system has genuine plausible uses in energy technology such as dye sensitized solar cells where DBS played an important role.<sup>263</sup>

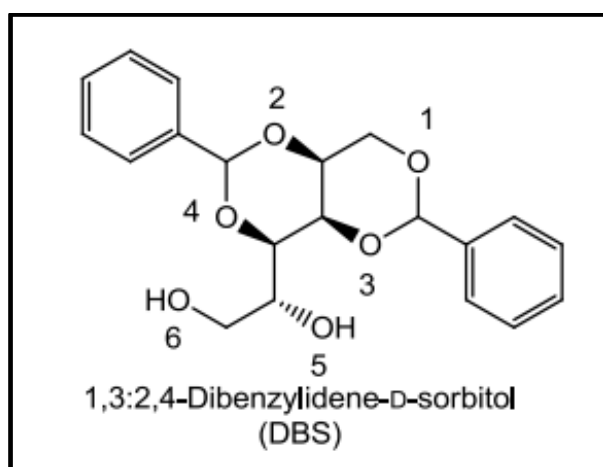


Figure 4-3: Typical Butterfly structure of DBS.<sup>242</sup>

It is worth noting that when talking about complex systems such as DES or ionic solvents, which are basically ambient temperature ionic melts, one should be cautious about the number and the kind of supramolecular interactions that could result from using a gelator such as DBS. At present, although solvent effects on gelation can often be well predicted for organic solvents,<sup>80</sup> it is currently not possible to predict gelation in ionic liquids or DESs.<sup>196</sup> As such, we were unsure whether or not these experiments using DBS as a

gelator for DESs would be successful. However, we considered DBS a good candidate gelator because it assembles through a combination of hydrogen bonds and solvophobic interactions, the balance of which has been shown to vary depending on the solvent in which assembly is taking place of as such, we reasoned that there was the scope for this gelator to adapt to the solvent environment in which it finds itself, and hence achieve self assembly.<sup>62</sup> In the following sections it is going to be detailed how to produce certain DES-gels based on DBS. The resulting material is a complex mixture of gelator and ionic liquid which is compatible and stable.

As described in Chapter 1, the benzylidene groups of DBS form the ‘wings’ and the sorbitol backbone the ‘body’ with the type of solvent playing a key role in controlling the precise assembly mode. It is thought that the way in which DBS self assembles is mediated by the aromatic part and the most external 6-hydroxy group, which forms intermolecular hydrogen bridges with the acetal oxygens of DBS “neighbours”, hence being crucial for the self-assembly event.<sup>62</sup> The result is the formation of fibres in a hierarchical manner and the building of the gel network with certain characteristics that are related with the nature of the solvent and the energy available in the system which affect solubility.<sup>264,265</sup> We hoped that this assembly mode would be compatible with DESs, and furthermore would not impact adversely on the properties and diffusional conductivity of the DES itself.

## 4.2. Preparation of natural deep eutectic solvents

First the preparation of the DESs based on glycols was performed. Figure 4-4 presents the different DESs investigated in this study. It should be noted here that these mixtures are very hygroscopic.

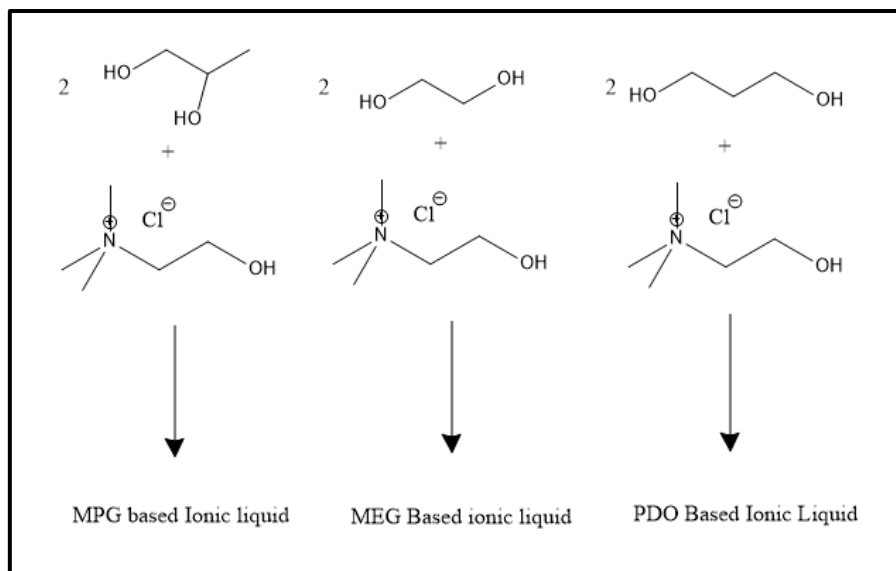


**Figure 4-4:** The basic procedure to form the Ionic liquid based on the two main components. Proportions are two molecules of glycol every one of choline chloride.

MPG (mono propylene glycol), MEG (mono ethylene glycol) and PDO (1,3-propanediol), as shown in Figure 4-4, are one of the components. Choline chloride is another natural substance, which is a quaternary ammonium salt and acts as the acceptor or Brönsted acid in these DESs. In each case, we combined the components by means of heating as a mixture of solid (ChCl) and liquid (glycol) and hence forming the ionic liquid which is characterized by an increase of ionic conductivity of the resulting liquid. However, before doing so we needed to dry the liquid glycols, extracting the traces of water as much as possible. Thus, it was necessary to treat with desiccant substances. This process is quite difficult to quantify because of the highly hygroscopic nature of these glycols, which absorb water from ambient conditions. The protocol for drying MEG, PDO and MPG was, first, to add them to  $\text{MgSO}_4$  to eliminate traces of water and then

distil them under vacuum to avoid introduction of traces of ambient moisture before mixing or heating.

Table 4-1 presents the ionic conductivities of these systems as measured by an ionic conductivity meter (Jenway 4310). An increase in ionic conductivity can clearly be observed when the corresponding glycols are added, in dry conditions, to the corresponding amounts of choline chloride (ChCl:Glycol, 1:2).<sup>189</sup>

Ionic Conductivity (mS/cm)		
DES type	No Choline	Choline
MEG	0	8.29
PDO	0	3.32
MPG	0	1.51

**Table 4-1** Ionic conductivities values for the pure glycols and their corresponding mixtures with choline chloride in a molar ratio of 2:1.

As it can be seen in Table 4-1, there was no ionic conductivity for the glycols in the absence of choline chloride, meaning that no ionic conduction was possible at the level of the voltage applied. Once, the salt (choline chloride) was added, the supramolecular association was established and separation of charges occurred resulting in a kind of ionic melt.<sup>179</sup> Such low temperature melts have ionic conductivity and the ability to dissolve metal oxides, chlorides and salts of various metal ions as will be seen in the following sections.

### 4.3. Preparation of ionic deep eutectic gels

After preparation of the DESs as described above, some attempts were made to prepare DES gels from them. As mentioned previously, DBS fits ideally with applications that require gelation in glycol based solvents. Thus, because one of the components of the prepared ionic liquid is a glycol, we reasoned there was a chance of gelating that environment. We therefore attempted to prepare gels using DBS and ionic liquids (based on PDO, MPG and MEG) with several gelator concentrations as indicated in Table 4.2.

Ionic liquid	ChCl+PDO		ChCl+MPG		ChCl+MEG	
Gelator (DBS) Concentration	3%	5%	3%	5%	3%	5%
Gelation	no	yes	no	yes	no	yes
Appearance	turbid	turbid	turbid	turbid	clear	clear

**Table 4-2** Various combinations of DBS with the prepared DES based on glycols and ChCl.

The first concentration tested was 3% wt/vol of DBS in ionic liquid (30 mg of DBS /1 mL ionic solvent). Gelation at this concentration did not occur in any of the liquids tested, that is to say, gels were not formed when adding 3% of DBS in every tested ionic liquid (PDO, MPG and MEG). Usually lower concentrations<sup>62</sup> (less than 1%) of DBS in glycol solvents are enough to trigger gelation, which means the minimum gelator concentration is normally quite low. As such, we can conclude that the presence of choline chloride significantly suppresses the gelation of DBS in glycol solvent environments. We might hypothesise that this is the result of competitive interactions between choline chloride and the gelator, which prevent the DBS from establishing a self-assembled nanoscale network

of its own. It is possible to speculate that choline chloride may limit the hydrogen bonding ability of DBS by competing for such interactions – for example, hydrogen bond interactions between O-H groups and chloride anions are well known<sup>266</sup> After this failed gelation, we then went on to test higher concentrations, i.e., 5% of DBS. Pleasingly, the result of this experiment was the formation of robust gels (Figure 4-5) – as far as we know, this is the first time that a choline chloride glycol based ionic liquid has been gelled. We refer to these new systems as DES-gels. The gelation occurred spontaneously at room temperature after cooling from the elevated temperatures achieved with the help of a heat gun needed to dissolve all prepared DESs and DBS. Gelation was also easily triggered by ultrasound, taking much less time to gelate (10 seconds) than compared with the normal ambient conditions of gelation (ca. one hour). Figure 4-6 presents the Tgel values. The Tgel value is highest for MEG > PDO > MPG – this would suggest that more thermally stable gels are formed in the more polar medium as MEG is the most polar of these solvents.

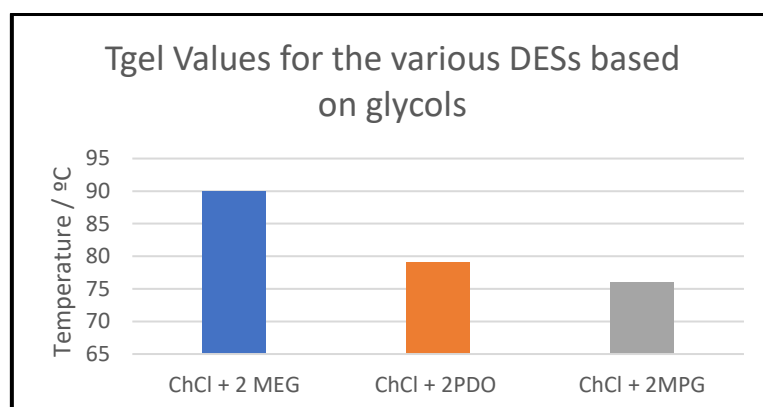


**Figure 4-5** Tgel determined for the first set of prepared DESs.

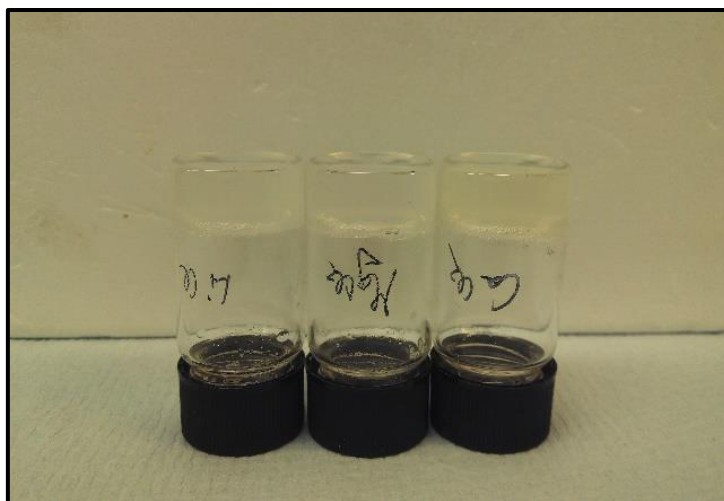


**Figure 4-6** Picture of ionogels as an example of the kind of gels that are obtained by combining DBS and various DESs.

The transparency of these gels is important (Figure 4-6), as it demonstrates that we are not simply achieving ‘gel-like’ materials as a result of gelator insolubility (which is often observed at high gelator loadings such as 5%), but rather achieving a well dispersed nanoscale network within the deep eutectic solvent phase.

#### **4.4. Comparing ionic conductivity of ionic liquids and their respective ionogels**

One of the key properties that we are interested in is the ionic conductivity of the resulting ionogels. A key aspect, explored previously with ionogels,<sup>267</sup> is whether these systems have conductivities close to, or the same as, the neat liquids – this would suggest high dynamics within the gel. With that goal in mind, an experiment was designed using an ionic conductometer (Jenway 4310, Figure 4-7) calibrated with two different calibration solutions of KOH and NaCl (defined concentrations) to make sure the range of measurement was accurate. This allowed us to compare ionic conductivity levels of both liquid and solid-like states. Temperature ramps were programmed and executed. The

expected increase of conductivity vs temperature as ionic mobility increases was thus recorded.

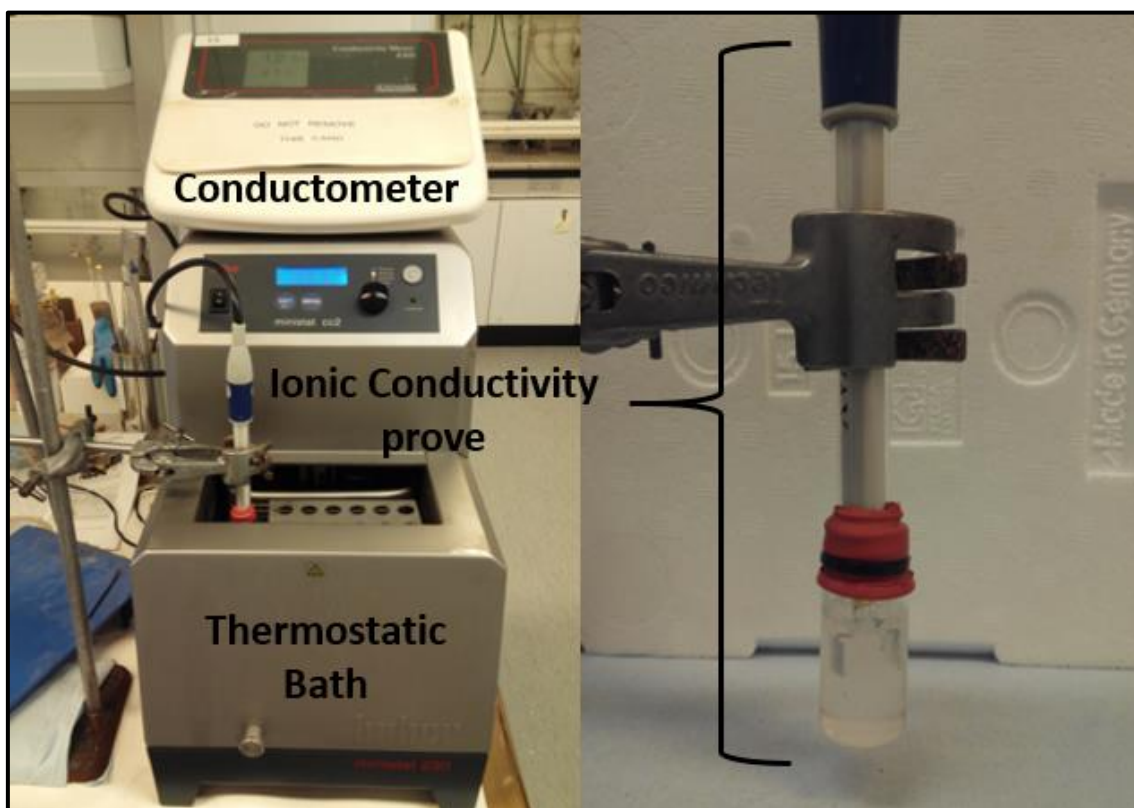


**Figure 4-7** Set up which is used in order to measure ionic conductivities versus temperature. In the image above can be identified the various parts of the set up: Conductometer, probe and the programmable thermostatic Bath.

Temperature can be measured using the bath and conductivity meter respectively. So two temperatures are noted, the first is indicated by the bath digital thermometer and the second is the thermometer in the conductivity probe which is integrated in the conductivity meter and hence accurately tracks the inside of the probe. In the end, the temperatures used were the result of the average between these two temperatures. Table 4-3 presents the conductivities of the DES and the DEGs at 25°C and then reports the percentage difference between them.

	MEG	PDO	MPG
DES	8.29	3.32	1.51
DEG	7.38	2.77	2.42
% Variation	89.02	83.43	160

**Table 4-3** Values of ionic conductivities expressed in mS/cm

These results indicate that for MEG and PDO based gels there is just a slight decrease in ionic conductivity compared with the respective ionic liquids. This could correspond to the fact that the presence of gel networks slightly hinder or prevent the free movement and propagation of ions inside the gel – indeed such effects might to some extent be expected. Pleasingly, at 5% loading, the lowering of conductivity is relatively small, suggestive of largely free ion mobility. The third behaviour (MPG) is quite unexpected according to these criteria, because the conductivity increased when the gel was formed. We suggest that the MPG ionic liquid studied here was not fully homogeneous and complete solution of the choline chloride was not possible at the proposed 1:2 molar ratio at room temperature but the reasons are unclear.

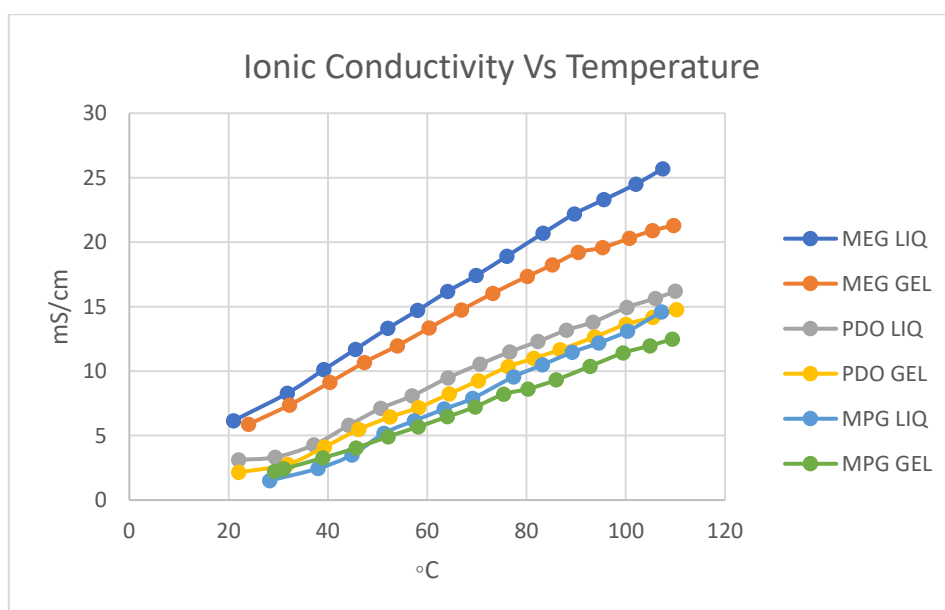


**Figure 4-8:** presents the influence of temperature of the ionic conductivity of the DESs and the corresponding DEGs.

As temperature was increased, so did the conductivities (Figure 4-8). There are two possible reasons for this – increased ionic mobility at higher temperatures, and lower viscosity at higher temperatures (see below). In each case, the conductivities of the DEGs are slightly lower than those of the DESs – as noted above, we suggest this is a result of the gel scaffold slightly inhibiting ionic transport. Nonetheless, all of these DEGs are highly effective ionic conductors.

Furthermore, we note that on raising temperature, the conductivity of the DEGs in MPG became lower than that of the liquid form of this solvent, as expected – inverting the somewhat unexpected behaviour at room temperature. Indeed, in general terms, all of the liquid forms increased their conductivities more on heating than did the gels (i.e. the conductivity gap between liquid and gel increases on increasing temperature). We suggest that although for both liquids and gels, the ions will become more mobile and hence more conducting, the liquid form will also become significantly less viscous. In contrast, the gel form remains converts into a sol when temperature is increased, and as such, the bulk viscosity will not change significantly. For this reason, the conductivity of the liquids benefits from both ionic mobility and lower viscosity on heating, whereas in the gel form, only the ionic mobility increases the conductivity. It seems that the lower IC in gels at higher temperatures is due to the fact that more substances are introduced in the original IL (DBS) and this lower the ability of the ionic environment to transport charges.

#### 4.5. Increasing ionic force in Ionogels

Knowing that the MEG DEGs was the best performing gel in terms of ionic conductivity (IC) and indeed was comparable with the IC of lithium ion battery electrolytes<sup>268</sup> (i.e., within the range of 1-10 mS/cm) we decided to proceed and investigate this system in more detail. We were fascinated with the report of next generation aluminium ion batteries (as potential replacements for lithium ion batteries) recently reported in *Nature*<sup>269</sup> in which DESs played a critical role in the stability of the device. Also, there is significant recent interest in improving lithium ion and calcium ion batteries. The electrochemical window of the electrolyte is sufficiently broad that there is a large gap in electrical potential where chemical species that are part of the cell (aluminium ion and some complexes of it) were stable, soluble and potentially mobile within the electrolyte. One of the requirements of this kind of electrolyte is the ability to dissolve any chemical substance that may appear during reaction in the electrochemical device. With this concept in mind, an experiment was performed to test such solubility properties, and the stability of ionogels when salts (an ionic force) were present. Obviously, adding extra ionic substances may affect not only the formation of the gel itself, but also the ionic conductivity of it. Adding salts changes the potential interactions that could be formed between gelator and the liquid-like phase on the molecular level. Thus, there is a risk of affecting the self-assembly of the scaffold of the gel because this process relies on supramolecular interactions and as such any variation or modification of them could result in its failure.

Several vials with various salts (metal chlorides) were dissolved in the DES based on MEG. Concentrations are given in the following table. Increasing concentrations were tested in order to discover the maximum solubilities of these salts in the proposed DES-gels based on MEG.

	MOLARITY							
MEG	0.05	0.1	0.5	1	2	3	4	6
NaCl	no	no	no	no	no	no	no	no
KCl	sol	no						
LiCl	sol	sol	sol	sol	sol	sol	sol	sol
MgCl <sub>2</sub>	sol	sol	sol	sol	no	no	no	no
CaCl <sub>2</sub>	sol	sol	sol	sol	no	no	no	no
FeCl <sub>3</sub>	sol	sol	sol	sol	sol	sol	no	no
AlCl <sub>3</sub>	no	no	no	no	no	no	no	no

**Table 4-4** Solubility test for determining the saturation concentration of these chlorides in MEG based ionic liquid. Where **sol** means soluble, **no** means no soluble in such concentration conditions.

As can be seen in Table 4-4, various concentrations of different chloride salts were tested to track the limit of solubility of those substances in the MEG/Choline Chloride based DES. This is important because solubilities have to be high and complete to make a potential electrolyte for an electrochemical device such a battery. Different salts were tested in order to evaluate potential uses of these ionic liquids under different types of chemistries or potential chemical reactions in these batteries. Lithium, magnesium, calcium and iron chlorides were the most soluble in this MEG/choline chloride DES. In contrast sodium, potassium and aluminium chlorides were quite insoluble in these conditions.

Having these results in mind, the logical and obvious next step was to test gelation on these saturated solutions of DES. The proposed concentration was 1M for all the salts. Gelator was added (DBS) and dissolved by heating in order to promote a sol state and later gelation. Three DES solutions were gelled – those containing Li<sup>+</sup> (even up to 6 M), Mg<sup>2+</sup> (1M) and Ca<sup>2+</sup>(1M), while that containing Fe<sup>3+</sup> did not form a gel. We suggest because FeCl<sub>3</sub> is a very strong Lewis acid, potential supramolecular interactions can hinder the interactions that are needed in order to self-assemble the 3D gel nanostructure. In recent studies, there has been intense work trying to develop some electrolyte additives

which solve problems that affect the longevity of lithium batteries. Such an approach is quite supramolecular in terms of adding a substance (additive)<sup>270</sup> at a certain concentration that can affect the whole solubility of the system particularly avoiding the generation of dendritic crystalline growths<sup>271</sup> inside the cells after a high number of cycles. This supramolecular formulation approach using an additive that modifies the solubility capabilities of an electrolyte is basically the same concept as that explained for the previous experiment. It is also worth noting that lithium, magnesium and calcium compatible electrolytes as explored here could have a significant impact on battery technology development.<sup>272,273</sup>

We thus prepared gels which included 1 M LiCl, MgCl<sub>2</sub> and CaCl<sub>2</sub> and then went on to perform conductivity testing. Initially, we monitored the ionic conductivity of these DES liquids in the absence of the gel network (Figure 4-9).

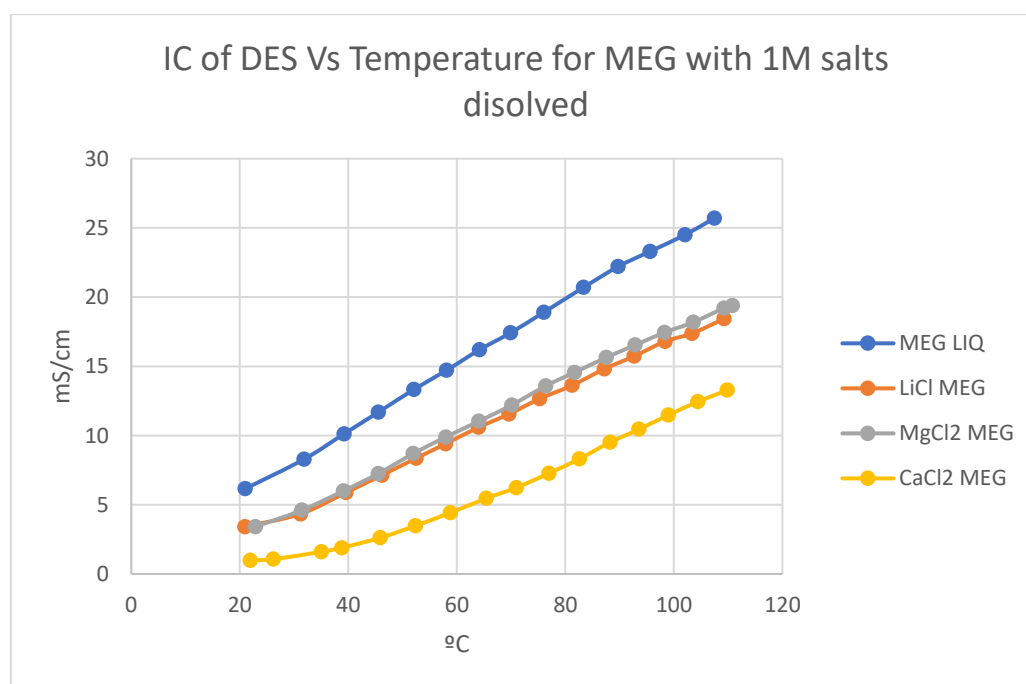


**Figure 4-9:** Ionic conductivity Vs Temperature for MEG DES with 1M salts dissolved

In the graph above it can be seen that addition of these salts at 1M concentration reduces the ionic conductivity of the electrolyte to approximately 66% of the original value for  $\text{Li}^+$  and  $\text{Mg}^{2+}$  and to ca. 33% of the original value in the presence of  $\text{Ca}^{2+}$ . These effects are maintained on increasing temperature. It seems plausible that these relatively charge dense ions help prevent ionic conductivity by inducing stronger ion pairing in the liquid-like phase and hence limiting the mobility of the free ions.

We then went on to compare the conductivity of the DES-gels to those of the native DES liquids with and without ionic additives. (Figure 4-10)

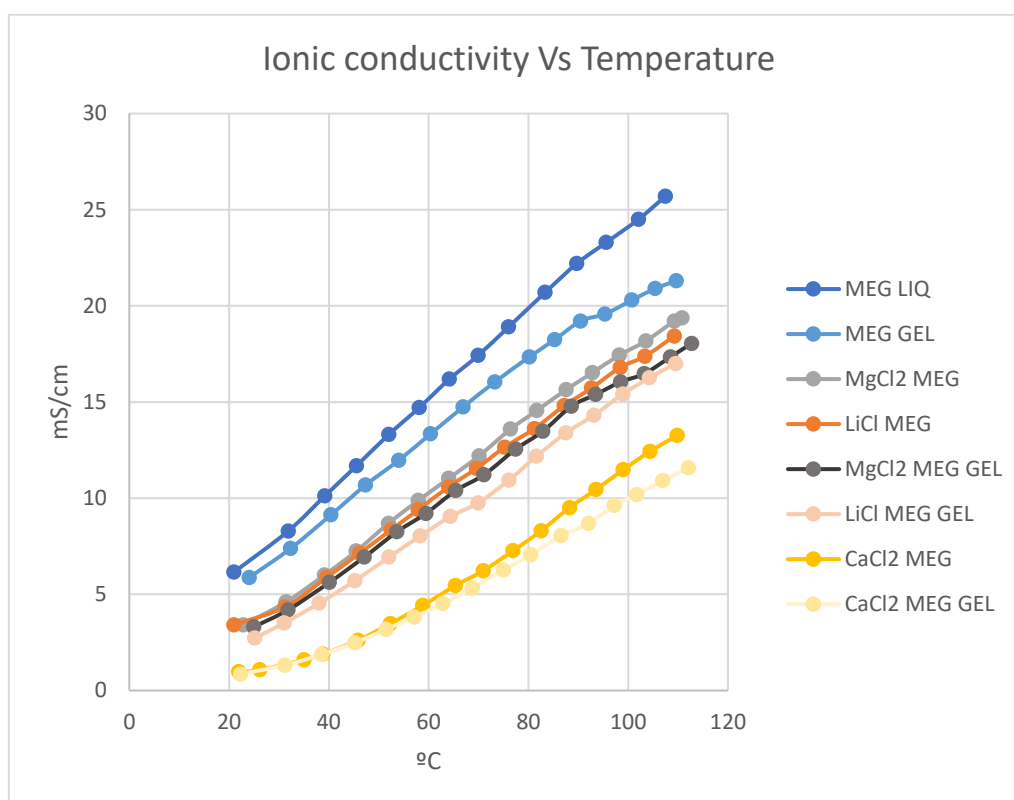


**Figure 4-10** Conductivities Vs temperature of DESs and DESs Gels with some salts.

It can be seen clearly that the addition of gelator only slightly decreases the conductivity in each case from that observed for the DES liquid with the same ionic additive. Therefore, remarkably the presence of the gel network does not significantly affect the overall conductivity even in the presence of ionic additives. As such, it is clear that the

impact of ionic additives on conductivity occurs as a result of modification of the structuring of the liquid – this happens either in the absence or the presence of the gel network in the same way. Once again, it can be observed that on increasing temperature the gels increase in conductivity slightly less than the liquids – as earlier we suggest that although ionic mobility increases in both cases, in the gels there is not the same decrease in viscosity as in the liquids. In summary, this experiment clearly demonstrates that gelation still occurs when ionic strength of relevant salts is increased to relatively high levels, a situation that is highly relevant with regard to electrolytes for battery or supercapacitor applications. In particular, we would conclude that this system is particularly appropriate for use in  $\text{Li}^+$  or  $\text{Mg}^{2+}$  batteries (conductivities of 3-4  $\text{mScm}^{-1}$  under ambient conditions of temperature), but is perhaps less suitable for use in  $\text{Ca}^{2+}$  batteries (conductivity of only ca. 1  $\text{mScm}^{-1}$  under ambient conditions).

#### **4.6. Gelation of DESs based on components other than glycols**

After investigating the saline ionogel described above and gaining insight into the kind of salts that are compatible with these gelation conditions, we became interested in exploring whether our DES-gels could be made from natural resources and also exhibit high IC values. Clearly, a move away from MEG would be beneficial in this regard. The search for non-toxic, cheap and biocompatible materials that meet strongest environmental requirements are increasingly becoming requirements for technologies, especially for ones which are expected to have great societal impact. Indeed, in general terms, this is one of the key advantages of using DES technology and gelation systems such as DBS which are based on natural product materials. Even the DES gels described above have significant environmental advantages over traditional ionic liquids, however, we reasoned they may be improved further. After research into the potential and

possibilities<sup>167 274 174</sup> of the choline chloride based DESs. a range of Lewis bases were selected and tested. Figure 4-11 presents the materials tested and used.

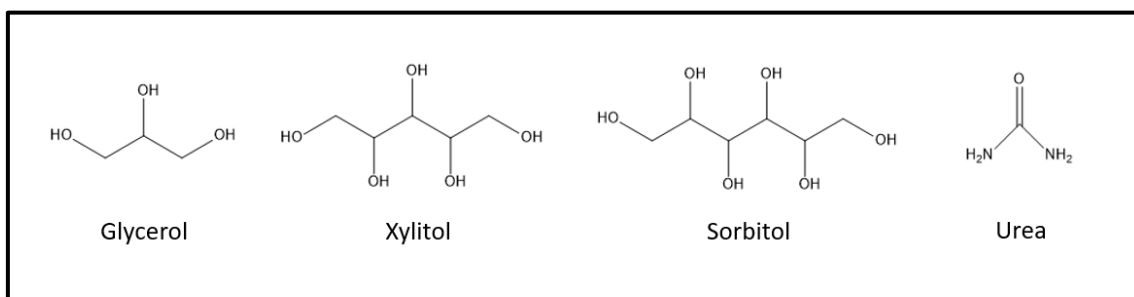


**Figure 4-11** Molecular structures of different potential molecules to be combined with Choline Chloride to form various DES's.

The molecules above demonstrate the relative versatility of these DESs and illustrate their ability to be tuned and designed (engineered tunability) in order to meet the requirements of any specific electrolyte application. Notice that depending on the nature of the molecule (which exist as more or less viscous liquids in each case), the final viscosity of the generated IL will be dependent on the viscosity of the liquid of origin with some exceptions that are related to the kind of supramolecular interactions that are formed. In these particular cases, it should be highlighted that urea and ChCl, both of which are solids, could be combined to form the eutectic mixture after mild warming with a heat gun and a viscous liquid is then formed which is stable at ambient conditions. In this example, therefore, the suppression of melting point of the individual components within the eutectic mixture is particularly clearly visualised.

All DESs were then prepared using a proportion of 2:1 for the molar ratio of neutral molecule:ChCl. Initially, all the liquids were tested in terms of ionic conductivity using the set-up described previously. It should be noted that some of these liquids had particularly high viscosities and it was important to try and ensure that no bubbles were affecting the measurements at the electrodes. Figure 4-12 presents the results for IC of the prepared liquids.

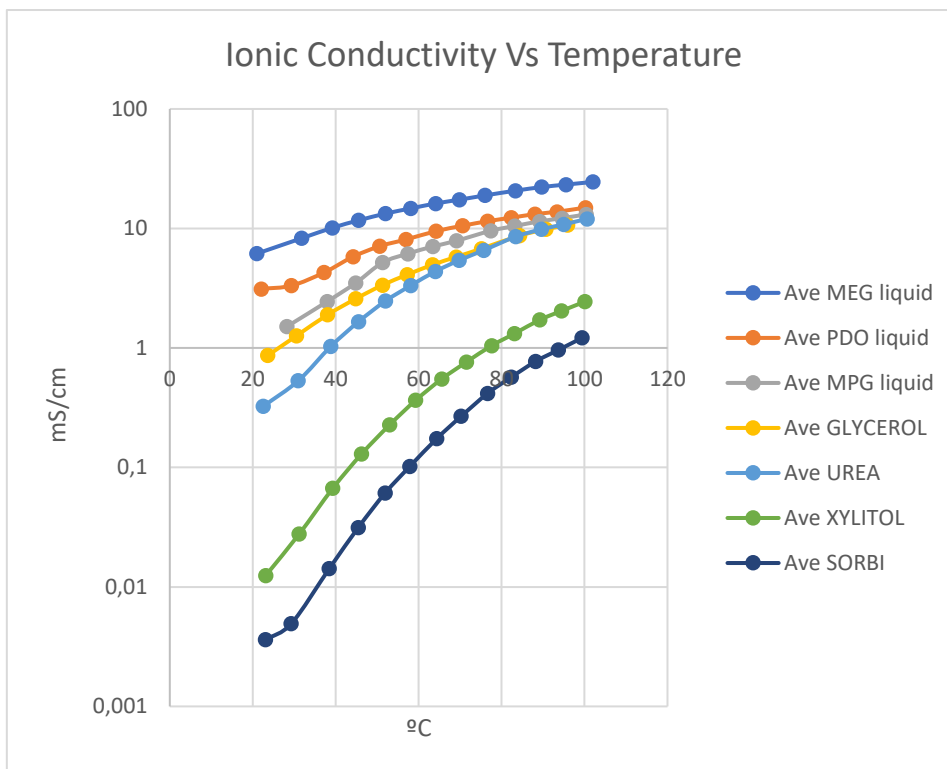


**Figure 4-12:** Logarithmic graph of the IC of the natural IL prepared from various combinations. “Ave” meaning average measurement of temperatures between the bath temperature and the prove temperature.

It can be seen that the range of different DESs produced have very diverse behaviours in terms of IC. As we will see, this behaviour is primarily related to the relative viscosity of the resulting liquids. Sorbitol makes the most viscous system, and is hence the least conductive, while MEG forms the least viscous system and is hence the most conductive. This relation of viscosities and ionic conductivities are measured in the following experiments by using the rheometer. This result is compatible with the idea of viscosity affecting the diffusion capacities of the ions, thus the ionic conductivity as described above. Of the renewable replacements for MEG, glycerol appeared to be the most effective at ambient temperatures, while the urea based system also became an effective conductor on heating.

#### 4.7. Gelating second generation DESs based on ChCl and hydrogen bond donors

Our next experiment was to attempt to gelate these second generation DESs using DBS as a gelator system. The DESs were prepared and DBS was added at 5% concentration. We were delighted to observe that all mixtures gelled completely or partially, giving more or less robust gels. This is a pleasing result showing that the diverse gelation potential of DBS for this kind of ChCl system. Indeed, this agrees with our hypothesis that DBS, by combining different interactions in its self-assembly mode, is a highly versatile and flexible gel-forming system.

After verification of formation of Deep Eutectic Gels (DEGs), conductivity measurements were performed. Figure 4-13 presents the results.

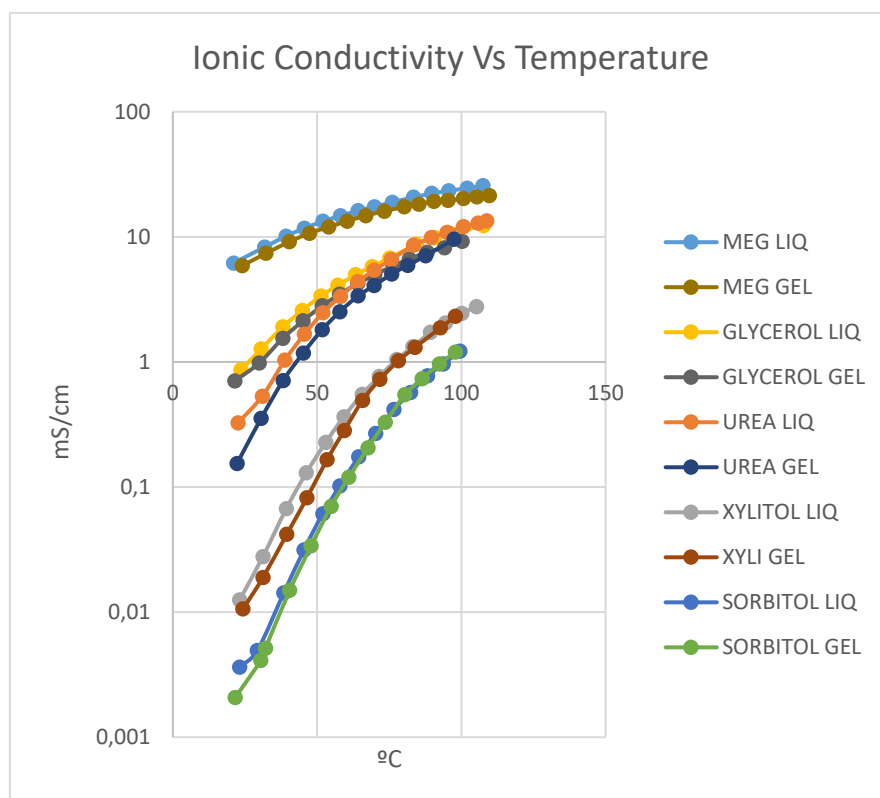


**Figure 4-13:** Logarithmic representation of IC measurements comparing and highlighting the small difference in IC between the IL and their respective Ionogels.

Essentially, conductivity was retained in each case, with the DEGs showing slightly lower conductivity than the native DESs. This clearly demonstrates that gelation of these liquids does not have a significant adverse impact on their conductivity profile, irrespective of the structure of the DES being immobilised. A gel is a viscoelastic material but this macroscopic feature has to be reinterpreted at the molecular level. The porosity of these solid-like materials is important for conductivity and energy applications. Broadly, it can be considered in these DEGs, there is a matrix formed by self-assembled gelators and a “sea” which is formed by solvent and other substances that can be dissolved in it. Freedom of movement is permitted by the labile interactions that the solvent contains with itself and with the molecules dissolved in it. This means that an apparently solid material (at least rheologically) can have similar properties in terms of diffusion to a liquid. The results are therefore very encouraging due to the similarity of ionic conductivity between liquid and immobilised versions of DES-gels reported here. Given the relevance of ionogels in a wide-range of applications, we suggest that these DES-gels have considerable potential for new applications. This is a consequence of the dynamic internal behaviour of gels and the specific charge propagation mechanism within these systems.

#### **4.8. Rheological properties of DESs.**

As outlined above, the ionic conductivity of these materials is of primary importance, but this ionic conductivity will be directly related to macroscopic properties such as viscosity, temperature and concentration of charge carrier (choline chloride). Indeed, the importance of viscosity has been discussed in the preceding sections. We therefore measured the viscosities of various DESs using Malvern Instruments Kinexus Pro Plus rheometer. A parallel plate geometry was used, with an upper plate of 20 mm in diameter,

and a gap between the geometries of 1 mm. The process of analysis of the viscosity involves the following steps.

1. The DES was placed in the rheometer plate.
2. Viscosity program was set for a ramp of temperatures.
3. The plate was lowered until it was in contact with the viscous DES.
4. The experiment starts and viscosity is recorded as temperature increases.
5. The viscosity was lowered as normal due to the increase of temperature.

Viscosity measurements were performed against temperature for these DES's liquids and the results are presented in Figure 4-14.

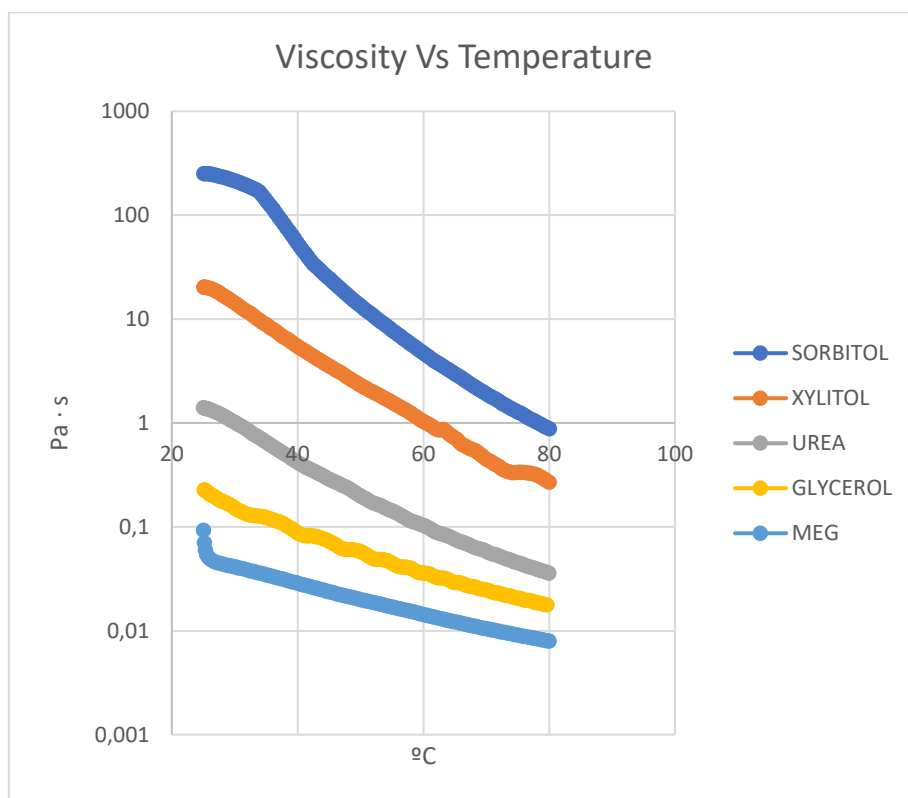


**Figure 4-14:** Viscosity versus temperature of the various prepared DESs.

As can clearly be seen, the most viscous DES is Sorbitol and the least viscous is MEG – this is in agreement with the comments made earlier, in which conductivity appeared to correlate inversely with viscosity. Indeed, viscosity is related to the self-diffusion

coefficient as can be seen in some studies made before with various electrolytes.<sup>275</sup> Diffusion is a key parameter that depends on temperature, as a result of supramolecular interactions between molecules within the DES – and it is evident from Figure 4-15 that viscosity decreases with temperature. As such, we can clearly state that DES conductivity depends primarily on viscosity.

#### **4.9. Rheological properties of ionogels**

As described above, the DEGs retain ionic conductivity at levels almost exactly the same as the original DESs. However, it is important to ensure that these ionogels are indeed actually gels, and not any other kind of material. Rheology was therefore performed to demonstrate that the gels have viscoelastic properties characteristic from solid-like materials. By doing this characterization, some values of elastic components can be determined and these describe how stiff and/or robust those gels are. The instrument employed was a KinexusMalvern Instruments Kinexus Pro Plus rheometer.

#### **4.10. Sample preparation**

In order to test DEGs in terms of their rheological properties, disks of gels were made. It is difficult to handle this kind of ionogel because they have hygroscopic properties, i.e., they tend to absorb a lot of moisture from the surrounding air. In principle, handling gel disks in open air conditions is not the ideal situation to test them. In this case, apparently there is no clear solution to this particular issue, so the sample disks were made in closed conditions as shown in Figure 4-15 and rapidly tested in the rheometer. A small cover like the shown in the picture below was used to avoid contact with the surrounding air. Figure 4-15, presents the whole process for the sample preparation.

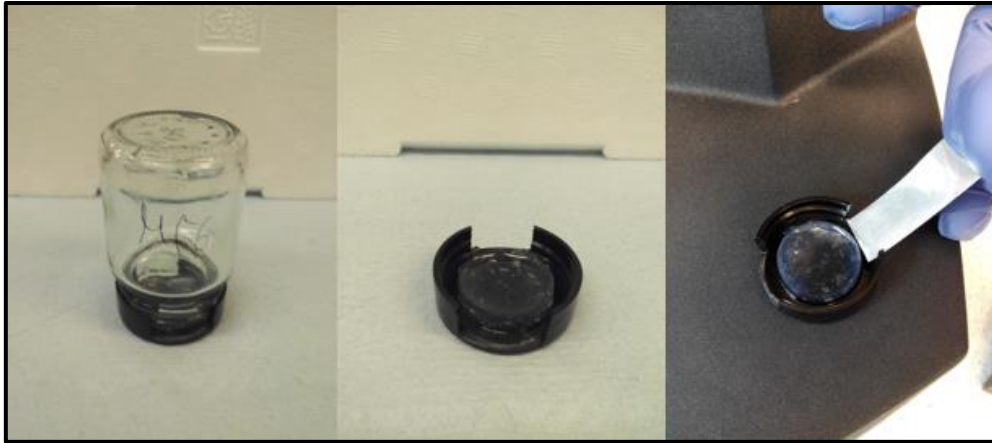


**Figure 4-15:** Procedure of preparations of disc of gels. The obtained disk can be handled in one piece until it is placed in the rheometer for testing.

As shown in the picture, the process of preparing the ionogels is explained in the following order.

1. An amount of gelator (100mg) was added to each jar.
2. The corresponding ionic liquid was added in certain volume (2mL) to get the 5% of DBS for each liquid.
3. The jar was immediately closed and heated with a heat gun to promote solution of both gelator and ionic liquid.
4. The jars were kept in an inverted position as in the first image and left overnight to form the gel.
5. Once the gel was formed a disk was retained in the lid as the second picture in the Figure above.
6. The gel was carefully moved from the lid to the rheometer plate where rheology was carried out.
7. Once the rheometer was programmed to perform the test, the plate was lowered to give a gap of 1 mm and the remains of gel after compression were removed by trimming.

The preparation of the disk for testing is very important. The objective is to prepare a whole piece of material that has not been cracked while handling from the mould (Jar lid) to the rheometer platform for later testing. As can be seen, these gels can be handled and moved, which is relatively unusual for supramolecular gels, many of which are very soft, and easily damaged, even at loadings as high as 5%. This clearly demonstrates the relative robustness of these DEGs materials.

Rheology characterizes a viscoelastic material and provides quantitative information. The  $G'$  (elastic portion) and  $G''$  (viscous portion) values can be determined in certain conditions of shear strain % and frequency. These values show how viscous and how elastic, (i.e., how stiff), tested gels are. As an example, when a gel is forming it changes from a liquid state to a solid one. In such a sol-gel transition, the liquid phase starts to become a more viscous solution due to the progress of self-assembly. The viscous component is the most important one (a higher value than the elastic one) then there is a transition from the sol state to an increasingly more solid and elastic one. In such a process, the  $G'$  and  $G''$  profile become more similar until they reach one another and the elastic component overtakes the viscous one, at which point the gel is almost formed until it matures. For a gel, the  $G'$  value should be at least an order of magnitude larger than  $G''$  and effectively independent of frequency.

Figures 4-16, 4-17, 4-18 present the response of different DEGs formed by MEG, MPG and PDO respectively to increasing strain. In this experiment the sample starts as a gel, with  $G'' \gg G'$  and then as strain increases, eventually reaches a point where  $G'' > G'$  and the enhanced strain leads to breakdown of the gel into a sol.

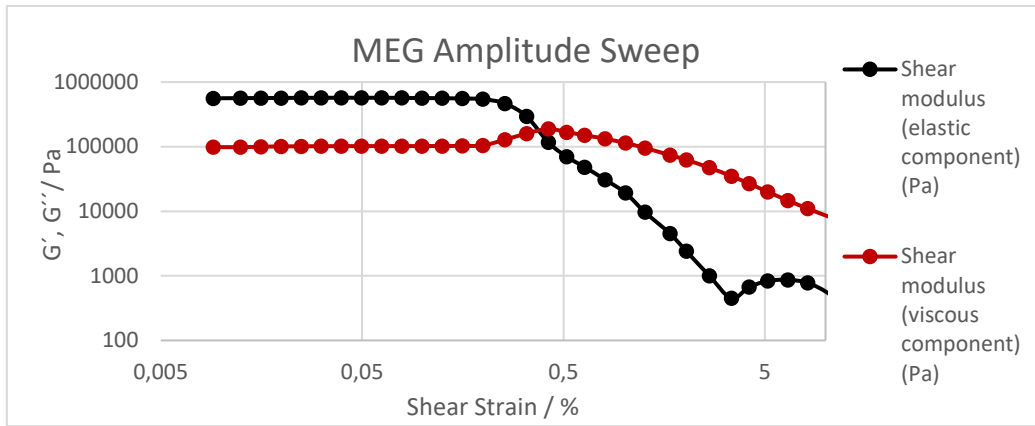


**Figure 4-16:** Amplitude Sweep Rheogram for MEG based ionogel.

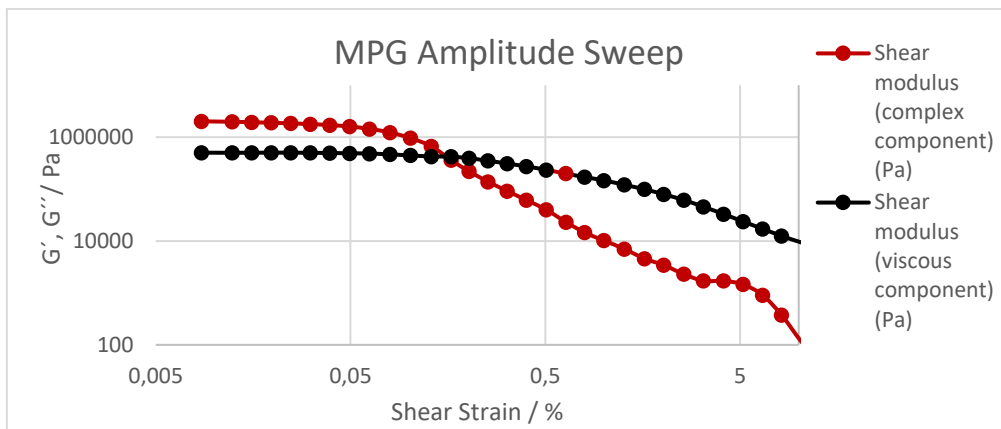


**Figure 4-17:** Amplitude Sweep Rheogram for MPG based ionogel.

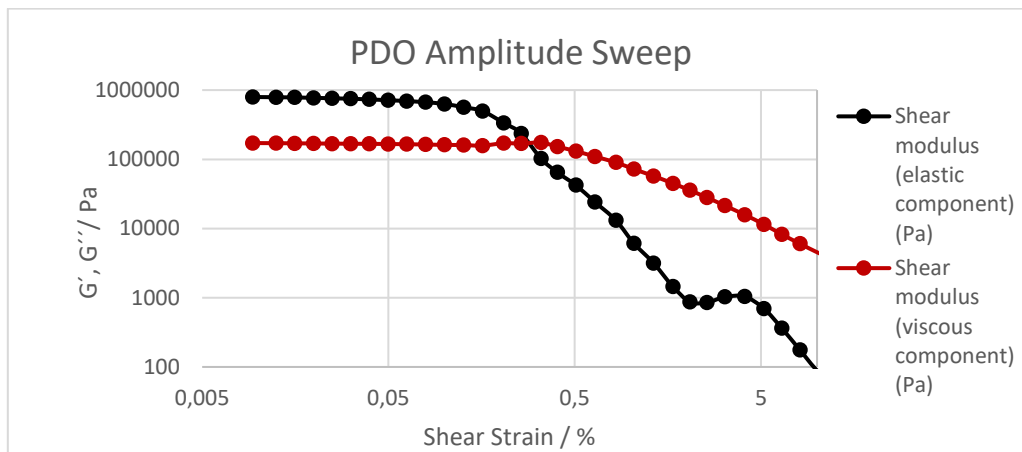


**Figure 4-18:** Amplitude Sweep Rheogram for PDO based ionogel.

We can extract a number of pieces of information from these graphs. Firstly, the values of  $G'$  and  $G''$  in the linear viscoelastic region (figure 4-19) (LVR, i.e. the part of the graph where they are constant, and the behaviour is solid-like). We selected a shear strain of 0.0495% as representing the middle of the LVR, Furthermore, we can determine the shear strain at which these gels are broken down, and  $G'' > G'$ .

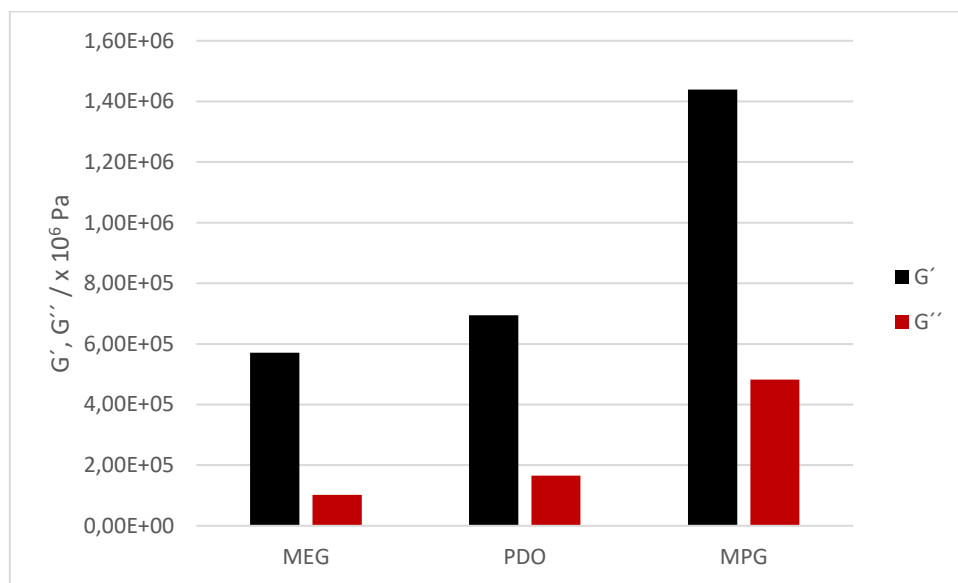


**Figure 4-19** Comparison of the viscoelastic components of the ionogels that have been tested (MEG, MPG and PDO)

From the results above it can be highlighted that MPG is the stiffest gel that has been tested compared to the other ones. Indeed, with a  $G'$  value of  $1.6 \times 10^6$  Pa, this is a very stiff gel indeed, particularly given that it is constructed only from non-covalent interactions. In the Figure 4-19 we can see that the  $G'$  value of the PDO DES-gel was  $7 \times 10^5$  Pa, while that of MEG was only ca.  $6 \times 10^5$  Pa. It is interesting to note that the stiffer gel based on MPG is actually less conductive than the more flexible gel network based on MEG. This suggests that the stiffness of the gel network formed when using MPG may act to inhibit ion mobility to a greater extent within the nanoscale structuring. As

such, we would conclude that it may be desirable to have relatively flexible gel networks in order to facilitate conductivity and electronic applications.

Furthermore, we considered the amount of strain required to break down these gels. MPG-based DEGs were more sensitive to strain than PDO, which in turn were more sensitive than MEG. So, the values of  $G'$  and  $G''$  cross over are 0.42, 0.165 and 0.330 respectively with MEG, MPG and PDO.

It is often seen that stiffer networks can be broken down more easily on application of strain as they are less able to flex, and therefore have greater fragility. This is clearly the case here. Obviously, for practical applications, resistance to strain is a desirable characteristic. Given that this is best observed for MEG, which also has a more flexible network giving rise to greater conductivity, it would suggest that limiting  $G'$ , while still obtaining effective gels, may be a useful way of optimising such materials for electronic applications.

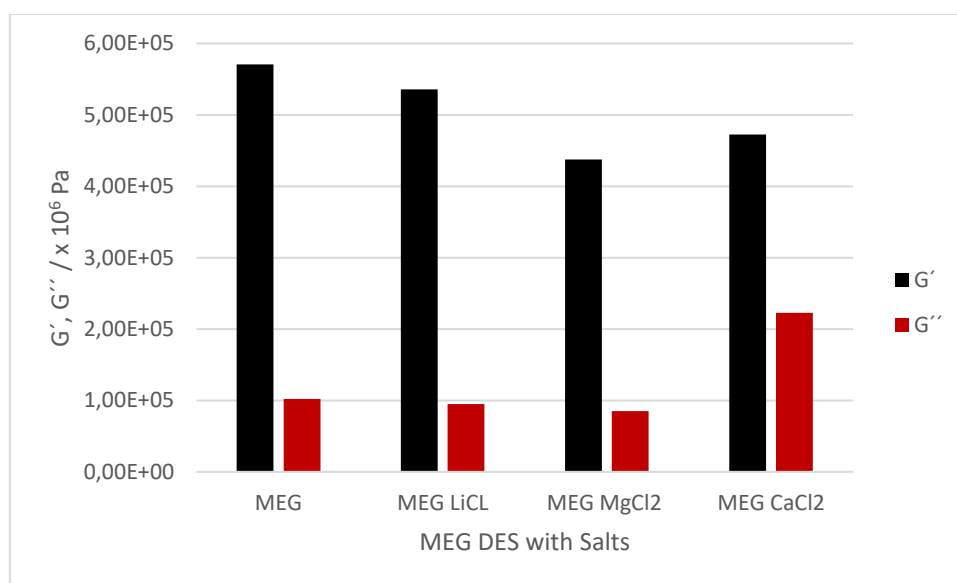


**Figure 4-20** Values of  $G'$  and  $G''$  for the various ionogels with different kind of salts dissolved.

We then investigated the impact of ionic additives on the rheological performance (Figure 4-20). In general, given that rheology typically has errors of  $\pm 10\%$ , the impact of these ionic additives is relatively small. As such, effective gels can be formed in each case, and there is no major evidence of the ionic additives affecting the structuring and rheological performance of the gel-phase network. The one exception to this is  $\text{Ca}^{2+}$ , which showed a significantly higher  $G''$  value than three other gels, which may indicate the gel is being significantly destabilised by the presence of this additive. It was notable that this system also had significantly lower conductivity as described earlier in the chapter.

We then went on to compare the strength of the DEGs generated with the full range of different components. Disks of various DEGs were prepared. The ones tested in the rheometer are based on Glycerol, Sorbitol, Xylitol and Urea (Figures 4-21, 4-22, 4-23, 4-24.) It is worth mentioning that, as previously seen, such ionic liquids have different viscosities, it is expected that at least the viscous component of the gel should be different from the one in MEG based ionogels.

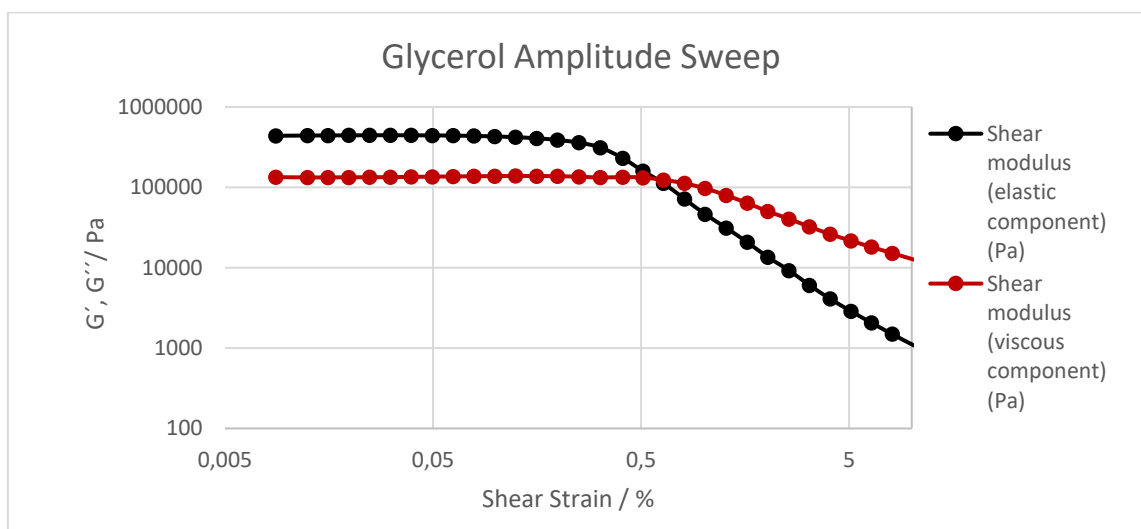


**Figure 4-21:** Amplitude Sweep Rheogram for Glycerol based IG.

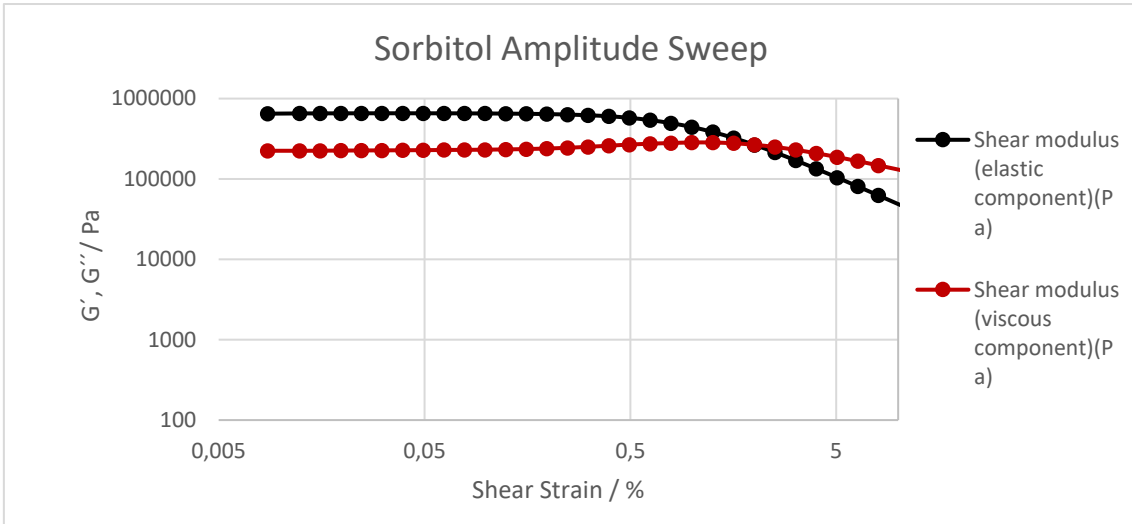


**Figure 4-22:** Amplitude Sweep Rheogram for Sorbitol based IG.

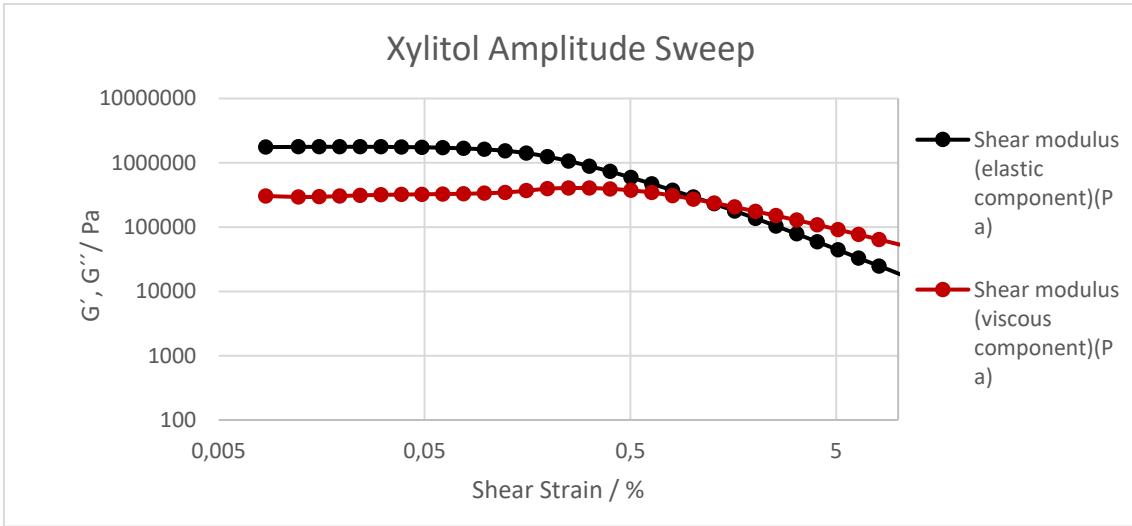


**Figure 4-23:** Amplitude Sweep Rheogram for Xylitol based IG.

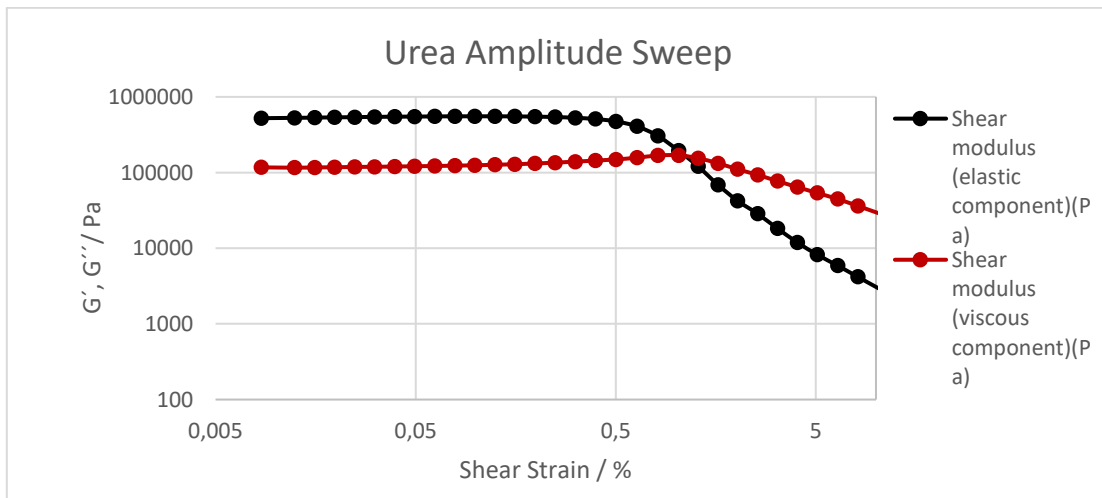


**Figure 4-24:** Amplitude Sweep Rheogram for Urea based IG.

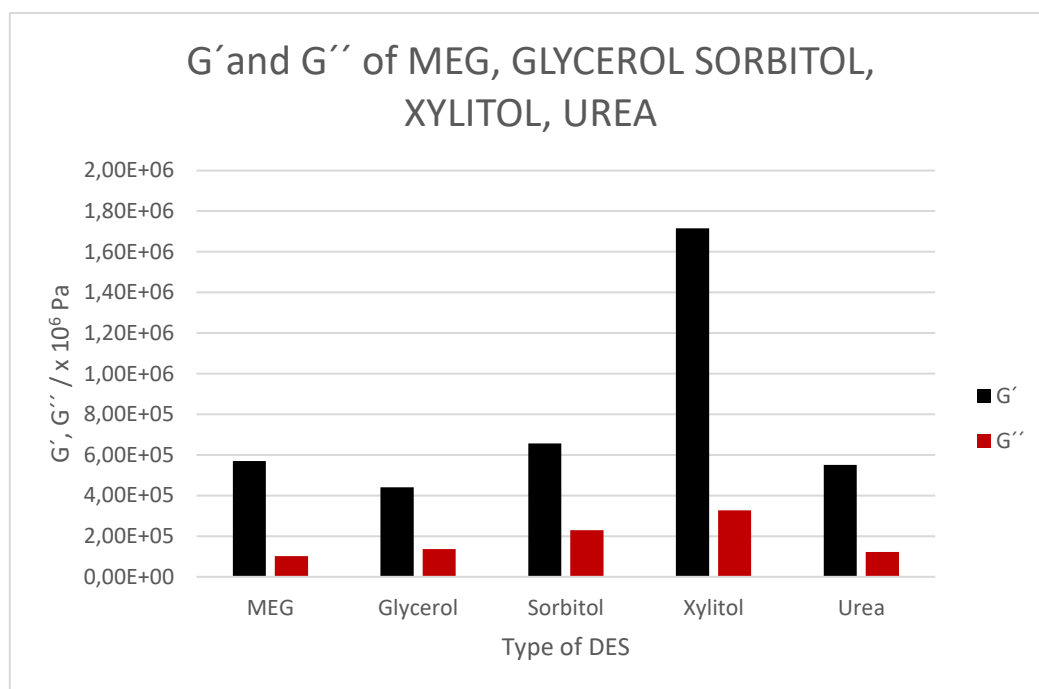


**Figure 4-25** Various values of viscoelastic  $G'$  and  $G''$  for the prepared ionogels.

Interestingly, of these additional systems, it is the IG based on glycerol which is the least stiff of the gels (Figure 4-25). This was also the most conductive. However, the fact it has lower stiffness than MEG did not translate into higher conductivity – so clearly gel network stiffness is not the only factor at play in controlling materials conductivity performance. Urea is the second most flexible gel, and was also the second most conductive. Xylitol was the stiffest gel and was also one of the worse conductors. However, we would have expected sorbitol to form a very stiff gel, based on its low conductivity, and it does not. This again suggests that although rheology may be partially responsible for conductivity, it cannot alone be used to correlate with conductivity – it is important to remember that the viscosity of the liquid phase itself is also significantly different for each of these fluids, which will presumably impact on the overall gel properties.

#### **4.11. Electron Microscopy of Ionogels**

Imaging of gels were required in order to demonstrate that a self-assembled nanostructured gel scaffold was indeed being formed. Several imaging techniques are available to observe materials at the nanoscale. In the particular case of DEGs based on choline chloride DESs, the practical problem is that we require dry conditions in order to put those gels inside the high vacuum chambers which are used in TEM and SEM. If the ionogels are dried, meaning the glycol is removed by high vacuum conditions, ChCl will precipitate because of the consequent solubility supersaturation of the increasing concentration of ChCl. This is a significant problem that apparently has no simple solution. In some research and related investigations of ionogels based on traditional ionic liquids, smart and quite simple strategies to overcome this limitation were employed, in terms of extracting the ionic liquid from inside the gel by diffusion.<sup>197</sup> The technique used for sample preparation was to introduce a piece of ionogel into water and self-diffusion of the ionic liquid inside the gel into the surrounding water enabled solvent exchange within the gel scaffold. Several washes were needed (3 washes) during several days (3 days) always assuming no effect of solvent change on assembly gel. The ionic liquid of the ionogel was hence removed while maintaining the 3D gel scaffold. Samples were cryo-dried in the metallic grids which are used in TEM and on the aluminium stubs which are used in SEM. In the following sections, the technique used here and the images collected will be shown and explained.

#### **4.12. SEM images of ionogels**

The first attempt at imaging was made using the SEM technique, which is the most commonly used for this kind of samples. As indicated above, the preparation of the sample is a key step in the generation of genuine and realistic gel scaffold images. The

process explained above (soaking in water for self-diffusion of inner DES) was used first to remove the ionic solvent of the ionogels and secondly a drying step was employed to gently remove by cryo-drying the remaining water inside the original ionogel. In the end, we obtained images such as those in Figure 4-26 for MEG (a), PDO (b) and MPG (c) DEGs.

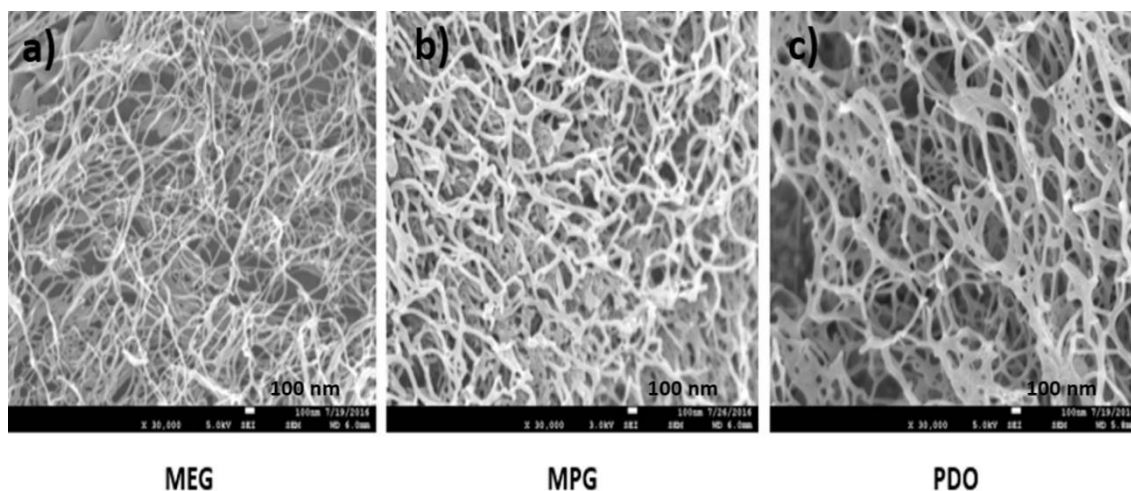


**Figure 4-26** SEM images of various gels at 30 thousand magnifications each.

It can be seen clearly that 3D networks, which are a characteristic of gel-phase materials, are present. DBS is clearly able to self-assemble into nanofibers even in in complex environments such as ionic liquids. These images support the visual observation of gelation and fully support the rheological properties described above. In each case, the nanofibrillar network looks relatively similar. It might be suggested that the network formed in MPG appears somewhat more rigid than that formed in MEG, in agreement with the greater stiffness observed rheologically, but it is difficult to draw definite conclusions given the potential perturbations to network which can occur during both solvent exchange and drying steps.

After this experiment, we then attempted to observe MEG DEGs with ionic additives, specifically LiCl, MgCl<sub>2</sub> and CaCl<sub>2</sub>. Figure 4.27 show the SEM images that were collected after the same treatment explained as above. It is important to notice that depending on the solubilities of the various salts, the treatment with water may not be able to remove them completely. In this case, the three salts are completely soluble in water.

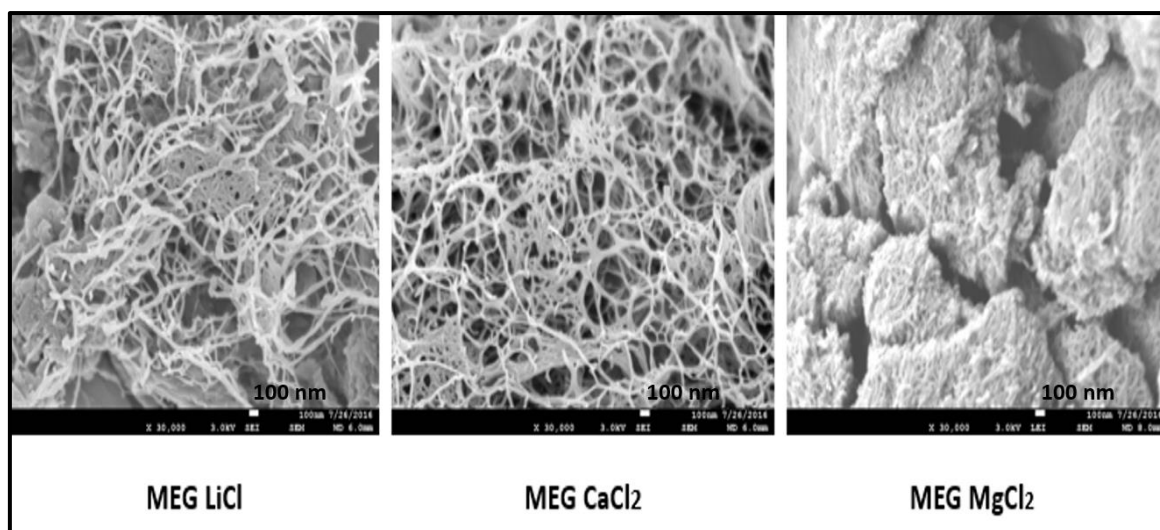


**Figure 4-27** SEM Images of various gels at 30 thousand magnifications each.

3D networks were identified and some of them were highly compacted. In order to get good images gels must be as porous as possible. In the first two images (MEG LiCl and MEG CaCl<sub>2</sub>) porous networks are imaged. In the third picture, a lack of porosity can be observed in the preparation of these samples, resulting in pieces of materials which are too packed to clearly observe the 3D networks – although some fibres can clearly still be visualised. This probably just indicates less complete removal of solvent and ionic additives in the latter case.

### 4.13. TEM images of ionogels

TEM imaging was also used in order to visualise the nanostructuring of the various ionogel scaffolds. The preparation of the samples was achieved following the same procedure as explained before of self-diffusion and substitution of internal ionic liquid by water and later cryodrying. Figure 4-28 corresponds to MEG, MPG and PDO based DEG-gels. In each case, nanofibrillar architectures can be observed deposited on the TEM grid.

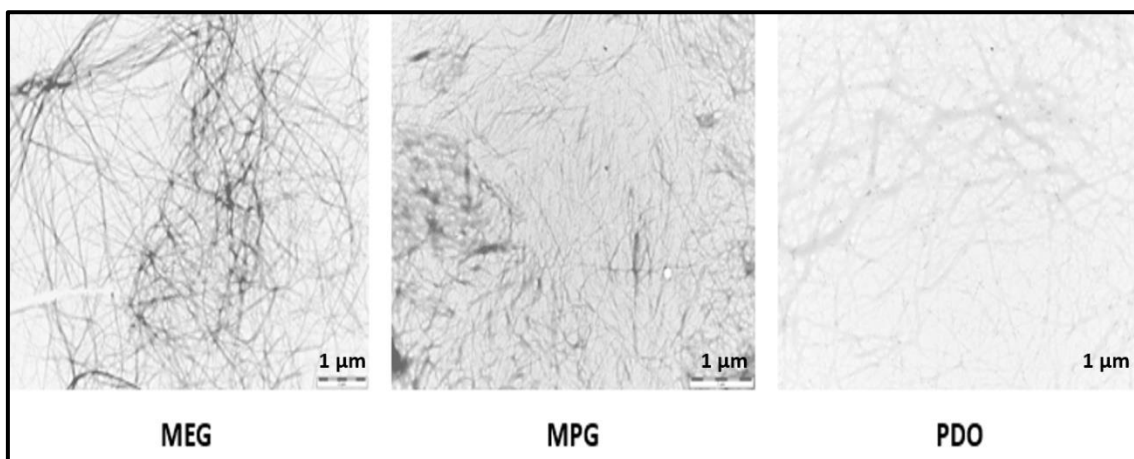


**Figure 4-28** TEM Images of various gels of MEG, MPG and PDO thousand magnifications respectively.

When a 1M concentration of salt was added to the ionogel the images in Figure 4-29 were obtained. The presence of ionic salts at 1M concentration did not significantly disrupt the nanofibrillar morphology, in agreement with the observation that macroscopic gelation still occurred for these samples.

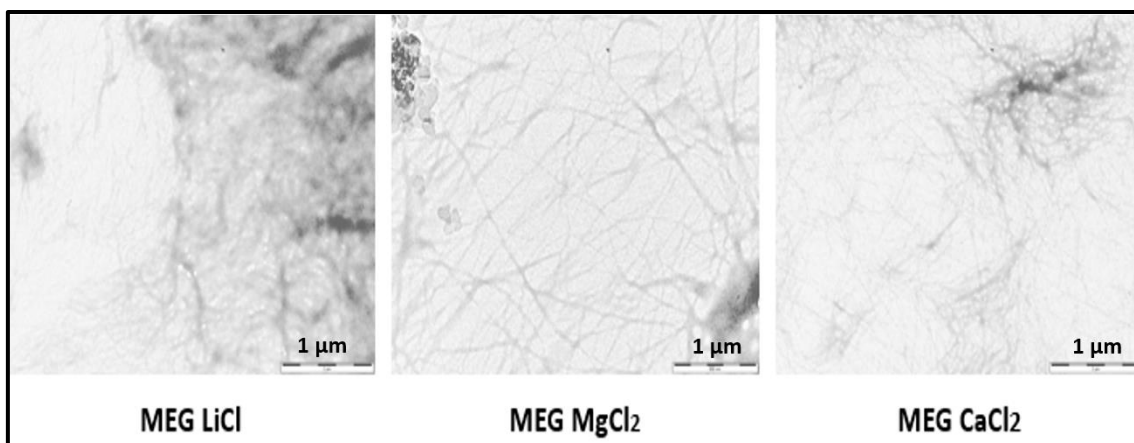


**Figure 4-29** TEM Images of various gels of MEG mixed with various salts at 1M

Figure 4-30 and 4-31 illustrates the TEM images for DES-gels made from Glycerol, Sorbitol, Xylitol and Urea. The scale bar is 1 micrometre and in each case, no stain was used to increase the contrast. Some fibres were observed in the Glycerol and Sorbitol samples, although we suggest that, the lack of an adequate stain for these fibres is the reason why there is not enough contrast, and it is not easy to distinguish fibres with accuracy, although it is evident that there are some nanofibers present.

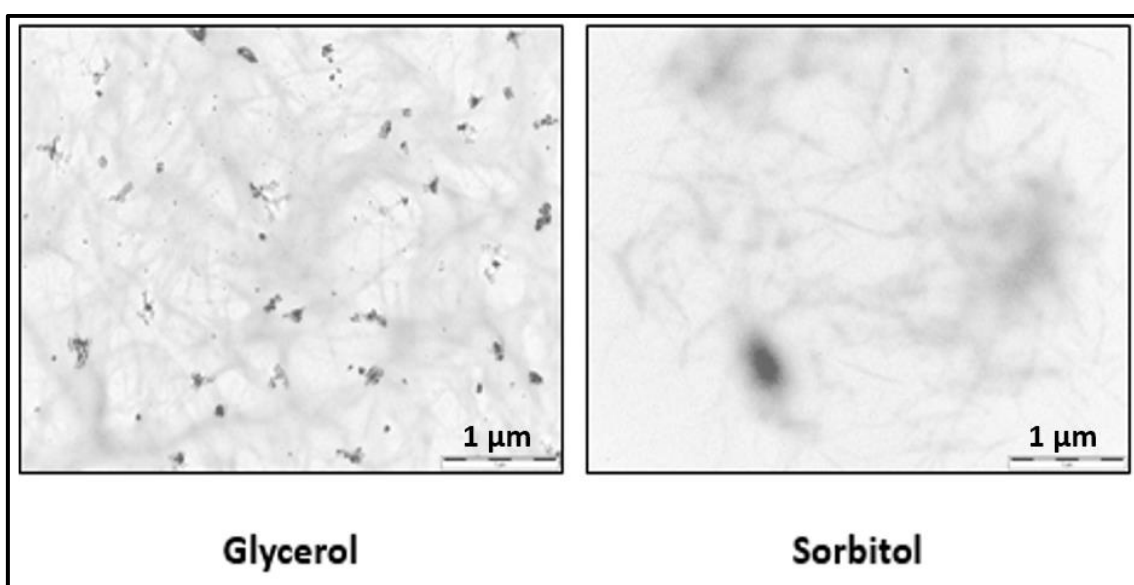


**Figure 4-30** TEM images of 1 micron for the glycerol and Sorbitol ionogels.

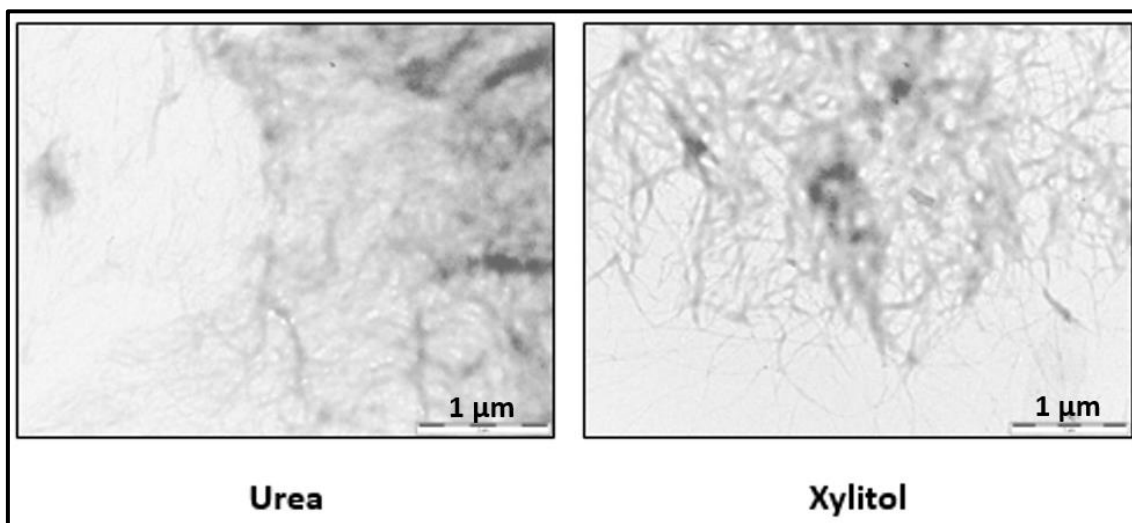


**Figure 4-31** TEM images of 1 micron for the Urea and Xylitol ionogels.

Figure 4-31 illustrates that the DES-gels formed from urea and xylitol with choline chloride also form nanofibrillar structures. Clearly, all of the samples investigated have DBS nanofibres within them, demonstrating the outstanding versatility of this simple, industrially viable gelation system, and its capacity to immobilise a wide range of DES-gels.

#### **4.14. Sonication and ionic conductivity**

The final experiment performed on these systems was a qualitative investigation of the effect of ultrasound on the ionic conductivity of the DEGs.

The role of sonication in this case is to find if a stimulation such as sonication can affect the ionic conductivity due to an enhancement of diffusing parameters of the ionic species that allows ionic conductivity of the material. The incorporation of an stimuli increases the level of agitation and can affect the supramolecular interactions that contributes to the viscosity level of the eutectic system.

This experiment was designed in such a manner that the whole ionic conductometer was moved next to the ultrasonic bath. The conductivity probe was introduced in the gel sample and the system was heated until complete solution of the DEGs was obtained. Once the gel was completely melted and the probe was situated inside the melted gel, gelation occurred so the material was solidified inside the probe and vial. The whole vial and conductivity probe apparatus was then sealed and cooled to room temperature. Then the first conductivity measurement was made generating the ionic conductivity for the DEGs – equivalent to those previously reported. The ultrasound bath (Elmasonic P 37kHz, 120W effective power) was then activated, and the sample immersed. On activating the ultrasound, the conductivity increased by roughly by 10 mS/cm as shown in the graph below. When ultrasonic stimulus was stopped then the ionic conductivity decreased to the original value making the effect reversible. This is a remarkable increase in conductivity. This could be due, at least partially, to the local heating effect when microbubbles appear, such local instant heating can affect the viscosity of the deep eutectic solvent inside the matrix and thus the self-diffusion parameters that affect directly to the free- movement of molecules and thus indirectly to the ionic conduction mechanisms. The temperature of the ultrasonic bath was thermoregulated and didn't increase at any time. The effect of ultrasound was immediate Figure 4-32.

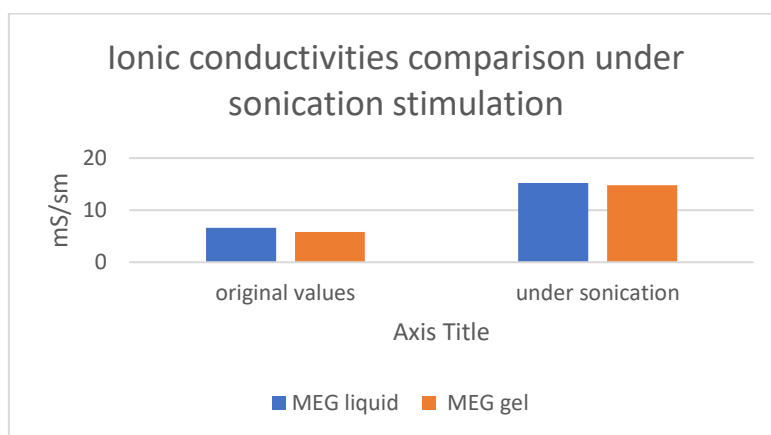


**Figure 4-32:** Effect on the ionic conductivity of the DES liquids and gel made of ChCl and MEG.

The mechanism of ultrasound in normal solvents creates microbubbles with peaks of high pressure (energy) that normally are used to stimulate supramolecular reactions and processes such as dissolving and self-assembly of nanostructures (graphene solutions, fracture of solids and precipitates, plastic welding).<sup>276</sup> As such, ultrasound affects physical interactions between molecules such as supramolecular bonds depending on the frequency and the intensity of the stimulus. Such processes have been used in medical applications to promote healing of wounds in diabetic patients which were really difficult to seal<sup>277</sup> and heal.<sup>278</sup> Nature has many processes where diffusion and supramolecular interactions are needed to evolve the different biophysical and biochemical mechanisms they have.

The experiment showed that actually there was a significant increase of ionic conductivity while sonicating such samples.<sup>279</sup> The increase was roughly double the original conductivity of MEG and immediately declined when the stimulation was removed or stopped. We were not sure if this response of DESs under sonication conditions was produced by an increase of local temperature inside the ionic conductivity probe or due to the theoretical increase of molecular mobility and decrease of viscosity in the material inside.<sup>280</sup> The gel remained stable under sonication under at least 5 min of stimulation.

Interestingly, the same effect was observed for both the DES liquid and the DES gel. It is plausible to consider that ultrasound disrupts non-covalent interactions between ions, and hence enhances the ionic mobility, which is the conductivity route in each of these materials.

#### **4.15. Conclusions.**

It can be confirmed that a new family of DEGs have been created. A set of deep eutectic solvents (DESs) have been made and all tested hydrogen bond donor/choline chloride based systems have been gelled using 1,3;2,4-dibenzylidenesorbitol (DBS). These gels could tolerate ionic species such as  $\text{Li}^+$ ,  $\text{Mg}^{2+}$  and  $\text{Ca}^{2+}$  but could not form in the presence of other ions such  $\text{Fe}^{3+}$  and  $\text{Al}^{3+}$ , which could not dissolve in the DES medium. The resulting DEGs almost completely retain the ionic conductivity of the original DES liquids. There were some differences in the temperature response of the liquids and the gels, which could perhaps be assigned to differences in viscosity response of the media. The gel nature of the formed ionogels was tested and verified by the basic tools available such as rheology and TEM and SEM imaging. There was some evidence from rheology that softer, more flexible gels were formed in those DESs with better conductivity, and that more rigid, stiffer gels were formed in systems with lower conductivity. This suggests that the ionic nature of the DES may have an impact on the rheological performance of the gels formed. Gel stiffness often emerges from the compatibility of the gelator with the precise solvent conditions. In summary, these gels are able to achieve good conductivities, in some cases with fully bio-derived systems.

##### **4.15.1. Suggested Future Work**

The potential of these kind of DEGs for electrolyte applications is evident. The tunability that can be achieved using different combinations of components in the mixture of DES liquids is extraordinarily broad. This leads to a special versatility in the preparation of electrolytes for various possible chemistries. Thus, there is considerable importance of such DES room temperature melts with an extraordinarily broad electrochemical window. The fact that these room temperature melts can be gelled easily is of practical use

because it avoids the risk of leakage and reduces the volatility of the electrolyte. Being a supramolecular gel improves the processability because the material incorporates the property of reversibility on the production line, depending on the surrounding conditions of temperature, pressure, ultrasonic stimulation, presence of additional chemicals etc. It is known that this can significantly assist with the process of loading a gel electrolyte into a device, as it can be loaded as a liquid, and then allowed to form a gel in situ, hence maximising contact with electrodes. We suggest that in analogy with other research on ionogels, there is significant potential for electrolytes such as this, only based on more renewable feedstocks than traditional ionic liquids, to find application in solar cell technology, lithium (or other) ion batteries and capacitors for energy storage.

## Chapter 5 Conclusions and future work

The main aim of this project was to study the different aspects of dynamic behaviour in supramolecular gels. That idea led us to study three main phenomena in these particular gels which have been described in each chapter. Gels are formed by self-assembly processes which could be considered as a bottom up process where gelator self-interact by means of supramolecular interactions which sustain the resulting 3D network. This evolving process in the construction of the gel is known as gelation and the rate at which this happens has been one of the key questions addressed in this project. Secondly, we knew that gels are solid like materials with a high content of solvent (99% W). This potentially allows diffusion of molecules through the gel matrix thus we were interested in studying such diffusion in between two similar gels that are placed into contact by means of the creation of gel-gel interface. Finally, we developed a DBS based ionogels for a family of choline chloride DESs. In the following sections, the main conclusion for each chapter are highlighted. Also, some potential future ideas that could be developed from the presented work are described.

### 5.1. Thermodynamics and Kinetics of gelation.

This chapter focusses on the thermodynamics and kinetics of a two-component gelator system based on a peptide dendron acid combined with an amine. Understanding thermodynamic and kinetic aspects of gel formation is a critical step to inform LMWG design. The self-assembly process of certain molecules is limited by the stability of the structures that are formed as a result of a hierarchical organized process. The Solvent plays an important role in the process of self-assembly. This formation can occur over a wide range of timescales, from seconds to hours. In this work 12 different combination of dendrons and amines have been tested and each one of them had diverse kinetic and

thermodynamic behaviours. Thus, we used three different methods to study the kinetics of gelation on three different length scales – rheology (macroscopic), CD spectroscopy (nanoscale) and NMR (molecular scale), thus providing a degree of quantitative insight into the self-assembly event. We have developed a rheological method for the study of rapid gel formation (in the seconds timescale). Fitting with an exponential model, adjusted with least square regression analysis, provided an accurate description of the experimental data recorded. We concluded that those gels which are thermodynamically most stable are not necessarily those which are formed the fastest.

## **5.2. Diffusion processes at gel-gel interfaces**

In this chapter we report diffusion across a gel-gel interface, and in particular compares and contrast the diffusion of small molecules which are mobile within the gel with the diffusion of the small molecules that actually self-assemble into the solid-like fibres. Such gel-gel diffusion processes are underinvestigated and are important in helping to understand release processes that gels can have when they are loaded with functional chemicals (controlled release). We find that although as expected, small molecules diffuse rapidly through the gel, even those small molecules which are part of the solid-like network can also diffuse and exchange across the gel-gel interface. This latter process is quantified in detail – it is slower than the diffusion of fully mobile small molecules but we propose it occurs via a mechanism in which the two-component complex disassembles and the individual parts can then move. We find that the amine is slightly more mobile than the acid dendron, which may reflect the latter being more integrated in the gel network through hydrogen bonding. The diffusion of self-assembled nanofibre components has important consequences for the ability of supramolecular gels to self-

self-heal as a result of this delicate equilibrium between the free available components and the solid network.

### **5.3. Ionic conductivity of Deep Eutectic gels.**

Chapter Four reports the gelation capabilities of certain choline chloride based deep eutectic solvents (DESs) using 1,3;2,4-dibenzylidenesorbitol (DBS) as gelator. Remarkably effective gels form across a wide-range of DESs – we describe these as DEGs. We monitor the ionic conductivity of the DEGs which have been created in order to gain insight into the diffusion characteristic of ionic components within the gel. The results demonstrate conductivities for the DEGs which are very similar to those of the DESs themselves, indicating that the ionic components do not suffer from problems of immobilisation through interaction with the self-assembled gel nanofibres. These results are encouraging as they are the first example of supramolecular gels made for these specific kinds of DESs, and suggest potential applications, for example as gel electrolytes in battery applications.

### **5.4. Summary**

All together the work has contributed to the understanding dynamic processes that these soft materials inherently possess. Smart materials have to be increasingly investigated by understanding the dynamic phenomena of such materials so that design and applications in this field can be developed and improved. The know-how produced in this research, ranging from the design and fabrication of the diffusion cell; to the development of methodologies such as the ones used to measure kinetics of gel formation; and the development of a new family of ionogels based on a range of deep eutectic solvents, could help and inform other researchers to better understand and study such materials. Hopefully most of the complete sections of this research such as the diffusion studies and the DEGs will be published so that others will benefit as I did from others' research.

## Chapter 6 Experimental

For ease of reference, experimental procedures are presented largely according to their order of appearance in this thesis.

### 6.1. General Experimental Methods.

All necessary compounds required for the synthesis were purchased from commercial suppliers and used without purification. Thin layer chromatography (TLC) was performed on Merck aluminium-backed plates coated with 0.25 nm silica gel 60. Flask column chromatography was performed on silica gel 60 supplied by Fluka.

NMR was recorded on a JEOL ECX 400 spectrometer ( $^1\text{H}$  400 MHz,  $^{13}\text{C}$  100 MHz). The various deuterated solvents which were used were  $\text{d}_4$  methanol and  $\text{d}_8$ -Toluene which were also used to reference chemical shifts. Mass spectrometric data was collected using a Bruker Micro-TOF mass Spectrometer. FTIR spectra were recorded on a Perkin Elmer Spectrum FT-IR spectrometer. Melting points were measured on a Stuart SMP3 apparatus. T<sub>gel</sub> values were recorded in glass vials with a diameter of 1cm using a thermoregulated oil bath Ministat cc2 Huber. Rheological measurements were performed in a Malvern Instrument Kinexus Pro+ Rheometer Fitted with a parallel plate geometry with an interface software to program experiments called 'rSpace'. The ionic conductivity readings were collected in a Jenway 4310 conductivity meter with a probe made of platinum with a thermocouple to measure temperature. Circular Dichroism was measured on a Jasco J810 CD spectrometer which included a thermoregulated system that could cool and warm the experimental conditions. SEM and TEM were carried out in the Department of Biology at University of York using a JEOL JSM-7600F (SEM) and (TEM). AFM was recorded in the Solvay facilities of Brussels using a Dimension Icon

AFM from Bruker. The ultrasound bath was an Elmasonic P 37kHz, 120W effective power, 5 litres.

## 6.2. Chapter 2 and 3 syntheses.

### 6.2.1. Synthesis of L or D lysine methyl ester dihydrochloride<sup>207</sup>

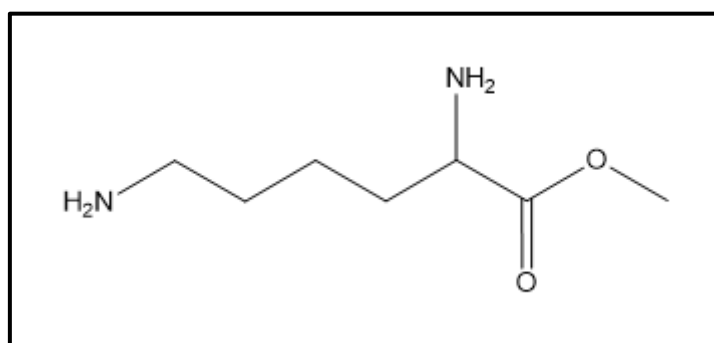


**Figure 6-1** Molecular structure of Lysine methyl ester dihydrochloride  
Molecular Formula:  $C_7H_{16}N_2O_2$   
Molecular Weight:  $160.22 \text{ g}\cdot\text{mol}^{-1}$

L- or D-Lysine monohydrochloride (2.5 g, 13.68 mmol) was dissolved in methanol (27.5 mL, 0.678 mol). Then 2,2-dimethoxypropane (70 mL, 0.52 mol) was added followed by concentrated hydrochloric acid (4.5 mL 36%, 52 mmol). The mixture was refluxed for 3 hours and stirred overnight at room temperature. The crude reaction mixture was evaporated in a rotary evaporator and the remaining oil was dissolved in the minimum amount of methanol to which was then added an ice cooled amount of ether (ca. 100 mL). After that a series of recrystallizations were carried out. A white powder was obtained as the final product.<sup>207</sup> **Yield L:** 84.81%, 1.86 g / **Yield D:** 76.15%, 1.67g . All other data were in agreement with those previously published.<sup>1</sup>

Colourless solid, **m.p.** 207-210 °C  
**<sup>1</sup>H-NMR** (400 MHz, MeOH-*d*<sub>4</sub>)  $\delta$ : 4.25 (t, *CHNH*<sub>2</sub>, *J* = 8Hz, 1H), 3.92 (s, *CO*<sub>2</sub>*CH*<sub>3</sub>, 3H), 3.09 (t, *CH*<sub>2</sub>*NH*<sub>2</sub>, <sup>3</sup>*J* = 8 Hz, 2H), 2.06 – 1.58 (br m, 3x*CH*<sub>2</sub>, 6H).  
**<sup>13</sup>C-NMR** (400 MHz, MeOH-*d*<sub>4</sub>)  $\delta$ : 170.58 (*CH*<sub>2</sub>*COOMe*), 53.63, 52.65 (*NH*<sub>2</sub>*CHCOOCH*<sub>3</sub>), 39.05 (*NH*<sub>2</sub>*CH*<sub>2</sub>*CH*<sub>2</sub>), 29.27 (*NH*<sub>2</sub>*CHCH*<sub>2</sub>), 26.29 (*NH*<sub>2</sub>*CH*<sub>2</sub>*CH*<sub>2</sub>), 21.50 (*NH*<sub>2</sub>*CH*<sub>2</sub>*CH*<sub>2</sub>*CH*<sub>2</sub>).

**IR:**  $\tilde{\nu}$  = 2943 (s), 1974 (w), 1739 (s), 1603 (m), 1583 (w), 1505 (s), 1450 (m), 1289 (w), 1228 (s), 1196 (m), 1160 (m), 1142 (w), 1097 (w), 1038 (m), 1002 (m), 952 (m), 928 (m), 856(m),741(m), 524(m).

**HRMS:**  $[M+H]^+$  ( $C_7H_{17}N_2O_2$ ) Calcd. *m/z* = 161.1285; Measured *m/z* = 161.1283 Mean Error 0.8 ppm

$[\alpha]_D^{20} = +24.1$  (c=1.0, MeOH) (L-enantiomer)  $[\alpha]_D^{20} = -23.9$  (c=1.0, MeOH) (D-enantiomer)

See appendix for spectra data.

### 6.2.2. BOC protection of L or D Lysine

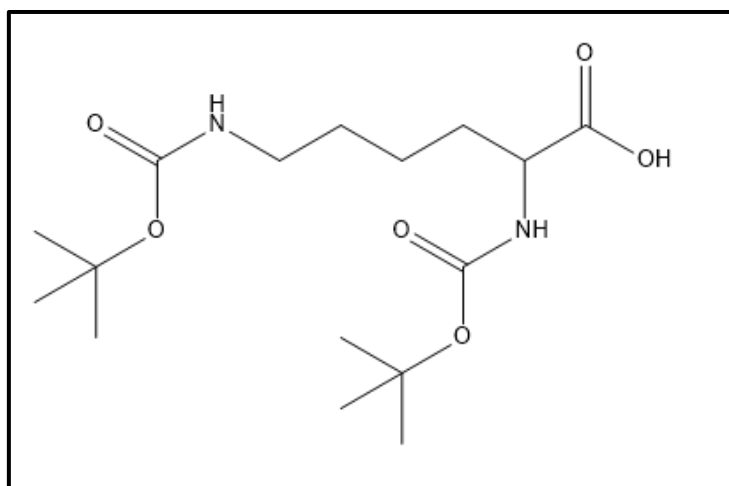


Figure 6-2 Molecular Structure of (Boc)<sub>2</sub>-Lys-OH

Molecular Formula: C<sub>16</sub>H<sub>30</sub>N<sub>2</sub>O<sub>6</sub>

Molecular Weight: 346.42 g·mol<sup>-1</sup>

A solution of NaOH was added to the reaction flask (13.31 mL, 1M, 13.31 mmol), followed by L-Lysine monohydrochloride (2.00 g, 13.69 mmol) and then <sup>t</sup>BuOH (10.27 mL, 107.39 mmol). The reaction mixture was stirred and then (Boc)<sub>2</sub>O (5.70 g, 27.39 mmol) was added. A precipitate was generated during addition. After the addition, heating was started and the temperature was raised to 40 °C for an hour. The mixture was left stirring at room temperature overnight. The crude reaction mixture was extracted with hexane. Then the organic phase was washed with a sodium bicarbonate solution Saturated. The resulting aqueous phase was acidified by a careful addition of saturated hydrogen sulphate solution. The resulting turbid reaction mixture is extracted by EtOAc several times. The resulting organic phase was washed with distilled water and wash with brine and magnesium sulphate. The solvent was removed by rotary evaporation, and the obtained powder recrystallized from hexane. <sup>208</sup>

**Yield L.** 69.5%, 3.3 g. / **Yield D.** 73.7%, 3.5 g.

Colourless solid. **m.p.** 139-143 °C

**<sup>1</sup>H-NMR** (400 MHz, MeOH-d<sub>4</sub>) δ: 6.82 (d, 1H, CONH), 6.58 (t, 1H, CONH), 4.05 (q, 1H, J=4Hz COCH(R)NH), 3.03 (t, 2H, CH<sub>2</sub>CH<sub>2</sub>NH), 1.80 (m, 2H, CH<sub>2</sub>CH<sub>2</sub>CH), 1.66 (m, 2H, CH<sub>2</sub>CH<sub>2</sub>CH), 1.44 (s, 6H; CCH<sub>3</sub>).

**<sup>13</sup>C-NMR** (400 MHz, MeOH-d<sub>4</sub>) δ: 176.26 (CO<sub>2</sub>H), 158.57 (CONH), 158.16 (CONH), 80.43 (OC(CH<sub>3</sub>)<sub>3</sub>), 79.83 (OC(CH<sub>3</sub>)<sub>3</sub>), 54.83 (COCH(R)NH), 40.99 (CH<sub>2</sub>NH), 32.45, 30.54, (All CH<sub>2</sub>), 28.8 (CH<sub>3</sub>), 24.16 (All CH<sub>2</sub>);

**IR:**  $\tilde{\nu}$  = 3334 (w), 2977 (w), 2933 (m), 1689 (s), 1517.12 (s), 1365 (s), 1248 (s) 1159 (s), 1047 (m), 736.3 (w)

**HRMS:** [M + Na]<sup>+</sup> (C<sub>16</sub>H<sub>30</sub>N<sub>2</sub>NaO<sub>6</sub>) Calc d. m/z = 369.1983; Measured m/z = 369.1996 Mean Error -4.3 ppm

See appendix for data Spectra.

### 6.2.3. Coupling of L-(Boc)<sub>2</sub>-Lys-OH and L(Lys)-OMe.

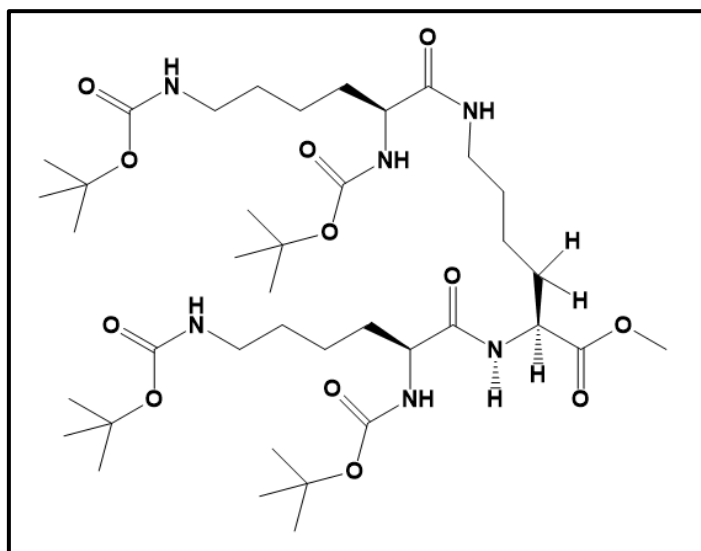


**Figure 6-3** Molecular structure of G2 ((Boc)<sub>2</sub>-Lys)<sub>2</sub>-Lys-OMe  
Molecular Formula: C<sub>39</sub>H<sub>72</sub>N<sub>6</sub>O<sub>12</sub>  
Molecular Weight: 817.04 g·mol<sup>-1</sup>

(Boc)<sub>2</sub>-Lys-OH (2.5 g, 6.2 mmol) was suspended in EtOAc (24 mL, 0.25 mol) and NEt<sub>3</sub> (0.87 mL, 6.2 mmol), then L-Lys-OMe (1.00 g, 6.24 mmol) was added so that a suspension was obtained. The mixture was cooled and treated under vacuum and nitrogen to remove the remaining air from the flask. TBTU (2-(1H-benzotriazole-1-yl)-1,1,3,3-

tetramethylammonium tetrafluoroborate) was added (2.39 g, 7.44 mmol) and the reaction mixture was left with stirring at room temperature overnight. The precipitate was removed by filtration and the filtrate was washed with NaHCO<sub>3</sub> (satd. aq), NaHSO<sub>4</sub> (aq 1 M) and NaHCO<sub>3</sub> (satd. aq), and finally with water then dried over MgSO<sub>4</sub>. The solvent was evaporated and the product was purified by flash chromatography (MeOH:CH<sub>2</sub>Cl<sub>2</sub>:NEt<sub>3</sub>, 5:95:0.1). The parameters of the column were diameter (6.5 cm), with 10 cm height of silicagel (300 mL approx.) Every column had a maximum charge of product of 1.75g, otherwise the product would not separate well.<sup>17</sup>

**Yield: L, L, stereoisomer** 83%, 2.03 g. / **Yield: D, D, stereoisomer** 73%, 1.78 g.

Colourless solid, m.p. 74-79°C; R<sub>f</sub> = 0.45 (CH<sub>2</sub>Cl<sub>2</sub>/MeOH/Et<sub>3</sub>N 90:10:0.1)

**<sup>1</sup>H-NMR** (400 MHz, MeOH-d<sub>4</sub>) δ: 8.24 (s, 1H; CONH), 7.95 (s, 1H, CONH), 6.70 (s, 1H, NHBoc), 6.58 (s, 1H, NHBoc), 4.37 (q, J=4 1H, COCH(R)NH), 4.06 (q, J=5.6Hz, 1H, COCH(R)NH), 3.96 (q, J= 5.6Hz, 1H, COCH(R)NH), 3.71 (s, 3H, CO<sub>2</sub>CH<sub>3</sub>), 3.18 (q, J=8Hz, 2H; CH<sub>2</sub>CH<sub>2</sub>(R)NH), 3.04 (q, J=6.8 4H; CH<sub>2</sub>CH<sub>2</sub>(R)NH), 1.84 (m, 6H, CH<sub>2</sub>CH<sub>2</sub>CH), 1.72 (m, 4H, CH<sub>2</sub>CH<sub>2</sub>CH), 1.58 (m, 6H, CH<sub>2</sub>CH<sub>2</sub>CH<sub>2</sub>) 1.43 (s, 12H; CCH<sub>3</sub>).

**<sup>13</sup>C-NMR** (400 MHz, MeOH-d<sub>4</sub>) δ: 175.79 (CO<sub>2</sub>Me, 1C), 174.39 (CONH, 2C), 158.97 (COOC(CH<sub>3</sub>)<sub>3</sub>), 158.23 (COOC(CH<sub>3</sub>)<sub>3</sub>), 80.98 (OC(CH<sub>3</sub>)<sub>3</sub>), 80.25 (OC(CH<sub>3</sub>)<sub>3</sub>), 56.64 (COCH(R)NH), 56.17 (COCH(R)NH), 53.91 (COCH(R)NH), 53.14 (CO<sub>2</sub>CH<sub>3</sub>), 41.43 (CH<sub>2</sub>NH), 40.23 (CH<sub>2</sub>NH), 33.51 (CH<sub>2</sub>CH<sub>2</sub>NH), 31.04, 29.20(C(CH<sub>3</sub>)<sub>3</sub>), 24.67, (All CH<sub>2</sub>).

**IR:**  $\tilde{\nu}$  = 3313 (w), 2976 (m), 2932 (m), 1690 (m), 1514 (s), 1247 (s), 1247 (s) 1165 (s), 1392 (m), 1366 (m), 1250 (m), 1172 (s) cm<sup>-1</sup>

**HRMS:** [M + H]<sup>+</sup> (C<sub>39</sub>H<sub>73</sub>N<sub>6</sub>O<sub>12</sub>) Calc. *m/z* = 817.530; Measured *m/z* = 817.528 Mean Error -2.9 ppm

[ $\alpha$ ]<sub>D</sub><sup>20</sup> = -10.7 (c=1.0, MeOH)

[ $\alpha$ ]<sub>D</sub><sup>20</sup> = +11.2 (c=1.0, MeOH)

See Appendice for data spectra.

#### 6.2.4. Coupling of Boc-Phe-OH and Lys-OMe.

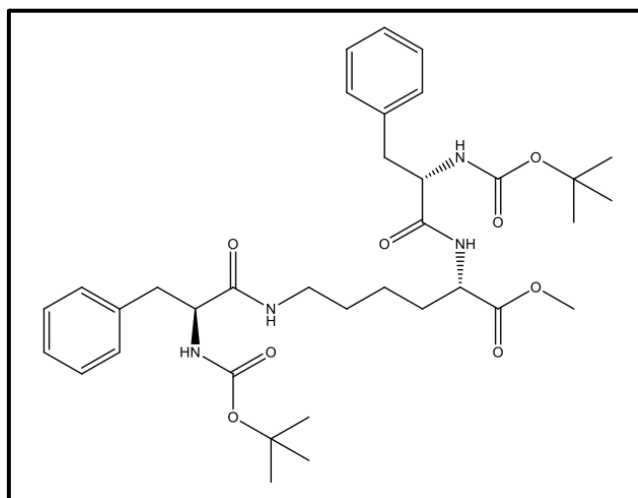


**Figure 6-4** Molecular structure G2 (Boc-Phe)<sub>2</sub>-Lys-OMe  
Molecular Formula: C<sub>35</sub>H<sub>50</sub>N<sub>4</sub>O<sub>8</sub>  
Molecular Weight: 654.79 g·mol<sup>-1</sup>

The Boc-Phe-OH (2.15 g, 8.10 mmol) was suspended in EtAc (32.41 mL, 0.33 mol) and NEt<sub>3</sub> (1.36 mL, 9.7 mmol), then the LysOMe (0.64 g, 4.05 mmol) was added so that a suspension was obtained. Then the mixture was cooled down and treated under vacuum and nitrogen to remove the remaining air of the flask. The TBTU was added (3.12 g, 9.7 mmol) and the reaction mixture was left with stirring and at room temperature overnight. The precipitate was removed by physical filtration and the filtrate was washed several times following a NaHCO<sub>3</sub> (aq), NaHSO<sub>4</sub> (aq) and NaHCO<sub>3</sub> (aq) order, finally was washed with water and the solution was dried with MgSO<sub>4</sub> then the solvent was evaporated and the product was dried. The product was purified by flash chromatography. The chosen solvent mixture was MeOH:CH<sub>2</sub>Cl<sub>2</sub>:NEt<sub>3</sub> (1:9:0.1) ratio respectively. The parameters of the column were 6.5 cm of diameter, and 10 cm of silicagel content (300 mL approx.). Every column had a maximum charge of product of 0.5g. This compound has some separation problems so the amount introduced in the flash chromatography was less than for other dendrons.

**Yield:** 71.69%, 1.9 g.

White solid, **m.p.** 108-110 °C; **Rf** = 0.70 (CH<sub>2</sub>Cl<sub>2</sub>/MeOH/Et<sub>3</sub>N 90:10:0.1);

**[α]<sub>D20</sub>** = +4.5 (c=1.0, MeOH)

**<sup>1</sup>H-NMR** (400 MHz, MeOH-d<sub>4</sub>) δ: 7.25 – 7.21 (m, Ar-H, 10H), 4.42-4.35 (t, Ar-CH<sub>2</sub>-CH-NH<sub>2</sub>, 2H), 4.37 (t, NHCHCOHN, 2H) 4.28 (t, NHCHCOOMe, J = 8 Hz, 1H), 3.69 (s, COOCH<sub>3</sub>, 3H), 3.14-3.10 (m, Ph-CH<sub>2</sub>-CHNH, 4H), 3.05-2.78 (m, CO-HN-CH<sub>2</sub>-CH<sub>2</sub>, 2H), 1.79 – 1.68 (m, MeCOO-CH-CH<sub>2</sub>-CH<sub>2</sub>-CH<sub>2</sub>-CH<sub>2</sub>-NH, 6H), 1.36 (s, Boc-CH<sub>3</sub>, 18H).

**<sup>13</sup>C-NMR** (400 MHz, MeOH-d<sub>4</sub>) δ: 174.67, 174.47, 174.03 (2x NH-CH-CO-NH and HCOOCH<sub>3</sub>), 157.79 (2x HNCOOC(CH<sub>3</sub>)<sub>3</sub>), 138.78, 138.75 (2x Ar-C<sub>q</sub>-CH<sub>2</sub>), 130.63, 129.68, 127.93, 27.86, (all Ar-C), 80.78 (2x C(Boc)), 57.79, 57.32 (both Ar-CH<sub>2</sub>-CH-NH), 55.02 NHCHCOOMe), 52.94 (COOCH<sub>3</sub>), 40.01 CH<sub>2</sub>-CH<sub>2</sub>-CH<sub>2</sub>-NH, 39.75 (COOCH<sub>3</sub>-CH<sub>2</sub>-CH<sub>2</sub>), 39.49 2x (Ar-CH<sub>2</sub>), 32.32 (MeCOO-CH-CH<sub>2</sub>-CH<sub>2</sub>-CH<sub>2</sub>-CH<sub>2</sub>-NH), 28.89 (6x Boc-CH<sub>3</sub>), 23.99 (MeCOO-CH-CH<sub>2</sub>-CH<sub>2</sub>-CH<sub>2</sub>-CH<sub>2</sub>-NH).

**IR:**  $\tilde{\nu}$  = 3300 (m), 2978 (m), 2930 (m), 2421 (m), 1742 (m), 1646 (s), 1534 (s), 1419 (s), 1365 (w), 1164 (m), 698 (m),

**HRMS:** [M + Na]<sup>+</sup> (C<sub>35</sub>H<sub>50</sub>N<sub>4</sub>O<sub>8</sub>Na) Calcd.  $m/z$  = 677.3519; Measured  $m/z$  = 677.3520 Mean Err -0.6 ppm; [M + H]<sup>+</sup> (C<sub>35</sub>H<sub>51</sub>N<sub>4</sub>O<sub>8</sub>) Calcd.  $m/z$  = 655.3694; Measured  $m/z$  = 655.370141 Mean Err -1.0 ppm

See Appendice for data spectra.

### 6.2.5. Coupling of Boc-Ala-OH and Lys-OMe.

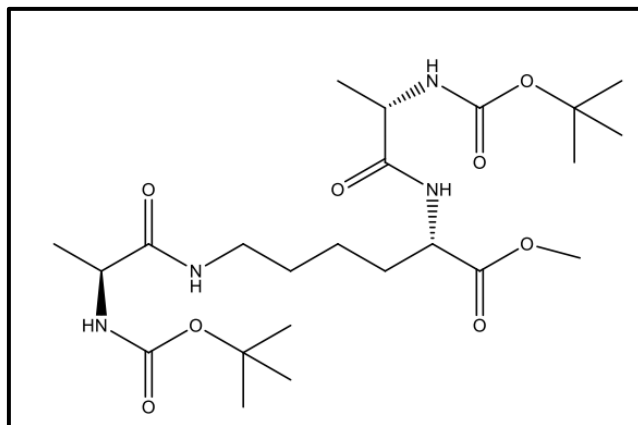


**Figure 6-5** Molecular structure G2 (Boc-Ala)<sub>2</sub>-Lys-OMe  
Molecular Formula: C<sub>23</sub>H<sub>42</sub>N<sub>4</sub>O<sub>8</sub>  
Molecular Weight: 502.60 g·mol<sup>-1</sup>

The Boc-Ala-OH (2.15 g, 11.3 mmol) was suspended in EtOAc (45.45 mL, 0.46 mol) and NEt<sub>3</sub> (1.91 mL, 13 mmol), then the Lys-OMe (0.9 g, 5.6 mmol) was added so that a suspension was obtained. Then the mixture was cooled down and treated under vacuum and nitrogen to remove the remaining air of the flask. The TBTU was added (4.37

g, 13.6 mmol) and the reaction mixture was left with stirring and at room temperature overnight. The precipitate was removed by physical filtration and the filtrate was washed several times following a NaHCO<sub>3</sub> (aq), NaHSO<sub>4</sub> (aq) and NaHCO<sub>3</sub> (aq) order, finally was washed with water and the solution was dried with MgSO<sub>4</sub> then the solvent was evaporated and the product was dried. The product was purified by flash chromatography. The chosen solvent mixture was MeOH:CH<sub>2</sub>Cl<sub>2</sub>:NEt<sub>3</sub> (1:9:0.1) ratio respectively. The parameters of the column were 6.5 cm of diameter, and 10 cm of silicagel content (300 mL approx.). the column was charged with a maximum charge of product of 1,75g.

**Yield:** 80.54%, 2.3 g.

Colourless highly viscous liquid, **R<sub>f</sub>** = 0.68 (CH<sub>2</sub>Cl<sub>2</sub>/MeOH/Et<sub>3</sub>N 90:10:0.1);

**[α]<sub>D</sub><sup>20</sup>** = -13.3 (c=1.0, MeOH)

**<sup>1</sup>H-NMR** (400 MHz, MeOH-d<sub>4</sub>) δ: 4.37 (q, HN-CH-COOCH<sub>3</sub>, J = 4.7 Hz, 1H), 4.11 – 4.03 (m, 2x -CH-NHBoc, 2H), 3.70 (s, COOCH<sub>3</sub>, 3H), 3.19 (t, CO-HN-CH<sub>2</sub>-CH<sub>2</sub>, 2H), 1.86-1.52 (m, MeCOO-CH-CH<sub>2</sub>-CH<sub>2</sub>-CH<sub>2</sub>-CH<sub>2</sub>-NH, 6H), 1.44 (s, Boc-CH<sub>3</sub>, 18H), 1.29 (2x d, both Ala-CH<sub>3</sub>, , J = 7.2 Hz, 6H).

**<sup>13</sup>C-NMR** (400 MHz, MeOH-d<sub>4</sub>) δ: 176.22, 176.12 (both NH-CH-CO-NH), 174.17 (CHCOOCH<sub>3</sub>), 157.78 (2x HNCOOC(CH<sub>3</sub>)<sub>3</sub>), 80.74 (2xC(Boc)), 55.02 (NHCHCOOMe), 52.89 (COOCH<sub>3</sub>), 51.93, 51.52 (CH<sub>3</sub>-CH-NH), 40.04 (CO-NH-CH<sub>2</sub>-), 32.26, 29.89 (MeCOO-CH-CH<sub>2</sub>-CH<sub>2</sub>-CH<sub>2</sub>-CH<sub>2</sub>-NH), 28.84 (6x Boc-CH<sub>3</sub>), 23.95 (MeCOO-CH-CH<sub>2</sub>-CH<sub>2</sub>-CH<sub>2</sub>-CH<sub>2</sub>-NH), 18.79, 18.58 (both Ala-CH<sub>3</sub>).

**IR:**  $\tilde{\nu}$  = 3300.43 (w), 2977 (w), 1654 (w), 1514 (m), 1450 (s), 1365 (s), 1246 (m), 1162 (w), 11068 (s), 1020 (m), 856 (s), 781 (s),

**HRMS:** [M + Na]<sup>+</sup> (C<sub>23</sub>H<sub>42</sub>N<sub>4</sub>O<sub>8</sub>Na) Calcd. *m/z* = 525.2906; Measured *m/z* = 525.289 Mean Err -2.3 ppm; [M + H]<sup>+</sup> (C<sub>23</sub>H<sub>43</sub>N<sub>4</sub>O<sub>8</sub>) Calcd. *m/z* = 503.3088; Measured *m/z* = 503.7541 Mean Err -2.4 ppm

See Appendice for data spectra.

### 6.2.6. Coupling of Boc-Val-OH and Lys-OMe

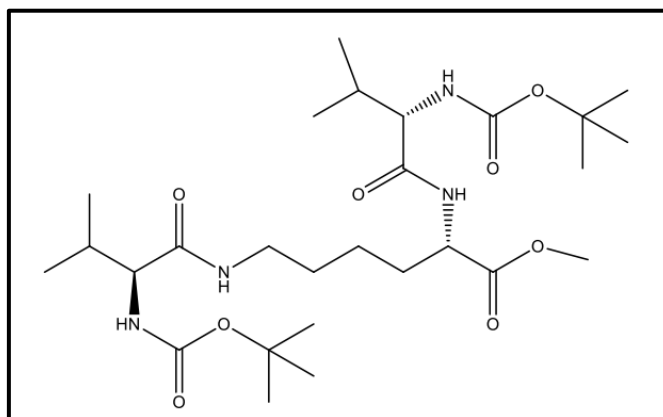


**Figure 6-6** Molecular structure G2 (Boc-Val)<sub>2</sub>-Lys-OMe  
Molecular Formula: C<sub>27</sub>H<sub>50</sub>N<sub>4</sub>O<sub>8</sub>  
Molecular Weight: 558.36 g·mol<sup>-1</sup>

The Boc-Val-OH (2.5 g, 9.9 mmol) was suspended in EtOAc (39.61 mL, 0.4032 mol) and NEt<sub>3</sub> (1.66 mL, 11.8 mmol), then the Lys-OMe (0.7921 g, 4.95 mmol) was added so that a suspension was obtained. Then the mixture was cooled down and treated under vacuum and nitrogen to remove the remaining air of the flask. The TBTU was added (3.81 g, 11.8 mmol) and the reaction mixture was left with stirring and at room temperature overnight. The precipitate was removed by physical filtration and the filtrate was washed several times following a NaHCO<sub>3</sub> (aq), NaHSO<sub>4</sub> (aq) and NaHCO<sub>3</sub> (aq) order, finally was washed with water and the solution was dried with MgSO<sub>4</sub> then the solvent was evaporated and the product was dried. The product was purified by flash chromatography. The chosen solvent mixture was MeOH:CH<sub>2</sub>Cl<sub>2</sub>:NEt<sub>3</sub> (1:9:0.1) ratio respectively. The parameters of the column were 6.5 cm of diameter, and 10 cm of silicagel content (300 mL approx.). Every column had a maximum charge of product of 1,75g, otherwise the product wouldn't separate well.

**Yield:** 68%, 1.9 g.

Colourless solid, **m.p.** 116-117 °C;

**R<sub>f</sub>** = 0.39 (CH<sub>2</sub>Cl<sub>2</sub>/MeOH/Et<sub>3</sub>N 90:5:0.1);

**[α]<sub>D20</sub>** = -26.9 (c=1.0, MeOH)

**<sup>1</sup>H-NMR** (400 MHz, MeOH-d<sub>4</sub>) δ: 4.38 (q, HN-CH-COOCH<sub>3</sub>, J = 4.7 Hz, 1H), 3.93, 3.81 (2x d, both -CH-NHBoc, J = 8 Hz, 2H), 3.70 (s, COOCH<sub>3</sub>, 3H), 3.19 (t, CO-HN-CH<sub>2</sub>-CH<sub>2</sub>, J = 5.8 Hz, 2H), 2.00 (m, 2x (CH<sub>3</sub>)<sub>2</sub>-CH-CH-NHBoc, 2H), 1.84-1.72 (m, MeCOO-CH-CH<sub>2</sub>-CH<sub>2</sub>-CH<sub>2</sub>-CH<sub>2</sub>-NH, 6H), 1.44 (s, Boc-CH<sub>3</sub>, 18H), 0.97, 0.93 (2x d, 4x Val-CH<sub>3</sub>, J = 3.4 Hz, 12H).

**<sup>13</sup>C-NMR** (400 MHz, MeOH-d<sub>4</sub>) δ: 174.68, 174.56 (both NH-CH-CO-NH), 173.85 (CHCOOCH<sub>3</sub>), 157.92 (2x HNCOOC(CH<sub>3</sub>)<sub>3</sub>), 80.49 (2x C(Boc)), 61.84, 61.24 (both (CH<sub>3</sub>)<sub>2</sub>-CH-CH-NHBoc), 53.54 (NHCHCOOMe), 52.59 (COOCH<sub>3</sub>), 39.73 (CO-NH-CH<sub>2</sub>-), 32.19, 31.9 (2x (CH<sub>3</sub>)<sub>2</sub>-CH-CH-NHBoc) 29.66 (MeCOO-CH-CH<sub>2</sub>-CH<sub>2</sub>-CH<sub>2</sub>-CH<sub>2</sub>-NH), 28.74 (6x Boc-CH<sub>3</sub>), 23.87 (MeCOO-CH-CH<sub>2</sub>-CH<sub>2</sub>-CH<sub>2</sub>-CH<sub>2</sub>-NH), 19.78, 19.72, 18.64, 18.6, (4x Val-CH<sub>3</sub>).

**IR:**  $\tilde{\nu}$  = 3299 (m), 2963 (m), 1745 (m), 1647 (s), 1527 (m), 1390 (m), 1365 (m), 1245 (m), 1163 (s), 1015 (m), 781 (w), 521 (m).

**HRMS:** [M + Na]<sup>+</sup> (C<sub>27</sub>H<sub>50</sub>N<sub>4</sub>O<sub>8</sub>Na) Calcd.  $m/z$  = 581.3524; Measured  $m/z$  = 581.3520 Mean Err 0.4 ppm; [M + H]<sup>+</sup> (C<sub>27</sub>H<sub>51</sub>N<sub>4</sub>O<sub>8</sub>) Calcd.  $m/z$  = 559.3709; Measured  $m/z$  = 559.3701 Mean Err -1.7 ppm

See Appendice for data spectra.

### 6.2.7. Hydrolysis of L and D G2 ((Boc)<sub>2</sub>Lys)<sub>2</sub>-Lys-OMe.

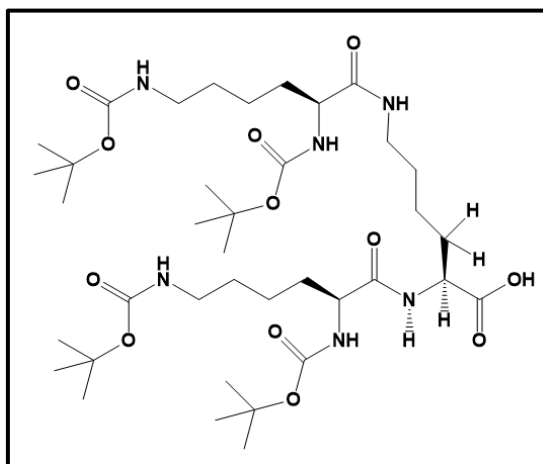


**Figure 6-7** Molecular structure G2 ((Boc)<sub>2</sub>Lys)<sub>2</sub>-Lys-OH

Molecular Formula: C<sub>38</sub>H<sub>70</sub>N<sub>6</sub>O<sub>12</sub>

Molecular Weight: 803.01 g·mol<sup>-1</sup>

The G2 ((Boc)<sub>2</sub>Lys)<sub>2</sub>-Lys-OMe dendron (0.60 g, 0.73 mmol) was dissolved in methanol (30 mL) under nitrogen.<sup>17</sup> NaOH<sub>(aq)</sub> solution (1 M, 2.16 mL, 2.16 mmol) was added and the reaction mixture left overnight with stirring. The crude reaction mixture was evaporated to dryness. After solvent removal, water (ca. 40 mL) was added and the

resulting viscous yellowish mixture was stirred until complete dissolution. Sonication was required in this last step. A precipitate was obtained on acidification with NaHSO<sub>4</sub> solution (x M) to pH=3. The precipitate was extracted with EtOAc (25 mL) and dried under high vacuum.

**Yield L,L, stereoisomer** : 71.25%, 0.42 g, **Yield D,D, stereoisomer** : 86.52%, 0.51 g.

Colourless solid, m.p. 90 – 100°C; *R<sub>f</sub>* = 0.15 (CH<sub>2</sub>Cl<sub>2</sub>/MeOH 90:10)

$[\alpha]_{\text{D}}^{20} = -10.7$  (c=1.0, MeOH) LL

$[\alpha]_{\text{D}}^{20} = +11.2$  (c=1.0, MeOH) DD

**<sup>1</sup>H-NMR** (400 MHz, MeOH-d<sub>4</sub>)  $\delta$ : 8.13 (s, 1H; CONH), 7.96 (s, 1H, CONH), 6.7 (s, 1H, NHBoc), 4.38 (q, *J*=1H, COCH(R)NH), 4.09 (q, *J*=8Hz, 1H, NHBoc), 3.95 (q, *J*= 8Hz, 1H, NHBoc), 3.19 (q, 1H; CH<sub>2</sub>CH<sub>2</sub>(R)NH), 3.03 (q, *J*=4Hz 2H; COCH(R)NH), 1.93-1.84 (m, 2H, CH<sub>2</sub>CH<sub>2</sub>CH), 1.89-1.67 (m, 2H, CH<sub>2</sub>CH<sub>2</sub>CH), 1.63-1.54 (m, 2H, CH<sub>2</sub>CH<sub>2</sub>CH<sub>2</sub>) 1.44 (s, 6H; CCH<sub>3</sub>).

**<sup>13</sup>C-NMR** (400 MHz, MeOH-d<sub>4</sub>)  $\delta$ : 175.36, 175.26, 174.26 (2xNH-CH-CO-NH CONH 2), 158.55 (COOC(CH<sub>3</sub>)<sub>3</sub> 4), 80.64 (OC(CH<sub>3</sub>)<sub>3</sub> 2), 79.83 (OC(CH<sub>3</sub>)<sub>3</sub> 2), 56.22 (COCH(R)NH), 55.84 (COCH(R)NH), 53.33 (COCH(R)NH), 41.05 (CH<sub>2</sub>NH 2), 33.04 (CH<sub>2</sub>NH), 32.23, 30.60, 29.67(All CH<sub>2</sub>), 28.82 (CH<sub>3</sub> 6), 28.77 (CH<sub>3</sub> 6), 24.23, 24.10 (All CH<sub>2</sub>);

**IR**:  $\tilde{\nu}$  = 3312 (w), 2933 (w), 1657 (m), 1514.13 (m), 1365 (m), 1247 (m), 1163 (s), 1046 (w) 1018 (w) 854 (w) 780 (w) 645 (w)

**HRMS**: [M + H]<sup>+</sup> (C<sub>38</sub>H<sub>71</sub>N<sub>6</sub>O<sub>12</sub>) Calcd. *m/z* = 803.5151; Measured *m/z* = 803.5154 Mean Error -3.6 ppm

See Appendice for data spectra.

### 6.2.8. Hydrolysis of G2 ((Boc)Phe)<sub>2</sub>-Lys-OMe.

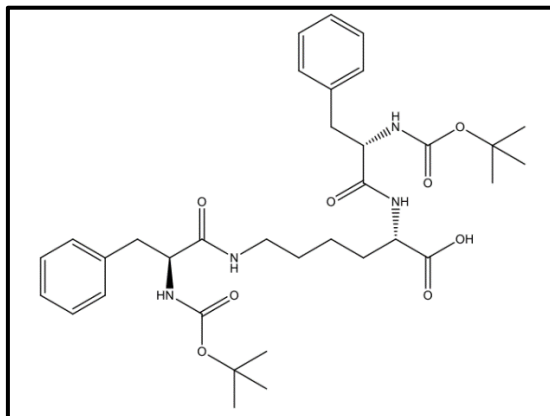


**Figure 6-8** Molecular structure G2 ((Boc)Phe)<sub>2</sub>-Lys-OH  
Molecular Formula: C<sub>34</sub>H<sub>48</sub>N<sub>4</sub>O<sub>8</sub>  
Molecular Weight: 640.77 g·mol<sup>-1</sup>

((Boc)Phe)<sub>2</sub>-Lys-OMe (0.6 g, 1.19 mmol) was dissolved in methanol (38 mL).<sup>17</sup> The air of the flask was then evacuated by vacuum and filled with pure nitrogen. Once an inert atmosphere was reached the NaOH<sub>(aq)</sub> solution (2.7 mL, 2.7 mmol) was added. Then the reaction mixture was left overnight under stirring. The reaction crude was evaporated by rotary evaporation, this is a critical step because rising the temperature above 40 °C would decompose the obtained compound. After solvent removal, some water (52.5 mL, 2.92 mol) was added and the resulting viscous yellowish compound was stirred until complete solution. Sonication was required in this last step. A precipitate was obtained when acidifying with NaHSO<sub>4</sub> solution to pH=3. The precipitate was extracted with EtOAc (24 mL) and dried under high vacuum.

**Yield:** 86.5%, 0.51 g, Colourless solid.

Colourless solid, **m.p.** 100-102 °C; [ $\alpha$ ]<sub>D20</sub> = +15.4 (c=1.0, MeOH)

**<sup>1</sup>H-NMR** (400 MHz, MeOH-d<sub>4</sub>)  $\delta$ : 8.18 (s, 1H; CONH), 7.93 (s, 1H, CONH), 7.40 (s, 1H, CONH), 7.26 – 7.21 (m, Ar-H, 10H), 4.43-4.34 (m, Ar-CH<sub>2</sub>-CH-NH, 2H), 4.26 (d, NHCHCOOH,  $\Delta J$  = 8 Hz, 1H), 3.14-3.10 (m, Ph-CH<sub>2</sub>-CHNH, 4H), 3.04-3.00 (m, COHN-CH<sub>2</sub>-CH<sub>2</sub>, 2H), 2.86 – 2.78 (m, CO-HN-CH<sub>2</sub>-CH<sub>2</sub>, 2H), 1.83 – 1.69 (m, MeCOO-CH-CH<sub>2</sub>-CH<sub>2</sub>-CH<sub>2</sub>-CH<sub>2</sub>-NH, 6H), 1.37 (s, Boc-CH<sub>3</sub>, 18H).

**<sup>13</sup>C-NMR** (400 MHz, MeOH-d<sub>4</sub>)  $\delta$ : 175.07, 174.53, 174.26 (2x NH-CH-CO-NH and HCOOH), 157.54, 155.51 (2x HNCOOC(CH<sub>3</sub>)<sub>3</sub>), 138.66, 138.54 (2x Ar-C<sub>q</sub>-CH<sub>2</sub>), 130.41, 129.35, 127.73, 127.66, (all Ar-C), 80.58 (2x C<sub>q</sub>(Boc)), 57.62, 57.16 (both Ar-CH<sub>2</sub>-CH-NH), 53.43 NHCHCOOH), 40.01 (Ar-CH<sub>2</sub>-CH-NH), 39.86 (Ph-CH<sub>2</sub>-CHNH), 32.30

(HCOO-CH-CH<sub>2</sub>-CH<sub>2</sub>-CH<sub>2</sub>-NH), 28.68 (6x Boc-CH<sub>3</sub>), 23.84 (HCOO-CH-CH<sub>2</sub>-CH<sub>2</sub>-CH<sub>2</sub>-NH).

**IR:**  $\tilde{\nu}$  = 3287 (m), 2930 (m), 1661 (s), 1630 (s), 1583 (s) 1392 (m), 1366 (m), 1246 (m), 1165 (s), 1021 (w), 698 (m),

**HRMS:** [M + Na]<sup>+</sup> (C<sub>34</sub>H<sub>48</sub>N<sub>4</sub>O<sub>8</sub>Na) Calcd. m/z = 663.33833; Measured m/z = 663.336435 Mean Err 3 ppm

See Appendice for data spectra.

### 6.2.9. Hydrolysis of G2 (Boc-Ala)<sub>2</sub>-Lys-OMe.

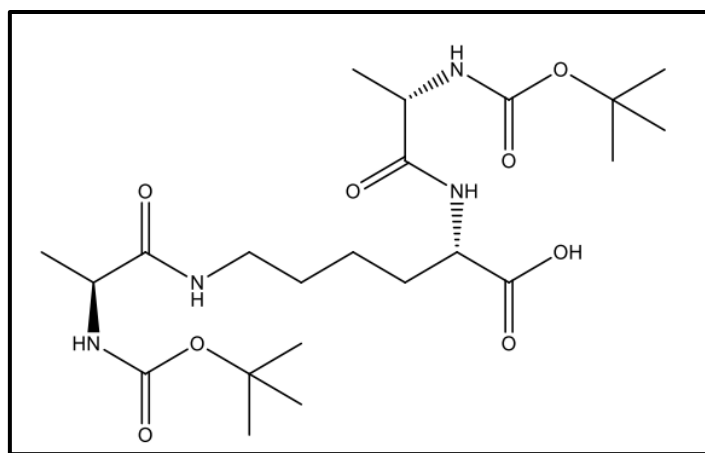


**Figure 6-9** Molecular structure G2 (Boc-Ala)<sub>2</sub>-Lys-OH

Molecular Formula: C<sub>22</sub>H<sub>40</sub>N<sub>4</sub>O<sub>8</sub>

Molecular Weight: 488.57 g·mol<sup>-1</sup>

The G2 (Boc-Ala)<sub>2</sub>-Lys-OMe dendron (0.6 g, 1.19 mmol) was dissolved in methanol (48.92 mL, 1.2 mol).<sup>17</sup> The air of the flask was then evacuated by vacuum and filled with pure nitrogen. Once an inert atmosphere was reached the NaOH<sub>(aq)</sub> solution (3.52 mL, 3.52 mmol) was added. Then the reaction mixture was left overnight under stirring. The reaction crude was evaporated by rotary evaporation, this is a critical step because rising the temperature above 40 °C would decompose the obtained compound. After solvent removal, some water (68.5 mL, 3.8 mol) was added and the resulting viscous yellowish compound was stirred until complete solution. Sonication was required in this last step. A precipitate was obtained when acidifying with NaHSO<sub>4</sub> solution to pH=3. The precipitate was extracted with EtOAc (24 mL) and dried under high vacuum.

**Yield:** 94%, 0.55 g, Colourless solid.

White solid  $[\alpha]_{D20}$  = -17.1 (c=1.0, MeOH)

**<sup>1</sup>H-NMR** (400 MHz, MeOH-*d*<sub>4</sub>)  $\delta$ : 8.18 (s, 1H; CONH), 7.92 (s, 1H, CONH), 6.78 (s, 1H, CONH), 4.37 (q, HN-CH-COOH, *J* = 4.5 Hz, 1H), 4.12 – 4.03 (m, 2x -CH-NHBoc, 2H), 3.19 (t, CO-HN-CH<sub>2</sub>-CH<sub>2</sub>, 2H), 1.88-1.54 (m, MeCOO-CH-CH<sub>2</sub>-CH<sub>2</sub>-CH<sub>2</sub>-CH<sub>2</sub>-NH, 6H), 1.44 (s, Boc-CH<sub>3</sub>, 18H), 1.31- 1.29 (2x d, both Ala-CH<sub>3</sub>, , *J* = 7.2 Hz, 6H).

**<sup>13</sup>C-NMR** (400 MHz, MeOH-*d*<sub>4</sub>)  $\delta$ : 175.93, 175.88 (both NH-CH-CO-NH), 175.14 CHCOOH), 157.57 (2x HNCOOC(CH<sub>3</sub>)<sub>3</sub>), 80.53 (2x C(Boc)), 53.32 (NHCHCOOH), 51.70, 51.4 (both CH<sub>3</sub>-CH-NH), 39.91 (CO-NH-CH<sub>2</sub>-), 32.26, 29.71 (COOH-CH-CH<sub>2</sub>-CH<sub>2</sub>-CH<sub>2</sub>-CH<sub>2</sub>-NH), 28.73 (6x Boc-CH<sub>3</sub>), 23.76 (COOH-CH-CH<sub>2</sub>-CH<sub>2</sub>-CH<sub>2</sub>-CH<sub>2</sub>-NH), 18.66, 18.36 (both Ala-CH<sub>3</sub>).

**IR:**  $\tilde{\nu}$  = 3301 (w), 2978 (w), 1654 (m), 1519 (m), 1450 (m), 1365 (m), 1247 (m), 1161 (s), 1068 (w), 1020 (w), 854 (w), 585 (w),

**HRMS:** [M + Na]<sup>+</sup> (C<sub>22</sub>H<sub>40</sub>N<sub>4</sub>O<sub>8</sub>Na) Calcd. *m/z* = 511.2722; Measured *m/z* = 511.2738 Mean Err -3.4 ppm; [M + H]<sup>+</sup> (C<sub>22</sub>H<sub>41</sub>N<sub>4</sub>O<sub>8</sub>) Calcd. *m/z* = 489.2906; Measured *m/z* = 489.2919 Mean Err -3.3 ppm

See Appendice for data spectra.

#### 6.2.10. Hydrolysis of G2 (Boc-Val)<sub>2</sub>-Lys-OMe.

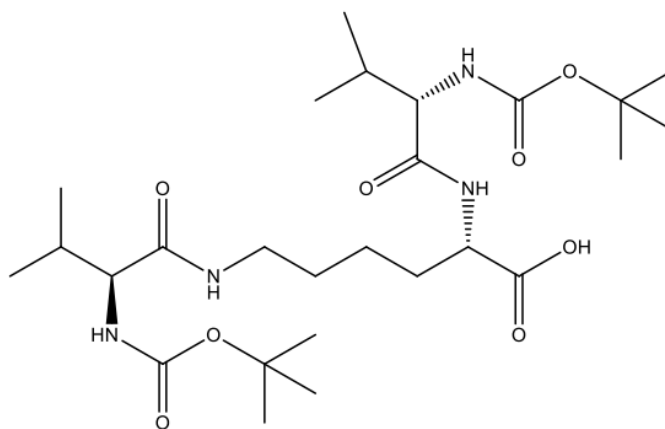


**Figure 6-10** Molecular structure G2 (Boc-Val)<sub>2</sub>-Lys-OH

Molecular Formula: C<sub>26</sub>H<sub>48</sub>N<sub>4</sub>O<sub>8</sub>

Molecular Weight: 544.68 g·mol<sup>-1</sup>

The G2 (BocVal)<sub>2</sub>-Lys-OMe dendron (0.6 g, 1.075 mmol) was dissolved in methanol (44.06 mL, 1.08 mol).<sup>17</sup> The air of the flask was then evacuated by vacuum and filled with pure nitrogen. Once an inert atmosphere was reached the NaOH<sub>(aq)</sub> solution (3.17 mL, 3.17 mmol) was added. Then the reaction mixture was left overnight under stirring. The reaction crude was evaporated by rotary evaporation, this is a critical step because rising the temperature above 40 °C would decompose the obtained compound. After

solvent removal, some water (61 mL, 3.4 mol) was added and the resulting viscous yellowish compound was stirred until complete solution. Sonication was required in this last step. A precipitate was obtained when acidifying with NaHSO<sub>4</sub> solution to pH=3. The precipitate was extracted with EtOAc (24 mL) and dried under high vacuum.

**Yield:** 83.7%, 0.49 g, Colourless solid.

Colourless solid, **m.p.** 90-94 °C; [ $\alpha$ ]<sub>D20</sub> = -19.4 (c=1.0, MeOH)

**<sup>1</sup>H-NMR** (400 MHz, MeOH-d<sub>4</sub>)  $\delta$ : 8.17 (s, 1H; CONH), 8.01 (s, 1H, CONH), 6.59 (s, 1H, COOH), 4.37 (q, HN-CH-COOH, J = 4.5 Hz, 1H), 3.93, 3.79 (2x d, both -CH-NHBoc, J = 8 Hz, 2H), 3.19 (t, CO-HN-CH<sub>2</sub>-CH<sub>2</sub>, J = 5.8 Hz, 2H), 2.03 (m, 2x (CH<sub>3</sub>)<sub>2</sub>-CH-CH-NHBoc, 2H), 1.87-1.54 (m, COOH-CH-CH<sub>2</sub>-CH<sub>2</sub>-CH<sub>2</sub>-CH<sub>2</sub>-NH, 6H), 1.45 (s, Boc-CH<sub>3</sub>, 9H), 0.99, 0.94 (2x d, 4x Val-CH<sub>3</sub>, J = 3.4 Hz, 12H).

**<sup>13</sup>C-NMR** (400 MHz, MeOH-d<sub>4</sub>)  $\delta$ : 175.05, 174.57 (both NH-CH-CO-NH), 174.55 (CHCOOH), 157.95-157.92 (2x HNCOOC(CH<sub>3</sub>)<sub>3</sub>), 80.5 (2x C(Boc)), 61.81, 61.31 (both (CH<sub>3</sub>)<sub>2</sub>-CH-CH-NHBoc), 53.37 (NHCHCOOMe), 40.81 (CO-NH-CH<sub>2</sub>-), 32.15, 31.94 (2x (CH<sub>3</sub>)<sub>2</sub>-CH-CH-NHBoc) 29.68 (COOH-CH-CH<sub>2</sub>-CH<sub>2</sub>-CH<sub>2</sub>-CH<sub>2</sub>-NH), 28.74 (6x Boc-CH<sub>3</sub>), 23.92 (COOH-CH-CH<sub>2</sub>-CH<sub>2</sub>-CH<sub>2</sub>-CH<sub>2</sub>-NH), 19.78, 18.62, 18.55, (4x Val-CH<sub>3</sub>).

**IR:**  $\tilde{\nu}$  = 3296 (w), 2964 (w), 1647.95 (m), 1528 (m), 1365 (m), 1245 (m), 1161 (s), 1017 (w), 871 (w), 781 (w), 648 (w).

**HRMS:** [M + Na]<sup>+</sup> (C<sub>26</sub>H<sub>48</sub>N<sub>4</sub>O<sub>8</sub>Na) Calcd.  $m/z$  = 545.3534; Measured  $m/z$  = 567.3364 Mean Err 3.4 ppm; [M + H]<sup>+</sup> (C<sub>26</sub>H<sub>49</sub>N<sub>4</sub>O<sub>8</sub>) Calcd.  $m/z$  = 545.35; Measured  $m/z$  = 545.3545 Mean Err -2.2 ppm

See Appendice for characterization spectra.

### **6.3. Assay, analysis, materials and methods.**

#### **6.3.1. Procedure for determining $T_{gel}$ values - Chapter 2.**

$T_{gel}$  values were determined using a high precision thermoregulated bath able to program temperature ramps at various speeds. Gels were prepared in 2 mL vials (diameter = 7mm) and introduced into the thermoregulated bath held by a vial rack. Vials and gels inside were checked every 20 seconds to make sure that  $T_{gel}$  point was visually registered – at this point the gel was no longer able to sustain its shape. The programmed temperature ramp was 5°C/min.

#### **6.3.2. Electron Microscopy (TEM) – Chapter 3.**

The Department of Biology at the University of York have a service technology facility for imaging in TEM, run by the technician Meg Stark. Preparation of samples was dependent on the nature of the material Toluene based gels and DES gels were thus analysed in different ways. The protocol for each is described as follows.

##### **6.3.2.1. Toluene based gels sample preparation for TEM**

A small piece of gel was taken with a spatula and was lightly rubbed against a copper grid standard for TEM purposes. The samples were then left to evaporate for at least 30 min to ensure complete removal of solvent before introducing the sample into the high vacuum chamber of the TEM. No stain was used with any sample because the incompatibility between aqueous and organic solvents – for this reason contrast was reduced.

##### **6.3.2.2. DES based gels sample preparation for TEM**

A piece of ionogel was taken and the DES substituted by suspension of the material in water. The procedure was to add distilled water in an 8 mL vial with a piece of ionogel in it. After 3 days of diffusion of the ionic liquid inside, and

replacing the water every day to improve DES extraction from the gel, final samples were prepared. TEM copper grids were lightly rubbed with each gel sample, and the samples were left to dry for at least 1 hour.

### **6.3.3. SEM sample preparation – Chapter 3.**

SEM samples were also analysed with Meg Stark of the Technology Facility, Department of Biology, University of York. One of the most important steps to obtain effective SEM images of these materials is to dry the samples gently enough to avoid changes in the 3D nanostructure. Two methods were employed to evaporate the toluene based gels:

#### **6.3.3.1. Freeze-drying method**

Gels were prepared at a concentration of 10 mM, placed on an aluminium stub and introduced into a flask closed to air and cooled down with liquid nitrogen placed in a Dewar bottle. The flask was inserted on to a high vacuum line for several hours until removal of the solvent was complete. The sample was then allowed to warm to ambient conditions and the vacuum removed. The samples on the stubs were then prepared for SEM analysis. This treatment enable us to obtain more porous xerogels for more effective imaging of the expanded nanostructures. Thermal equilibration on heating back to ambient conditions under vacuum was performed to avoid potential condensation of moisture into samples, and thus, destruction of the obtained nanostructure.

#### **6.3.3.2. Ambient drying method**

The ambient drying method involved simple drying of the gel open to the surrounding air at room temperature. This technique produces gels which have less porosity than those produced by the freeze-drying method. The process consists of taking a small piece of toluene based gel and placing it on an aluminium stub. Samples were left to dry in the bench covered by a beaker to

avoid dust particles or excessive flow of air. After that samples were placed in the SEM cavity and sputtered by a thin layer of palladium to avoid overcharges when focussing the beam of electrons inside the SEM chamber.

#### **6.3.4. AFM technique - Chapter 3**

The device used was the Dimension Icon AFM from Bruker which had several modes and probes, including Contact mode, Tapping mode and Peak Force. A process of calibration and alignment of the laser was required. The device was used as part of a 3-month training programed visit to the Solvay facilities in Brussels to perform nanomechanics measurements of polymers and AFM imaging.

##### **6.3.4.1. Preparation of samples.**

The preparation of samples was achieved by self-drying at ambient temperature and pressure following the same procedure as that used in the SEM ambient drying method. Samples were covered by a glass flask to prevent moisture and dust in the sample. The result was very effective in terms of yielding high definition images, even though the drying method was very simple.

#### **6.3.5. Kinetics of gelation by circular dichroism spectroscopy - Chapter 2.**

Various kinetic measurements were performed in the CD spectrometer (Jasco J810 circular dichromator fitted with a Peltier cooler and heating bath and a temperature control unit). The cell used was a 1.0 mm quartz cell. There were two main different gel formation processes to study:(i) hot sol-gel transitions and (ii) ambient temperature mixing of the two components to achieve liquid-gel transition. The solvent used was a mixture of methylcyclohexane/dioxane (95/5) and the concentration of gel was 5mM

### **6.3.5.1. Hot sol-gel transition gel formation.**

In this method, both components were mixed in the CD cell and the gel was brought to the sol state by heating with a heat gun. When everything was mixed and dissolved, the cell was immediately introduced in the CD spectrometer and a wavelength was selected according to the maximum absorption of CD signal for each molecule. The collection of CD signal vs time starts before the CD cell cools down, so the signal does not gain intensity until the sol-gel transition is reached by the sudden and spontaneous drop of temperature of the gel inside the cell.

### **6.3.5.2. Cold (25°C) sol-gel transition formation.**

This method was used to measure the gel formation kinetics when gels are formed at room temperature on simple mixing. The gel components are mixed when the cell is placed in the CD chamber so collection of data starts before mixing. On mixing the components, the gelation process starts, as reflected in the increase in CD signal, which comes from the nanoscale gel chirality. The result is a collection of data that is represented in the form of CD signal versus experimental time.

### **6.3.6. Kinetics of gelation by VT <sup>1</sup>H-NMR spectroscopy – Chapter 2.**

When using VT NMR to track the concentrations of dendrons and amines concentration, Gels were prepared by mixing two different solutions (amines and Dendrons) of 10 mM, each which had diphenylmethane (5 mM) as an internal standard for later integration, using d8 toluene as the deuterated solvent. The NMR tube was filled with the two solutions introduced as liquids and gels formed spontaneously inside the tube. To promote a homogeneous gel, the NMR tube was heated using a heat gun and the gel redissolved, and subsequently cooled down. After leaving all the gels overnight for cooling and aging, each gel was tested using VT-NMR where temperatures were raised from 25 to 90°C in intervals of 5°C of increase. A subsequent cooling period (sudden decrease of temperature

as rapid as the NMR could cool it down) was used to track how long the gel components take to self-assemble from a sol state at the highest temperature. This method allows us to quantify how much of each component is mobile at each temperature during a cooling cycle, and hence gain insight into both thermodynamics and kinetics.

#### **6.3.6.1. Procedure Kinetic data VT-<sup>1</sup>H-NMR - Chapter 2**

The Kinetic data is obtained by integrating the various signals that come from the spectra collected. The series of spectra are programmed to reach 90°C where gels are fully dissolved in sol state, this makes the composition of the amines and dendrons completely visible and quantifiable. As an example, in the Figure 6-1 the set of spectra of <sup>1</sup>H-NMR is shown where the peaks are integrated and converted in the concentration profiles versus time of analysis. Thus, concentration of the visible substance that is detected in in the <sup>1</sup>H-NMR is the substance that remains soluble while the process of gelation is ongoing. This way it can be calculated the speed of gelation if the process is sufficiently slow.

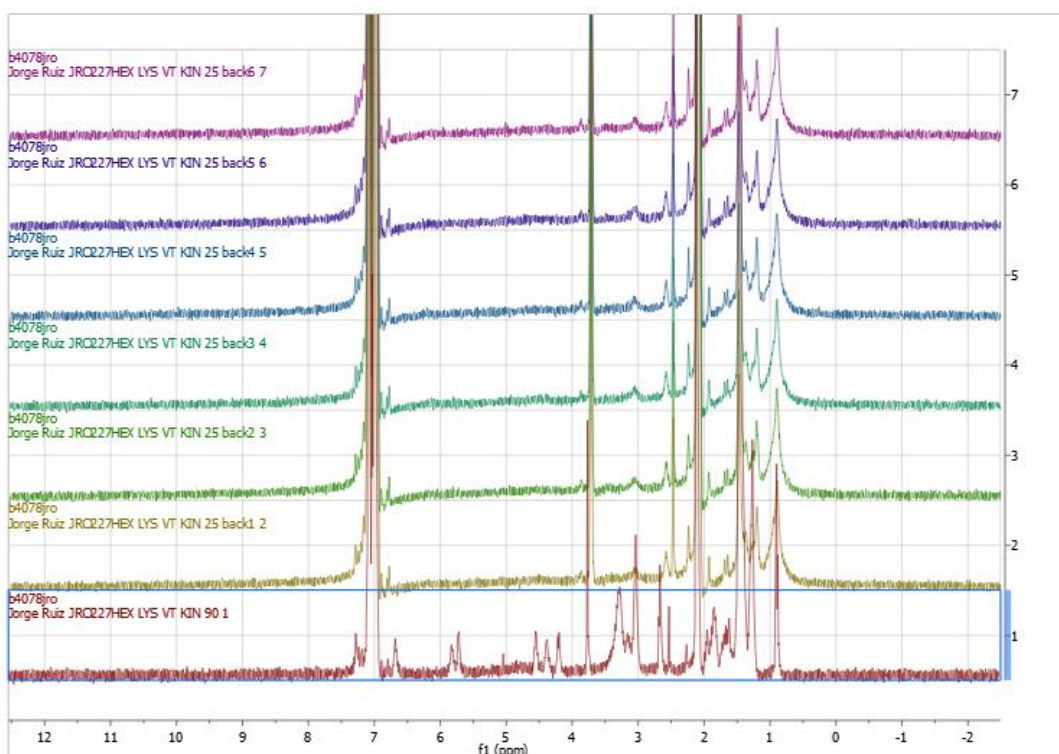


**Figure 6-11** Concentration profile of the process of cooling a NMR tube from 90 to 25 with HEX LYS gel.

After this experiment, peaks corresponding to LYS dendron and to the amines (HEX, NAPH or PHEN) can be integrated. So, we obtain a table of concentrations versus time for each temperature. Table 6-1

HEX LYS Dendron		
Time min	temperature	concentration
0	90	4.2
14	25	0.5
26	25	0.65
38	25	0.45
49	25	0.75
61	25	0.75
72	25	0.7

**Table 6-1** Correspondence with time in min temperature in °C and dendron concentration in mM

This can be plotted in a graph (Figure 6-2) to follow the concentration of available gelators (dendrons or amines) that remain as free moving and solvated substances right before they self-assemble.

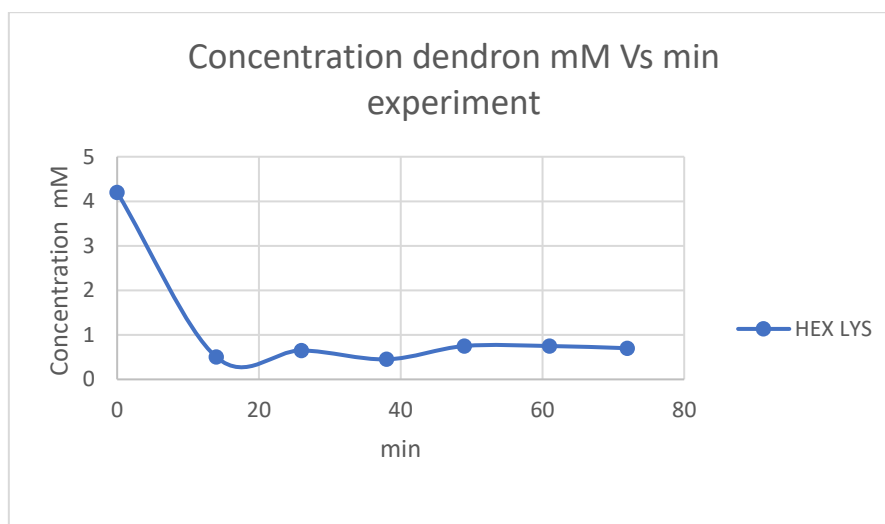


**Figure 6-12** Concentration profile of the process of gelation from hot conditions to the room temperature of the  $^1\text{H-NMR}$  process.

In this particular case, the method was not valid due to the really fast kinetics of gel formation when bringing the gel from the high temperature ( $90^\circ\text{C}$ ) to the room temperature ( $25^\circ\text{C}$ ) in which the gel should be formed. that is to say, the gelation trigger is the lowering of the temperature. Before we can detect that lowering of compounds that are forming the gel when temperature lower the gel is already formed. This long time required before the first analysis makes practically impossible the tracking of the kinetics of gel formation. If we could have a system with lower gelation speeds the concentration variation could be tracked and fitted to a model (linear or exponential) and the kinetic equations could be obtained.

#### **6.3.8. Ionic conductivity method. Chapter 4**

The ionic conductivity meter was a Jenway 4310 with a platinum probe. Calibration of the device was performed before taking any measurements, using a standard calibration

solution of NaCl 12.88 mS/cm (Hanna HI-7030L). Such conductivity was automatically detected by the device as the reference. 5 mL of DES was then introduced in an 8 mL vial. The conductivity probe had a temperature gauge inside of the glass tube. The probe was introduced in the vial full of ionic liquid until the two platinum plates were completely covered by liquid as represented in the Figure 6-3.



**Figure 6-13** Thermoregulated ionic conductivity set up and conductivity probe with the ionic liquid or gel inside.

When measuring the DES gels, the hot sol gel solution of ionic solvent and gelator was introduced in the vial and sonicated for ca. 1 minute to promote faster gelation. Comparison between the sonicated and non-sonicated ionogels led to similar ionic conductivity results. In order to produce variable temperature ionic conductivity measurements a thermoregulated bath was incorporated to the conductivity system.

### **6.3.9. Sonication ionic conductivity measurements**

Sonication measurements were made preparing the same vials with ionic liquids attached to the ionic conductivity probe in such a way that a complete seal was achieved to prevent water or moisture coming inside the ionic liquid. This is particularly important when introducing such a vial-probe in a water sonication bath. The whole conductivity meter system was then moved next to the sonication bath (Elmasonic P 37 kHz, 120 W effective

power, 5 litres). The conductivity measurements were made by activating the ultrasounds at 25°C and then compared with the original ionic conductivity of the DES liquid of gel without ultrasound stimulation.

#### **6.3.10. Rheology and viscosity measurements**

Rheology measurements were carried out in the Malvern Instruments Kinexus Pro Plus rheometer. The geometry selected was a parallel plate of 20mm of diameter and a gap in between geometries of 1 mm. When starting the experiment, the gels were squeezed until 1mm of distance was reached. The remains of the gel were removed before the experiment started. Most of the rheology experiment took 10Hz as the initial value to test the gels. In the following lines it is going to be described the various necessary steps to perform a typical rheological analysis for measuring their viscoelastic properties.

##### **6.3.10.1. Gel Disc preparation**

In a small glass jar of 15 mL the materials were introduced in terms of components (ionic liquids and DBS gelator or amines+dendrons+toluene). 2mL of the solution was heated with the top closed to prevent moisture contamination (ionic gels) or toluene evaporation. The jar was closed with the lid and the liquid sol was setting all the night on the internal part of the lid. Gels were cooled and kept overnight for them to get formed. The jar was opened and the gel was collected carefully from the lid surface trying not to crack it. After that, gels are placed carefully (avoiding any cracks) onto the Rheometer test platform and squeezed until sufficient pressure was exerted on the gel without damaging it. Figure 6-4 shows how the gel disc was removed from the ample vial and placed onto the testing platform of the Rheometer.



**Figure 6-14** Process of placing a formed gel inside a Jar and the careful extraction of it to the rheometer testing platform.

### **6.3.10.2. Viscosity test in rheology.**

The DES (liquid) was prepared in a jar. The ChCl/proton donator molar ratio was 0.5 for all tested compounds. The problem of moisture absorbance due to the inherent hygroscopic properties of this compound was neglected in this test due to the impossibility of avoiding such an absorption process. The DES was placed in the testing platform of the rheometer and the test plate lowered until complete contact was achieved. The software was programmed to collect viscosity versus temperature. A ramp of temperatures from 25°C to 80°C over 11 min which was considered appropriate due to the very close contact between the liquid and the rheometer platform.

### **6.3.11. Kinetics of gel formation in rheology – Chapter 2**

The main experiment in terms of kinetics of gelation was measuring the formation of a gel using their rheological properties. In this case there are two methods that have been applied which uses two different approaches to trigger gelation. In both cases the procedure uses an aluminium weight boat which is placed in between the supporting plate and the parallel plate (Figure 6-5) which feels the sol-gel transition when this is being produced.



**Figure 6-15** example of the set up where gels are introduced in liquid state and there is a transition to gel produce either the addition of a second component or the lowering of the temperature.

### 6.3.11.1. Cold (25°C) sol-gel transition formation. Chapter 2.

In this procedure the sol-gel transition is triggered by the addition of the second component. The concentration of the solutions of dendron and amine is 10 mM and when they are mixed a 5mM gel is produced in the rheometer platform. The procedure is placing the aluminium disposable boat in the platform, adding one of the components in solution and lowering the parallel plate geometry until the gap is 1 mm and it is in full contact with the liquid. The experiment is set up for a normal viscoelastic determination of a gel which basic parameters are 10 Hz and a strain % of 0.06 and a stable temperature of 25°C which were corresponding in all cases the linear region where toluene based gels were stable. After the rheometer started to collect data ( $G'$  and  $G''$ ) the second component was added, in most of cases an instant response of gel formation was notice and the data collection progressed during 30 min. Rheograms were collected and processed with a fitting that included a linear and exponential fitting in the same equation. The model and the real curve were fitted using the least Squares solution option in excel. Such transition triggered by the addition of the other component can be observed in Figure 6-6 as an example of the rheological process.

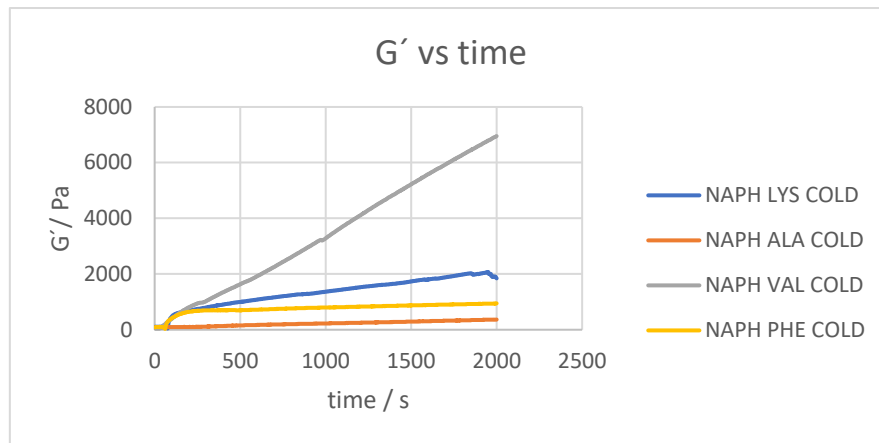


**Figure 6-16** the rheological response of the elastic modulus when adding the second component to the aluminium weight boat while the rheometer performs the analysis.

### 6.3.12. The Diffusion cell testing – Chapter 3

The process of putting two different gels into contact with a gel-gel interface requires the design, construction and use of a cell that could withstand the diffusion process conditions.

#### 6.3.12.1. Placing gels in the cell.

An Volume of gel (1 mL) was prepared in 8 mL vials. Gels have a final concentration of 5 mM, which means that the solutions of the two components each have a concentration of 10 mM. To these solutions a reference material (diphenylmethane) was also incorporated at a final concentration of 5mM. Those gels in vials were heated until they completely dissolved. The cell was ready to be filled with the gels and an aluminium barrier sealed with silicone was inserted to avoid the mixing of each gel when placing the materials inside the cell. Then, the gels were solidified with the help of lowering the temperature with an ice bath in contact with the external cell walls in about 3 min. Once the gels were in the solid state (3 min aprox), the barrier aluminium separator was removed, to bring the gels into contact for the first time, creating a gel-gel interface. The cell was placed

in a chamber containing a toluene reservoir (Figure 6-8) to maintain the solvation of the gels while diffusion took place. The diffusion experiment started (when the barrier was removed) and time was monitored.



**Figure 6-17** Diffusion Cell (left) with the two sides easily observed and an incubator with the diffusion chamber filled with several diffusion cells performing the experiment at controlled temperature.

#### 6.3.12.2. Sampling of the various regions of the cell.

Once the gels had been diffusing for a specific time the various regions of the cell were collected. Six different regions that were collected and sliced with the spatula parallelly to the gel-gel interface as indicated in Figure 6-9. The experiment was performed with several diffusion cell to run several experiments in parallel and, thus, having several diffusion times.



**Figure 6-18** Diffusion cell divided in each region (left) and the collection of the material corresponding to those regions in 8 mL vials.

Every region from the gel was placed in an 8 mL vial and dried under high vacuum to remove the solvent and then redissolved in 1mL of deuterated toluene for the later  $^1\text{H-NMR}$  analysis. In the end, six different NMR tubes were obtained representing the 6 different regions of the cell for a given diffusion time. The various NMR spectra were integrated in terms of proton signals to determine the corresponding concentrations of the different components in each region. This allowed analysis of concentrations and hence diffusion profiles.

### **6.3.12.3. Diffusion procedure for dendron analysis with CD**

As amines have been analysed in the diffusion tests, dendrons have been investigated to know more about the dynamics of their potential transfers in between the different gels through the interface. To do so, two similar gels were prepared HEX GELS where the only difference was the use of opposite stereochemical dendrons (LLL and DDD) and the concentration of those gels were 5mM. After the corresponding diffusion time, cells were collected and sampled as before with the only difference that the vials were weighted in order to prepare later the corresponding exact solutions of regions with certain concentration (0.625mM) in all analysed regions so the resulting signal intensity was result of the mixing of opposite stereoisomers rather than produced by a variation of concentration. Figure 6-10 is an example of CD spectra that is obtained for this kind of dendrons tracking the movement of the dendrons through the two different gels.

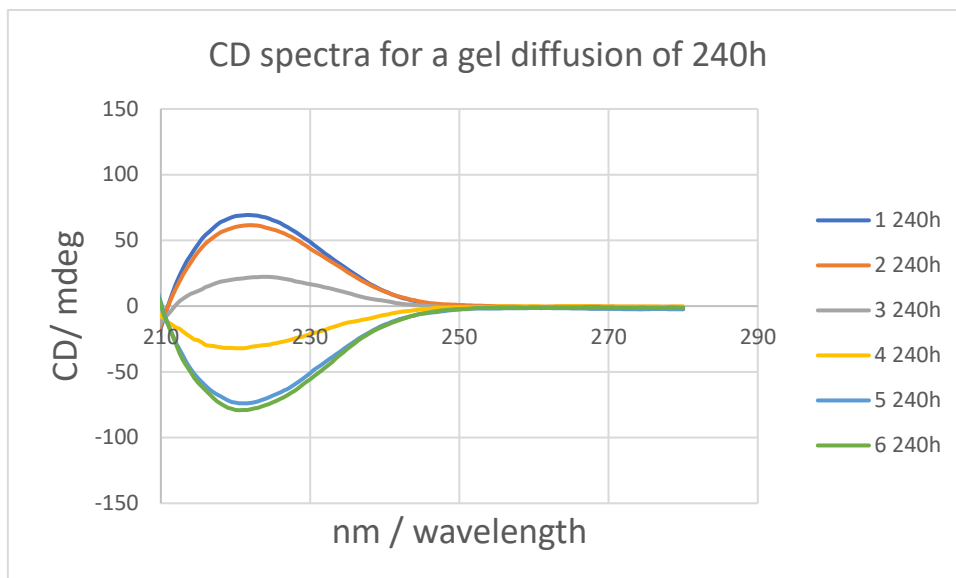


**Figure 6-19** Dendron diffusion profile of two gels in a transfer cell for a given time of 240h

#### 6.3.12.4. Diffusion coefficients D calculation.

Diffusion coefficients are obtained once a concentration profile is obtained. The concentration profile with the information of the gradient of concentration ( $\frac{\partial c}{\partial x}$ ) at certain time which allows us to determine the diffusion coefficient  $D$  ( $\text{cm}^2\text{s}^{-1}$ ) which corresponds to the diffusion pattern of certain gel (concentration) in certain conditions of temperature. Knowing the Fick's laws and if we assume that we have a cell in which the solute is present in half of the container, the concentration which is taken initially is 1mM. The concentration profile at any time can be expressed as:

$$C(x, t) = \frac{1}{2} \operatorname{erf} \left( \frac{x}{2\sqrt{DT}} \right) + \frac{1}{2} \quad \text{Equation 6-1}$$

Where  $C(x,t)$  is the concentration which depends on the position of the cell and the diffusion time,  $D$  the diffusion coefficient and  $T$  the diffusion time. Time ( $T$ ) and Position ( $x$ ) are variables that we know and  $D$  is the unknown parameter that we need to determine for the diffusion profiles that are obtained for several temperatures and substances (diphenylmethane, amines and dendrons).

This model can be fitted in the concentration profiles that we obtain from the diffusion experiments and thus, by fitting with a least square method we can obtain the value of  $D$  that best fits to any diffusion profile we could obtain. Figure 6-11 shows an example of how well the model fits with the obtained data at a given diffusion time.

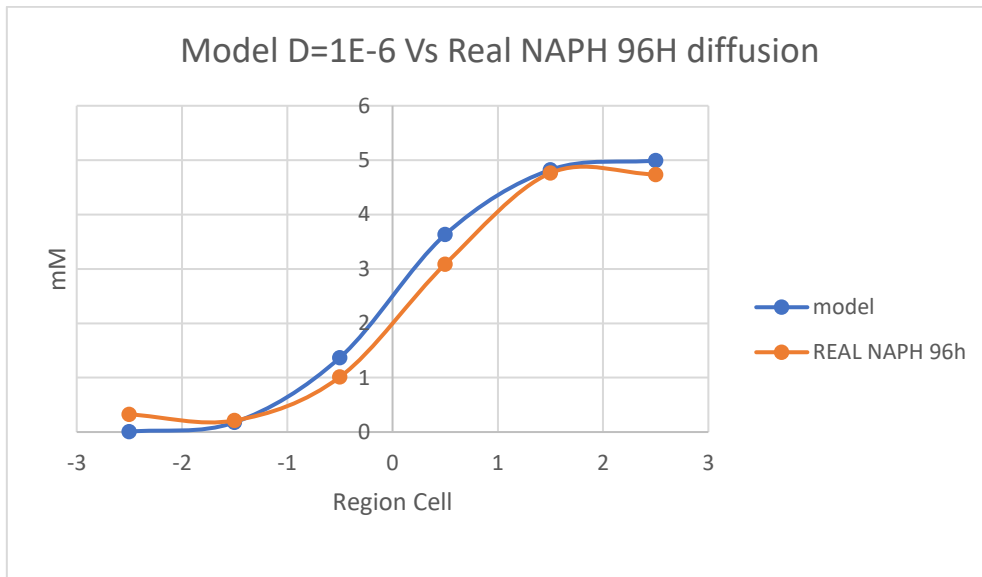


**Figure 6-20** Fitting of the Fickian model with a real diffusion profile of 96h at 25°C. The obtained value of Diffusion Coefficient is  $1 \cdot 10^{-6}$

The method used to adapt and fit the model to the experimental data is explained in the series of steps bellow:

1. Experimental data is presented as a table in excel.

Tiempo 24H	
mM Naph	Position (X)
4,85	1,46
4,83	0,88
3,56	0,29
0,39	-0,29
0,06	-0,88
0,00	-1,46

**Table 6-2** Experimental data of diffusion Naph for 24h at 25°C

2. The data is represented graphically:

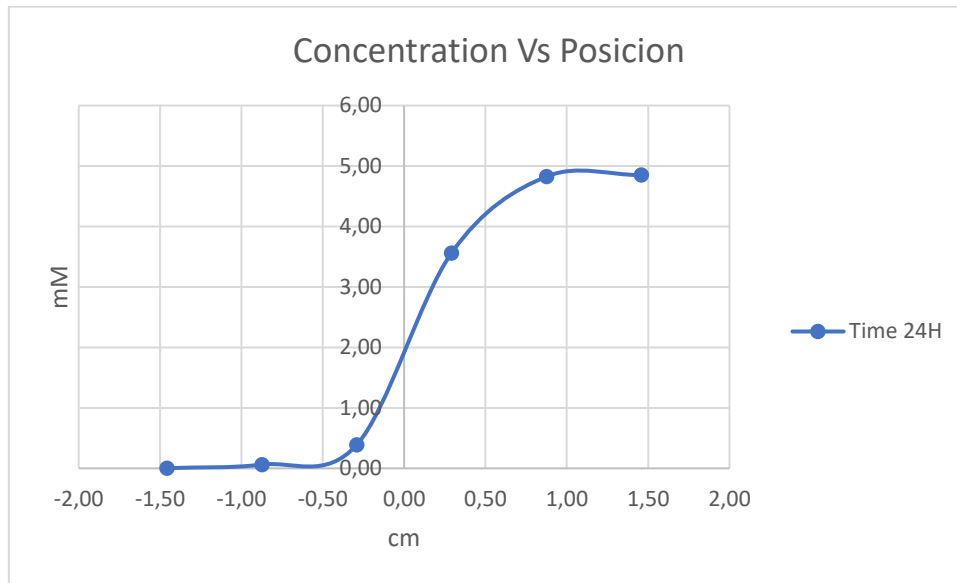


**Figure 6-21** Data of diffusion for Naph at 24h and 25°C

3. Then we create the fitting using the Fickian model bellow:

$$C(x, t) = \frac{1}{2} \operatorname{erf} \left( \frac{x}{2\sqrt{Dt}} \right) + \frac{1}{2} \quad \text{Equation 6-2}$$

So a table is created with the concentrations calculated from the data proposed of position, time and diffusion coefficient. Time should be in seconds and position in centimeters. For a given value of  $10^{-5} \text{ cm}^2\text{s}^{-1}$  we obtain this table of values.

Model 24h Naph 25°C			
[Naph] mM	position (cm)	time (s)	D24H ( $\text{cm}^2\text{s}^{-1}$ )
1,00E+00	1,46	86400	1,00E-07
1,00E+00	0,88		
9,87E-01	0,29		
1,33E-02	-0,29		
1,40E-11	-0,88		
0,00E+00	-1,46		

**Table 6-3** Calculated parameters of the model proposed for 24h diffusion time and  $10^{-7}$  of Diffusion constant.

Notice that the model proposed is giving maximum concentrations of 1mM. Because of this the resulting concentration is multiplied by 5 so it can be better adjusted to the experimental result where original concentration starts at 5mM. In the following table such transformations are represented:

[Naph]	[Naph] x 5	Position [cm]
1,00E+00	5,00	1,46
1,00E+00	5,00	0,88
9,87E-01	4,93	0,29
1,33E-02	0,07	-0,29
1,40E-11	0,00	-0,88
0,00E+00	0,00	-1,46

**Table 6-4** Concentration in mM multiplied by 5 and the position in cm

If concentration and position is represented, the following graph is obtained:

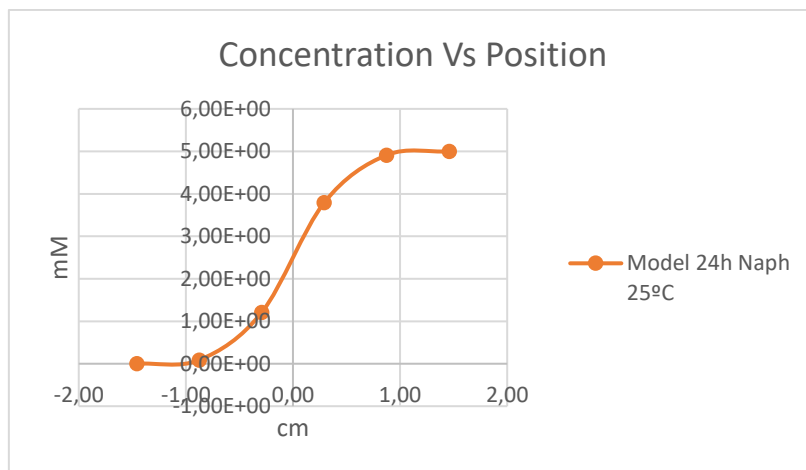


**Figure 6-22** Model representation of Naph concentration Vs Position for a given value of 86400 seconds (24h) and diffusion parameter of  $10^{-7} \text{ cm}^2\text{s}^{-1}$ .

4. If both graphs (experimental and real data) are represented, the following graph is obtained:

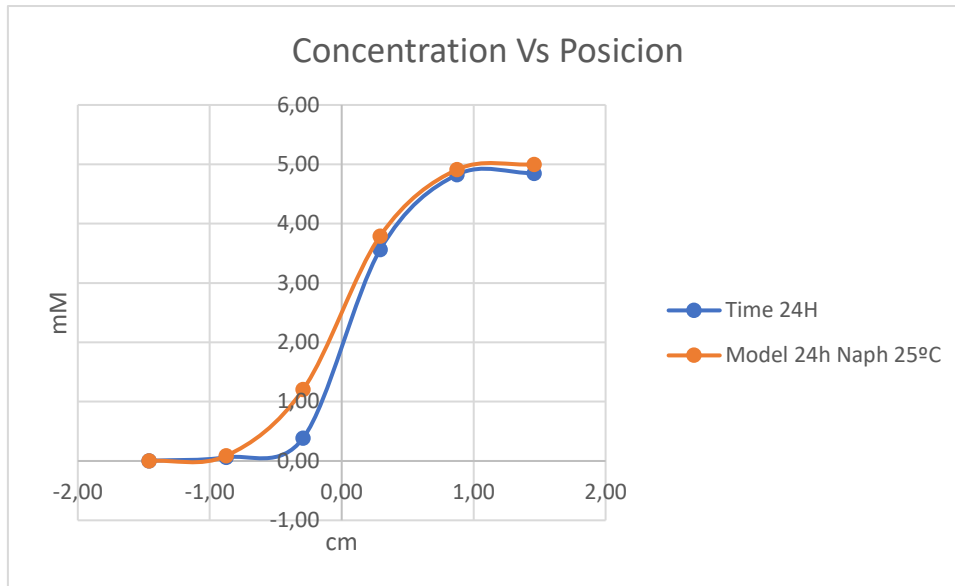


**Figure 6-23** Representation of both (Real and model) graphs for diffusion of Naph 24h and 25°C

- At this point the model should be as similar as possible to the real behaviour and the best value of the diffusion parameters are searched by the least squares method. To do so the difference between concentrations of both model and real behaviour are calculated. After that, such differences are summed and elevated to the square by using the formula SUMSQ[...] and selecting the differences that we calculated between concentrations of both model and real behaviour. In the table below is shown such a process.

[Naph] model	[Naph] real	$\Delta$ [Naph]	Square Summ
5,00E+00	4,85E+00	1,49E-01	0,755369928
4,91E+00	4,83E+00	8,68E-02	
3,79E+00	3,56E+00	2,30E-01	
1,21E+00	3,88E-01	8,20E-01	
8,82E-02	6,25E-02	2,57E-02	
1,13E-03	3,00E-03	-1,87E-03	

**Table 6-5** Differences between real and modelled [Naph]. Notice calculation of Square sum

Then a value of Diffusion is proposed such as  $10^{-7}$  and by using the solver function of Excel the best fitting is obtained.

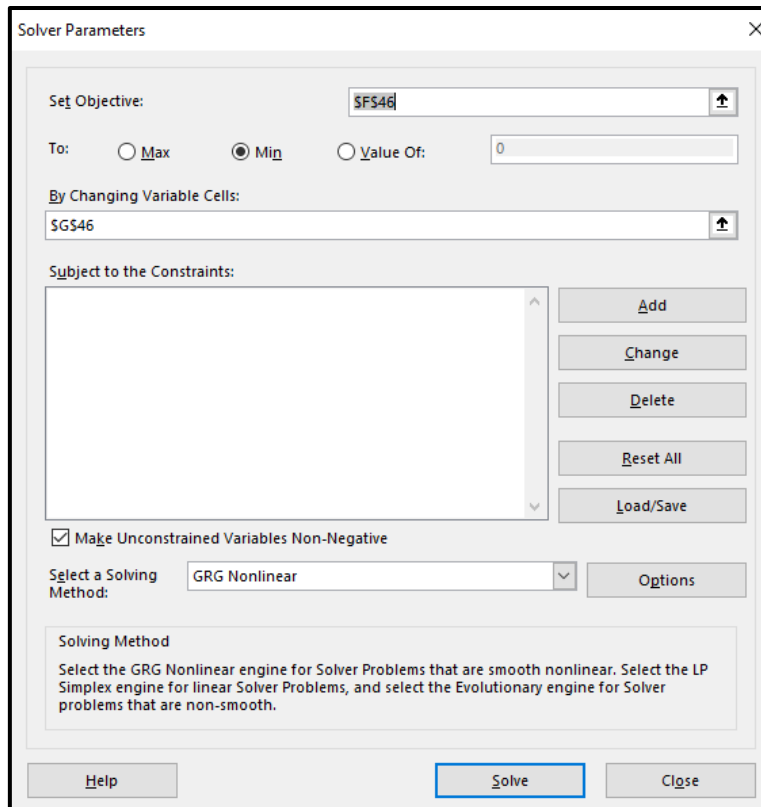


**Figure 6-24** Example of such calculation by using solver analysis tool where cell set objective is the SUMMSQ function and the variable cell is the corresponding to the diffusion rate cell.

6. Solve function of excel is used to get the best fitting between the curves (real and modelled), that is to say, the best value of D to get the best fitting of the curves.

When the best value is obtained the two curves looks like the following graph.

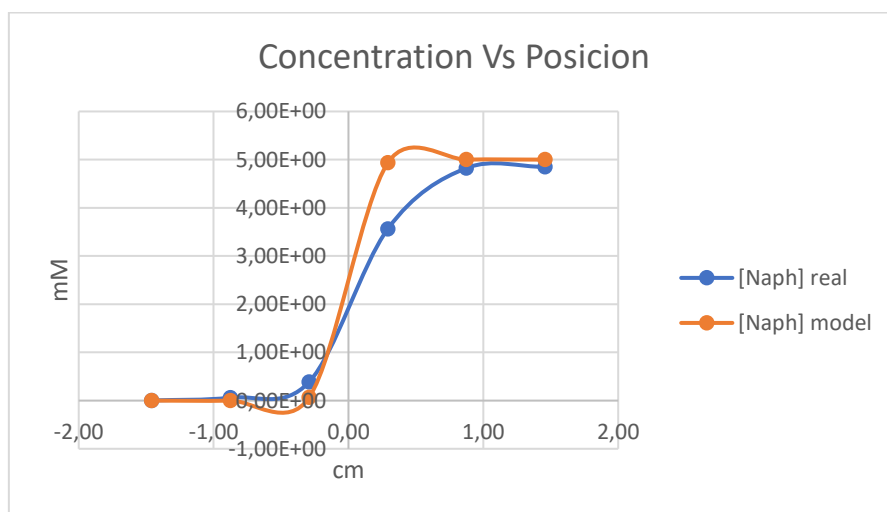


**Figure 6-25** Representation of modelled and real behaviour where the best fitting proposed is  $D = 10^{-6}$

In the appendice can be found the various calculationsn that have been done in order to find the best fitting for the various diffusion conditions (Temperature and natureof the substance) that were studied.

## References

- 1 H. R. Allcock, *Introduction to materials chemistry*, Wiley, 2008.
- 2 D. Stout, *Philos. Trans. R. Soc. Lond. B. Biol. Sci.*, 2011, **366**, 1050.
- 3 M. F. Ashby, *Materials and the Environment : Eco-informed Material Choice.*, Elsevier Science, 2012.
- 4 D. B. Amabilino, D. K. Smith and J. W. Steed, *Chem. Soc. Rev.*, 2017, **46**, 2404–2420.
- 5 J. N. Aneli, A. Jiménez and S. Kubica, *CHEMISTRY and PHYSICS of MODERN MATERIALS Processing, Production and Applications*, Apple Acad., 2014.
- 6 N. M. Sangeetha and U. Maitra, *Chem. Soc. Rev.*, 2005, **34**, 821–836.
- 7 A. R. Patel, *Curr. Opin. Food Sci.*, 2017, **15**, 1–7.
- 8 B. A. Westrin Anders Axelsson Guido Zacchi, *J. Control. Release*, 1994, **30**, 189–199.
- 9 P. Terech and R. G. Weiss, *Chem. Rev.*, 1997, **97**, 3133–3160.
- 10 M. Suzuki and K. Hanabusa, *Chem. Soc. Rev.*, 2010, **39**, 455–463.
- 11 E. R. Draper and D. J. Adams, *Chem*, 2017, **3**, 390–410.
- 12 J. Boekhoven, J. M. Poolman, C. Maity, F. Li, L. van der Mee, C. B. Minckenberg, E. Mendes, J. H. van Esch and R. Eelkema, *Nat. Chem.*, 2013, **5**, 433–437.
- 13 L. E. Buerkle and S. J. Rowan, *Chem. Soc. Rev.*, 2012, **41**, 6089–6102.
- 14 F. Huang and E. V. Anslyn, *Chem. Rev.*, 2015, **115**, 6999–7000.
- 15 J. W. Steed and J. L. Atwood, *Supramolecular chemistry*, Wiley, 2009.
- 16 D. P. Stevenson, *J. Am. Chem. Soc.*, 1955, **77**, 2350–2350.
- 17 G. M. Dykes, L. J. Brierley, D. K. Smith, P. T. McGrail and G. J. Seeley, *Chemistry*, 2001, **7**, 4730–4739.
- 18 J. L. Atwood and J. W. Steed, *Encyclopedia of supramolecular chemistry*, M. Dekker, 2004.
- 19 C. K. McLaughlin, G. D. Hamblin and H. F. Sleiman, *Chem. Soc. Rev.*, 2011, **40**, 5647.
- 20 A. Houlton and S. M. D. Watson, *Annu. Reports Sect. 'A' (Inorganic Chem.)*, 2011, **107**, 21–42.
- 21 Y. Bai, Q. Luo and J. Liu, *Chem. Soc. Rev.*, 2016, **45**, 2756–2767.
- 22 T. Schrader, G. Bitan and F.-G. Klärner, *Chem. Commun.*, 2016, **52**, 11318–11334.
- 23 Koji Oohora and Takashi Hayashi, *Curr. Opin. Chem. Biol.*, 2014, **19**, 154–161.
- 24 I. N. Berezovsky, E. Guarnera and Z. Zheng, *Prog. Biophys. Mol. Biol.*, 2017, **128**, 85–99.

- 25 G. M. Whitesides and M. Boncheva, *Proc. Natl. Acad. Sci. U. S. A.*, 2002, **99**, 4769–4774.
- 26 G. Yu, X. Yan, C. Han and F. Huang, *Chem. Soc. Rev.*, 2013, **42**, 6697–6722.
- 27 M. Zhang, K. Zhu, F. Huang, M. Zhang, K. Zhu and F. Huang, in *Supramolecular Chemistry*, John Wiley & Sons, Ltd, Chichester, UK, 2012.
- 28 P. Iqbal, J. A. Preece, P. M. Mendes, P. Iqbal, J. A. Preece and P. M. Mendes, in *Supramolecular Chemistry*, John Wiley & Sons, Ltd, Chichester, UK, 2012.
- 29 B. L. Feringa and W. R. Browne, Eds., *Molecular Switches*, Wiley-VCH Verlag GmbH & Co. KGaA, Weinheim, Germany, 2011.
- 30 T. Review, A. Coskun, M. Banaszak, R. D. Astumian, J. F. Stoddart and B. A. Grzybowski, *Chem. Soc. Rev.*, 2012, **41**, 306–312.
- 31 D. Bléger and S. Hecht, *Angew. Chem. Int. Ed.*, 2015, **54**, 11338–11349.
- 32 J. D. Watson and F. H. C. Crick, *Cold Spring Harb. Symp. Quant. Biol.*, 1953, **18**, 123–131.
- 33 F. Hof, S. L. Craig, C. Nuckolls and J. Rebek Jr., *Angew. Chemie Int. Ed.*, 2002, **41**, 1488–1508.
- 34 C. J. Pedersen, *J. Am. Chem. Soc.*, 1967, **89**, 2495–2496.
- 35 V. Balzani, *Pure Appl. Chem.*, 2008, **80**, 1631–1650.
- 36 Y.-C. Chen, T. Cao, C. Chen, Z. Pedramrazi, D. Haberer, D. G. de Oteyza, F. R. Fischer, S. G. Louie and M. F. Crommie, *Nat. Nanotechnol.*, 2015, **10**, 156–160.
- 37 S. H. Ko, M. Su, C. Zhang, A. E. Ribbe, W. Jiang and C. Mao, *Nat. Chem.*, 2010, **2**, 1050–1055.
- 38 K. Almdal, J. Dyre, S. Hvidt and O. Kramer, *Polym. Gels Networks*, 1993, **1**, 5–17.
- 39 N. M. Sangeetha and U. Maitra, *Chem. Soc. Rev.*, 2005, **34**, 821.
- 40 Wataru Kubo, Kei Murakoshi, T. Kitamura, Shigeo Yoshida, M. Haruki, Kenji Hanabusa, H. Shirai, A. Yuji Wada and S. Yanagida, *J. Phys. Chem.*, 2001, **105** (51), 12809–12815.
- 41 L. S. Jeon, S. Y. Kim, S. J. Kim, Y. G. Lee, M. S. Kang and Y. S. Kang, *J. Photochem. Photobiol. A Chem.*, 2010, **212**, 88–93.
- 42 Y. J. Kim, J. H. Kim, M.-S. Kang, M. J. Lee, J. Won, J. C. Lee and Y. S. Kang, *Adv. Mater.*, 2004, **16**, 1753–1757.
- 43 C.-C. Cheng and D.-J. Lee, *RSC Adv.*, 2016, **6**, 38223–38227.
- 44 P. D. Frischmann, L. C. H. Gerber, S. E. Doris, E. Y. Tsai, F. Y. Fan, X. Qu, A. Jain, K. A. Persson, Y.-M. Chiang and B. A. Helms, *Chem. Mater.*, 2015, **27**, 6765–6770.
- 45 W. H. Meyer, *Adv. Mater.*, 1998, **10**, 439–448.
- 46 M. M. P. M. Jansen, J. M. Verzijl, D. M. Burger and Y. A. Hekster, *Int. J. Pharm.*,

- 2013, **452**, 266–269.
- 47 K. J. Skilling, F. Citossi, T. D. Bradshaw, M. Ashford, B. Kellam and M. Marlow, *Soft Matter*, 2014, **10**, 237–256.
- 48 V. Mironov, T. Boland, T. Trusk, G. Forgacs and R. R. Markwald, *Trends Biotechnol.*, 2003, **21**, 157–61.
- 49 C. B. Highley, C. B. Rodell and J. A. Burdick, *Adv. Mater.*, 2015, **27**, 5075–5079.
- 50 Q. Wu, J. Wei, B. Xu, X. Liu, H. Wang, W. Wang, Q. Wang and W. Liu, *Sci. Rep.*, 2017, **7**, 41566.
- 51 S. V Murphy and A. Atala, *Nat. Biotechnol.*, 2014, **32**, 773–785.
- 52 A. Munaz, R. K. Vadivelu, J. St. John, M. Barton, H. Kamble and N.-T. Nguyen, *J. Sci. Adv. Mater. Devices*, 2016, **1**, 1–17.
- 53 T. J. Hinton, Q. Jallerat, R. N. Palchesko, J. H. Park, M. S. Grodzicki, H.-J. Shue, M. H. Ramadan, A. R. Hudson and A. W. Feinberg, *Sci. Adv.*, 2015, **1**, e1500758–e1500758.
- 54 M. M. Stanton, J. Samitier and S. Sánchez, *Lab Chip*, 2015, **15**, 3111–3115.
- 55 W. Shi, R. He and Y. Liu, *Eur. J. Biomed. Res.*, , DOI:10.18088/ejbmr.1.3.2015.pp3-8.
- 56 N. Mehrban, G. Z. Teoh and M. A. Birchall, *Int. J. Bioprinting*, 2016, **2**, 6–19.
- 57 J. W. Steed, *Chem. Commun.*, 2011, **47**, 1379–1383.
- 58 D. J. Cornwell, O. J. Daubney and D. K. Smith, , DOI:10.1021/jacs.5b09691.
- 59 D. Knani and D. Alperstein, *J. Phys. Chem. A*, 2017, **121**, 1113–1120.
- 60 P. S. Santos, M. G. Abiad, M. A. Carignano and O. H. Campanella, *Rheol. Acta*, 2012, **51**, 3–11.
- 61 W.-C. Lai, L.-J. Liu and P.-H. Huang, *Langmuir*, 2017, **33**, 6390–6397.
- 62 B. O. Okesola, V. M. P. Vieira, D. J. Cornwell, N. K. Whitelaw and D. K. Smith, *Soft Matter*, 2015, 4768–4787.
- 63 B. O. Okesola and D. K. Smith, *Chem. Commun.*, 2013, **49**, 11164.
- 64 W. Edwards and D. K. Smith, *J. Am. Chem. Soc.*, 2013, **135**, 5911–5920.
- 65 W. Edwards and D. K. Smith, *J. Am. Chem. Soc.*, 2014, **136**, 1116–1124.
- 66 J. G. Hardy, A. R. Hirst and D. K. Smith, *Soft Matter*, 2012, **8**, 3399–3406.
- 67 A. R. Hirst, J. F. Miravet, B. Escuder, L. Noirez, V. Castelletto, I. W. Hamley and D. K. Smith, *Chem. - A Eur. J.*, 2009, **15**, 372–379.
- 68 G. M. Dykes and D. K. Smith, *Tetrahedron*, 2003, **59**, 3999–4009.
- 69 S. S. Rohner, J. Ruiz-Olles and D. K. Smith, *RSC Adv.*, 2015, **5**, 27190–27196.
- 70 D. K. Smith, *Chem. Commun.*, 2006, 34–44.
- 71 M. Suzuki and K. Hanabusa, *Chem. Soc. Rev.*, 2009, **38**, 967–975.

- 72 R. G. Weiss, *J. Am. Chem. Soc.*, 2014, **136**, 7519–7530.
- 73 G. Fichman and E. Gazit, *Acta Biomater.*, 2014, **10**, 1671–1682.
- 74 N. Javid, S. Roy, M. Zelzer, Z. Yang, J. Sefcik and R. V. Ulijn, *Biomacromolecules*, 2013, **14**, 4368–4376.
- 75 A. P. McCloskey, E. R. Draper, B. F. Gilmore and G. Laverty, *J. Pept. Sci.*, 2017, **23**, 131–140.
- 76 A. Dasgupta, J. H. Mondal and D. Das, *RSC Adv.*, 2013, **3**, 9117.
- 77 R. Orbach, L. Adler-Abramovich, S. Zigerson, I. Mironi-Harpaz, D. Seliktar and E. Gazit, *Biomacromolecules*, 2009, **10**, 2646–2651.
- 78 A. R. Hirst, I. A. Coates, T. R. Boucheteau, J. F. Miravet, B. Escuder, V. Castelletto, I. W. Hamley and D. K. Smith, *J. Am. Chem. Soc.*, 2008, **130**, 9113–9121.
- 79 J. Raeburn and D. J. Adams, *Chem. Commun.*, 2015, **5170**, 5170–5180.
- 80 Y. Lan, M. G. Corradini, R. G. Weiss, S. R. Raghavan and M. A. Rogers, *Chem. Soc. Rev.*, 2015, **44**, 6035–6058.
- 81 and P.-D. H. Che-Min Chou and P.-D. Hong\*, *Macromolecules*, 2004, 5596–5606.
- 82 P. Dastidar, *Chem. Soc. Rev.*, 2008, **37**, 2699–2715.
- 83 A. Mallick, E.-M. Schön, T. Panda, K. Sreenivas, D. D. Díaz and R. Banerjee, *J. Mater. Chem.*, 2012, **22**, 14951–14963.
- 84 P. Terech, *Langmuir*, 2009, **25**, 8370–8372.
- 85 P. Jonkheijm, P. van der Schoot, A. P. H. J. Schenning and E. W. Meijer, *Science*, 2006, **313**, 80–83.
- 86 A. P. Constantinou and T. K. Georgiou, *Eur. Polym. J.*, 2016, **78**, 366–375.
- 87 B. Gyarmati, B. Á. Szilágyi and A. Szilágyi, *Eur. Polym. J.*, 2017, **93**, 642–669.
- 88 Rafael Tadmor, and Rafail L. Khalfin and Yachin Cohen\*, *Langmuir*, 2002, **18** (19), 7146–7150.
- 89 Jun-Ying Xiong, Janaky Narayanan, Xiang-Yang Liu, § Tan Kok Chong, and Shing Bor Chen and T.-S. Chung, *J. Phys. Chem*, 2005, **109** (12), 5638–5643.
- 90 E. A. Röessler, S. Stapf and N. Fatkullin, *Curr. Opin. Colloid Interface Sci.*, 2013, **18**, 172–182.
- 91 M. Suzuki, Y. Nakajima, M. Yumoto, M. Kimura, H. Shirai and K. Hanabusa, *Org. Biomol. Chem.*, 2004, **2**, 1155–1159.
- 92 K. K. Diehn, H. Oh, R. Hashemipour, R. G. Weiss and S. R. Raghavan, *Soft Matter*, 2014, **10**, 2632.
- 93 X. Yu, L. Chen, M. Zhang and T. Yi, *Chem. Soc. Rev.*, 2014, **43**, 5346–5371.
- 94 X. Huang, P. Terech, § and Srinivasa R. Raghavan and R. G. Weiss, *J. Am. Chem.*

- Soc*, 2005, **127** (12), 4336–4344.
- 95 X. Huang, S. R. Raghavan, A. Pierre Terech and R. G. Weiss, *J. Am. Chem. Soc.*, 2006, **128** (47), 15341–15352.
- 96 C. Ren, G. H. B. Ng, H. Wu, K.-H. Chan, J. Shen, C. Teh, J. Y. Ying and H. Zeng, *Chem. Mater.*, 2016, **28**, 4001–4008.
- 97 C. Ren, F. Chen, F. Zhou, J. Shen, H. Su and H. Zeng, *Langmuir*, 2016, **32**, 13510–13516.
- 98 K. Saalwächter, M. Gottlieb, R. Liu and W. Oppermann, *Macromolecules*, 2007, **40**, 1555–1561.
- 99 L. B. Romero-Zeron, F. M. Hum and A. Kantzas, *SPE Reserv. Eval. Eng.*, 2008, **11**, 439–453.
- 100 M. Avrami and Melvin, *J. Chem. Phys.*, 1939, **7**, 1103–1112.
- 101 M. Avrami, *J. Chem. Phys.*, 1940, **8**, 212–224.
- 102 M. Avrami, *J. Chem. Phys.*, 1941, **9**, 177–184.
- 103 C. Veerman, K. Rajagopal, C. S. Palla, D. J. Pochan, J. P. Schneider and E. M. Furst, *Macromolecules*, 2006, **39**, 6608–6614.
- 104 D. J. Cornwell, B. O. Okesola and D. K. Smith, *Soft Matter*, 2013, **9**, 8730–8736.
- 105 S. Cantekin, Y. Nakano, J. C. Everts, P. van der Schoot, E. W. Meijer and A. R. A. Palmans, *Chem. Commun.*, 2012, **48**, 3803–3805.
- 106 A. Dawn and H. Kumari, *Chem. - A Eur. J.*, 2018, **24**, 762–776.
- 107 N. A. K. Mezmarich and B. J. Love, *Macromolecules*, 2011, **44**, 3548–3555.
- 108 D. T. N. Chen, Q. Wen, P. A. Janmey, J. C. Crocker and A. G. Yodh, *Annu. Rev. Condens. Matter Phys.*, 2010, **1**, 301–322.
- 109 T. B. Goudoulas and N. Germann, *Food Hydrocoll.*, 2017, **66**, 49–60.
- 110 I. Fernández Farrés and I. T. Norton, *Food Hydrocoll.*, 2014, **40**, 76–84.
- 111 A. Gabriele, F. Spyropoulos and I. T. Norton, *Food Hydrocoll.*, 2009, **23**, 2054–2061.
- 112 A. Baral, S. Basak, K. Basu, A. Dehsorkhi, I. W. Hamley and A. Banerjee, *Soft Matter*, 2015, **11**, 4944–4951.
- 113 A. E. Steam, E. M. Irish and H. Eyring, *J. Phys. Chem.*, 1940, **44**, 981–995.
- 114 R. S. Brodkey and H. C. Hershey, *Transport phenomena : a unified approach*, Brodkey Pub, 1988.
- 115 J. P. Şek, *Am. Inst. Chem. Eng.*, 1996, **42**, 3333–3339.
- 116 W. J. McManamey, J. T. Davies, J. M. Woollen and J. R. Coe, *Chem. Eng. Sci.*, 1973, **28**, 1061–1069.
- 117 M. Liang, R. Harder and I. K. Robinson, *Int. Union Crystallogr. J.*, 2014, **1**, 172–178.

- 118 Yao Xin, Henrietta Mitchell, and Heather Cameron and S. A. Allison\*, *J. Phys. Chem.*, 2005, **110** (2), 1038–1045.
- 119 K. Starchev, A. Jean Sturm, G. Weill and C.-H. Brogren, *J. Phys. Chem.*, 1997, **101** (29), 5659–5663.
- 120 J. H. Masliyah and S. Bhattacharjee, *Electrokinetic and colloid transport phenomena*, Wiley-Interscience, 2006.
- 121 A. Dawn, K. S. Andrew, D. S. Yufit, Y. Hong, J. P. Reddy, C. D. Jones, J. A. Aguilar and J. W. Steed, *Cryst. Growth Des.*, 2015, **15**, 4591–4599.
- 122 M. R. Saboktakin and R. M. Tabatabaei, *Int. J. Biol. Macromol.*, 2015, **75**, 426–436.
- 123 M. Tokita, *Gels*, 2016, **2**, 17.
- 124 D. P. Birnie, D. M. Kaz and D. J. Taylor, *J. Sol-Gel Sci. Technol.*, 2009, **49**, 233–237.
- 125 M. Zare, A. Roustaei, K. Alba and I. A. Frigaard, *J. Nonnewton. Fluid Mech.*, 2016, **238**, 212–223.
- 126 D. D. Díaz, E. Morin, E. M. Schön, G. Budin, A. Wagner and J.-S. Remy, *J. Mater. Chem.*, 2011, **21**, 641–644.
- 127 J.-C. L. Anda Vintiloiu, *J. Control. Release*, 2008, **125**, 179–192.
- 128 J. Labille, A. Nicolas Fatin-Rouge and J. Buffle, *Langmuir*, 2007, **23** (4), 2083–2090.
- 129 M. L. Veyries, G. Couarraze, S. Geiger, F. Agnely, L. Massias, B. Kunzli, F. Faurisson and B. Rouveix, *Int. J. Pharm.*, 1999, **192**, 183–193.
- 130 P. Gao, X. Nie, M. Zou, Y. Shi and G. Cheng, *J. Antibiot. (Tokyo)*, 2011, **64**, 625–634.
- 131 I. D. John and H. N. More, *Res. J. Pharm. Tech*, 2008, **1**, 502–506.
- 132 S. Bajaj, A. Whiteman and B. Brandner, *Contin. Educ. Anaesthesia, Crit. Care Pain*, 2011, **11**, 39–43.
- 133 C. D. Jones and J. W. Steed, *Chem. Soc. Rev.*, 2016, **45**, 6546–6596.
- 134 W. Ha, J. Yu, X. Song, J. Chen and Y. Shi, *ACS Appl. Mater. Interfaces*, 2014, **6**, 10623–10630.
- 135 O. Ordeig, S. Y. Chin, S. Kim, P. V. Chitnis and S. K. Sia, *Sci. Rep.*, 2016, **6**, 22803.
- 136 T. J. Dubinsky, C. Cuevas, M. K. Dighe, O. Kolokythas and J. H. Hwang, *Am. J. Roentgenol.*, 2008, **190**, 191–199.
- 137 E. S. Dolinina and E. V. Parfenyuk, *Curr. Drug Deliv.*, , DOI:10.2174/1567201813666161021103714.
- 138 D. J. Cornwell, B. O. Okesola and D. K. Smith, *Angew. Chemie - Int. Ed.*, 2014, **53**, 12461–12465.

- 139 E. J. Howe, B. O. Okesola and D. K. Smith, *Chem. Commun.*, 2015, **51**, 7451–7454.
- 140 P. R. A. Chivers and D. K. Smith, *Chem. Sci.*, 2017, **8**, 7218–7227.
- 141 H. Wipf, *Phys. Scr.*, 2001, **T94**, 43.
- 142 C. Chipot and J. Comer, *Sci. Rep.*, 2016, **6**, 35913.
- 143 R. Kimmich, *Principles of Soft-Matter Dynamics*, Springer Netherlands, Dordrecht, 2012.
- 144 M. Yemloul, E. Steiner, A. Robert, S. Bouguet-Bonnet, F. Allix, B. Jamart-Grégoire, D. Canet and M. méthodologie RMN, *J. Phys. Chem. B*, 2011, **115**, 2511–2517.
- 145 J. Tritt-Goc, A. Rachocki and M. Bielejewski, *Soft Matter*, 2014, **10(39)**, 7810–7818.
- 146 J. Kowalczyk, A. Rachocki, M. Bielejewski and J. Tritt-Goc, *J. Colloid Interface Sci.*, 2016, **472**, 60–68.
- 147 A. Pluen, P. A. Netti, R. K. Jain and D. A. Berk, *Biophys. J.*, **77**, 542–552.
- 148 Y. Saito, H. Kataoka and A. M. Stephan, *Macromolecules*, 2001, **34 (20)**, 6955–6958.
- 149 Y. Aihara, S. Arai and K. Hayamizu, *Electrochim. Acta*, 2000, **45**, 1321–1326.
- 150 M. S. Islam and C. A. J. Fisher, *Chem. Soc. Rev.*, 2014, **43**, 185–204.
- 151 K. Samprovalaki, P. T. Robbins and P. J. Fryer, *J. Food Eng.*, 2012, **111**, 537–545.
- 152 J. Crank, *The Mathematics of Diffusion*, 2nd Editio., 1975.
- 153 C. García-Aparicio, I. Quijada-Garrido and L. Garrido, *J. Colloid Interface Sci.*, 2012, **368**, 14–20.
- 154 A. M. Stephan, *Eur. Polym. J.*, 2006, **42**, 21–42.
- 155 J. G. Kim, B. Son, S. Mukherjee, N. Schuppert, A. Bates, O. Kwon, M. J. Choi, H. Y. Chung and S. Park, *J. Power Sources*, 2015, **282**, 299–322.
- 156 J. C. Bachman, S. Muy, A. Grimaud, H.-H. Chang, N. Pour, S. F. Lux, O. Paschos, F. Maglia, S. Lupart, P. Lamp, L. Giordano and Y. Shao-Horn, *Chem. Rev.*, 2016, **116**, 140–162.
- 157 J. B. Goodenough and P. Singh, *J. Electrochem. Soc.*, 2015, **162**, A2387–A2392.
- 158 A. Manthiram, X. Yu and S. Wang, *Nat. Rev. Mater.*, 2017, **2**, 16103.
- 159 J. S. Wilkes, *Green Chem.*, 2002, **4**, 73–80.
- 160 A. S. Dworkin, H. R. Bronstein and M. A. Bredig, *Discuss. Faraday Soc.*, 1961, **32**, 188–196.
- 161 M. Anouti, in *Electrochemistry in Ionic Liquids*, Springer International Publishing, Cham, 2015, pp. 217–252.
- 162 R. Hayes, G. G. Warr and R. Atkin, *Chem. Rev.*, 2015, **115 (13)**, 6357–6426.

- 163 F. Bresme, M. González-Melchor and J. Alejandre, *J. Phys. Condens. Matter*, 2005, **17**, S3301–S3307.
- 164 A. Rupp, N. Roznyatovskaya, H. Scherer, W. Beichel, P. Klose, C. Sturm, A. Hoffmann, J. Tübke, T. Koslowski and I. Krossing, *Chem. - A Eur. J.*, 2014, **20**, 9794–9804.
- 165 T. Erdmenger, C. Guerrero-Sanchez, J. Vitz, R. Hoogenboom and U. S. Schubert, *Chem. Soc. Rev.*, 2010, **39**, 3317–3333.
- 166 D. Zhao, Y. Liao and Z. Zhang, *CLEAN – Soil, Air, Water*, 2007, **35**, 42–48.
- 167 E. L. Smith, A. P. Abbott and K. S. Ryder, *Chem. Rev.*, 2014, **114**, 11060–11082.
- 168 Y. Dai, J. Van Spronsen, G. J. Witkamp, R. Verpoorte and Y. H. Choi, *J. Nat. Prod.*, 2013, **76**, 2162–2173.
- 169 M. Ruesgas-Ramón, M. C. Figueroa-Espinoza and E. Durand, *J. Agric. Food Chem.*, 2017, **65**, 3591–3601.
- 170 A. Pandey, Bhawna, D. Dhingra and S. Pandey, *J. Phys. Chem. B*, 2017, **121**, 4202–4212.
- 171 R. P. Swatloski, J. D. Holbrey and R. D. Rogers, *Green Chem.*, 2003, **5**, 361.
- 172 Q. Wen, J.-X. Chen, Y.-L. Tang, J. Wang and Z. Yang, *Chemosphere*, 2015, **132**, 63–69.
- 173 K. Radošević, M. Cvjetko Bubalo, V. Gaurina Srček, D. Grgas, T. Landeka Dragičević and I. Radojčić Redovniković, *Ecotoxicol. Environ. Saf.*, 2015, **112**, 46–53.
- 174 Q. Zhang, K. De Oliveira Vigier, S. Royer and F. Jérôme, *Chem. Soc. Rev.*, 2012, **41**, 7108–7146.
- 175 Q. Li, J. Jiang, G. Li, W. Zhao, X. Zhao and T. Mu, *Sci. China Chem.*, 2016, **59**, 571–577.
- 176 C. Ma, Y. Guo, D. Li, J. Zong, X. Ji, C. Liu and X. Lu, *J. Chem. Eng. Data*, 2016, **61**, 4172–4177.
- 177 F. H. Hurley and T. P. Wier, *J. Electrochem. Soc.*, 1951, **98**, 203.
- 178 A. P. Abbott, G. Capper, D. L. Davies, R. K. Rasheed and V. Tambyrajah, *Chem. Commun. (Camb)*, 2003, 70–71.
- 179 G. García, S. Aparicio, R. Ullah and M. Atilhan, *Energy & Fuels*, 2015, **29**, 2616–2644.
- 180 Clément Comminges, Rachid Barhdadi, A. Michel Laurent and M. Troupel, *J. Chem. Eng. Data*, 2006, **51** (2), 680–685.
- 181 T. Koller, M. H. Rausch, P. S. Schulz, M. Berger, P. Wasserscheid, I. G. Economou, A. Leipertz and A. P. Fröba, *J. Chem. Eng. Data*, 2012, **57**, 828–835.
- 182 K. R. Harris and M. Kanakubo, *J. Chem. Eng. Data*, 2016, **61**, 2399–2411.
- 183 Q. Chen, X. Li, X. Zang, Y. Cao, Y. He, P. Li, K. Wang, J. Wei, D. Wu and H. Zhu, *RSC Adv.*, 2014, **4**, 36253–36256.

- 184 L. Sun, O. Morales-Collazo, H. Xia and J. F. Brennecke, *J. Phys. Chem. B*, 2015, **119**, 15030–15039.
- 185 S. Tsuzuki, *ChemPhysChem*, 2012, **13**, 1664–1670.
- 186 L. Bahadori, M. H. Chakrabarti, N. S. A. Manan, M. A. Hashim, F. S. Mjalli, I. M. AlNashef and N. Brandon, *PLoS One*, 2015, **10**, e0144235.
- 187 Y. Cui, K. D. Fulfer, J. Ma, T. K. Weldeghiorghis and D. G. Kuroda, *Phys. Chem. Chem. Phys.*, 2016, **18**, 31471–31479.
- 188 I. R. Sasselli, I. P. Moreira, R. V. Ulijn and T. Tuttle, *Org. Biomol. Chem.*, 2017, **15**, 6541–6547.
- 189 A. Popescu, *Bulg. Chem. ...*, 2014, **46**, 452–457.
- 190 D. Wileńska, I. Anusiewicz, S. Freza, M. Bobrowski, E. Laux, S. Uhl, H. Keppner and P. Skurski, *Mol. Phys.*, 2015, **113**, 630–639.
- 191 ‡ and Katsumi Tochigi\* and H. Yamamoto§, , DOI:10.1021/JP073839A.
- 192 J. Le Bideau, L. Viau and A. Vioux, *Chem. Soc. Rev.*, 2011, **40**, 907–925.
- 193 N. K. and and T. Nakashima, , DOI:10.1021/LA015523E.
- 194 K. Hanabusa, H. Fukui, M. Suzuki and H. Shirai, *Langmuir*, 2005, **21**, 10383–10390.
- 195 \*,† Jason E. Bara, ‡ Sonja Lessmann, ‡ Christopher J. Gabriel, † Evan S. Hatakeyama, † and Richard D. Noble and ‡ Douglas L. Gin†, , DOI:10.1021/IE0704492.
- 196 A. Maršavelski, V. Smrečki, R. Vianello, M. Žinić, A. Moguš-Milanković and A. Šantić, *Chemistry*, 2015, **21**, 12121–8.
- 197 T. Kataoka, Y. Ishioka, M. Mizuhata, H. Minami and T. Maruyama, *ACS Appl. Mater. Interfaces*, 2015, **7**, 23346–23352.
- 198 N. Mohmeyer, D. Kuang, P. Wang, H.-W. Schmidt, S. M. Zakeeruddin and M. Grätzel, , DOI:10.1039/b604021g.
- 199 J.-D. Decoppet, T. Moehl, S. S. Babkair, R. A. Alzubaydi, A. A. Ansari, S. S. Habib, S. M. Zakeeruddin, H.-W. Schmidt and M. Grätzel, *J. Mater. Chem. A*, 2014, **2**, 15972–15977.
- 200 C. Mukesh, R. Gupta, D. N. Srivastava, S. K. Nataraj and K. Prasad, *RSC Adv.*, 2016, **6**, 28586–28592.
- 201 H. Qin and M. J. Panzer, *ChemElectroChem*, 2017, **4**, 2556–2562.
- 202 O. Miyawaki, C. Omote and K. Matsuhira, *Biopolymers*, 2015, **103**, 685–691.
- 203 V. Adibnia and R. J. Hill, *Cit. J. Rheol.*, , DOI:10.1122/1.4948428.
- 204 S. Meysam Hashemnejad and S. Kundu, , DOI:10.1021/acs.langmuir.7b01531.
- 205 M. M. Van Schooneveld, V. W. A. De Villeneuve, R. P. A. Dullens, D. G. A. L. Aarts, M. E. Leunissen and W. K. Kegel, , DOI:10.1021/jp809659g.

- 206 M. Driffield, D. M. Goodall, A. S. Klute, A. David K. Smith and K. Wilson, *Langmuir*, 2002, **18** (22), 8660–8665.
- 207 C. E. Davies, T. D. Heightman, S. a. Hermitage and M. G. Moloney, *Synth. Commun.*, 1996, **26**, 687–696.
- 208 W. E. Keller, G. Van Look, G. Wersin and M. A. Sanner, *Org. Synth.*, 1985, **63**, 160–170.
- 209 A. K. Jana, S. K. Das and G. Panda, *Tetrahedron*, 2012, 10114–10121.
- 210 T. I. Al-Warhi, H. M. A. Al-Hazimi and A. El-Faham, *J. Saudi Chem. Soc.*, 2012, **16**, 97–116.
- 211 C. A. G. N. Montalbetti and V. Falque, *Tetrahedron*, 2005, **61**, 10827–10852.
- 212 J. S. Foster, J. M. Zurek, N. M. S. Almeida, W. E. Hendriksen, V. A. A. Le Sage, V. Lakshminarayanan, A. L. Thompson, R. Banerjee, R. Eelkema, H. Mulvana, M. J. Paterson, J. H. Van Esch and G. O. Lloyd, *J. Am. Chem. Soc.*, 2015, **137**, 14236–14239.
- 213 V. J. Nebot and D. K. Smith, *Techniques for the Characterisation of Molecular Gels*, 2014.
- 214 C. Pradal, K. S. Jack, L. Grøndahl and J. J. Cooper-White., *Biomacromolecules*, 2013, **14**, 3780–3792.
- 215 R. Hassan, A. Gobouri and I. Zaafarany, *Adv. Biosens. Bioelectron.*, 2013, **2**, 12–20.
- 216 G. Gottarelli, S. Lena, S. Masiero, S. Pieraccini and G. P. Spada, *Chirality*, 2008, **20**, 471–485.
- 217 J. F. Miravet and B. Escuder, in *Functional Molecular Gels*, ed. RSC Soft Matter No., 2014, pp. 117–156.
- 218 P. S. Weiss, *ACS Nano*, 2008, **2**, 1085–1087.
- 219 E. R. Draper, T. O. McDonald and D. J. Adams, *Chem. Commun.*, 2015, **51**, 6595–6597.
- 220 L. Johansson and J. Löfroth, *J. Chem. Phys.*, 1993, **98**, 7471–7479.
- 221 R. Metzler, J.-H. Jeon and A. G. Cherstvy, *BBA - Biomembr.*, 2016, **1858**, 2451–2467.
- 222 P. D. Anne Marie Helmenstine, What Is Diffusion? Chemistry Definition, <https://www.thoughtco.com/definition-of-diffusion-604430>.
- 223 E. De la Barrera, *Nat. Struct. Mol. Biol.*, 2005, **12**, 280–280.
- 224 B. P. van Milligen, P. D. Bons, B. A. Carreras and R. Sánchez, *Eur. J. Phys.*, 2005, **26**, 913–925.
- 225 Diffusion of Dye in Agar - YouTube, <https://www.youtube.com/watch?v=eebPrMpKG7c>, (accessed 23 October 2017).
- 226 C. Rest, R. Kandaneli and G. Fernández, *Chem. Soc. Rev.*, 2015, **44**, 2543–2572.

- 227 X.-Y. Zhao, Q. Cao, L.-Q. Zheng and G.-Y. Zhang, *Colloids Surfaces A Physicochem. Eng. Asp.*, 2006, **281**, 67–73.
- 228 F. Pop, C. Melan, I. Danila, M. Linares, D. Beljonne, D. B. Amabilino and N. Avarvari, *Chem. - A Eur. J.*, 2014, **20**, 17443–17453.
- 229 S. Strandman and X. X. Zhu, *Gels*, 2016, **2**, 16.
- 230 K. Venkata Rao, D. Miyajima, A. Nihonyanagi and T. Aida, *Nat. Chem.*, 2017, 1–7.
- 231 F. Yao and J. K. Weiyuan, *Expert Opin. Drug Deliv.*, 2010, **7**, 429–444.
- 232 G. Yu, X. Yan, C. Han and F. Huang, *Chem. Soc. Rev.*, 2013, **42**, 6697.
- 233 S. Gits-Leon, F. Lefaucheux and M. C. Robert, *J. Cryst. Growth*, 1987, **84**, 155–162.
- 234 S. Cantekin, D. W. R. Balkenende, M. M. J. Smulders, A. R. A. Palmans and E. W. Meijer, *Nat. Chem.*, 2011, **3**, 42–46.
- 235 F. Tantakitti, J. Boekhoven, X. Wang, R. V. Kazantsev, T. Yu, J. Li, E. Zhuang, R. Zandi, J. H. Ortony, C. J. Newcomb, L. C. Palmer, G. S. Shekhawat, M. O. de la Cruz, G. C. Schatz and S. I. Stupp, *Nat. Mater.*, 2016, **15**, 469–476.
- 236 T. Fukui, S. Kawai, S. Fujinuma, Y. Matsushita, T. Yasuda, T. Sakurai, S. Seki, M. Takeuchi and K. Sugiyasu, *Nat. Chem.*, 2016, **9**, 493–499.
- 237 Y. Shi, J. Zhang, L. Pan, Y. Shi and G. Yu, *Nano Today*, 2016, **11**, 738–762.
- 238 Z. Chang, C. Li, Y. Wang, B. Chen, L. Fu, Y. Zhu, L. Zhang, Y. Wu and W. Huang, *Sci. Rep.*, 2016, **6**, 28421.
- 239 W. Zuo, R. Li, C. Zhou, Y. Li, J. Xia and J. Liu, *Adv. Sci.*, 2017, 1–21.
- 240 X. Wang, R. S. Chandrabose, S. E. Chun, T. Zhang, B. Evanko, Z. Jian, S. W. Boettcher, G. D. Stucky and X. Ji, *ACS Appl. Mater. Interfaces*, 2015, **7**, 19978–19985.
- 241 X. Li, L. Liu, X. Wang, Y. S. Ok, J. A. W. Elliott, S. X. Chang and H.-J. Chung, *Sci. Rep.*, 2017, **7**, 1685.
- 242 B. O. Okesola, D. K. Smith, S. Babel and E. Al., *Chem. Soc. Rev.*, 2016, **97**, 219–243.
- 243 I. Volovych, Y. Kasaka, M. Schwarze, Z. Nairoukh, J. Blum, M. Fanun, D. Avnir and R. Schomäcker, *J. Mol. Catal. A Chem.*, 2014, **393**, 210–221.
- 244 S. Magdeldin, S. Enany, Y. Yoshida, B. Xu, Y. Zhang, Z. Zureena, I. Lokamani, E. Yaoita and T. Yamamoto, *Clin. Proteomics*, 2014, **11**, 16.
- 245 P. C. Marr and A. C. Marr, *Green Chem.*, 2016, **18**, 105–128.
- 246 T. P. Lodge and T. Ueki, *Acc. Chem. Res.*, 2016, **49**, 2107–2114.
- 247 D. V. Wagle, H. Zhao and G. A. Baker, *Acc. Chem. Res.*, 2014, **47**, 2299–2308.
- 248 M. H. Chakrabarti, F. S. Mjalli, I. M. Alnashef, M. A. Hashim, M. A. Hussain, L. Bahadori and C. T. J. Low, *Renew. Sustain. Energy Rev.*, 2014, **30**, 254–270.

- 249 K. Suzuki, M. Yamaguchi, M. Kumagai, N. Tanabe and S. Yanagida, *Comptes Rendus Chim.*, 2006, **9**, 611–616.
- 250 H. L. Hsu, C. F. Tien, Y. T. Yang and J. Leu, *Electrochim. Acta*, 2013, **91**, 208–213.
- 251 H. Usui, H. Matsui, N. Tanabe and S. Yanagida, *J. Photochem. Photobiol. A Chem.*, 2004, **164**, 97–101.
- 252 W. Li, Y. Pang, J. Liu, G. Liu, Y. Wang and Y. Xia, *RSC Adv.*, 2017, **7**, 23494–23501.
- 253 H. C. Moon, T. P. Lodge and C. D. Frisbie, *Chem. Mater.*, 2015, **27**, 1420–1425.
- 254 K. (Kelvin) Fu, Y. Gong, J. Dai, A. Gong, X. Han, Y. Yao, C. Wang, Y. Wang, Y. Chen, C. Yan, Y. Li, E. D. Wachsman and L. Hu, *Proc. Natl. Acad. Sci.*, 2016, **113**, 7094–7099.
- 255 S. Khandelwal, Y. K. Tailor and M. Kumar, *J. Mol. Liq.*, 2016, **215**, 345–386.
- 256 N. Koganti, J. R. Mitchell, R. N. Ibbett and T. J. Foster, *Biomacromolecules*, 2011, **12**, 2888–2893.
- 257 S. Casali, M. Gungormusler, L. Bertin, F. Fava and N. Azbar, *Biochem. Eng. J.*, 2012, **64**, 84–90.
- 258 D. Wischral, J. Zhang, C. Cheng, M. Lin, L. M. G. De Souza, F. L. P. Pessoa, N. Pereira and S. T. Yang, *Bioresour. Technol.*, 2016, **212**, 100–110.
- 259 T. Carvalho, V. Augusto, A. R. Brás, N. M. T. Lourenço, C. A. M. Afonso, S. Barreiros, N. T. Correia, P. Vidinha, E. J. Cabrita, C. J. Dias, M. Dionísio and B. Roling, *J. Phys. Chem. B*, 2012, **116**, 2664–2676.
- 260 G. Oltean, M. Valvo, L. Nyholm and K. Edström, *Thin Solid Films*, 2014, **562**, 63–69.
- 261 B. M. Savoie, M. A. Webb and T. F. Miller, *J. Phys. Chem. Lett.*, 2017, **8**, 641–646.
- 262 A. Vlad, N. Singh, J. Rolland, S. Melinte, P. M. Ajayan and J.-F. Gohy, *Sci. Rep.*, 2014, **4**, 4315.
- 263 L. Tao, Z. Huo, Y. Ding, Y. Li, S. Dai, L. Wang, J. Zhu, X. Pan, B. Zhang, J. Yao, M. K. Nazeeruddin and M. Grätzel, *J. Mater. Chem. A*, 2015, **3**, 2344–2352.
- 264 W.-C. Lai and C.-H. Wu, *J. Appl. Polym. Sci.*, 2010, **115**, 1113–1119.
- 265 W.-C. Lai and Y.-C. Lee, *RSC Adv.*, 2016, **6**, 98042–98051.
- 266 R. Stefanovic, M. Ludwig, G. B. Webber, R. Atkin and A. J. Page, *Phys. Chem. Chem. Phys.*, 2017, **19**, 3297–3306.
- 267 K. Hanabusa, K. Hiratsuka, M. Kimura and H. Shirai, *Chem. Mater.*, 1999, **11**, 649–655.
- 268 Q. Li, J. Chen, L. Fan, X. Kong and Y. Lu, *Green Energy Environ.*, 2016, **1**, 1–25.
- 269 M.-C. Lin, M. Gong, B. Lu, Y. Wu, D.-Y. Wang, M. Guan, M. Angell, C. Chen, J. Yang, B.-J. Hwang and H. Dai, *Nature*, 2015, **520**, 324–328.

- 270 A. Tornheim, M. He, C.-C. Su and Z. Zhang, *J. Electrochem. Soc.*, 2017, **164**, A6366–A6372.
- 271 R. Miao, J. Yang, Z. Xu, J. Wang, Y. Nuli and L. Sun, *Sci. Rep.*, 2016, **6**, 21771.
- 272 H. Tian, T. Gao, X. Li, X. Wang, C. Luo, X. Fan, C. Yang, L. Suo, Z. Ma, W. Han and C. Wang, *Nat. Commun.*, 2017, **8**, 14083.
- 273 A. Ponrouch, C. Frontera, F. Bardé and M. R. Palacín, *Nat. Mater.*, 2015, **15**, 169–172.
- 274 A. P. Abbott, D. Boothby, G. Capper, D. L. Davies and R. K. Rasheed, *J. Am. Chem. Soc.*, 2004, **126**, 9142–9147.
- 275 K. R. Harris and M. Kanakubo, *J. Phys. Chem. B*, 2016, **120**, 12937–12949.
- 276 A. Siddiq and E. Ghassemieh, *Mech. Mater.*, 2008, **40**, 982–1000.
- 277 L. Claes and B. Willie, *Prog. Biophys. Mol. Biol.*, 2007, **93**, 384–98.
- 278 S. R. Young and M. Dyson, *Ultrasonics*, 1990, **28**, 175–180.
- 279 S. B. Agarwal, *Ultrasonics*, 1980, **18**, 270–72.
- 280 J. Jossinet, B. Lavandier and D. Cathignol, *Ultrasonics*, 1998, **36**, 607–613.

## Appendix.

### L-LysOMe. Characterization spectra. <sup>207</sup>

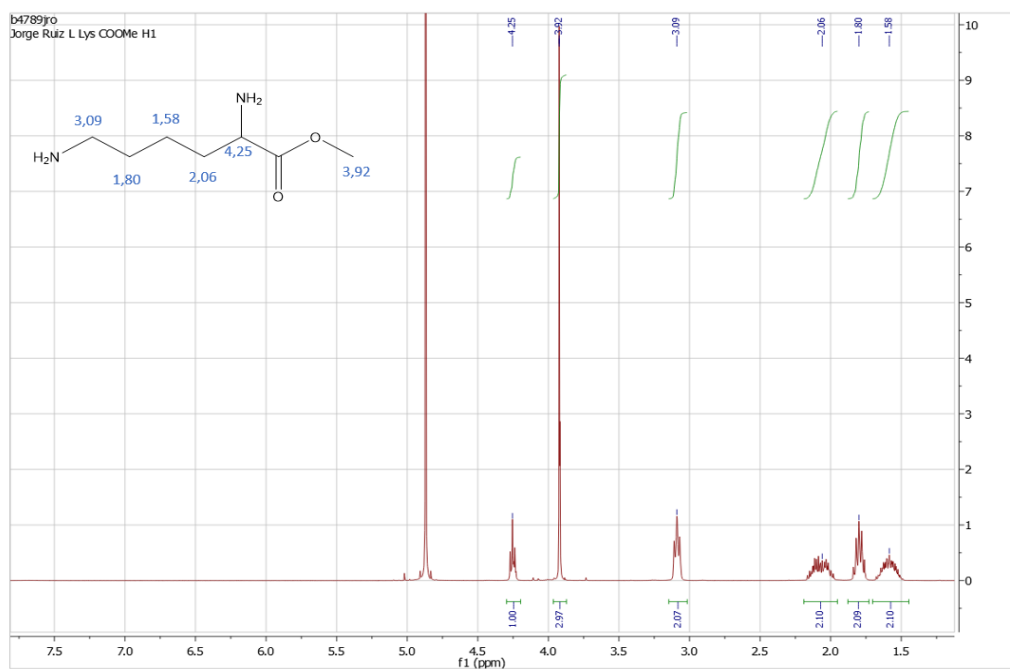


Figure 6-26 <sup>1</sup>H-NMR L-Lysine methyl ester dihydrochloride.

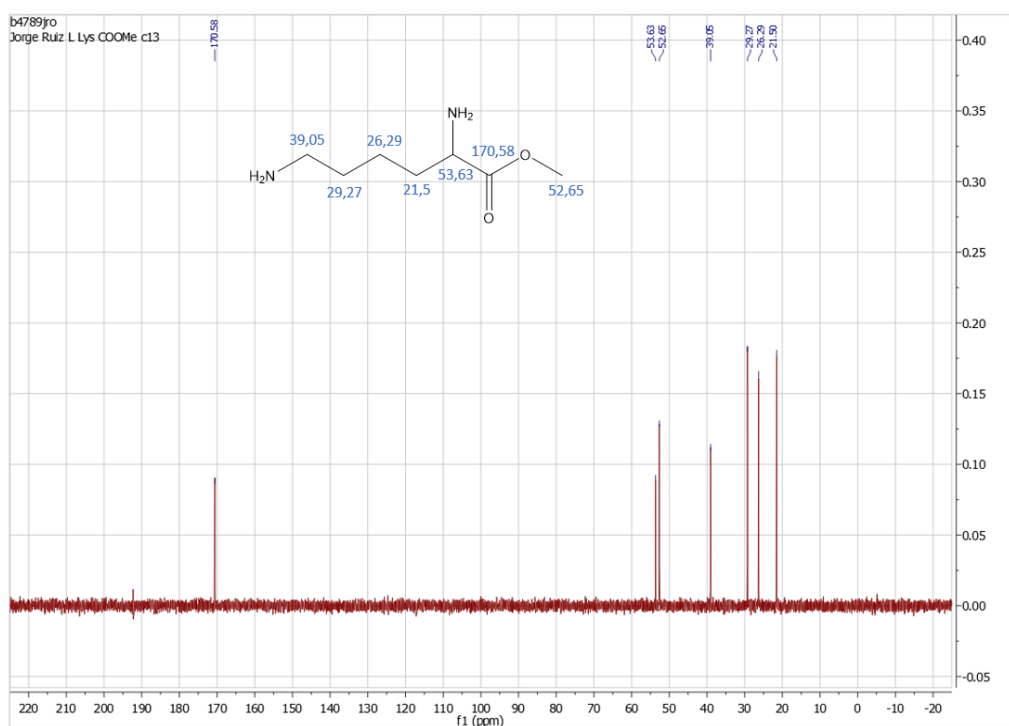


Figure 6-27 <sup>13</sup>C NMR L-Lysine methyl ester dihydrochloride.

York - Chemistry - Mass Spectrometry Service Report

L Lys COOMe

Analysis Information

Acquisition Date 03/10/2018 15:37:46

Analysis Filename dks61203jr\_P1-D-8\_01\_294.d  
 Method 400p\_scn1260\_2c1s.m  
 Submission Name dks61203jr  
 Instrument micrOTOF  
 ESI Positive

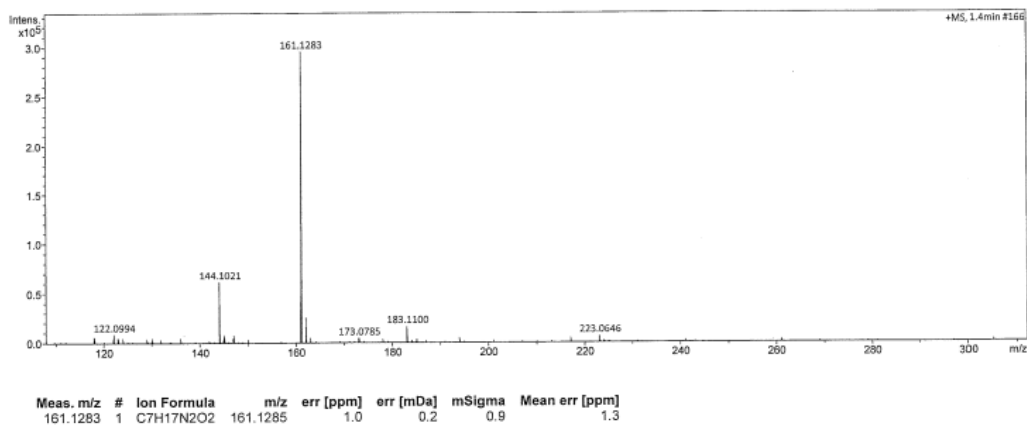


Figure 6-28 Mass spectrum of L-Lysine methyl ester dihydrochloride

D-LysOMe. Characterization Spectra.

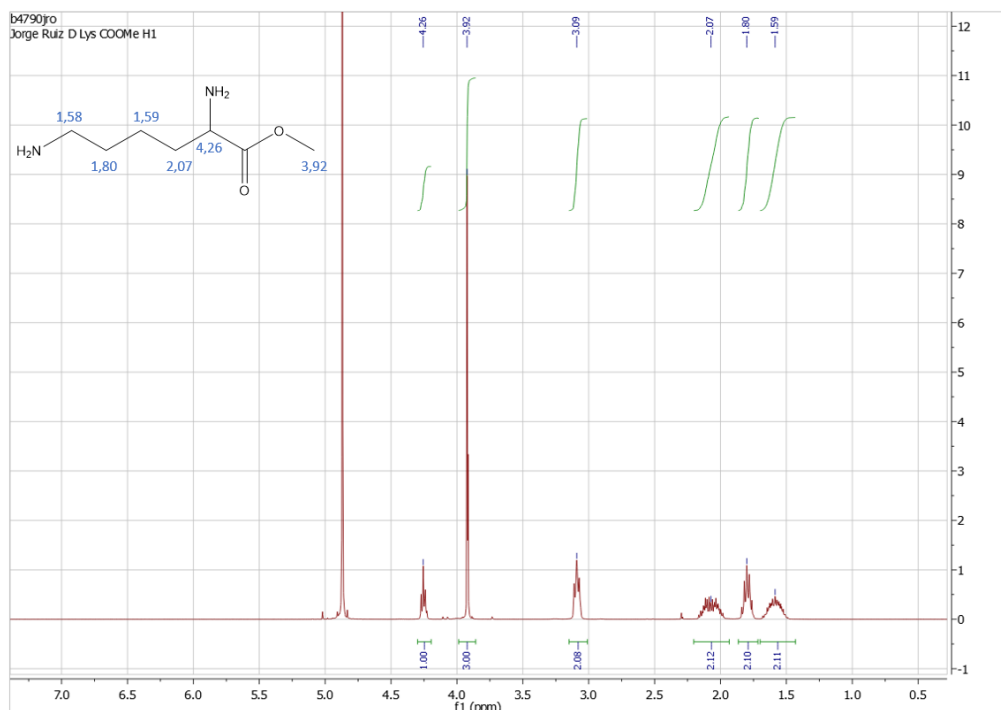


Figure 6-29 <sup>1</sup>H-NMR of D-Lysine methyl ester dihydrochloride.

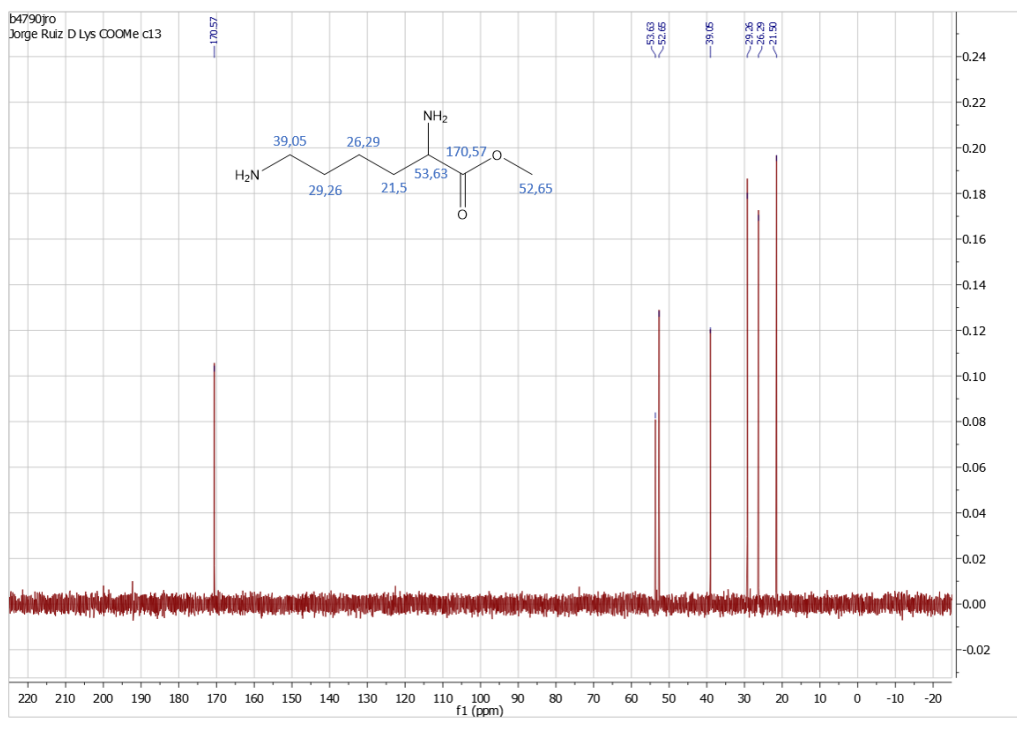


Figure 6-30 <sup>13</sup>C NMR of D-Lysine methyl ester dihydrochloride.

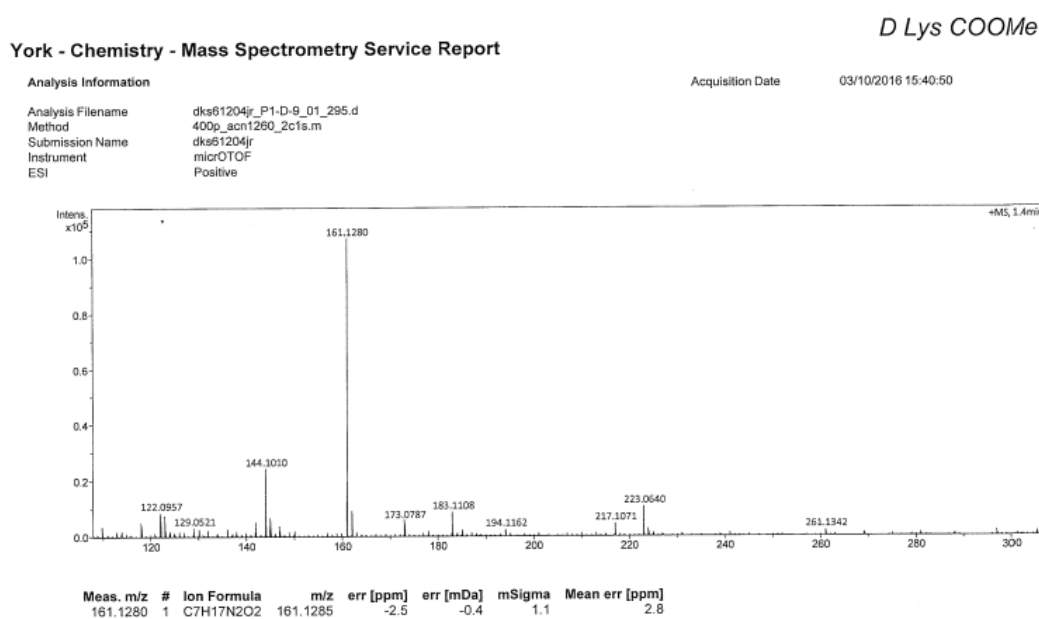
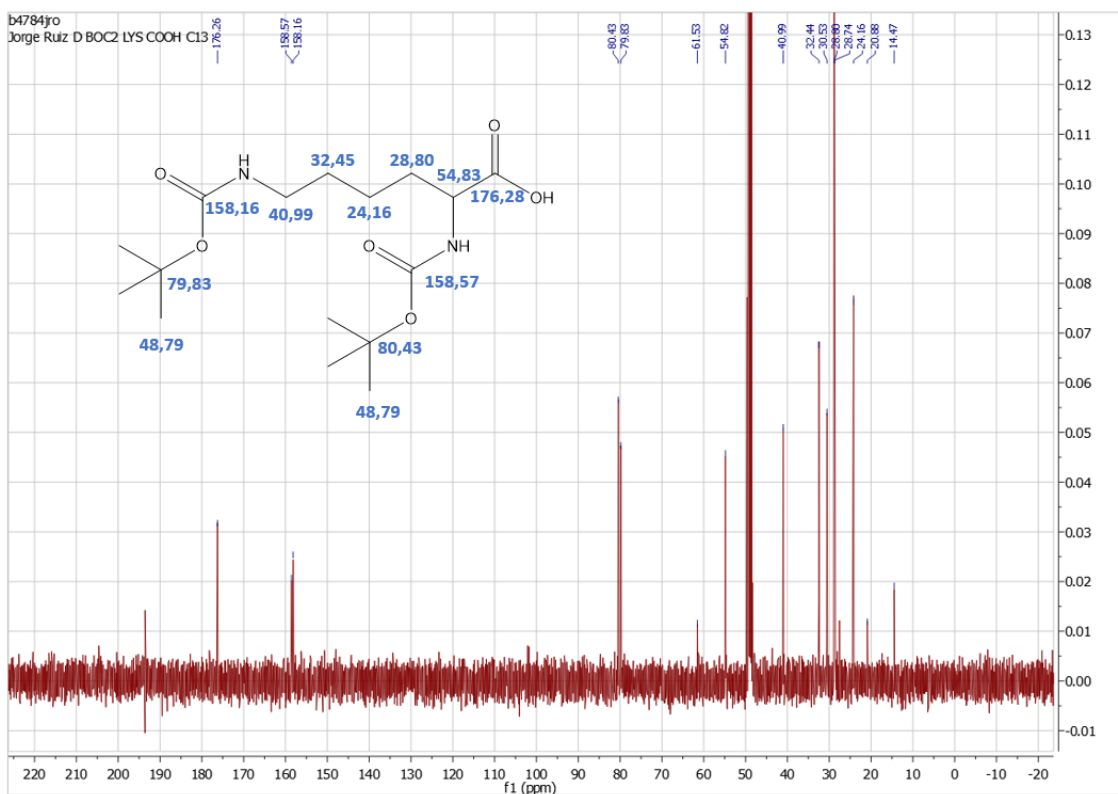
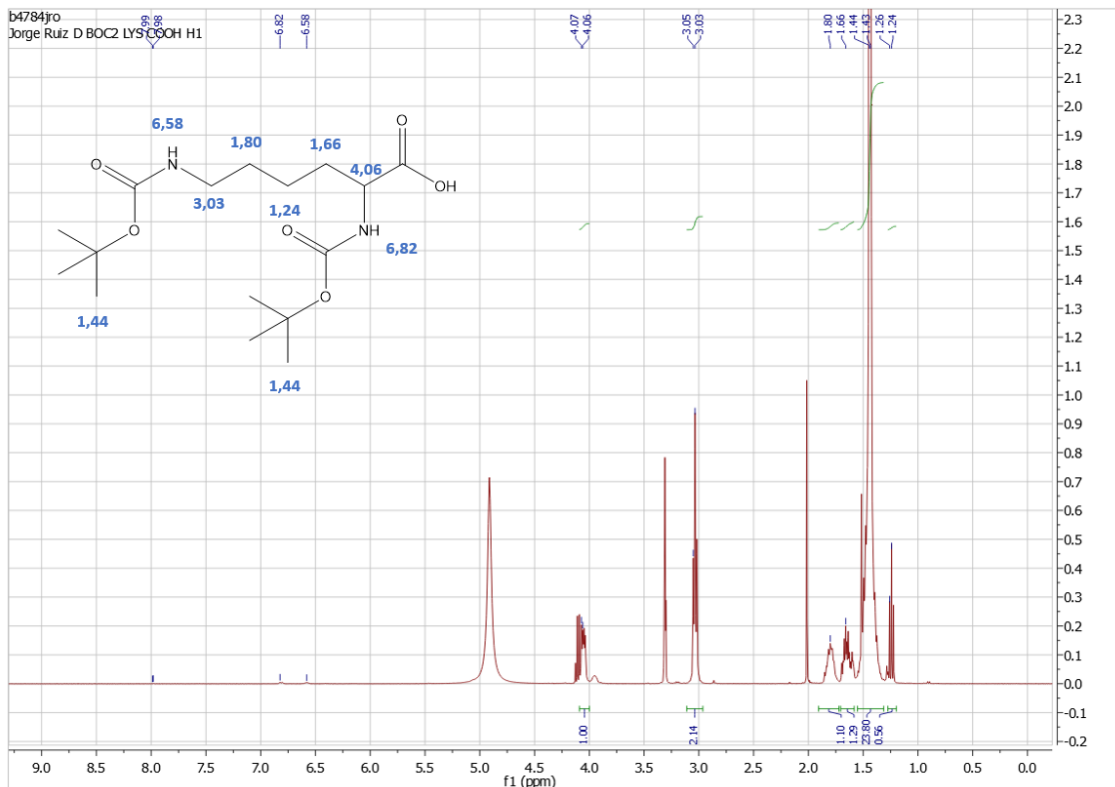


Figure 6-31 Mass spectrum of D-Lysine methyl ester dihydrochloride





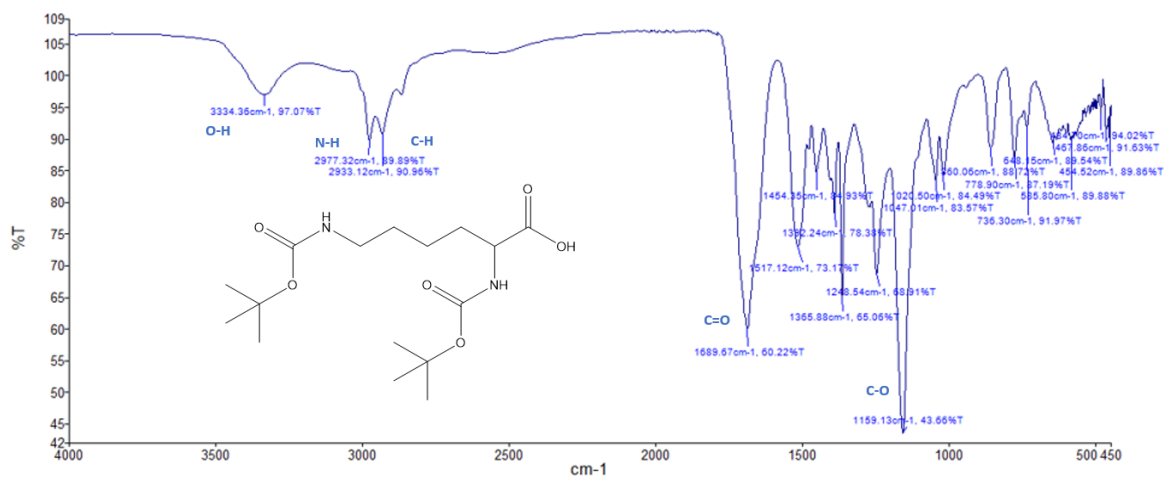


Figure 6-36 FTIR spectra of G1 (Boc)<sub>2</sub>-Lys-OH

York - Chemistry - Mass Spectrometry Service Report

*L(boc)<sub>2</sub> Lys OH*

Analysis Information

Acquisition Date

03/10/2016 15:31:39

Analysis Filename dks61201jr\_P1-D-6\_01\_292.d  
 Method 400p\_acn1260\_2c1s.m  
 Submission Name dks61201jr  
 Instrument micrOTOF  
 ESI Positive

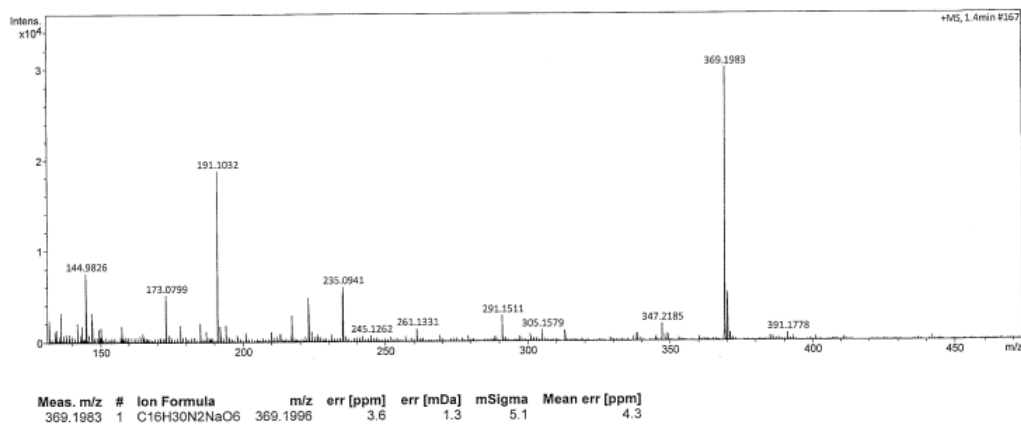


Figure 6-37 Mass spectra of G1 L-(Boc)<sub>2</sub>-Lys-OH

York - Chemistry - Mass Spectrometry Service Report

D(boc)<sub>2</sub> Lys OH

Analysis Information

Acquisition Date 03/10/2016 15:34:41

Analysis Filename dks61202jr\_P1-D-7\_01\_293.d  
 Method 400p\_acn1260\_2c1s.m  
 Submission Name dks61202jr  
 Instrument micrOTOF  
 ESI Positive

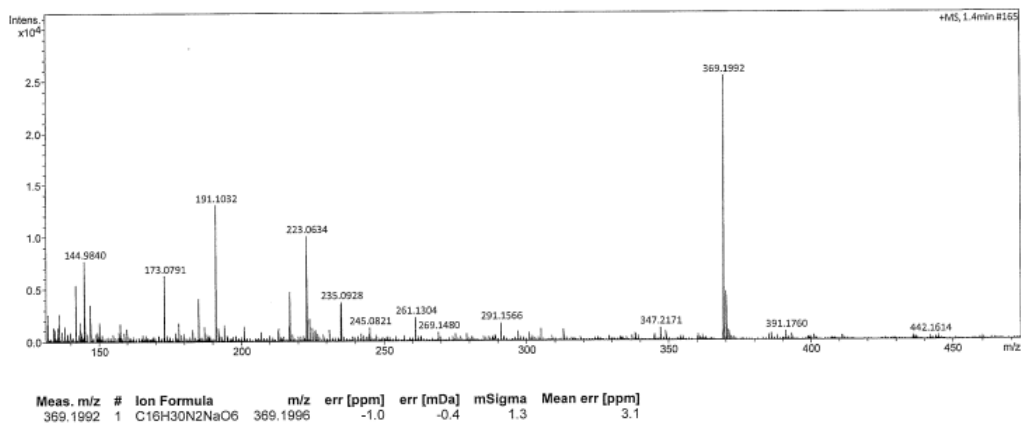


Figure 6-38 Mass spectra of G1 D-(Boc)<sub>2</sub>-Lys-OH

G2 ((Boc)<sub>2</sub>-Lys)<sub>2</sub>-Lys-OMe Characterization data.

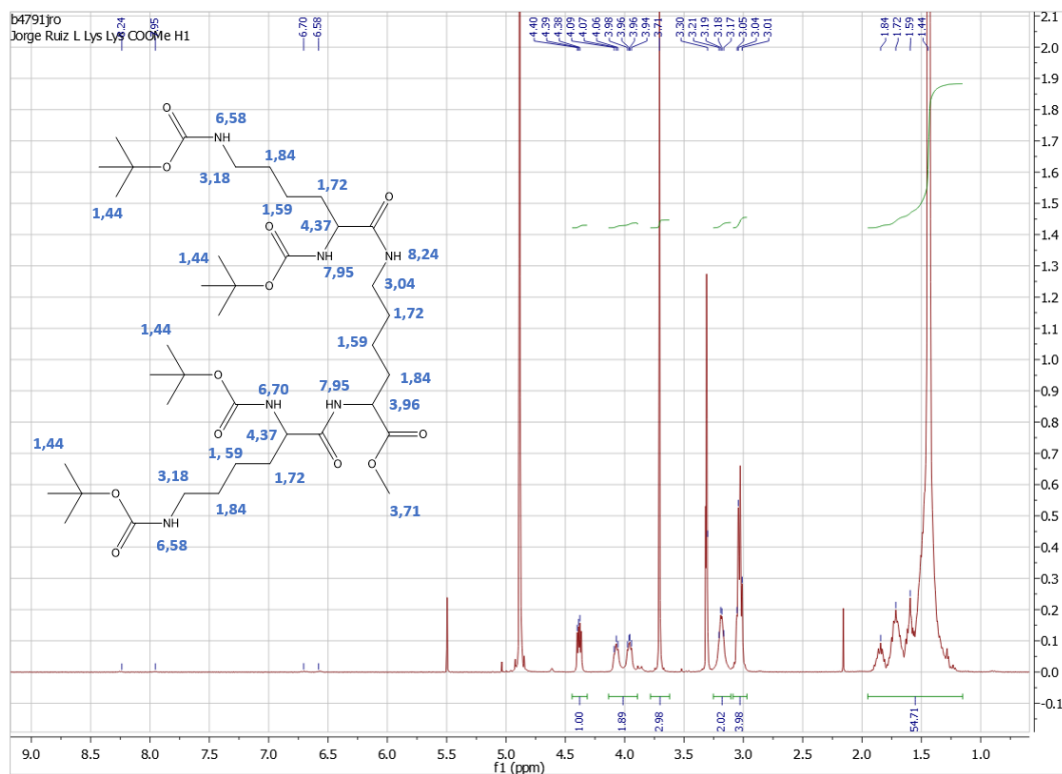


Figure 6-39 <sup>1</sup>H-NMR of G2 L-((Boc)<sub>2</sub>-Lys)<sub>2</sub>-Lys-OMe.

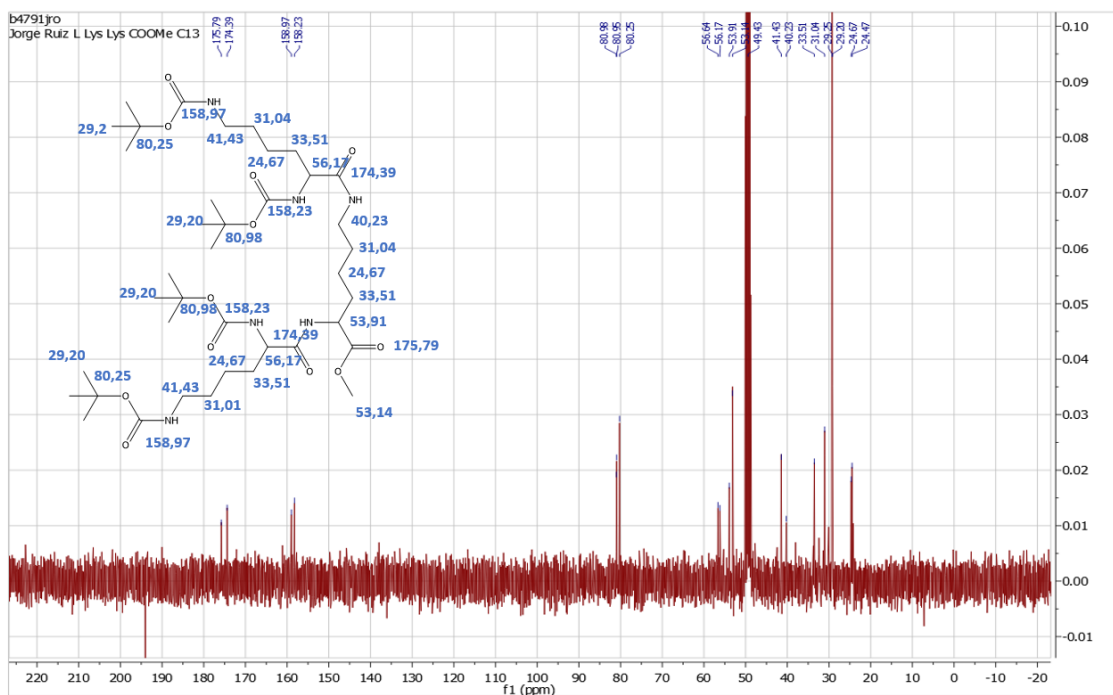


Figure 6-40  $^{13}\text{C}$  NMR of G2 L-((Boc) $_2$ -Lys) $_2$ -Lys-OMe.

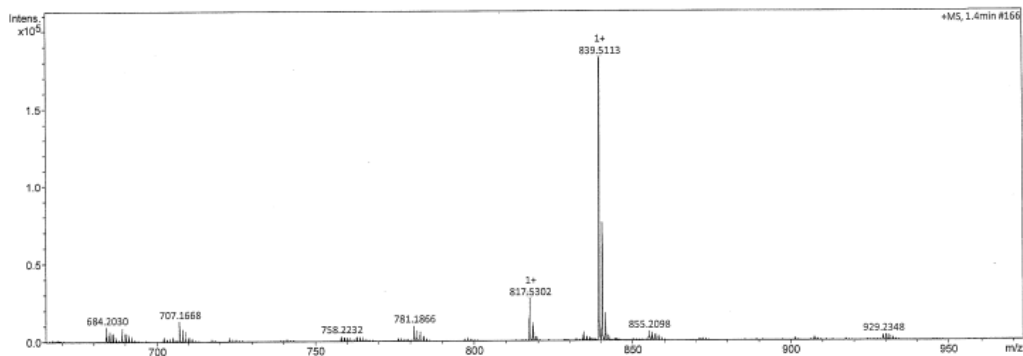
York - Chemistry - Mass Spectrometry Service Report

L Lys Lys COOMe

Analysis Information

Acquisition Date 03/10/2016 13:37:25

Analysis Filename dks61194jr\_P1-C-7\_01\_282.d  
 Method 800p\_acn1260\_2c1s.m  
 Submission Name dks61194jr  
 Instrument micrOTOF  
 ESI Positive



Meas. m/z	#	Ion Formula	m/z	err [ppm]	err [mDa]	mSigma	Mean err [ppm]
817.530178	1	C <sub>39</sub> H <sub>73</sub> N <sub>6</sub> O <sub>12</sub>	817.528098	-2.5	-2.1	22.2	-2.9
839.511293	1	C <sub>39</sub> H <sub>72</sub> N <sub>6</sub> NaO <sub>12</sub>	839.510042	1.5	1.3	22.8	-1.7

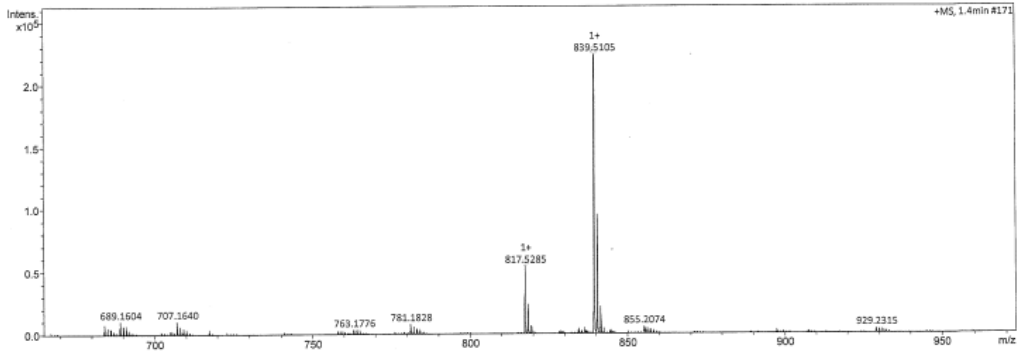
Figure 6-41 Mass Spectra of G2 L-((Boc) $_2$ -Lys) $_2$ -Lys-OMe.

York - Chemistry - Mass Spectrometry Service Report

Analysis Information

Acquisition Date 03/10/2016 13:40:28

Analysis Filename dks61195jr\_P1-C-8\_01\_283.d  
 Method 800p\_acn1260\_2c1s.m  
 Submission Name dks61195jr  
 Instrument micrOTOF  
 ESI Positive



Meas. m/z	#	Ion Formula	m/z	err [ppm]	err [mDa]	mSigma	Mean err [ppm]
817.528502	1	C <sub>39</sub> H <sub>73</sub> N <sub>6</sub> O <sub>12</sub>	817.528098	-0.5	-0.4	12.3	-0.2
839.510532	1	C <sub>39</sub> H <sub>72</sub> N <sub>6</sub> NaO <sub>12</sub>	839.510042	0.6	0.5	19.7	-0.6

Figure 6-42 Mass Spectra of G2<sub>D</sub>-((Boc)<sub>2</sub>-Lys)<sub>2</sub>-Lys-OMe.

G2 (Boc-Phe)<sub>2</sub>-Lys-OMe Characterization data.

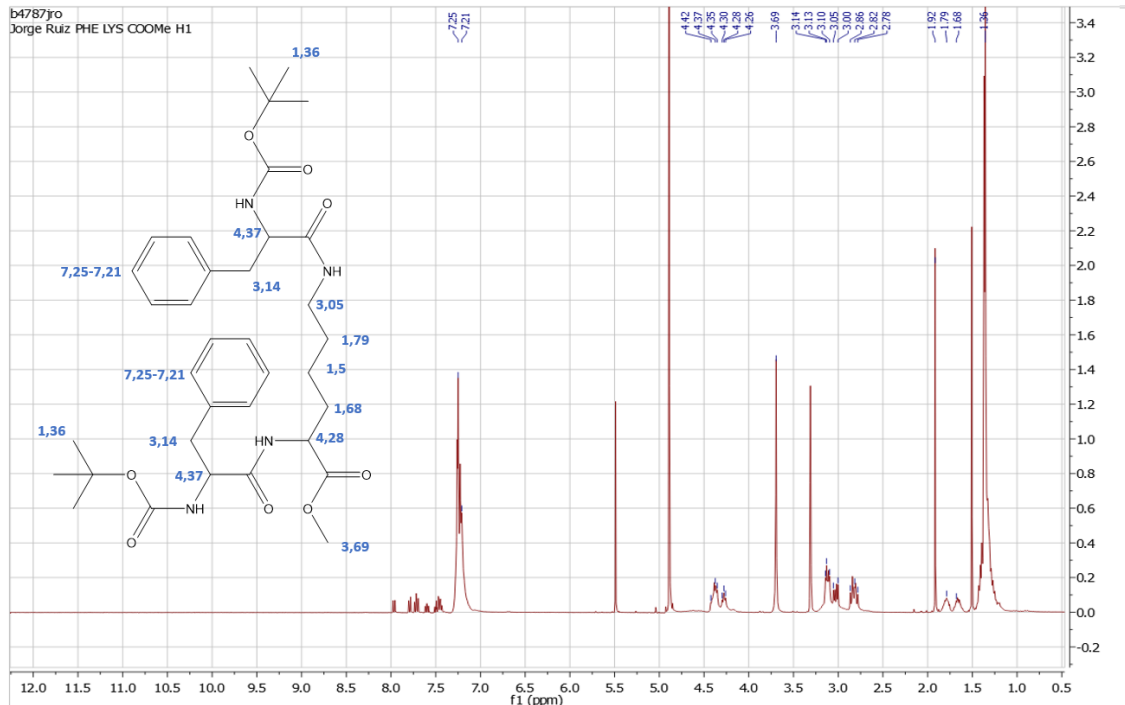


Figure 6-43 <sup>1</sup>H-NMR of G2<sub>L</sub>-(Boc-Phe)<sub>2</sub>-Lys-OMe.



## G2 (Boc-Ala)<sub>2</sub>-Lys-OMe Characterization data.

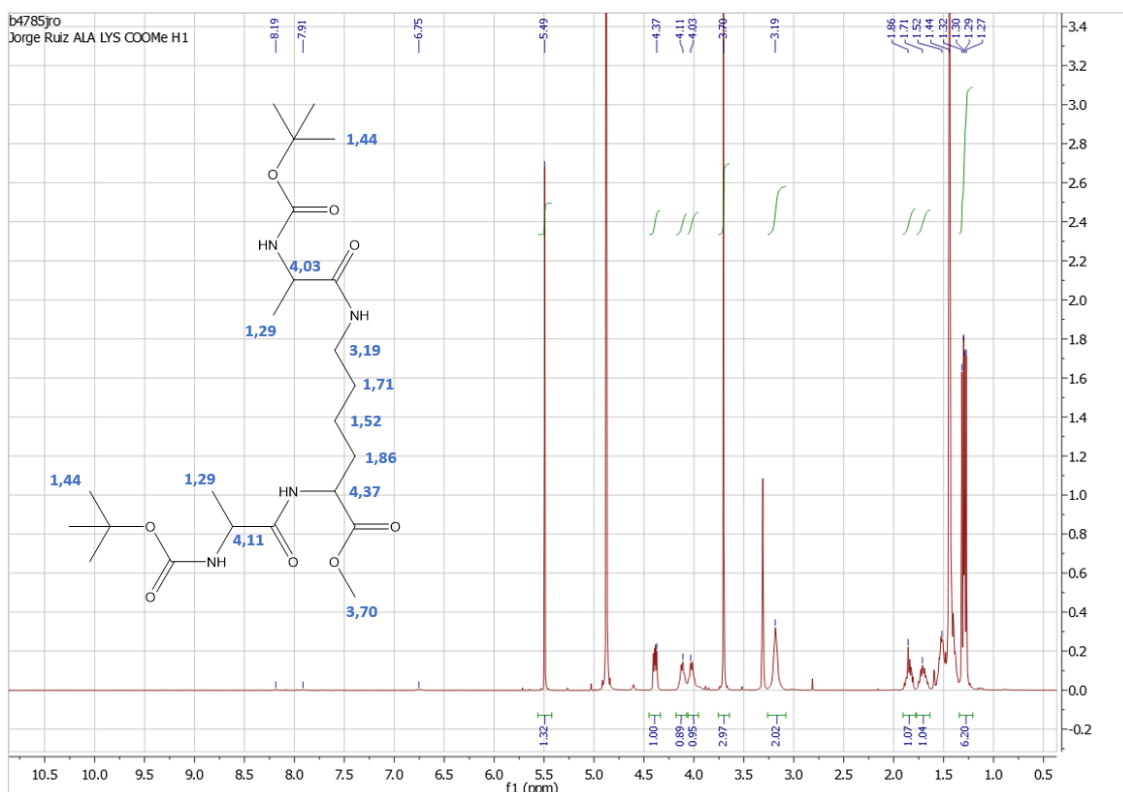


Figure 6-46 <sup>1</sup>H-NMR of G2 L-(Boc-Ala)<sub>2</sub>-Lys-OMe.

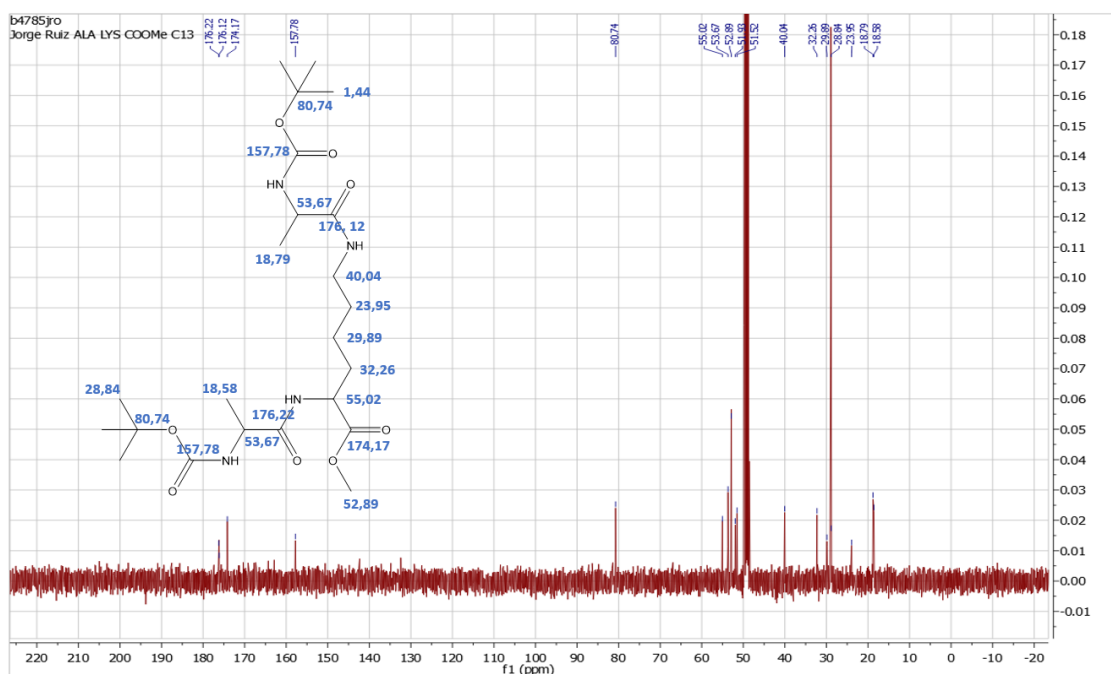


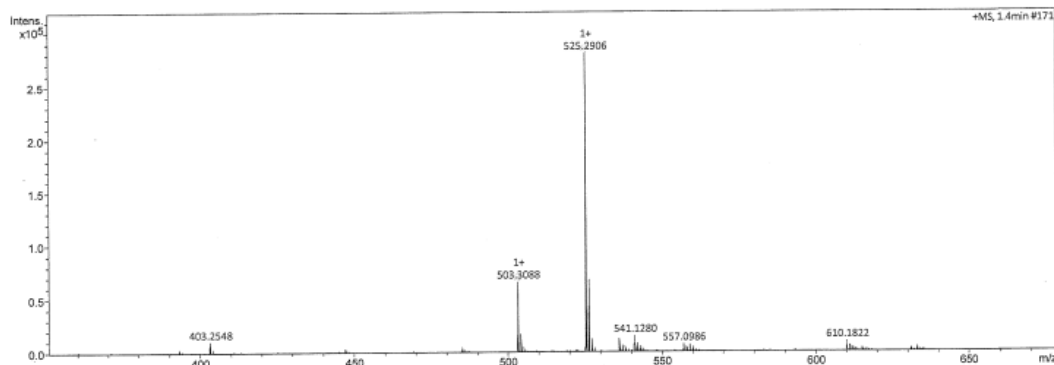
Figure 6-47 <sup>13</sup>C NMR of G2 L-(Boc-Ala)<sub>2</sub>-Lys-OMe.

Analysis Information

Acquisition Date

03/10/2016 13:43:32

Analysis Filename dks61196jr\_P1-C-9\_01\_284.d  
 Method 600p\_acn1260\_2c1s.m  
 Submission Name dks61196jr  
 Instrument micrOTOF  
 ESI Positive



Meas. m/z	#	Ion Formula	m/z	err [ppm]	err [mDa]	mSigma	Mean err [ppm]
503.30832	1	C23H43N4O8	503.307541	2.6	1.3	7.6	-2.4
525.290611	1	C23H42N4NaO8	525.289485	2.1	1.1	15.6	-2.3

Figure 6-48 Mass Spectra of G2<sub>L</sub>-(Boc-Ala)<sub>2</sub>-Lys-OMe.

G2 (Boc-Val)<sub>2</sub>-Lys-OMe Characterization data.

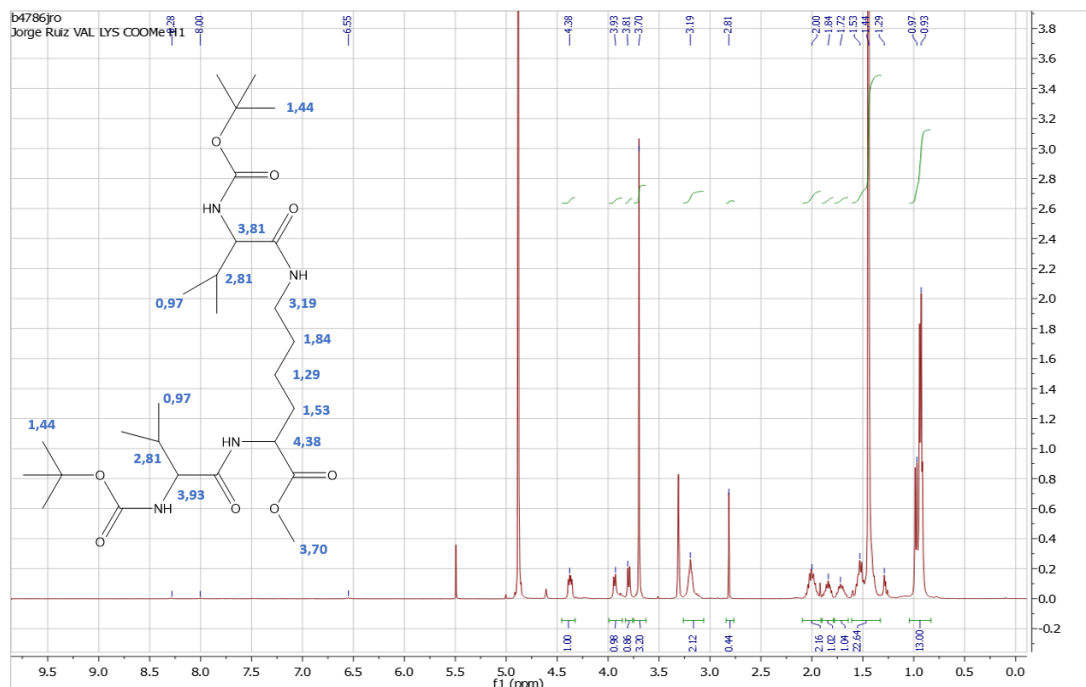


Figure 6-49 <sup>1</sup>H-NMR of G2<sub>L</sub>-(Boc-Val)<sub>2</sub>-Lys-OMe.





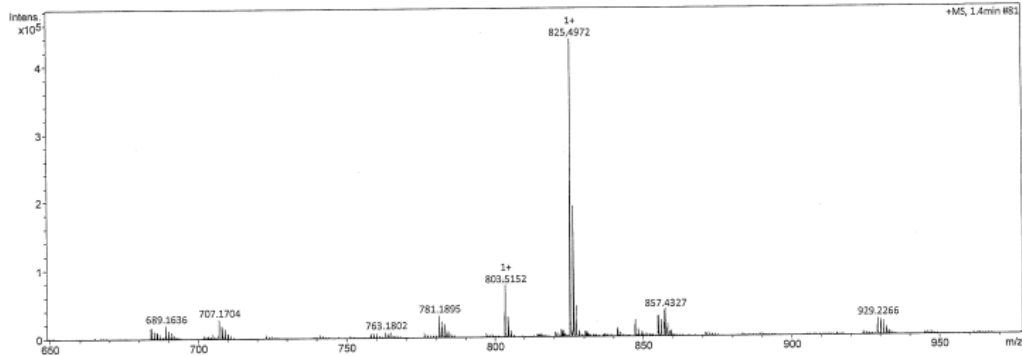
L Lys COOH

York - Chemistry - Mass Spectrometry Service Report

Analysis Information

Acquisition Date 03/10/2016 10:11:31

Analysis Filename dks61186jr\_P1-B-8\_01\_273.d  
Method 800px\_acn1260\_2c1s.m  
Submission Name dks61186jr  
Instrument micrOTOF  
ESI Positive



Meas. m/z	#	Ion Formula	m/z	err [ppm]	err [mDa]	mSigma	Mean err [ppm]
803.515154	1	C38H71N6O12	803.512448	-3.4	-2.7	22.2	-3.6
825.497157	1	C38H70N6NaO12	825.494392	-3.3	-2.8	8.1	-3.0

Figure 6-54 Mass Spectra of G2 L((Boc)<sub>2</sub>-Lys)<sub>2</sub>-Lys-OH.

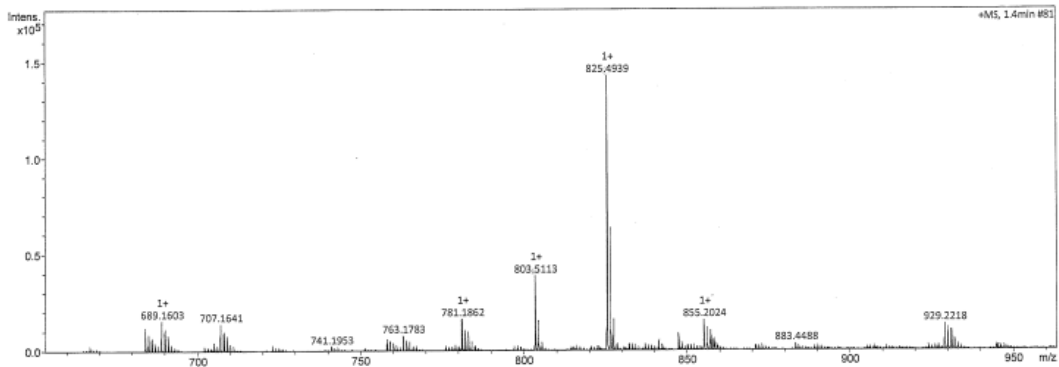
D Lys COOH

York - Chemistry - Mass Spectrometry Service Report

Analysis Information

Acquisition Date 03/10/2016 10:14:34

Analysis Filename dks61187jr\_P1-B-9\_01\_274.d  
Method 800px\_acn1260\_2c1s.m  
Submission Name dks61187jr  
Instrument micrOTOF  
ESI Positive



Meas. m/z	#	Ion Formula	m/z	err [ppm]	err [mDa]	mSigma	Mean err [ppm]
803.511315	1	C38H71N6O12	803.512448	-1.4	-1.1	19.9	0.7
825.493886	1	C38H70N6NaO12	825.494392	-0.6	-0.5	3.5	0.9

Figure 6-55 Mass Spectra of G2 ((Boc)<sub>2</sub>-Lys)<sub>2</sub>-Lys-OH.







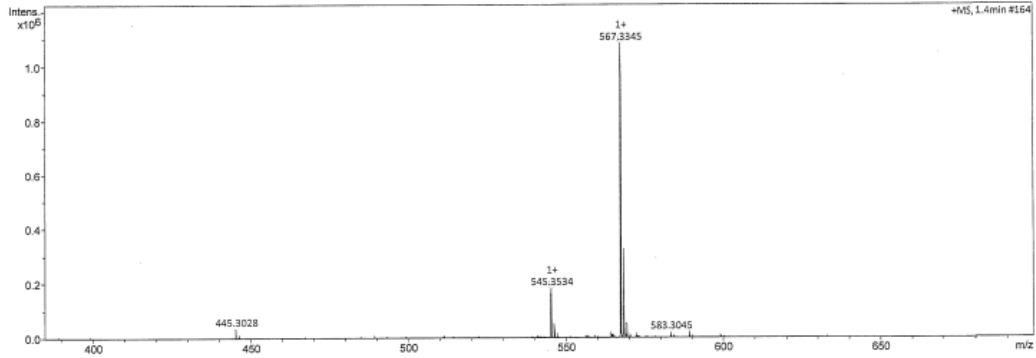


## York - Chemistry - Mass Spectrometry Service Report

## Analysis Information

Analysis Filename dks61189jr\_P1-C-2\_01\_276.d  
Method 600p\_acn1260\_2c1s.m  
Submission Name dks61189jr  
Instrument micrOTOF  
ESI Positive

Acquisition Date 03/10/2016 10:20:40



Meas. m/z	#	Ion Formula	m/z	err [ppm]	err [mDa]	mSigma	Mean err [ppm]
545.353397	1	C26H49N4O8	545.354491	-2.0	-1.1	11.4	2.2
567.334505	1	C26H48N4NaO8	567.336435	-3.4	-1.9	6.3	3.4

Figure 6-64 Mass Spectra of G2 (Boc-Val)<sub>2</sub>-Lys-OH

# Diffusion coefficients calculations

## Diphenylmethane Diffusion Coefficient.

### Diphenylmethane Diffusion coefficient

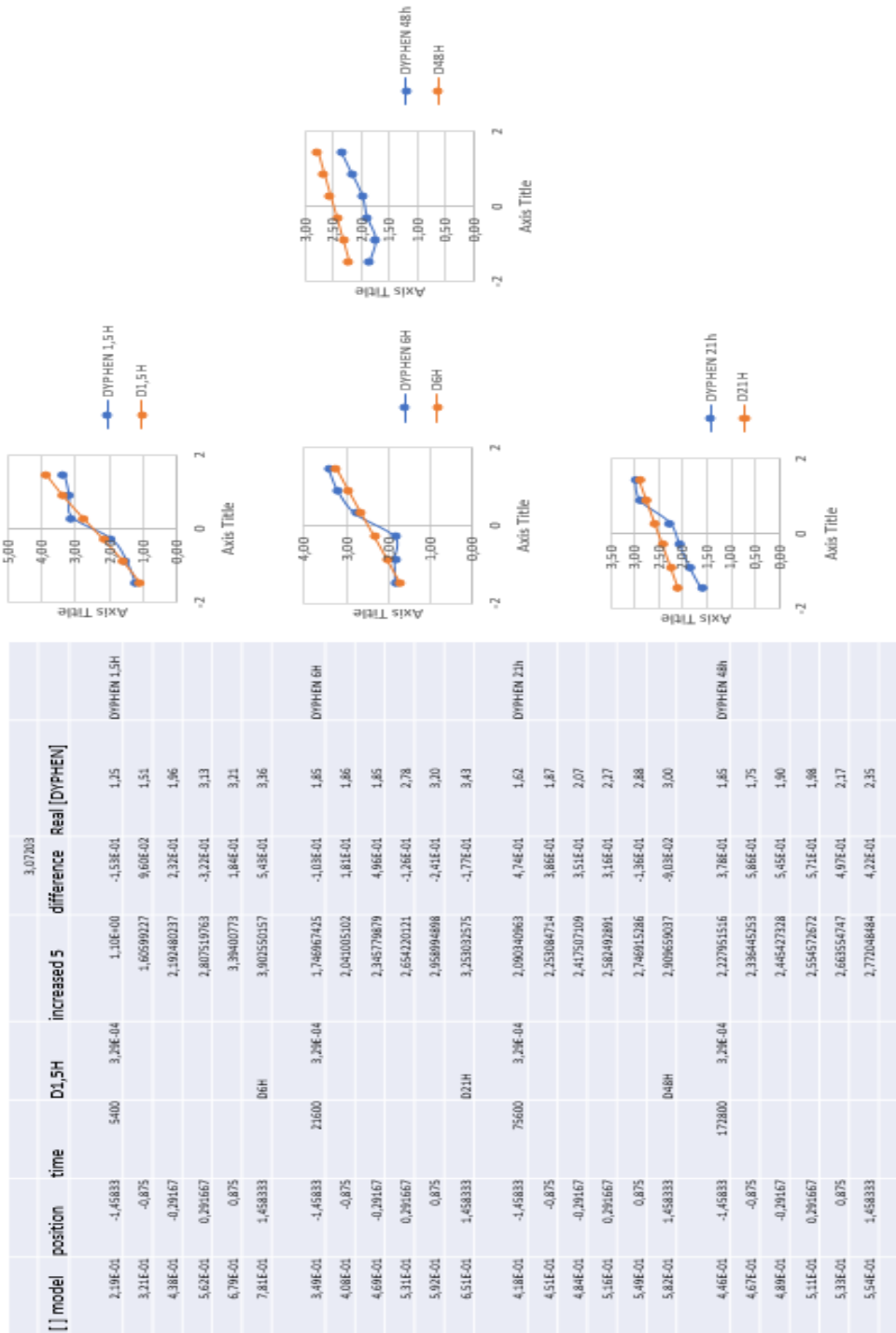


Figure 6-65 Diphenylmethane Diffusion Coefficient

# Naph diffusion coefficient at 25°C

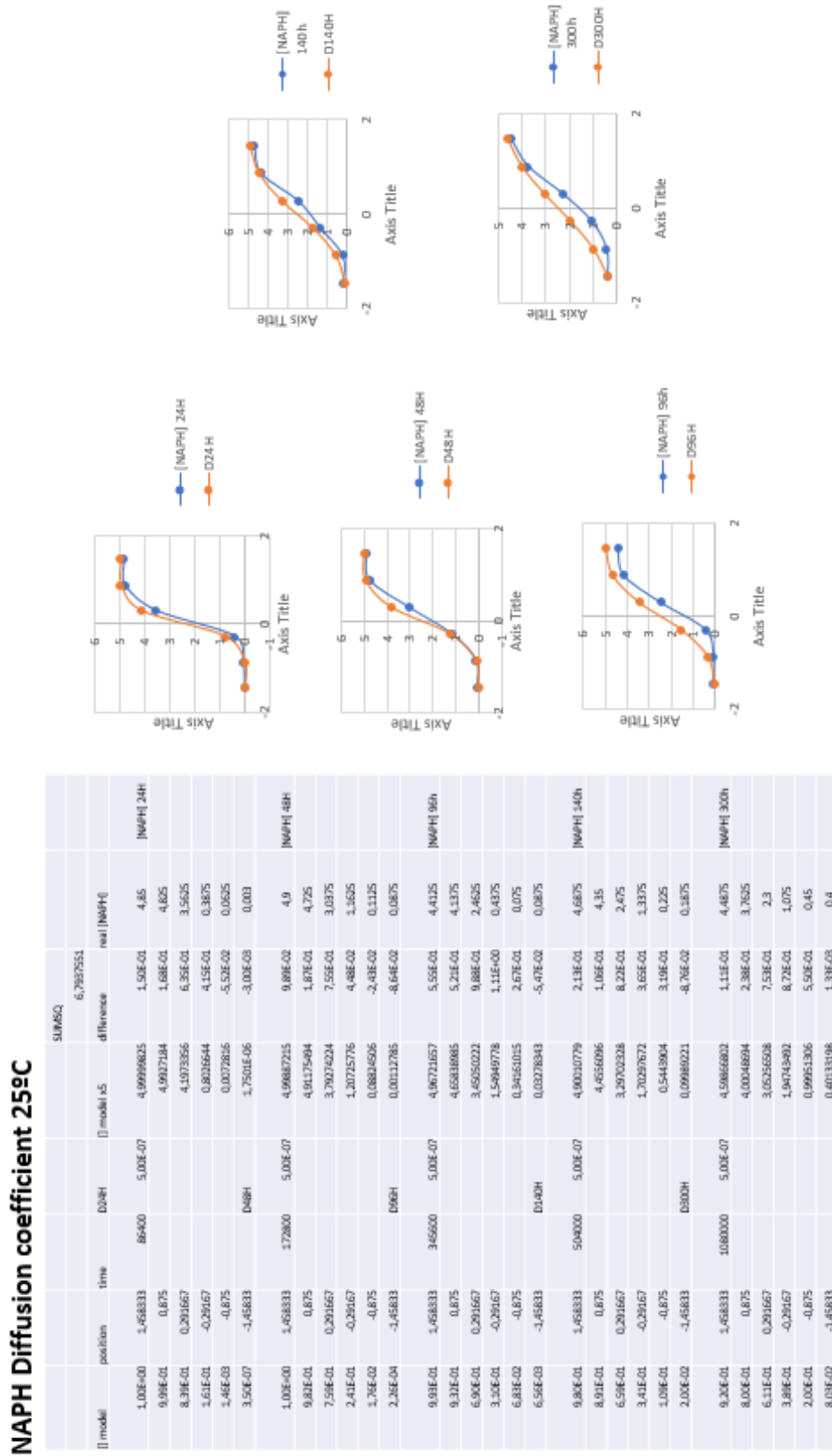


Figure 6-66 Naph Diffusion Coefficient at 25°C

# Hex diffusion coefficient at 25°C

## HEX Diffusion coefficient 25°C

[I] model	position	time	D0xH	[I] model	ΔS	difference	RMSE	RMSE [HEX]
			86400		6,879E-05	-3,25E-01	3,236766	
1,38E-05	-1,45833	0,875			0,00685247	-2,95E-01	0,33	[HEX] 24H
5,94E-08	-0,2967				1,04104568	-0,58E-02	1,10	
2,01E-01	0,39667				3,9679542	-2,04E-01	4,20	
7,99E-01	0,875				4,970314753	4,20E-01	4,55	
9,94E-01	1,45833		D48H		4,99995121	4,25E-01	4,58	
1,00E+00	-1,45833	172800			0,007567708	-5,42E-01	0,55	[HEX] 48H
3,76E-02	-0,875				0,18125755	-3,12E-01	0,50	
2,77E-01	-0,2967				1,36061521	-6,00E-01	1,98	
7,29E-01	0,39667				3,617038479	-1,16E-01	3,73	
9,62E-01	0,875				4,81189245	1,45E-01	4,67	
9,98E-01	1,45833		D96H		4,900432202	5,91E-02	4,93	
1,89E-02	-1,45833	345600			0,00032832	-2,85E-01	0,38	[HEX] 96h
1,04E-01	-0,875				0,521040866	1,96E-01	0,33	
3,37E-01	-0,2967				1,667472749	-1,38E-01	1,83	
6,63E-01	0,39667				3,312527251	-5,37E-01	3,85	
8,96E-01	0,875				4,478959134	2,29E-01	4,25	
9,82E-01	1,45833		D140H		4,909917168	6,00E-01	4,25	
4,13E-02	-1,45833	504000			0,206350075	-0,36E-02	0,30	[HEX] 140h
1,49E-01	-0,875				0,743915621	4,44E-01	0,30	
3,64E-01	-0,2967				1,821050943	-7,89E-02	1,90	
6,38E-01	0,39667				3,178939057	7,89E-02	3,10	
8,51E-01	0,875				4,356084379	-1,89E-02	4,28	
9,59E-01	1,45833		D300H		4,70639525	4,19E-01	4,38	
1,18E-01	-1,45833	1080000			0,589055946	4,14E-01	0,18	[HEX] 300h
2,38E-01	-0,875				1,191768654	4,67E-01	0,73	
4,05E-01	-0,2967				2,051258097	-0,37E-02	2,13	
5,94E-01	0,39667				2,968741903	-2,06E-01	3,18	
7,62E-01	0,875				3,808200136	-1,67E-01	3,98	
8,82E-01	1,45833				4,410894054	2,61E-01	4,15	

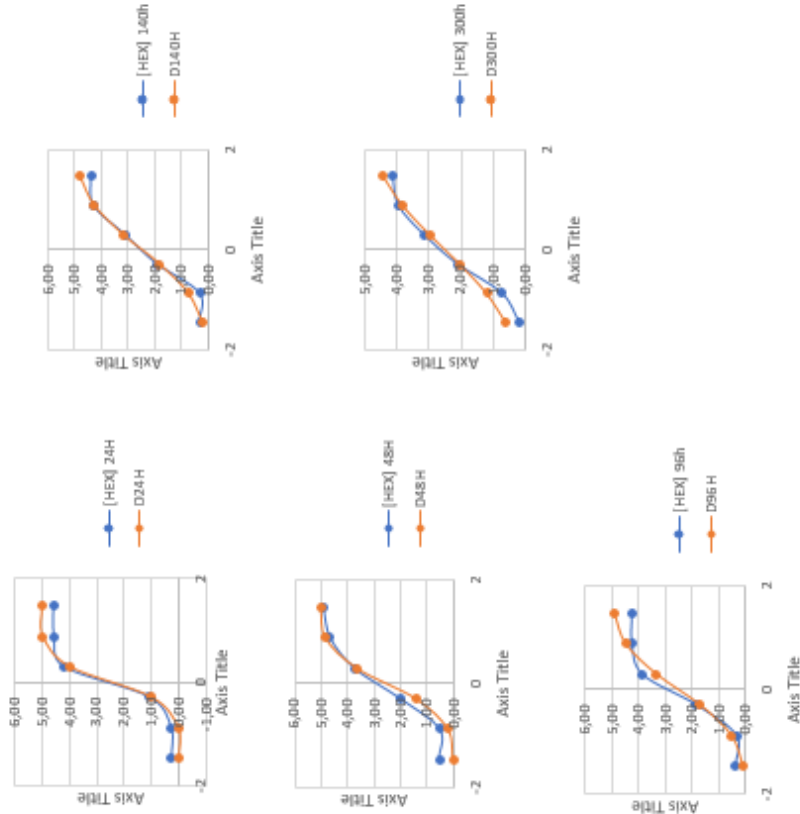


Figure 6-67 Hex Diffusion Coefficient at 25°C

# Naph diffusion coefficient at 5°C

NAPH Diffusion coefficient 5°C

[] model		position	time	D24H	[] model's	difference	real [NAPH]	SUMSQ
								6.383958
1.00E+00	1.458333	86400	3.00E-07	5.00E+00	4.25E-01	4.575	[NAPH] 24H	
1.00E+00	0.875			4.996696	5.62E-01	4.4375		
9.00E-01	0.291667			4.996529	8.00E-01	3.7		
1.00E-01	-0.291667			0.500471	2.38E-01	0.2625		
6.00E-05	-0.875			0.000304	-3.00E-01	0.3		
7.51E-11	-1.458333	096H		3.76E-10	-1.87E-01	0.1875		
9.99E-01	1.458333	345600	3.00E-07	4.996594	4.34E-01	4.5625	[NAPH] 96H	
9.73E-01	0.875			4.863335	3.38E-01	4.525		
7.39E-01	0.291667			3.695393	5.70E-01	3.125		
2.65E-01	-0.291667			1.304607	8.42E-01	0.4625		
2.73E-02	-0.875			0.136665	-1.51E-01	0.2875		
6.81E-04	-1.458333	0140H		0.003406	-1.09E-01	0.1125		
9.98E-01	1.458333	504000	3.00E-07	4.979993	5.05E-01	4.475	[NAPH] 140h	
9.44E-01	0.875			4.721073	3.34E-01	4.3875		
7.02E-01	0.291667			3.510997	6.35E-01	2.875		
2.98E-01	-0.291667			1.489603	8.15E-01	0.675		
5.38E-02	-0.875			0.278927	2.04E-01	0.075		
4.00E-03	-1.458333	0216H		0.020007	7.51E-03	0.0125		
9.84E-01	1.458333	777600	3.00E-07	4.918103	4.81E-01	4.4375	[NAPH] 216h	
9.00E-01	0.875			4.499529	2.50E-01	4.25		
6.65E-01	0.291667			3.326561	6.27E-01	2.7		
3.35E-01	-0.291667			1.679439	1.15E+00	0.525		
1.00E-01	-0.875			0.500471	4.63E-01	0.0375		
1.64E-02	-1.458333			0.081897	6.90E-03	0.075		

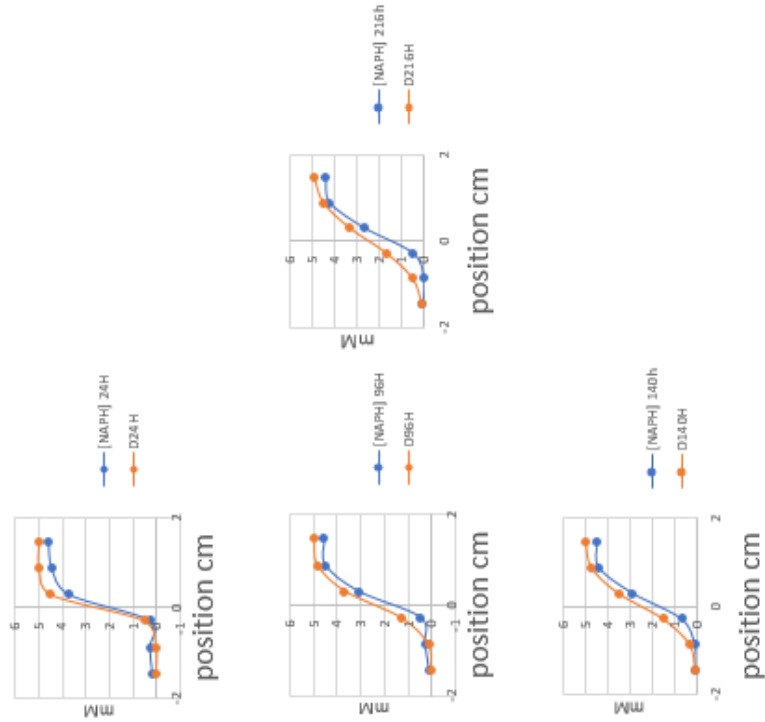


Figure 6-68 Naph diffusion coefficient at 5°C

# Hex diffusion coefficient at 5°C

## HEX Diffusion coefficient 5°C

model	position	time	D24H	model\5	difference	real [HEX]	SUMSQ
0,00E+00	-1,45833	86400	1,00E-07	0,00E+00	-2,75E-01	0,275	6,363593
1,40E-11	-0,875			7,02E-11	-4,75E-01	0,475	
1,33E-02	-0,29167			0,066254	-8,09E-01	0,875	
9,87E-01	0,291667			4,933746	4,84E-01	4,45	
1,00E+00	0,875			5	3,50E-01	4,65	
1,00E+00	1,458333		D96H	5	1,50E-01	4,85	
1,45E-08	-1,45833	345600	1,00E-07	7,27E-08	-3,25E-01	0,325	[HEX] 96H
4,37E-04	-0,875			0,002185	-1,48E-01	0,15	
1,34E-01	-0,29167			0,668153	-1,16E+00	1,825	
8,66E-01	0,291667			4,331847	2,32E-01	4,1	
1,00E+00	0,875			4,907815	3,73E-01	4,625	
1,00E+00	1,458333		D140H	5	2,75E-01	4,725	
2,18E-06	-1,45833	504000	1,00E-07	1,09E-05	-1,75E-01	0,175	[HEX] 140h
2,93E-03	-0,875			0,014629	-1,65E-01	0,2	
1,79E-01	-0,29167			0,895679	-5,54E-01	1,45	
8,21E-01	0,291667			4,104321	4,29E-01	3,675	
9,97E-01	0,875			4,985371	7,66E-01	4,225	
1,00E+00	1,458333		D216H	4,999989	8,00E-01	4,2	
1,09E-04	-1,45833	777600	1,00E-07	0,000543	-4,74E-01	0,475	[HEX] 216h
1,33E-02	-0,875			0,066254	-1,84E-01	0,25	
2,30E-01	-0,29167			1,148865	-6,51E-01	1,8	
7,70E-01	0,291667			3,851135	-2,74E-01	4,125	
9,87E-01	0,875			4,933746	5,84E-01	4,35	
1,00E+00	1,458333			4,999457	6,49E-01	4,35	

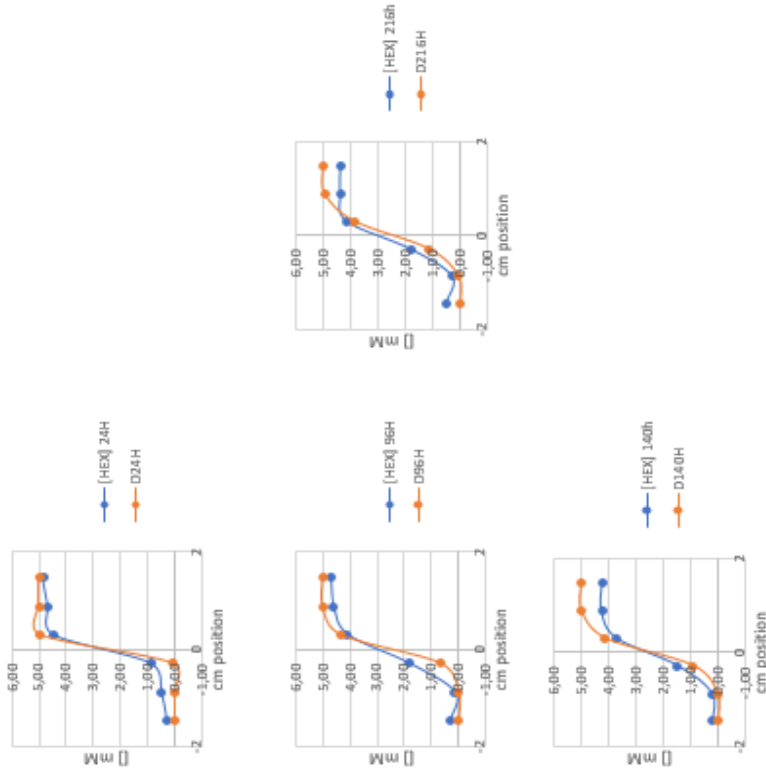


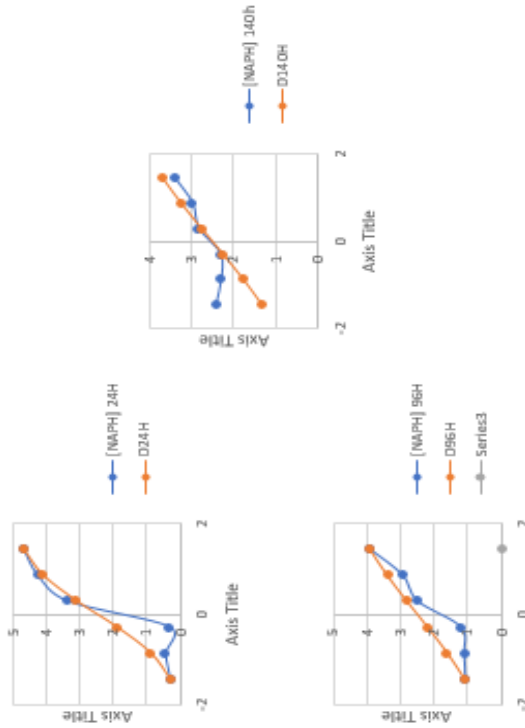
Figure 6-69 Hex diffusion coefficient at 5°C

# Naph diffusion coefficient at 45°C

## NAPH Diffusion coefficient 45°C

[ ] model	position	time	D24H	[ ] model x5	Difference	real [NAPH]
					SUMSQ	
					6,001474174	
9,38E-01	1,458333	86400	5,19E-06	4,69E+00	4,11E-02	4,65 [NAPH] 24H
8,22E-01	0,875	05-ago		4,11E+00	-1,26E-01	4,2375
6,21E-01	0,291667			3,104814483	-2,45E-01	3,35
3,79E-01	-0,29167			1,895185517	1,57E+00	0,325
1,78E-01	-0,875			0,888674092	4,39E-01	0,45
6,18E-02	-1,45833		D96H	0,308868348	-3,63E-03	0,3125
7,79E-01	1,458333	345600	5,19E-06	3,896789858	-4,07E-02	3,9375 [NAPH] 96H
6,78E-01	0,875			3,389825415	4,40E-01	2,95
5,61E-01	0,291667			2,805986186	3,06E-01	2,5
4,39E-01	-0,29167			2,194013814	9,94E-01	1,2
3,22E-01	-0,875			1,610174585	4,98E-01	1,1125
2,21E-01	-1,45833		D140H	1,103210142	2,82E-02	1,075
7,38E-01	1,458333	504000	5,19E-06	3,69073424	2,78E-01	3,4125 [NAPH] 140h
6,49E-01	0,875			3,244932396	2,57E-01	2,9875
5,51E-01	0,291667			2,733694779	-8,38E-02	2,8375
4,49E-01	-0,29167			2,246305221	-7,87E-02	2,325
3,51E-01	-0,875			1,755067604	-5,57E-01	2,3125
2,62E-01	-1,45833			1,30926576	-1,13E+00	2,4375

Figure 6-70 Naph Diffusion Coefficient at 45°C



# Hex diffusion coefficient at 45°C

## HEX Diffusion coefficient 45°C

model	position	time	D24H	model x5 difference	real [HEX]	SUMSQ
						6,426886
7,06E-02	-1,45833	86400	5,69E-06	0,353172	7,82E-02	[HEX] 24H
1,89E-01	-0,875			0,943564	5,94E-01	0,35
3,84E-01	-0,29167			1,921481	8,96E-01	1,03
6,16E-01	0,291667			3,078519	-7,21E-01	3,80
8,11E-01	0,875			4,056436	3,06E-01	3,75
9,29E-01	1,458333		D96H	4,646828	4,72E-01	4,18
2,31E-01	-1,45833	345600	5,69E-06	1,155025	2,80E-01	0,88
3,29E-01	-0,875			1,647445	-2,76E-02	1,68
4,42E-01	-0,29167			2,207616	3,08E-01	1,90
5,58E-01	0,291667			2,792384	-7,33E-01	3,53
6,71E-01	0,875			3,352555	-1,72E-01	3,53
7,69E-01	1,458333		D140H	3,844975	1,45E-01	3,70
2,71E-01	-1,45833	504000	5,69E-06	1,356169	3,56E-01	1,00
3,57E-01	-0,875			1,786936	1,37E-01	1,65
4,52E-01	-0,29167			2,257609	7,58E-01	1,50
5,48E-01	0,291667			2,742391	5,42E-01	2,20
6,43E-01	0,875			3,213064	5,88E-01	2,63
7,29E-01	1,458333			3,643831	1,52E+00	2,13
						[HEX] 96H
						[HEX] 140h

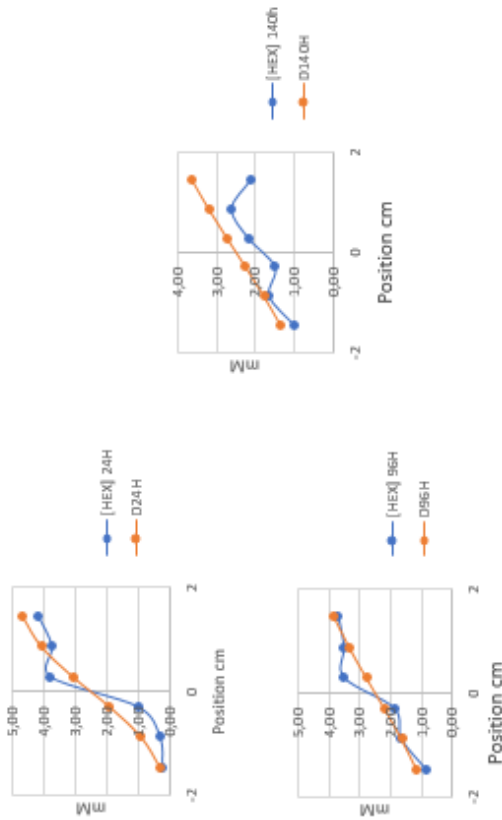


Figure 6-71 Hex diffusion coefficient at 45°C

